DEPARTMENT OF PHYSICS
INDIAN INSTITUTE OF TECHNOLOGY MADRAS
CHENNAI 600036

GENESIS OF MAGNETIC FIELDS DURING INFLATION: IMPLICATIONS OF DEVIATIONS FROM SLOW ROLL

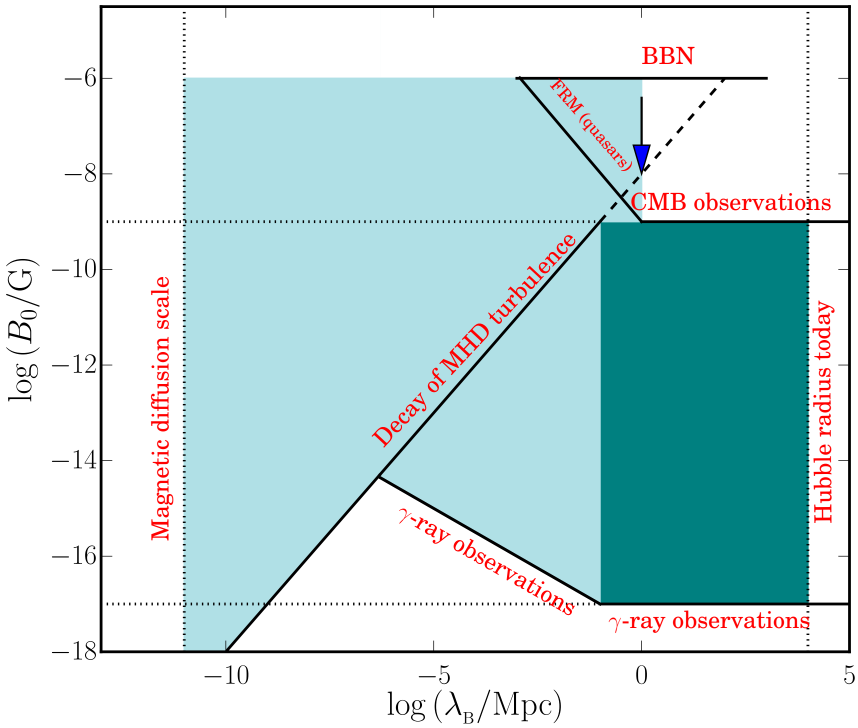

A thesis

Submitted by

SAGARIKA TRIPATHY

For the award of the degree

of

DOCTOR OF PHILOSOPHY

September 2023

DEPARTMENT OF PHYSICS
INDIAN INSTITUTE OF TECHNOLOGY MADRAS
CHENNAI 600036

GENESIS OF MAGNETIC FIELDS DURING INFLATION: IMPLICATIONS OF DEVIATIONS FROM SLOW ROLL

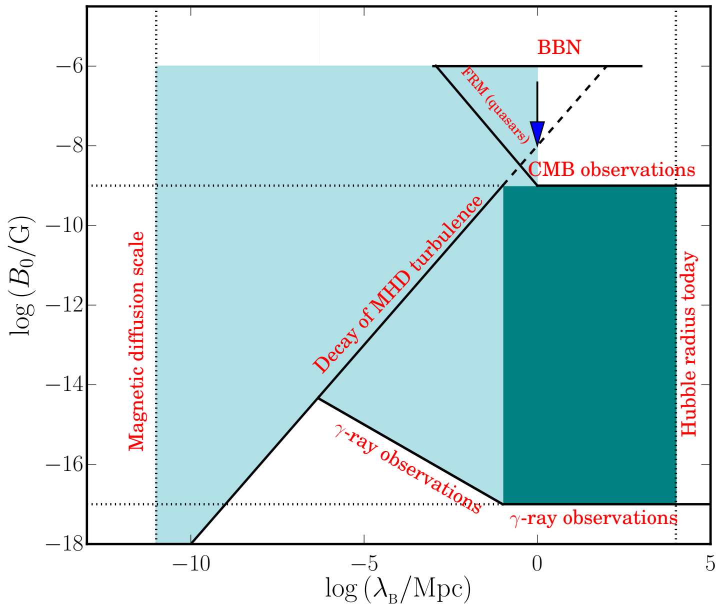

A thesis

Submitted by

SAGARIKA TRIPATHY

For the award of the degree

of

DOCTOR OF PHILOSOPHY

September 2023

Great dreams of great dreamers are always transcended.

Dr. A. P. J. Abdul Kalam

THESIS CERTIFICATE

This is to undertake that the thesis titled *'Genesis of magnetic fields during inflation: Implications of deviations from slow roll'* submitted by me to the Indian Institute of Technology Madras, for the award of Ph.D. is a bonafide record of the research work done by me under the supervision of Prof. L. Sriramkumar. The contents of this thesis, in full or in parts, have not been submitted to any other Institute or University for the award of any degree or diploma.

Chennai 600036 **Research Scholar**

Date: September 28, 2023

Research Guide

List of Publications

The publications arising out of the work described in this thesis are as follows.

• **Publications in refereed journals**

1. **S. Tripathy**, D. Chowdhury, R. K. Jain and L. Sriramkumar, *Challenges in the choice of the non-conformal coupling function in inflationary magnetogenesis*, Phys. Rev. D **105**, 063519 (2022) [arXiv:2111.01478 [astro-ph.CO]].

2. **S. Tripathy**, D. Chowdhury, H. V. Ragavendra, R. K. Jain and L. Sriramkumar, *Circumventing the challenges in the choice of the nonconformal coupling function in inflationary magnetogenesis*, Phys. Rev. D **107**, 043501 (2023) [arXiv:2211.05834 [astro-ph.CO]].

3. **S. Tripathy**, R. N. Raveendran, K. Parattu and L. Sriramkumar, *Amplifying quantum discord during inflationary magnetogenesis through violation of parity*, Phys. Rev. D **108**, 123512 (2023) [arXiv:2306.16168 [gr-qc]].

ACKNOWLEDGEMENTS

I wish to express my profound gratitude to my thesis supervisor, Prof. L. Sriramkumar, for his exceptional guidance, unwavering support, and invaluable mentorship throughout my entire Ph.D. journey. His expertise in the field, dedication to academic excellence, and commitment to both my academic and personal growth have been instrumental in shaping this research project. He has not only inspired my research but also broadened my horizons beyond the academic realm, introducing me to diverse subjects such as history, music, and art. I am deeply thankful for the privilege of working under his guidance.

I extend my heartfelt thanks to the chairperson of my doctoral committee—Prof. Arul Lakshminarayanan. His persistent motivation has been a driving force throughout the years. I would also like to thank the other members of the committee: Dr. Dawood Kothawala, Prof. James Libby, and Prof. Anil Prabhakar, for their insightful suggestions and valuable comments. Special thanks go to Dr. Dhiraj Hazra, Prof. Kandaswamy Subramanian, Dr. Matteo Braglia, Dr. Ramkishor Sharma, and Prof. Shiv Sethi for enlightening discussions on various aspects of cosmology during my Ph.D. journey.

I owe a debt of gratitude to my former officemate and collaborator, Dr. H. V. Ragavendra, who has played a pivotal role in shaping me as a researcher. His patient guidance, from clarifying basic doubts to teaching new tools and methods, has been indispensable. His advice and motivation sustained me through the ups and downs of my Ph.D. tenure. Additionally, his sense of humour and well-timed meme-sharing never failed to lift my spirits up during tough times. I extend my heartfelt appreciation to my collaborator and former colleague, Dr. Debika Chowdhury, for her patience during work-related discussions and her role as an inspiring figure in my academic journey. Her recommendations of exceptional food places in Chennai are warmly appreciated. I would also like to thank my brilliant collaborators—Dr. Rathul Nath Raveendran, Dr. Krishnamohan Parattu, and Dr. Rajeev Kumar Jain—for their thought-provoking discussions and invaluable contributions.

I want to thank my current colleagues, including Suvashis Maity, Alipriyo Hoory, Hari K., Dr. Md Riajul Haque, Dr. Subhajit Barman, and former colleagues Dr. Rahul Kothari, Dr. Pankaj Saha, Dr. Sampurn Anand, Dr. Ashmita Das, Dr. Sukannya Bhattacharya, and Dr. Debottam Nandi, for their kindness and support, which made my journey smoother. Our physics discussions, outings to watch countless movies (especially movies from MCU), and trips will forever hold a special place in my memories. To my friends—Amit, Anubhav, Atanu, Bibek, Buddha, Kanti, Kaushik, Namrata, Niharika, Sugandha, Sweta, and Vinod—I extend my heartfelt thanks for their faith, support, and encouragement at different stages of my life. I reserve a special place of gratitude for my closest friends from my B.Sc. days—Monica, Sushree, and Tulika—whose constant encouragement and invaluable contribution to my all-round development have consistently driven me towards achieving my goals while keeping me grounded.

I express my deepest appreciation to my partner, Sougata Guha, who has been a continuous source of inspiration and support for the past eight years. His guidance and encouragement have been instrumental in shaping my ability to think critically. I am forever indebted to him for showing me the right way to understand physics. I could not have navigated this challenging journey without his steadfast support and assistance, which has helped me maintain my mental peace in the face of adversity.

My heartfelt thanks go to my parents for nurturing me into becoming the dignified and independent individual I am today. Their perseverance, faith, and motivation have made it possible for me to pursue my career in science. I also extend my gratitude to my sister and brother-in-law for their help and support and for giving me the most priceless present of all—their child, Suhan. Last but not least, I want to express my appreciation to my in-laws for being my loving and supportive second family, cheering me on at every step of this journey.

ABSTRACT

KEYWORDS: Inflation, Primordial magnetic fields, Non-conformal coupling, Violation of parity, Cosmic microwave background, Evolution of the quantum state of electromagnetic fields

Magnetic fields permeate the entire universe, extending from the smallest to the largest observable length scales. In galaxies and clusters of galaxies, the strength of the observed magnetic fields is of order $\mu\,\mathrm{G}$, with their coherence lengths ranging from Kpc to Mpc. In addition, very weak magnetic fields with a lower bound of the order of $10^{-17}\,\mathrm{G}$ are observed in the voids in the intergalactic medium, which are coherent over scales above $1\,\mathrm{Mpc}$. According to the standard paradigm, the strong magnetic fields observed in galaxies and clusters are a result of the amplification of pre-existing, weaker, seed magnetic fields via physical phenomena such as the dynamo mechanism. Due to the absence of complex plasma and magnetohydrodynamical processes, the magnetic fields present in intergalactic voids on cosmological scales (i.e. over 1–$10^4\,\mathrm{Mpc}$) are least likely to be affected by astrophysical phenomena. Hence, they can be considered as suitable regions in space for the investigation of the origin of the seed fields.

The seed magnetic fields could be generated from quantum fluctuations in the vacuum state of the electromagnetic fields during the early stages of the evolution of the universe. Such fields are referred to as primordial magnetic fields (PMFs). Since the energy density of magnetic fields decay with the expansion of the universe, the strength of the seed fields generated in the early universe, especially during inflation, will rapidly die down, and hence will not lead to the observed strengths of the fields today. Therefore, in order to produce magnetic fields that are consistent with the current observations, according to the popular theory of inflationary magnetogenesis, the seed magnetic fields on cosmological scales are generated by breaking the conformal invariance of the conventional electromagnetic action.

To understand the origin and evolution of the PMFs, we first need to understand the physics of inflation. Inflation corresponds to a period of accelerated expansion that is expected to have occurred during the early stages of the radiation dominated epoch. It is often invoked to overcome the shortcomings of the hot big bang model, such as the horizon and flatness problems. A canonical scalar field (often referred to as the inflaton) that is slowly rolling down the potential is one of the simplest ways to achieve inflation. In order to generate large scale magnetic fields during inflation, the conformal invariance of the standard electromagnetic action is broken by coupling

the electromagnetic field to the inflaton. In addition, a parity violating term is often included in the action to generate helical magnetic fields. It has been found that, in such situations, one of the two states of polarization of the electromagnetic modes evolves to a higher amplitude than the other during the later stages of inflation. The magnetic fields generated through such mechanisms will not be diluted during inflation and can evolve to the observed strengths today.

The form of the non-conformal coupling function that is widely used in the literature generally involves a power of the scale factor. Such a form for the coupling function leads to power spectra of magnetic fields that are of the desired shape and amplitude. However, in a more realistic scenario wherein inflation is driven by a scalar field, it is appropriate to work with coupling functions which capture the dynamics of the field. In inflationary models wherein the inflaton rolls slowly, the resulting scalar power spectrum has a nearly scale invariant form. Such spectra are largely consistent with the recent data on the anisotropies in the cosmic microwave background (CMB). However, with an interest in improving the fit to the CMB data and to understand the possible primordial origin of black holes, a plethora of inflationary models have been proposed which generate features in the scalar power spectrum over large and small scales. These models involve potentials which lead to nontrivial dynamics—specifically, departures from slow roll—and it is interesting to investigate the generation of magnetic fields in such scenarios.

In this thesis, we shall first understand the challenges that arise in the generation of magnetic fields in single field models of inflation that lead to deviations from slow roll. Thereafter, we shall discuss the manner in which such challenges can be circumvented using two field models of inflation. Lastly, we shall utilize different measures to understand the evolution of the quantum state of helical electromagnetic fields during inflation. In what follows, we have briefly outlined below three pieces of work that have been completed in these contexts, which constitute this thesis. (The reference numbers in this abstract correspond to the manuscripts listed earlier under publications and preprints.)

• *On the challenges in the choice of the non-conformal coupling function in inflationary magnetogenesis*: PMFs are generated during inflation by considering actions that break the conformal invariance of the electromagnetic field. To break the conformal invariance, the electromagnetic fields are coupled either to the inflaton or to the scalar curvature. Also, a parity violating term is often added to the action in order to enhance the amplitudes of the primordial electromagnetic fields. In this work [1], we examine the effects of deviations from slow roll inflation on the spectra of nonhelical as well as helical electromagnetic fields. We find that, in the case of the coupling to the scalar curvature, there arise certain challenges in generating electromagnetic fields of the desired shapes and strengths even in slow roll inflation. When the field is coupled to the inflaton, it is possible to construct model-dependent coupling functions which lead to nearly scale invariant power spectra of the magnetic fields in slow roll inflation. However, we show that sharp features in the scalar power spectrum generated due to departures from slow roll inflation inevitably lead to strong features in the power spectra of the electromagnetic fields. Moreover, we find that such effects can also considerably suppress the strengths of the generated electromagnetic fields over the scales of cosmological interest. We illustrate these aspects with the aid of inflationary models that have been considered to produce specific features in the scalar power spectrum. Further, we find that, in such situations, if the strong features in the electromagnetic power spectra are to be undone, the choice of the coupling function requires considerable fine tuning. We discuss the wider implications of the results we obtain.

•*Circumventing the challenges in the choice of the non-conformal coupling function in inflationary magnetogenesis*: As is well known, in order to generate magnetic fields of observed amplitudes during inflation, the conformal invariance of the electromagnetic field has to be broken by coupling it either to the inflaton or to the scalar curvature. Couplings to scalar curvature pose certain challenges even in slow roll inflation and it seems desirable to consider couplings to the inflaton. It can be shown that, in slow roll inflation, to generate nearly scale invariant magnetic fields of adequate strengths, the non-conformal coupling to the inflaton has to be chosen specifically depending on the inflationary model at hand. In an earlier work [1], we had shown that, when there arise sharp departures from slow roll inflation leading to strong features in the scalar power spectra, there inevitably arise sharp features in the spectra of the electromagnetic fields, unless the non-conformal coupling functions are extremely fine tuned. In particular, we had found that, if there occurs an epoch of ultra slow roll inflation (that is often required either to lower scalar power on large scales or to enhance power on small scales), then the strength of the magnetic field over large scales can be severely suppressed. In this work [2], we examine whether these challenges can be circumvented in models of inflation involving two fields. We show that the presence of the additional scalar field allows us to construct coupling functions that lead to magnetic fields of required strengths even when there arise intermediate epochs of ultra slow roll inflation. However, we find that the features in the spectra of the magnetic fields that are induced due to the departures from slow roll inflation cannot be completely ironed out. We make use of the code MagCAMB to calculate the effects of the magnetic fields on the anisotropies in the CMB and investigate if the spectra with features are broadly consistent with the current constraints.

• *Amplifying quantum discord during inflationary magnetogenesis through violation of parity*: It is well known that, during inflation, the conformal invariance of the electromagnetic action has to be broken in order to produce magnetic fields of observed strengths today. Often, to further enhance the strengths of the magnetic fields, parity is also assumed to be violated when the fields are being generated. In this work [3], we examine the evolution of the quantum state of the Fourier modes of the non-conformally coupled and parity violating electromagnetic field during inflation. We utilize tools such as the Wigner ellipse, squeezing parameters and quantum discord to understand the evolution of the field. We show that the violation of parity leads to an enhancement of the squeezing amplitude and the quantum discord (or, equivalently, in this context, the entanglement entropy) associated with a pair of opposite wave vectors for one of the two states of polarization (and a suppression for the other state of polarization), when compared to the case wherein parity is conserved. We highlight the similarities between the evolution of the Fourier modes of the electromagnetic field when parity is violated during inflation and the behaviour of the modes of a charged, quantum, scalar field in the presence of a constant electric field in a de Sitter universe. We briefly discuss the implications of the results we obtain.

TABLE OF CONTENTS

LIST OF TABLES

Table **Title** **Page**

LIST OF FIGURES

ABBREVIATIONS

IGM	Inter Galactic Medium
MHD	Magnetohydrodynamics
LSS	Large Scale Structure
PMFs	Primordial Magnetic Fields
CMB	Cosmic Microwave Background
FLRW	Friedmann-Lemaître-Robertson-Walker
COBE	Cosmic Background Explorer
WMAP	Wilkinson Microwave Anisotropy Probe
ADM	Arnowitt-Deser-Misner
BICEP	Background Imaging of Cosmic Extragalactic Polarization
UHECRs	Ultra High-Energy Cosmic Rays
FRM	Faraday Rotation Measure
BBN	Big Bang Nucleosynthesis
HESS	High Energy Stereoscopic System
LAT	Large Area Telescope
MAGIC	Major Atmospheric Gamma Imaging Cherenkov Telescope
VERITAS	Very Energetic Radiation Imaging Telescope Array System
EW	Electroweak
CAMB	Code for Anisotropies in the Microwave Background
PBHs	Primordial Black Holes
QCD	Quantum Chromodynamics
QP	Quadratic Potential
QP-WS	Quadratic Potential With Step
SM	Starobinsky Model
SM-WS	Starobinsky Model With Step
SFM	Small Field Model
SFM-WS	Small Field Model With Step
PI	Punctuated Inflation
USR	Ultra Slow Roll
TFM	Two Field Model

NOTATIONS

The notations used in this thesis have been listed below in the order of their appearance in the thesis.

Notation	Description
$\hbar$	Reduced Planck's constant, $1.054 \times 10^{-34}\,\mathrm{J\,s}$
c	Speed of light, $299792458\,\mathrm{m\,s^{-1}}$
$M_{_{\mathrm{Pl}}}$	Reduced Planck mass, $2.435 \times 10^{18}\,\mathrm{GeV/c^2}$
G	Universal gravitational constant, $6.674 \times 10^{-11}\,\mathrm{N\,kg^{-2}\,m^2}$
t	Cosmic time
$\boldsymbol{x}$	Position vector
η	Conformal time
N	E-fold
$a(t)$	Scale factor describing the universe
H	Hubble parameter
H_0	Hubble constant, value of the Hubble parameter today
$H_{_{\mathrm{I}}}$	(Nearly) Constant value of Hubble parameter in (slow roll) de Sitter inflation
ρ	Energy density
w	Parameter describing the equation of state
p	Pressure
ϕ	Scalar field driving inflation
$V(\phi)$	Potential describing the scalar field ϕ
V_0	Parameter determining the energy scale of potential in the single and two field models of inflation
η_{i}	Conformal time when the initial conditions are imposed on perturbations
η_{e}, $-1/k_e$	Conformal time at the end of inflation
V_ϕ	$\mathrm{d}V/\mathrm{d}\phi$, Derivative of the potential V with respect to the scalar field ϕ
$V_{\phi\phi}$	$\mathrm{d}^2V/\mathrm{d}\phi^2$, Second derivative of the potential V with respect to ϕ
z	Redshift
T^{μ}_{ν}	Stress-energy tensor
$\mathcal{N}$	Lapse function
$\mathcal{N}^i$	Shift vector

Notation	**Description**
h_{ij}	Spatial metric
$\rho_{\rm I}$	Background energy density during inflation
ϵ_n	n-th slow roll parameter
Ω_Λ^0	Dimensionless energy density of the cosmological constant today
$\Omega_{\rm m}^0$	Dimensionless energy density of non-relativistic matter at present
k	Comoving wave number of the perturbations
$\mathcal{R}(\eta, \boldsymbol{x})$	Curvature perturbation at the spacetime coordinates $(\eta, \boldsymbol{x})$
$\gamma_{ij}(\eta, \boldsymbol{x})$	Tensor perturbation at the spacetime coordinates $(\eta, \boldsymbol{x})$
$S_2[\mathcal{R}]$	Second order action governing the curvature perturbations
$S_2[\gamma_{ij}]$	Second order action governing the primary tensor perturbations
f_k	Fourier mode function describing the scalar perturbations, corresponding to the wave number k
v_k	Fourier mode of the Mukhanov-Sasaki variable associated with the scalar perturbations, corresponding to the wave number k
h_k	Fourier mode of the tensor perturbations, corresponding to the wave number k
u_k	Fourier mode of the Mukhanov-Sasaki variable associated with the tensor perturbations, corresponding to the wave number k
$\epsilon_{ij}^\lambda(\boldsymbol{k})$	Polarization tensor of the gravitational waves, with the indices $\lambda = (+, \times)$ denoting the two states of polarization
$\mathcal{P}_{\rm S}(k)$	Power spectrum of the curvature perturbations
$\mathcal{P}_{\rm T}(k)$	Power spectrum of the primary tensor perturbations
$n_{\rm S}$	Spectral index of primordial scalar power spectrum
$n_{\rm T}$	Spectral index of primordial tensor power spectrum
r	Tensor-to-scalar ratio
k_*	Pivot scale
$\lambda_{\rm B}$	Coherence length of magnetic fields
B_0	Present day amplitude of magnetic fields
A^μ	Electromagnetic four vector potential
$F_{\mu\nu}$	Electromagnetic field tensor
$\widetilde{F}_{\mu\nu}$	Dual electromagnetic field tensor
σ	Positive or negative helicity of the electromagnetic modes
γ	Helicity parameter
$J(\phi), I(\phi)$	Non-conformal/Non-minimal coupling function in the electromagnetic action

Notation	Description
A^i	Electromagnetic three vector potential
$\epsilon_{\lambda i}^{\boldsymbol{k}}$	Polarization vector of the electromagnetic vector potential (with $\lambda = (1,2)$) corresponding to the wave vector $\boldsymbol{k}$ in the i-spatial direction
$\bar{A}_k$	Fourier mode function describing the electromagnetic vector potential corresponding to the wave number k
$\mathcal{A}_k$	Redefined Fourier mode function of the electromagnetic vector potential corresponding to the wave number k
$\mathcal{P}_{\mathrm{B}}(k)$	Power spectrum of the primordial magnetic fields
$\mathcal{P}_{\mathrm{E}}(k)$	Power spectrum of the primordial electric fields
n_{B}	Spectral index of the power spectrum of the primordial magnetic field
n_{E}	Spectral index of power spectrum of the primordial electric field
R	Scalar curvature
H_{e}	Value of Hubble parameter at the end of inflation
N_{e}	E-fold at the end of inflation
$\mathcal{P}_{\mathrm{B}}^{0}(k)$	Power spectrum of the magnetic field today
a_{e}	Scale factor at the end of inflation
a_0	Scale factor today
T_{e}	Temperature of the universe at the onset of radiation domination epoch
T_0	Temperature of the universe today
g_{e}	Effective number of relativistic degrees of freedom at the onset of radiation domination epoch
g_0	Effective number of relativistic degrees of freedom today
m	Mass of the inflaton when described by potentials such as quadratic potential and gpunctuated inflation model
ϕ_{i}	Value of the scalar field at the beginning of its evolution
$\epsilon_{1\mathrm{i}}$	Value of the first slow roll parameter at the beginning of the evolution of ϕ
N_*	E-fold at which the pivot scale k_* leaves the Hubble radius, when counted from the end of inflation

Notation	Description
ϕ_0	Value of the scalar field at which the step is introduced in potentials leading to slow roll; where the slope changes in the potential of the second Starobinsky model; value of the field at the inflection point in models of ultra slow roll and punctuated inflation
$\Delta\phi$	Width of the step introduced in potentials leading to slow roll; parameter determining the change of slope in the smoothed form of the potential in the second Starobinsky model
$\Delta\phi_1$	Parameters that determine the duration of the transition between the non-conformal coupling functions
J_1, J_{0+}, J_{0-}	Constants that ensure that the non-conformal coupling function reduces to unity at the end of inflation
A_+	Slope of the potential in the first stage of second Starobinsky model
A_-	Slope of the potential in the second stage of second Starobinsky model
ΔA	Difference between the slopes in second Starobinsky model, i.e. $A_- - A_+$
η_1, $-1/k_1$	Conformal time at the onset of ultra slow roll
$\hat{\rho}_{\mathrm{B}}$	Operator corresponding to the energy density associated with the magnetic field
$\hat{\rho}_{\mathrm{E}}$	Operator corresponding to the energy density associated with the electric field
A_{S}	Amplitude of primordial scalar power spectrum
η_k	Conformal time at which the mode with wave number leaves the Hubble radius
χ	Scalar field that drives inflation
$V(\chi)$	Potential describing the scalar field χ
m_ϕ, m_χ	Masses of scalar fields in two field models of inflation
χ_0	Points of turn in background trajectory in field space of two field models
χ_{i}	Value of the second scalar field at the beginning of its evolution
ϕ_1, χ_1	Values of the scalar fields at the point of transition in two field models
$\delta\sigma$	Adiabatic perturbation in the two field models
δs	Entropy perturbation in the two field models

Notation	Description
v_k^σ	Mukhanov-Sasaki variable associated with the curvature perturbation corresponding to the wave number k
v_k^s	Mukhanov-Sasaki variable associated with the isocurvature perturbation corresponding to the wave number k
$\mathcal{R}_{k1}, \mathcal{R}_{k2}$	Curvature perturbation in two field models
$\mathcal{S}_{k1}, \mathcal{S}_{k2}$	Isocurvature perturbation in the two field models
$\mathcal{P}_{\mathcal{S}}(k)$	Power spectrum of the isocurvature perturbations
$\mathcal{R}_k^{\mathrm{mag}}$	Secondary curvature perturbation induced by magnetic fields during inflation
$\Delta\chi$	Parameters that determine the duration of the transition between the non-conformal coupling functions
$P_{\mathrm{EM}}(k)$	Power spectrum of the fluctuations in energy density of electromagnetic fields
$\mathcal{P}_{\mathcal{R}}^{\mathrm{mag}}(k)$	Scalar power spectrum associated with the inflationary magnetic mode
k_{min}	Smallest wave number to leave the Hubble radius during inflation
ℓ	Multipole
C_ℓ	CMB angular power spectrum corresponding to the multipole ℓ
$\mathcal{L}$	Lagrangian density in Fourier space
$\mathcal{H}$	Hamiltonian density in Fourier space
$\mathcal{A}_{\boldsymbol{k}\mathrm{R}}^\sigma$	Real part of the redefined Fourier mode $\mathcal{A}_{\boldsymbol{k}}^\sigma$
$\mathcal{A}_{\boldsymbol{k}\mathrm{I}}^\sigma$	Imaginary part of the redefined Fourier mode $\mathcal{A}_{\boldsymbol{k}}^\sigma$
$\mathcal{A}_{-\boldsymbol{k}}^\sigma$	Redefined Fourier mode of the electromagnetic vector potential corresponding to the wave vector $-\boldsymbol{k}$
$\mathcal{P}_{\boldsymbol{k}}^\sigma$	Conjugate momentum associated with the Fourier mode $\mathcal{A}_{-\boldsymbol{k}}^\sigma$
$\mathcal{P}_{-\boldsymbol{k}}^\sigma$	Conjugate momentum associated with the Fourier mode $\mathcal{A}_{-\boldsymbol{k}}^\sigma$
$\Psi(\mathcal{A}, \eta)$	Wave function describing a given mode of the electromagnetic fields
$\mathcal{N}(\eta)$	Time-dependent, complex normalization function wave function
$1/\Omega(\eta)$	Width of the Gaussian wave function $\Psi(\mathcal{A}, \eta)$
$W(\mathcal{A}, \mathcal{P}, \eta)$	Wigner function
V	Covariance matrix
r	Squeezing parameter
φ	Squeezing angle

Notation	Description
$\rho_{\rm red}(x_2, x_2', \eta)$	Reduced density matrix of the system obtained after tracing out the degree of freedom associated with wave vector $\boldsymbol{k}$
$\mathcal{S}$	Entanglement entropy
p_n	Eigen values of the reduced density matrix $\rho_{\rm red}(x_2, x_2', \eta)$
$\psi_n(x)$	Energy eigenstates of the harmonic oscillator
δ	Quantum discord

CHAPTER 1
INTRODUCTION

1.1 MAGNETIC FIELDS IN THE UNIVERSE

Magnetic fields are observed in the entire universe, extending from the astrophysical to the cosmological scales (in this context, see the reviews [1–10]). The Earth and the Sun have dipolar magnetic fields of order $1\,\mathrm{G}$, sustained for billions of years due to the dynamo mechanism [11–14]. In galaxies and clusters of galaxies, the strength of the observed magnetic fields is of the order of μG, with their coherence length scales ranging from Kpc to Mpc [15–20]. Apart from these, very weak magnetic fields with a lower bound of order $10^{-17}\,\mathrm{G}$ are observed in the voids in the intergalactic medium (IGM), which are coherent over scales above $1\,\mathrm{Mpc}$ [21–24].

On small scales, such as in astronomical objects like the Earth, Sun, stars and planets, magnetic fields can dissipate their energy through turbulent and thermal motions of astrophysical plasma. This behaviour also applies, to some extent, to the galactic magnetic fields, including those in the Milky Way galaxy. However, weak magnetic fields on larger distance scales may not have sufficient time to dissipate their energy into motions in the plasma. Once amplified through mechanisms like the dynamo, these magnetic fields can maintain their strength over time scales comparable to the age of the universe.

According to the conventional paradigm, the strong magnetic fields observed in galaxies and clusters of galaxies are produced due to the amplification of already existing weaker magnetic fields through different physical phenomena such as the dynamo mechanism. However, the existing data on magnetic fields in galaxies and clusters of galaxies do not provide direct constraints on the properties and origin of the seed fields. One of the reasons is due to the uncertainties associated with the intricate details of dynamo mechanism operating in galaxies and clusters. Therefore, the only potential opportunity to gain insight into the nature of the initial seed fields is to search for regions in the universe where these fields might exist in their original form, undistorted by the plasma and magnetohydrodynamical (MHD) processes. One such possibility is the IGM, specifically the voids in the large scale structure (LSS). The seed magnetic fields could have been generated through astrophysical processes such as the Biermann battery [25, 26]. But these processes can not explain the large scale magnetic fields present in voids. If weak magnetic fields were indeed present in the very early stages of the universe, they would have experienced limited amplification due to the absence of dynamo processes in the voids. Cosmologically produced magnetic fields could have evolved over time, being diluted by the expansion of the universe. Therefore, potential measurements of magnetic fields in the IGM using observational techniques in the radio, microwave, and γ-ray frequencies could provide essential clues regarding the origin of the seed fields. Such magnetic fields, which are generated through cosmological processes, are called primordial magnetic fields (PMFs).

This thesis focuses on investigating magnetic fields that arise from cosmological processes, particularly during the inflationary epoch of the early universe. Inflation offers an efficient mechanism for the generation and evolution of magnetic fields. The magnetic fields are expected to have arisen out of quantum fluctuations which are inevitably present at the onset of inflation. We will discuss the inflationary epoch of the universe later in this chapter. Our research involves exploring the generation of magnetic fields in various non-trivial inflationary scenarios which leads to interesting signatures of the primordial perturbations on the cosmic microwave background (CMB). We shall also assess how consistent the amplitudes of these magnetic fields are with the observational bounds.

In this chapter, we shall discuss the physics of inflation and the constraints on the magnetic fields present in the voids in the IGM. The chapter is organized as follows. In the next section, we shall outline the essential ideas associated with the hot big bang model. In Sec. 1.3, we shall introduce the metric describing the homogeneous and isotropic universe and discuss the equations governing its dynamics. Thereafter, in Sec. 1.4, we shall discuss the horizon problem, a crucial drawback of the hot big bang model and, in Sec. 1.5, we shall explain how an epoch of inflation helps in overcoming the drawback. We shall also discuss the manner in which inflation can be achieved with the aid of a single, canonical scalar field, and introduce the so-called slow roll parameters. Further, in Sec. 1.6, we shall describe the generation of the scalar and tensor perturbations in an inflationary scenario driven by a single, canonical scalar field. We shall also outline the evaluation of the power spectra characterizing these perturbations in slow roll inflation. Next, in Sec. 1.7, we shall outline the popular mechanisms for the origin of the large scale magnetic fields observed today. In Sec. 1.8, we shall describe the theoretical and observational constraints on the magnetic fields. Lastly, in Sec. 1.9, we shall outline the organization of the thesis.

Before we proceed further, let us clarify a few points regarding the conventions and notations that we shall work with. To begin with, we shall assume that gravitation is described by the general theory of relativity. We shall work with natural units such that $\hbar = c = 1$, and set the reduced Planck mass to be $M_{_{\mathrm{Pl}}} = (8\,\pi\,G)^{-1/2}$. We shall adopt the signature of the metric to be $(-,+,+,+)$. Note that Latin indices will represent the spatial coordinates, except for k which will be reserved for denoting the wave number. We shall assume that the smooth background universe is described by the *spatially flat* Friedmann-Lemaître-Robertson-Walker (FLRW) line-element characterized by the scale factor a. We shall represent the cosmic time as t and the conformal time as η. Also, an overdot and an overprime will denote differentiation with respect to the cosmic and conformal time coordinates, respectively. Moreover, $H = \dot{a}/a$ will represent the Hubble parameter. Lastly, N will represent the number of e-folds.

1.2 THE HOT BIG BANG MODEL

The prevailing cosmological model that provides the most comprehensive understanding of the universe from its earliest moments to its current state is widely known as the hot big bang model (for discussions in this context, see the textbooks [27–35]). There are two critical pieces of observational evidence that support this model. The first of these observations is the expansion of the universe as described by the Hubble's law in the nearby or local universe. As we shall discuss below, the expanding universe can be described in terms of the scale factor a, which is the ratio of the physical distance to the comoving distance between, say, two galaxies in the universe. The second observational evidence that supports the hot big bang model is the discovery of the CMB and the extent of its isotropy. In general theory of relativity, from the conservation of energy, it can be shown that the energy density of non-relativistic (or pressureless) matter and radiation decay as the inverse of the third and fourth powers of the scale factor, respectively [36]. The presence of the CMB indicates that the expansion of the universe started from a hot and dense state dominated by radiation. As the universe cooled down due to the expansion, the initial epoch of radiation domination transits to the epoch of matter domination.

During the initial period of radiation domination, the universe consisted of an opaque plasma of relativistic particles. Soon after the time of transition from the epoch of radiation domination to that of matter domination, the photons decoupled from the baryonic plasma and started propagating freely through space. In other words, following decoupling, the universe became transparent and it is the freely streaming photons that constitute the CMB which we observe today. Therefore, the CMB photons are remnants from the early universe and they carry information about the universe prior to decoupling. While the CMB is observed to be highly isotropic, it also carries small anisotropies of about 1 part in 10^5. Over the last few decades, successive generations of space-based observational missions such as the Cosmic Background Explorer (COBE) [37–44], Wilkinson Microwave Anisotropy Probe (WMAP) [45–47] and Planck [48–52] have played a crucial role in measuring the anisotropies in the CMB with ever-increasing precision. The data collected from these satellites have immensely helped in constraining the parameters that describe the hot big bang model.

Despite the tremendous success of the hot big bang model, it cannot provide an appropriate explanation for certain puzzles such as the overall isotropy of the CMB, viz. the fact that the photons arriving at us from even opposite directions of the sky exhibit nearly identical temperatures. It also cannot explain the origin of anisotropies in the CMB. This has led to the exploration of scenarios beyond the hot big bang model that can account for the evolution of the universe while remaining consistent with the observational data. The most promising resolution to the shortcomings of the hot big bang model is the introduction of a brief period of inflation preceding the epoch of radiation domination, a period during which the universe undergoes accelerated expansion (for detailed discussions in this context, see the reviews [53–64]). The primordial perturbations are believed to have been generated from the quantum fluctuations inevitably present during the early stages of inflation, which are amplified into classical perturbations due to the rapid expansion of the universe. The anisotropies observed in the CMB are the imprints of the primordial perturbations. Post-decoupling, during the epoch of matter domination, the perturbations grow and form the LSS, such as galaxies and clusters of galaxies that we observe in the universe today.

1.3 THE HOMOGENEOUS UNIVERSE

As we had mentioned, we shall assume that the homogeneous and isotropic background universe is described by the *spatially flat* FLRW line-element. The line-element characterized by the scale factor a is given by

$$\mathrm{d}s^2 = -\mathrm{d}t^2 + a^2(t)\,\mathrm{d}\boldsymbol{x}^2, \tag{1.1}$$

where t and $\boldsymbol{x}$ represent the cosmic time coordinate and the comoving spatial coordinates. The quantity $\eta = \int \mathrm{d}t/a(t)$ represents the so-called conformal time coordinate, in terms of which the above FLRW line-element can be expressed as

$$\mathrm{d}s^2 = a^2(\eta)\,\left(-\mathrm{d}\eta^2 + \mathrm{d}\boldsymbol{x}^2\right). \tag{1.2}$$

In other words, in terms of the time coordinate η, the FLRW line-element is conformally related to the line-element of Minkowski spacetime. Due to the symmetries of the FLRW line-element, the stress-energy tensor describing the matter fields can be expressed as

$$T^{\mu}_{\nu} = \begin{pmatrix} -\rho & 0 \\ 0 & p\,\delta^i_j \end{pmatrix}, \tag{1.3}$$

where ρ and p are time-dependent and homogeneous energy density and pressure associated with the matter fields that drive the expansion of the universe.

The Einstein field equations corresponding to the above metric and the stress-energy tensor are given by

$$H^2 = \frac{8\,\pi\,G}{3}\rho = \frac{\rho}{3\,M_{\rm Pl}^2}, \tag{1.4a}$$

$$\frac{\ddot{a}}{a} = -\frac{4\pi G}{3}(\rho + 3\,p) = -\frac{1}{6M_{\rm Pl}^2}(\rho + 3\,p), \tag{1.4b}$$

where $H = \dot{a}/a$ represents the Hubble parameter and the overdot denotes differentiation with respect to the cosmic time. These equations are often referred to as the Friedmann and the Raychaudhuri equations. The above two equations can be combined to arrive at the following continuity equation which reflects the conservation of the above stress-energy tensor:

$$\dot{\rho} + 3\,H\,(\rho + p) = 0. \tag{1.5}$$

If we are given that the energy density ρ and pressure p are governed by a constant equation of state patameter w so that $p = w\,\rho$, the above continuity equation can be immediately integrated to obtain that

$$\rho(a) \propto a^{-3\,(1+w)}. \tag{1.6}$$

During radiation and matter domination (i.e. when $w = 1/3$ and $w = 0$), for such a behaviour of ρ, the Friedmann equation (1.4a) can be integrated to obtain that $a(t) \propto t^{1/2}$ and $a(t) \propto t^{2/3}$, respectively.

1.4 THE HORIZON PROBLEM

As we mentioned earlier, the hot big bang model has certain shortcomings, the most important of which is the horizon problem. Consider the situation in the model wherein the universe is initially dominated by radiation and later by matter. In such a case, it can be shown that, the angle subtended by a region in the CMB sky that was causally connected at the time of decoupling will be approximately 1°. But, we find that photons arriving at us from even two widely separated points in the sky (i.e. points which were causally disconnected at the time of decoupling) share the same physical properties, such as the temperature. This issue is known as the horizon problem and it cannot be explained solely on the basis of the hot big bang model.

There is another way of stating the horizon problem. From the behaviour (1.6) of the energy density ρ, it is easy to show that the comoving Hubble radius $(a\,H)^{-1}$ behaves as

$$(a\,H)^{-1} \propto a^{(1+3\,w)/2}. \tag{1.7}$$

Therefore, if the universe was initially dominated by the energy density of radiation ($w = 1/3$) and later that of matter ($w = 0$), in both the epochs, the comoving Hubble radius grows monotonically with the expansion of the universe. Since the comoving wave lengths k^{-1} are constant in time, it is then clear that all the modes of cosmological interest will be *outside* the Hubble radius at sufficiently early times. In other words, the modes will not be within a causally connected domain during the early stages of evolution of the universe.

1.5 RESOLUTION OF THE HORIZON PROBLEM VIA INFLATION

To resolve the horizon problem, there should arise an epoch *prior* to the period of radiation domination wherein the comoving Hubble radius $(a\,H)^{-1}$ *decreases* with time. In such a situation, provided the duration of this epoch is adequately long, all the comoving wave numbers of cosmological interest will be well inside the Hubble radius during the early stages of the epoch. A decreasing comoving Hubble radius implies that

$$\frac{\mathrm{d}}{\mathrm{d}t}(aH)^{-1} < 0, \tag{1.8}$$

which, in turn, leads to

$$\ddot{a} > 0. \tag{1.9}$$

This condition suggests that the universe needs to go through an epoch of accelerated expansion at a very early stage of its evolution in order to overcome the horizon problem. Such an epoch is called as inflation. Often, for convenience, the scale factor during inflation is assumed to be of the de Sitter form, i.e. it is expected to behave as $a(t) \propto e^{H_{\rm I} t}$, where $H_{\rm I}$ is a constant Hubble parameter. In such a situation, the comoving Hubble radius behaves as

$$(a\,H)^{-1} \propto a^{-1}. \tag{1.10}$$

Such a behaviour ensures that the wave numbers of observational interest begin from sufficiently inside the Hubble radius implying they are within a causally connected domain during the early stages of inflation. They leave the Hubble radius during

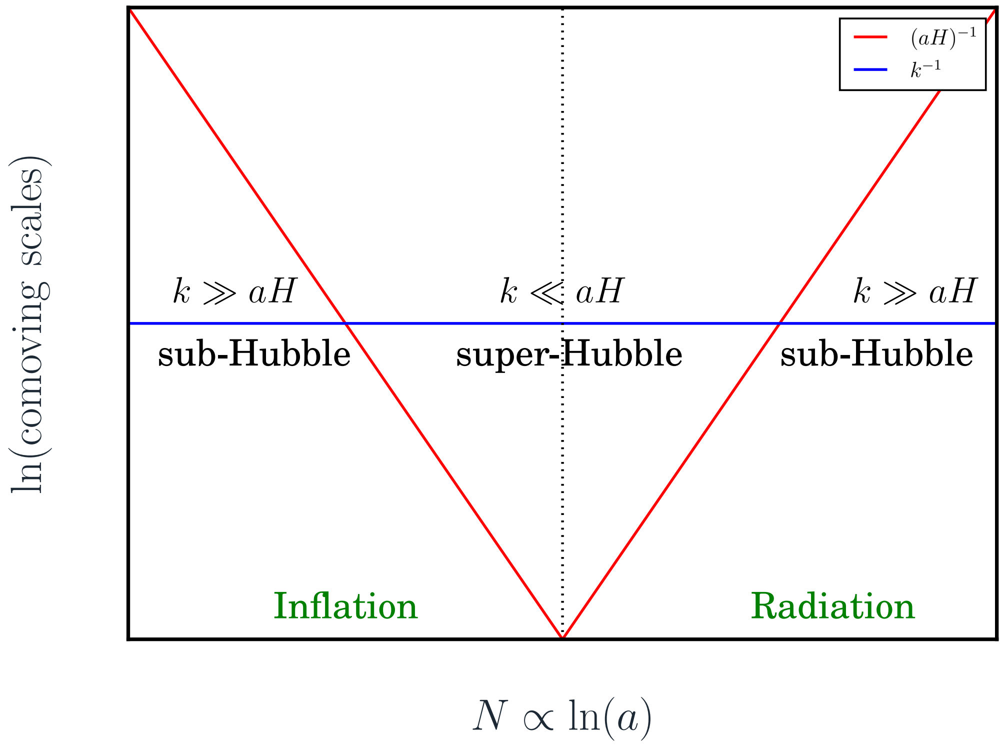

Figure 1.1: This figure depicts the evolution of the comoving Hubble radius $(a\,H)^{-1}$ (in red) and the comoving wave length k^{-1} (in blue) during the epochs of inflation and radiation domination. The evolution of these quantities have been plotted as a function of e-folds N. Note that, while the comoving wave length is not affected by the expansion, the comoving Hubble radius behaves as a^{-1} during inflation and as a during radiation domination. The shrinking comoving Hubble radius during inflation ensures that the wave lengths of observational interest begin from inside the Hubble radius at early times. The wave lengths leave the Hubble radius during the later stages of inflation and they reenter later during the epochs of radiation or matter domination.

inflation and reenter at later epochs. In Fig. 1.1, we have illustrated the behaviour of the comoving Hubble radius during inflation followed by the epoch of radiation domination. Since the comoving Hubble radius falls as the inverse power of the scale factor during inflation, while it is proportional to the scale factor during radiation domination, in the log-log plot, they have slopes of $+1$ and -1, respectively. It proves to be convenient to express the duration of inflation in terms of the number of e-folds, which is defined through the relation $a \propto \mathrm{e}^N$. The number of e-folds required to overcome the horizon problem is estimated to be approximately 60–70 [53–64]. In summary, the horizon problem can be effectively resolved by invoking a period of inflation during the early stages of the universe.

1.5.1 Driving inflation with a scalar field

As we can see from Eq. (1.4b), it is not possible to achieve inflation (i.e. $\ddot{a} > 0$) if we consider the energy density of the universe to be dominated by that of radiation or matter (i.e. when $\rho > 0$ and $w \geq 0$). Clearly, we require $(\rho + 3\,p) = (1 + 3\,w)\,\rho < 0$ in order to realize a period of accelerated expansion. One of the simplest ways to drive inflation is to consider a canonical scalar field (generally referred to as the inflaton, say, ϕ) that is slowly rolling down a potential, as illustrated in Fig. 1.2. The action describing the canonical scalar field that is governed by the potential $V(\phi)$ is given by

$$S[\phi] = -\int \mathrm{d}^4x\,\sqrt{-g}\,\left[-\frac{1}{2}\,\partial_\mu\phi\,\partial^\mu\phi + V(\phi)\right]. \tag{1.11}$$

In the spatially flat FLRW universe described by the line-element (1.1), the homogeneous scalar field satisfies the following equation of motion:

$$\ddot{\phi} + 3\,H\,\dot{\phi} + V_\phi = 0, \tag{1.12}$$

where $V_\phi = \mathrm{d}V/\mathrm{d}\phi$. The stress-energy tensor associated with the homogeneous scalar field resembles that of a perfect fluid whose energy density ρ_ϕ and pressure p_ϕ are given by

$$\rho_\phi = \frac{\dot{\phi}^2}{2} + V(\phi), \tag{1.13a}$$

$$p_\phi = \frac{\dot{\phi}^2}{2} - V(\phi). \tag{1.13b}$$

In order for the model to be stable, the potential is always assumed to be positive, which implies that $\rho_\phi > 0$. To achieve inflation, we require that $(\rho_\phi + 3\,p_\phi) < 0$ or, equivalently, $\dot{\phi}^2 < V$, implying that, to lead to an epoch of accelerated expansion, the the potential energy has to dominate the kinetic energy. Typically, the inflaton ϕ starts away from the minimum of the potential $V(\phi)$ and it rolls down slowly towards the minimum. Inflation usually ends as the field nears the bottom of the potential.

1.5.2 The slow roll parameters

While it is adequate if $\dot{\phi}^2 < V$ to achieve inflation, we also require a sufficient duration of inflation to overcome the horizon problem. The friction term in Eq. (1.12), viz. $3\,H\,\dot{\phi}$,

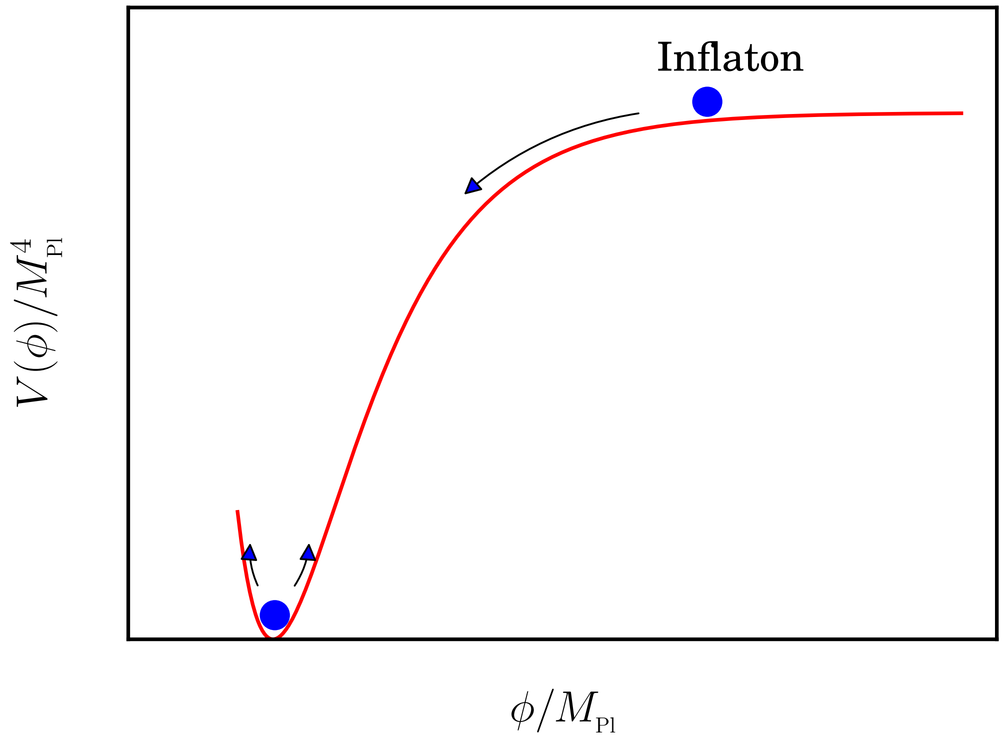

Figure 1.2: We have illustrated the shape of a typical inflationary potential $V(\phi)$ as a function of the field ϕ. The scalar field (in blue) slowly rolls down the potential (in red) during the early stages of inflation. One finds that inflation is terminated as the field approaches the bottom of the potential. Thereafter, the field starts oscillating at the bottom of the potential leading to the epoch referred to as (p)reheating.

ensures that the field rolls slowly down the potential. Therefore, if we start at a high enough value of the potential, it is guaranteed that we will have the required duration of inflation to overcome the horizon problem before the field reaches the bottom of the potential leading to the end of inflation. The conditions that guarantee a sufficient duration of inflation are given by

$$\dot{\phi}^2 \ll V(\phi), \tag{1.14a}$$

$$\ddot{\phi} \ll 3\,H\,\dot{\phi}. \tag{1.14b}$$

These conditions are often expressed in terms of dimensionless parameters called the slow roll parameters [53–64]. The first of these parameters is conventionally defined as

$$\epsilon_1 = -\frac{\dot{H}}{H^2} = -\frac{H_N}{H}, \tag{1.15}$$

where $H_N = {\rm d}H/{\rm d}N$, and we have made use of the relation ${\rm d}N/{\rm d}t = H$ in arriving at the final expression. It is useful to note that we can also write the parameter ϵ_1 in terms of the kinetic energy of the scalar field as follows

$$\epsilon_1 = \frac{\phi_N^2}{2M_{\rm Pl}^2}, \tag{1.16}$$

where $\phi_N = {\rm d}\phi/{\rm d}N$, which suggests that ϵ_1 is a positive definite quantity. The subsequent higher order slow roll parameters are defined as

$$\epsilon_{n+1} = \frac{{\rm d}\ln\epsilon_n}{{\rm d}N}, \tag{1.17}$$

where $n \geq 1$. In the slow roll limit, the Friedmann equation (1.4a) and the equation of motion (1.12) of the scalar field reduce to the following forms:

$$H^2 \simeq \frac{V}{3\,M_{\rm Pl}^2}, \tag{1.18a}$$

$$3\,H\,\dot{\phi} + V_\phi \simeq 0. \tag{1.18b}$$

Upon combining these equations, we can write the first two slow roll parameters in terms of the potential and its derivatives with respect to the field as follows:

$$\epsilon_1 \simeq \frac{M_{\rm Pl}^2}{2}\left(\frac{V_\phi}{V}\right)^2, \tag{1.19}$$

$$\epsilon_2 \simeq 2\,M_{\rm Pl}^2\left[\left(\frac{V_\phi}{V}\right)^2 - \frac{V_{\phi\phi}}{V}\right], \tag{1.20}$$

where $V_{\phi\phi} = {\rm d}V_\phi/{\rm d}\phi$. It is easy to show that the condition for inflation (i.e. $\ddot{a} > 0$) implies that $\epsilon_1 < 1$. In a typical slow roll inflationary scenario, the velocity of the field is assumed to be very small initially. Hence, the first slow roll parameter ϵ_1 starts with a small value and it increases slowly as the field rolls down the potential. As the field approaches the bottom of the potential, the parameter ϵ_1 crosses unity indicating the termination of inflation.

1.6 PERTURBATION THEORY AND POWER SPECTRA IN SLOW ROLL INFLATION

The precise measurements of the anisotropies in the CMB by the various satellite missions indicate that, although the universe was remarkably homogeneous and isotropic at the time of decoupling, there existed small inhomogeneities over all scales. As we mentioned, it is the quantum fluctuations associated with the scalar field that drives inflation which are supposed to be responsible for the generation of the perturbations during inflation. Due to the accelerated expansion of the universe, the tiny quantum fluctuations are amplified into small inhomogeneities or perturbations. These perturbations, in turn, act as the sources for the formation of structures during the epoch of matter domination. The fluctuations in the scalar field are coupled to the metric perturbations through the Einstein's equations. Based on their transformation properties on a spacelike hypersurface in a FLRW universe, the metric and matter perturbations can be classified into three categories as the scalar, vector, and tensor perturbations [53–64]. At the linear order, it can be shown that these perturbations evolve independently.

In this section, we shall first arrive at the equations governing the perturbations using the Arnowitt-Deser-Misner (ADM) formalism and thereafter go on to discuss the generation of perturbations. In the ADM formalism, a generic spacetime is described by the line-element [65–69]

$$\mathrm{d}s^2 = -\mathcal{N}^2\, \left(\mathrm{d}x^0\right)^2 + h_{ij}\, (\mathcal{N}^i\, \mathrm{d}x^0 + \mathrm{d}x^i)\, (\mathcal{N}^j\, \mathrm{d}x^0 + \mathrm{d}x^j), \tag{1.21}$$

where x^0 and x^i indicate the time and the spatial coordinates, $\mathcal{N}$ represents the lapse function, $\mathcal{N}^i$ denotes the shift vector, and h_{ij} represents the spatial metric such that $h_{ij}\, h^{jk} = \delta^i_j$. In other words, the metric tensor is given by

$$g_{\mu\nu} = \begin{pmatrix} -\mathcal{N}^2 + \mathcal{N}^i \mathcal{N}_i & \mathcal{N}_i \\ \mathcal{N}_i & h_{ij} \end{pmatrix}, \tag{1.22}$$

where $\mathcal{N}_i = h_{ij}\, \mathcal{N}^j$. In terms of the above line-element, the complete action describing the system of a canonical scalar field that is coupled to gravitation can be written as

$$\begin{aligned} S[\mathcal{N}, \mathcal{N}^i, \gamma_{ij}, \phi] &= \frac{1}{2} \int \mathrm{d}^4x\, \mathcal{N}\, \sqrt{\gamma}\, \biggl\{ M_{_{\mathrm{Pl}}}^2\, \left[R^{(3)} + \frac{1}{\mathcal{N}^2}\, \left(E_{ij}\, E^{ij} - E^2\right) \right] \\ &\quad + \frac{1}{\mathcal{N}^2}\, \left(\partial_0\phi - \mathcal{N}^i\, \partial_i\phi\right)^2 - \gamma^{ij}\, \partial_i\phi\, \partial_j\phi - 2\, V(\phi) \biggr\}, \end{aligned} \tag{1.23}$$

where $\gamma = \mathrm{det.}\ (\gamma_{ij})$, $R^{(3)}$ represents the spatial curvature, the quantity E_{ij} is given by

$$E_{ij} = \frac{1}{2}\, \left[\partial_0\gamma_{ij} - (\nabla_i \mathcal{N}_j + \nabla_j \mathcal{N}_i)\right] \tag{1.24}$$

with ∇_i denoting the covariant derivatives, and $E = h_{ij} E^{ij}$.

Since inflation is assumed to be driven by a scalar field, there are no vector sources during the epoch. The vector perturbations decay in the absence of a vector source. Therefore, we shall restrict our discussion to the scalar and tensor perturbations.

To describe the scalar perturbations, for convenience, we shall work in the so-called comoving gauge wherein the perturbations in the scalar field are zero. In such a case, the action (1.23) simplifies to the form

$$\begin{aligned} S[\mathcal{N},\mathcal{N}^i,\gamma_{ij},\phi] &= \frac{1}{2}\int \mathrm{d}^4x\,\mathcal{N}\,\sqrt{\gamma}\,\biggl\{M_{_{\mathrm{Pl}}}^2\left[R^{(3)}+\frac{1}{\mathcal{N}^2}\,\left(E_{ij}\,E^{ij}-E^2\right)\right] \\ &\quad +\frac{1}{\mathcal{N}^2}\,\left(\partial_0\phi\right)^2-2\,V(\phi)\biggr\}. \end{aligned} \tag{1.25}$$

As is well known, the lapse function $\mathcal{N}$ and the shift vector $\mathcal{N}^i$ act as Lagrange multipliers for the system. Upon varying the above action with respect to $\mathcal{N}$ and $\mathcal{N}^i$, we obtain the so-called energy and momentum constraints to be

$$R^{(3)}-2\,V(\phi)-\frac{1}{\mathcal{N}^2}\,\left(E_{ij}E^{ij}-E^2\right)-\frac{1}{\mathcal{N}^2}\,\left(\partial_0\phi\right)^2 = 0, \tag{1.26a}$$

$$\nabla_i\left[\frac{1}{\mathcal{N}}\,\left(E^i_j-\delta^i_j\,E\right)\right] = 0. \tag{1.26b}$$

In the FLRW universe, we shall assume that the scalar perturbations are described by the curvature perturbation $\mathcal{R}$ and the tensor perturbations are characterized by the spatial metric tensor h_{ij}. Under these assumptions, the spatial metric γ_{ij} can be written as

$$\gamma_{ij}=a^2(t)\,\mathrm{e}^{2\,\mathcal{R}}\,\mathrm{e}^{h_{ij}}. \tag{1.27}$$

If we now solve the constraint equations (1.26) up to the first order in the perturbations, we obtain the lapse function $\mathcal{N}$ and the shift vector $\mathcal{N}^i$ to be

$$\mathcal{N} = 1+\frac{\dot{\mathcal{R}}}{H}, \tag{1.28a}$$

$$\mathcal{N}_i = a\left[-\frac{1}{a\,H}\,\partial_i\mathcal{R}+\epsilon_1\,\partial_i(\nabla^{-2}\dot{\mathcal{R}})\right]. \tag{1.28b}$$

On substituting these expressions for the Lagrange multipliers in the action (1.25), we find that, at the quadratic order, the actions governing the scalar and tensor perturbations $\mathcal{R}$ and h_{ij} are given by [53–61, 65–73]

$$S_2[\mathcal{R}] = \frac{1}{2}\int \mathrm{d}\eta\int \mathrm{d}^3\boldsymbol{x}\,z^2\left[\mathcal{R}'^2-(\partial\mathcal{R})^2\right], \tag{1.29a}$$

$$S_2[h_{ij}] = \frac{M_{_{\mathrm{Pl}}}^2}{8}\int \mathrm{d}\eta\int \mathrm{d}^3\boldsymbol{x}\,a^2\,\left[h_{ij}'^2-(\partial h_{ij})^2\right], \tag{1.29b}$$

where $z=a\,M_{_{\mathrm{Pl}}}\,\sqrt{2\epsilon_1}$.

The primordial perturbations are expected to have originated from quantum fluctuations in the early universe. On quantization, the classical perturbations $\mathcal{R}$ and h_{ij} are elevated to be quantum operators. We can express these operators in terms of the Fourier mode functions, say, f_k and h_k, of the scalar and tensor perturbations as

$$\begin{aligned}\hat{\mathcal{R}}(\eta, \boldsymbol{x}) &= \int \frac{\mathrm{d}^3\boldsymbol{k}}{(2\,\pi)^{3/2}}\, \hat{\mathcal{R}}_{\boldsymbol{k}}(\eta)\, \mathrm{e}^{i\,\boldsymbol{k}\cdot\boldsymbol{x}} \\ &= \int \frac{\mathrm{d}^3\boldsymbol{k}}{(2\,\pi)^{3/2}} \left[\hat{a}_{\boldsymbol{k}}\, f_k(\eta)\, \mathrm{e}^{i\,\boldsymbol{k}\cdot\boldsymbol{x}} + \hat{a}^{\dagger}_{\boldsymbol{k}}\, f_k^{*}(\eta)\, \mathrm{e}^{-i\,\boldsymbol{k}\cdot\boldsymbol{x}}\right], \qquad (1.30\text{a}) \\ \hat{h}_{ij}(\eta, \boldsymbol{x}) &= \int \frac{\mathrm{d}^3\boldsymbol{k}}{(2\,\pi)^{3/2}}\, \hat{h}^{\boldsymbol{k}}_{ij}(\eta)\, \mathrm{e}^{i\,\boldsymbol{k}\cdot\boldsymbol{x}} \\ &= \int \frac{\mathrm{d}^3\boldsymbol{k}}{(2\,\pi)^{3/2}} \sum_{\lambda=(+,\times)} \left[\hat{b}^{\lambda}_{\boldsymbol{k}}\, \epsilon^{\lambda}_{ij}(\boldsymbol{k})\, h_k(\eta)\, \mathrm{e}^{i\,\boldsymbol{k}\cdot\boldsymbol{x}} + \hat{b}^{\lambda\dagger}_{\boldsymbol{k}}\, \epsilon^{\lambda *}_{ij}(\boldsymbol{k})\, h_k^{*}(\eta)\, \mathrm{e}^{-i\,\boldsymbol{k}\cdot\boldsymbol{x}}\right], \\ &\qquad (1.30\text{b})\end{aligned}$$

where the annihilation ($\hat{a}_{\boldsymbol{k}}, \hat{b}^{\lambda}_{\boldsymbol{k}}$) and creation ($\hat{a}^{\dagger}_{\boldsymbol{k}}, \hat{b}^{\lambda\dagger}_{\boldsymbol{k}}$) operators satisfy the following commutation relations:

$$\begin{aligned}\left[\hat{a}_{\boldsymbol{k}}, \hat{a}_{\boldsymbol{k}'}\right] &= \left[\hat{a}^{\dagger}_{\boldsymbol{k}}, \hat{a}^{\dagger}_{\boldsymbol{k}'}\right] = 0, \quad \left[\hat{a}_{\boldsymbol{k}}, \hat{a}^{\dagger}_{\boldsymbol{k}'}\right] = \delta^{(3)}(\boldsymbol{k} - \boldsymbol{k}'), \qquad (1.31\text{a}) \\ \left[\hat{b}^{\lambda}_{\boldsymbol{k}}, \hat{b}^{\lambda'}_{\boldsymbol{k}'}\right] &= \left[\hat{b}^{\lambda\dagger}_{\boldsymbol{k}}, \hat{b}^{\lambda'\dagger}_{\boldsymbol{k}'}\right] = 0, \quad \left[\hat{b}^{\lambda}_{\boldsymbol{k}}, \hat{b}^{\lambda'\dagger}_{\boldsymbol{k}'}\right] = \delta_{\lambda\lambda'}\, \delta^{(3)}(\boldsymbol{k} - \boldsymbol{k}'). \qquad (1.31\text{b})\end{aligned}$$

Also, the quantities $\epsilon^{\lambda}_{ij}(\boldsymbol{k})$ denote the polarization tensors associated with the gravitational waves, with $\lambda = (+, \times)$ denoting the two states of polarization. Note that the polarization tensors $\epsilon^{\lambda}_{ij}(\boldsymbol{k})$ satisfy the conditions $\delta^{im}\,\delta^{jn}\,\epsilon^{\lambda}_{ij}(\boldsymbol{k})\,\epsilon^{\lambda'}_{mn}(\boldsymbol{k}) = 2\,\delta_{\lambda\lambda'}$ and $k^i\,\epsilon_{ij}(\boldsymbol{k}) = 0$.

By varying the actions (1.29), we can arrive at the equations of motion governing the Fourier modes of the scalar and tensor perturbations to be

$$\begin{aligned}f_k'' + 2\,\frac{z'}{z}\,f_k' + k^2\,f_k &= 0, \qquad (1.32\text{a}) \\ h_k'' + 2\,\frac{a'}{a}\,h_k' + k^2\,h_k &= 0. \qquad (1.32\text{b})\end{aligned}$$

We can rewrite these equations in terms of another set of convenient quantities called the Mukhanov-Sasaki variables, which are defined as $v_k = z\,f_k$ and $u_k = a\,M_{_{\mathrm{Pl}}}\,h_k/\sqrt{2}$. In terms of these variables, the equations (1.32) reduce to the following forms:

$$v_k'' + \left(k^2 - \frac{z''}{z}\right) v_k = 0, \qquad (1.33\text{a})$$

$$u_k'' + \left(k^2 - \frac{a''}{a}\right) u_k \;=\; 0. \tag{1.33b}$$

The initial conditions on the variables v_k and u_k are imposed in the domain wherein $k \gg \sqrt{z''/z}$ for the scalar perturbations and $k \gg \sqrt{a''/a}$ for the tensor perturbations. These conditions are often referred to as the sub-Hubble limit, since in slow roll inflationary scenario, under these conditions, the wave numbers are sufficiently inside the Hubble radius. In this limit, the modes do not feel the curvature of spacetime and, as a result, they behave exactly as they would in Minkowski spacetime, i.e. they have the form

$$v_k(\eta) = u_k(\eta) = \frac{1}{\sqrt{2k}}\, \mathrm{e}^{-i\,k\,\eta}, \tag{1.34}$$

which is considered to be the initial condition for evolving the perturbations. The vacuum state associated with such initial conditions for the Mukhanov-Sasaki variables is known as the Bunch-Davies vacuum.

At late times such that $k \ll \sqrt{z''/z}$ and $k \ll \sqrt{a''/a}$, the wave numbers are well outside the Hubble radius. From the equations (1.33) governing the scalar and tensor Mukhanov-Sasaki variables v_k and u_k, it should be clear that, in the super-Hubble limit, the solutions can be expressed as

$$v_k(\eta) \;\simeq\; A_1\, z + B_1\, z \int \frac{\mathrm{d}\eta}{z^2}, \tag{1.35a}$$

$$u_k(\eta) \;\simeq\; A_2\, a + B_2\, a \int \frac{\mathrm{d}\eta}{a^2}, \tag{1.35b}$$

where A_1, B_1, A_2 and B_2 are constants. The first and the second terms in these solutions describe the growing and decaying modes. In slow roll inflation, at late times, the second terms are subdominant since they decay. Clearly, in such a case, $v_k \propto z$ and $u_k \propto a$, which implies f_k and h_k are constant in the super-Hubble limit. As we shall discuss below, in slow roll inflation, the exact solutions to the Mukhanov-Sasaki variables indeed exhibit such a behaviour in the super-Hubble limit.

Many models of inflation permit slow roll wherein the slow roll parameters $(\epsilon_1, \epsilon_2, \ldots)$ remain small until close to the end of inflation. Let us now discuss the solutions for the scalar and tensor mode functions in such slow roll inflationary scenarios. At the leading order in the slow roll approximation, one can show that the conformal Hubble parameter $\mathcal{H} = a\, H = a'/a$ can be expressed as

$$\mathcal{H} = \frac{a'}{a} \simeq \frac{1}{(1-\epsilon_1)\,\eta}. \tag{1.36}$$

Upon using this expression and the definition of z mentioned earlier, we can express the quantities z''/z and a''/a in terms of the first two slow roll parameters as follows (see, for instance, Refs. [62, 63, 74, 75]):

$$\frac{z''}{z} \simeq \left(2 + 3\,\epsilon_1 + \frac{3\,\epsilon_2}{2}\right)\frac{1}{\eta^2}, \tag{1.37a}$$

$$\frac{a''}{a} \simeq (2 + 3\,\epsilon_1)\,\frac{1}{\eta^2}. \tag{1.37b}$$

For such forms of z''/z and a''/a, the solutions to the Mukhanov-Sasaki equations (1.33) which satisfy the Bunch-Davies initial conditions (1.34) can be obtained to be

$$v_k(\eta) = \sqrt{-\frac{\pi\,\eta}{4}}\,\mathrm{e}^{\frac{i\pi}{2}\,[\nu_{\mathrm{S}}+1/2]}\,H^{(1)}_{\nu_{\mathrm{S}}}(-k\,\eta), \tag{1.38a}$$

$$u_k(\eta) = \sqrt{-\frac{\pi\,\eta}{4}}\,\mathrm{e}^{\frac{i\pi}{2}\,[\nu_{\mathrm{T}}+1/2]}\,H^{(1)}_{\nu_{\mathrm{T}}}(-k\,\eta), \tag{1.38b}$$

where $H^{(1)}_{\nu}(z)$ are the Hankel functions of the first kind, while the indices ν_{S} and ν_{T} are given by

$$\nu_{\mathrm{S}} \simeq \frac{3}{2} + \epsilon_1 + \frac{\epsilon_2}{2}, \tag{1.39a}$$

$$\nu_{\mathrm{T}} \simeq \frac{3}{2} + \epsilon_1. \tag{1.39b}$$

The statistical properties of the Gaussian primordial perturbations are characterized by their two-point correlations. In Fourier space, these quantities are described by the corresponding power spectra. The scalar and tensor power spectra—denoted as $\mathcal{P}_{\mathrm{S}}(k)$ and $\mathcal{P}_{\mathrm{T}}(k)$—are defined in terms of the operators $\hat{\mathcal{R}}_{\boldsymbol{k}}$ and $\hat{h}^{\boldsymbol{k}}_{ij}$ [cf. Eqs. (1.30)] as follows:

$$\langle 0|\hat{\mathcal{R}}_{\boldsymbol{k}}(\eta)\,\hat{\mathcal{R}}_{\boldsymbol{k}'}(\eta)|0\rangle = \frac{2\,\pi^2}{k^3}\,\mathcal{P}_{\mathrm{S}}(k)\,\delta^{(3)}(\boldsymbol{k}-\boldsymbol{k}'), \tag{1.40a}$$

$$\langle 0|\hat{h}^{\boldsymbol{k}}_{ij}(\eta)\,\hat{h}^{ij}_{\boldsymbol{k}'}(\eta)|0\rangle = \frac{2\,\pi^2}{k^3}\,\mathcal{P}_{\mathrm{T}}(k)\,\delta^{(3)}(\boldsymbol{k}-\boldsymbol{k}'), \tag{1.40b}$$

where $|0\rangle$ denotes the Bunch-Davies vacuum. On using the decomposition (1.30), the scalar and tensor power spectra can be written in terms of the mode functions (f_k, h_k) or the Mukhanov-Sasaki variables (v_k, u_k) as

$$\mathcal{P}_{\mathrm{S}}(k) = \frac{k^3}{2\,\pi^2}\,|f_k|^2 = \frac{k^3}{2\,\pi^2}\left|\frac{v_k}{z}\right|^2, \tag{1.41a}$$

$$\mathcal{P}_{_{\rm T}}(k) \;=\; 4\,\frac{k^3}{2\,\pi^2}\,\left|h_k\right|^2 = \frac{8}{M_{_{\rm Pl}}^2}\frac{k^3}{2\pi^2}\left|\frac{u_k}{a}\right|^2, \tag{1.41b}$$

with the right hand sides to be evaluated at late times during inflation. In slow roll inflation, on super-Hubble scales, the mode functions f_k and h_k associated with the solutions (1.38) to the scalar and tensor Mukhanov-Sasaki variables approach a constant value, as we have pointed out earlier. On using these asymptotic forms, the power spectra $\mathcal{P}_{_{\rm S}}(k)$ and $\mathcal{P}_{_{\rm T}}(k)$ evaluated at late times (i.e. as $\eta \to 0$) can be expressed as

$$\begin{aligned}\mathcal{P}_{_{\rm S}}(k) \;=\;& \frac{H_{_{\rm I}}^2}{8\,\pi^2\,M_{_{\rm Pl}}^2\,\epsilon_1}\biggl[1-2\,\epsilon_1-(2\,\epsilon_1+\epsilon_2)\ln\left(\frac{k}{k_*}\right)\\ &-\,(2\,\epsilon_1+\epsilon_2)\,\left(\gamma_{_{\rm E}}+\ln 2-2\right)\biggr],\end{aligned} \tag{1.42}$$

$$\mathcal{P}_{_{\rm T}}(k) \;=\; \frac{2\,H_{_{\rm I}}^2}{\pi^2\,M_{_{\rm Pl}}^2}\left[1-2\,\epsilon_1\ln\left(\frac{k}{k_*}\right)-2\,\epsilon_1\left(\gamma_{_{\rm E}}+\ln 2-1\right)\right], \tag{1.43}$$

where $H_{_{\rm I}}$ denotes the nearly constant Hubble parameter in slow roll inflation, k_* represents the so-called pivot scale at which the amplitude of the scalar power spectrum is often quoted, and $\gamma_{_{\rm E}}$ is the Euler-Mascheroni constant.

As we shall discuss below, apart from the scalar and tensor amplitudes, the quantities of observational interest are the scalar and tensor spectral indices $n_{_{\rm S}}$ and $n_{_{\rm T}}$. These are defined in terms of the scalar and tensor power spectra $\mathcal{P}_{_{\rm S}}(k)$ and $\mathcal{P}_{_{\rm T}}(k)$ in the following manner:

$$n_{_{\rm S}} \;=\; 1+\frac{{\rm d}\ln\mathcal{P}_{_{\rm S}}}{{\rm d}\ln k}, \tag{1.44}$$

$$n_{_{\rm T}} \;=\; \frac{{\rm d}\ln\mathcal{P}_{_{\rm T}}}{{\rm d}\ln k}. \tag{1.45}$$

It should be evident from the form of the power spectra (1.42)that, in the slow roll approximation, the scalar and tensor indices are given by $n_{_{\rm S}} = 1-2\,\epsilon_1-\epsilon_2$ and $n_{_{\rm T}} = -2\,\epsilon_1$. In other words, in a slow roll inflationary scenario, since the parameters ϵ_1 and ϵ_2 are small, the scalar and tensor power spectra are expected to be nearly scale invariant. Another quantity of observational interest is the tensor-to-scalar ratio r, which is defined as

$$r = \frac{\mathcal{P}_{_{\rm T}}(k)}{\mathcal{P}_{_{\rm S}}(k)}. \tag{1.46}$$

In slow roll approximation, if we ignore the weak scale dependence of the power spectra (1.42), the tensor-to-scalar ratio r can be obtained to be

$$r \simeq 16\,\epsilon_1 = -8\,n_{_{\rm T}}. \tag{1.47}$$

To compare with the observational data, the primordial scalar and tensor power spectra are often written in a simple power law form as follows:

$$\mathcal{P}_{\rm S}(k) = A_{\rm S}\left(\frac{k}{k_*}\right)^{n_{\rm S}-1}, \tag{1.48a}$$

$$\mathcal{P}_{\rm T}(k) = A_{\rm T}\left(\frac{k}{k_*}\right)^{n_{\rm T}}, \tag{1.48b}$$

where $A_{\rm S}$ and $A_{\rm T}$ are scalar and the tensor amplitudes, respectively. The scalar amplitude $A_{\rm S}$ is well constrained by the CMB data and is often referred to as COBE normalization [76]. According to the recent Planck data, the value of $A_{\rm S}$ is given by [51, 52]

$$\ln\left(10^{10}\,A_{\rm S}\right) = 3.044 \pm 0.014, \tag{1.49}$$

while the scalar spectral index is constrained to be $n_{\rm S} = 0.9649 \pm 0.0042$ at the pivot scale of $k_* = 0.05\,{\rm Mpc}^{-1}$. The most recent constraint on the tensor-to-scalar ratio from the Planck and BICEP/Keck array data is the upper bound of $r < 0.032$ [77, 78].

1.7 PRIMORDIAL MAGNETIC FIELDS

As we discussed earlier in Sec. 1.1, magnetic fields are present everywhere in the current universe over a wide range of length scales. The strength of magnetic fields can be measured using methods such as Faraday rotation and synchrotron emission. While the former method helps with measuring the line of sight component of the magnetic fields in galaxies and clusters of galaxies, the latter method helps measure the component of magnetic fields perpendicular to the line of sight in galaxies. To measure the magnetic fields present in stars and interstellar gas clouds, investigation of the Zeeman splitting of the spectral lines, particularly the $21\,{\rm cm}$ line from the neutral hydrogen, proves to be a useful method [79, 80]. Although the techniques of Faraday rotation and synchrotron emission are adequate for measuring the amplified magnetic fields with strengths of the order of $\mu\,{\rm G}$, they are unsuitable for probing the PMFs present in the IGM voids, which are expected to be considerably weaker in their strengths. The weakness is due to the absence of any structure to support the mechanism required to amplify the small seed fields. Also, the uncertainties in the amplification mechanism pose challenges to investigate the origin of these fields. To probe the magnetic fields present in the voids, the data from the measurements of anisotropies in the CMB, radio emission from distant quasars and high energy γ rays from blazars have proven to be useful, as they allow us to set limits on the strength of the magnetic fields. If these magnetic fields can be detected and measured, they can provide additional information about their evolution during the early stages of the universe. In Sec. 1.8, we shall discuss the observational constraints on magnetic fields present in the current universe [8, 10, 50, 81]. In this section, we shall broadly outline the two popular mechanisms that are believed to be responsible for the origin of large scale magnetic fields in the early universe.

The PMFs could have been generated through cosmological processes either during the inflationary epoch or during the electroweak (EW) and quantum chromodynamic (QCD) phase transitions which occur at temperatures of $T \sim 100\,\mathrm{GeV}$ and $T \sim 150\,\mathrm{MeV}$, respectively. During the phase transitions, the magnetic fields are produced by causal mechanisms (in this context, see, for example, Refs. [82–88, 88–90]). In these scenarios, it has been found that the correlation lengths of the magnetic fields (which are proportional to the inverse of the temperature) prove to be much smaller than the Hubble radius H^{-1}. Also, the generated magnetic fields are very weak and are damped rapidly. However, when the magnetic fields possess non-zero helicity, energy can be transferred from small to large scales—a process called the inverse cascade. Such helical magnetic fields generated during the phase transitions may possess adequate strengths to explain the magnetic fields observed today [91, 92].

Let us now turn to discuss the generation of magnetic fields during the epoch of inflation (in this regard, see, for instance, Refs. [7, 93–102]). Recall that the standard electromagnetic action which leads to the Maxwell's equations is invariant under the conformal transformations. Since the FLRW metric is conformally related to the metric of Minkowski spacetime, the solutions to the electromagnetic vector potential in FLRW spacetime are similar in form to the solutions in Minkowski spacetime. Such a behaviour leads to a rapid decay of the electromagnetic fields with the expansion of the universe (the magnetic field B behaves as the inverse square of the scale factor a). In particular, the accelerated expansion of the universe during inflation quickly dilutes the strengths of the fields. As the electromagnetic fields are supposed to have originated from the quantum vacuum, another way of stating this result is that no photons are created due to the expansion of the universe [103].

Hence, to generate large scale magnetic fields during inflation that can evolve to current observable strengths, the conformal invariance needs to be broken. As we shall discuss in the next chapter, this is often achieved by coupling the electromagnetic field to either the inflation or scalar curvature through terms such as: $J^2(\phi)\, F_{\mu\nu}\, F^{\mu\nu}$, $J(R)\, F_{\mu\nu}\, F^{\mu\nu}$ or even $R_{\alpha\beta\mu\nu}\, F^{\alpha\beta}\, F^{\mu\nu}$ (for more details in this context, see, for instance, Refs. [5, 6, 9, 93–95, 104–107]). Another way of breaking the conformal invariance is to assume that the gauge field is massive, which also breaks the gauge symmetry (in this regard, see, for instance, Ref. [108]). In this thesis, we shall focus on the generation of

PMFs during inflation wherein the electromagnetic field is non-conformally coupled to the inflaton.

1.8 OBSERVATIONAL CONSTRAINTS ON MAGNETIC FIELDS

Deciphering the characteristics of PMFs can help us understand their role in several astronomical and cosmological phenomena, such as the propagation of ultra high-energy cosmic rays (UHECRs), various aspects of radio astronomy and the formation of structure. As we mentioned earlier, using methods of Faraday rotation and synchrotron emission, magnetic fields have been observed in collapsed objects such as galaxies and clusters of galaxies. However, there is no direct detection of the magnetic fields in the IGM voids, which are regions far from the collapsed objects. Also, there is no direct detection of the magnetic fields generated during the very early phases of the universe due to various challenges. There are only observational bounds on the strengths of the magnetic field today (say, B_0) at different correlation lengths (say, λ_{B}). We can arrive at the constraints on the magnetic fields from the CMB, UHECRs, Faraday rotation measurements of distant quasars and observations of high energy gamma rays emitted by the blazars. In this section, we shall discuss the theoretical and observational constraints on the magnetic fields.

The observational upper bound of $B_0 < 10^{-9}\,\mathrm{G}$ with correlation lengths of cosmological scales, are primarily obtained from the Faraday rotation measure (FRM) of radio emissions from distant quasars [109–115] and the CMB [116–119]. The polarization plane of electromagnetic radiation changes its orientation when it propagates through an ionized medium containing magnetic fields. Based on this effect, the FRM observations provide an upper bound on the strength of magnetic fields in IGM voids. The total rotation angle of the polarized light is proportional to the so-called rotation measure (RM), which is given by [120]

$$RM = \frac{e^3}{2\,\pi\,m_{\mathrm{e}}^2\,c^4} \int \mathrm{d}l(z)\,\frac{n_{\mathrm{e}}(l) B_{\|}(l)}{1+z^2}, \tag{1.50}$$

where e and m_{e} are the charge and mass of the electron, n_{e} is the number density of free electrons, and $B_{\|}(l)$ is the component of the magnetic field parallel to the line of sight. The quantity z represents redshift, which is defined as

$$1 + z = \frac{a_0}{a}, \tag{1.51}$$

with a_0 denoting the scale factor today (i.e. at $t = t_0$). The distance element $\mathrm{d}l(z)$ is given by

$$\mathrm{d}l(z) = \frac{\mathrm{d}z}{H_0\,(1+z)\,\sqrt{\Omega_{\mathrm{m}}^0\,(1+z^3)+\Omega_\Lambda^0}}, \tag{1.52}$$

where H_0 is the value of the Hubble parameter today, while Ω_{m}^0 and Ω_Λ^0 represent the present day values of the dimensionless density parameters corresponding to matter and the cosmological constant, respectively. There can be three contributions to RM which source the extragalactic magnetic fields, usually listed as RM_{G}, RM_{IG} and RM_{S}. They represent the rotation measures arising due to galaxies, IGM, and the medium close to the source (such as the distant quasars), respectively. To arrive at constraints on the strengths of the magnetic fields in the IGM, the contributions due to the other two need to be removed. While this proves to be a useful probe to impose constraints on the magnetic fields in the IGM, the lack of information regarding magnetic fields in galaxies, which has the maximum contributions to the RM, raises problems in considering the FRM as the best choice for constraining the seed fields. The next-generation telescopes such as the Low-Frequency Array and Square Kilometre Array might provide us more information about the RM_{G}, which can help us arrive at better constraints on the PMFs [121].

Apart from the FRM of distant quasars, the upper bound of the order of nG on scales above $1\,\mathrm{Mpc}$ can also be obtained from the CMB data [122–127]. The PMFs can source the scalar, vector, and tensor perturbations, which can leave distinct imprints on the temperature and polarization angular power spectra of the CMB [124, 128–131]. Importantly, in the case of helical magnetic fields, the violation of parity can lead to cross-correlations between temperature and E and B polarization of the CMB. In addition, since the energy-momentum tensor corresponding to the PMFs is quadratic in nature, they can induce primordial non-Gaussianities, which can also leave their signatures on the CMB [50, 106, 132–134]. The coupling between the primordial plasma and the magnetic fields on small scales can affect the acoustic peaks of the CMB spectra due to the dissipation of the magnetic fields. Along with this, the dissipation of the non-thermal energy of magnetic fields into the energy of electrons prior to recombination can cause spectral distortions in the nearly perfect black body spectrum of CMB. Moreover, the presence of magnetic fields can affect Silk damping and the formation of LSS. Upon taking into account all these effects, one can arrive at constraints on the PMFs of coherent lengths comparable to the CMB scales to be of the order of nG that we mentioned above.

Another upper bound of order $10^{-6}\,\mathrm{G}$ can be arrived from the epoch of big bang nucleosynthesis (BBN) by studying the effects of the magnetic fields on the abundance of light elements, especially He^4 (in this context, see, for instance, Refs. [135–139]).

If magnetic fields are present during the epoch of BBN, they can change the expansion rate of the universe due to their contribution to the total energy density of the universe. The magnetic fields can also affect the reaction rates of weak processes like neutron-to-proton conversion and also modify the phase space of the electrons and positrons, which leads to changes in their statistical distributions. Taking all these effects into account, the above constraint is arrived at over the scales of Kpc-Gpc.

A lower bound on the magnetic fields in the IGM can be obtained from the observations of the high energy ($0.1\,\mathrm{GeV}$-$10\,\mathrm{TeV}$) blazars through γ-ray telescopes such as High Energy Stereoscopic System (HESS) [140] and the Fermi large area telescope (Fermi/LAT)[21, 141–143]. These high energy γ-rays interact with the extragalactic background light while propagating through the IGM voids. This interaction creates electron-positron pairs whose trajectories can be deflected by the magnetic fields present in the voids. When these electrons and positrons interact with the CMB photons via inverse Compton scattering, a cascade of secondary γ-rays are produced, which carry information about the magnetic fields present in the IGM voids. The cascade of secondary photons gives rise to two observable effects, which are an extended emission pattern around the initial point source of the γ-rays [144–146], and time delays observed in the γ-ray flares [147, 148]. If the distance scale over which the electron-positron pairs lose energy due to scattering is less than the correlation length of the magnetic fields, then the lower bound on the strength of magnetic fields decays as $\lambda_{_{\rm B}}^{-1/2}$. This generally happens in the case of magnetic fields with correlation lengths less than $1\,\mathrm{Mpc}$. If the distance scale is greater than the correlation length, it possesses constant amplitude, and it happens for magnetic fields with $\lambda_{_{\rm B}} > 1$ Mpc. These observations impose a lower bound of about $10^{-17}\,\mathrm{G}$ on the magnetic fields present in the IGM voids.

At the scale of $1\,\mathrm{Mpc}$, the strongest upper bounds on the magnetic fields arise from the CMB. For a nearly scale invariant spectrum of the PMFs, the Planck 2015 data leads to the upper limit on the present day strength of the magnetic field to be $B_0 < 2.0\,\mathrm{nG}$ [50]. The addition of the BICEP/Keck data and the data from the South Pole Telescope improves the limit to be $B_0 < 1.5\,\mathrm{nG}$, at 95% confidence level [149]. Other observational constraints are derived based on long term combined monitoring of γ-rays from the blazar 1ES 0229+200 in the energy range of 1-$100\,\mathrm{GeV}$ with Fermi/LAT and in the energy range above $200\,\mathrm{GeV}$ with Cherenkov telescopes such as MAGIC, HESS and VERITAS. These concurrent observations impose a lower bound of $B_0 > 1.8 \times 10^{-17}\,\mathrm{G}$

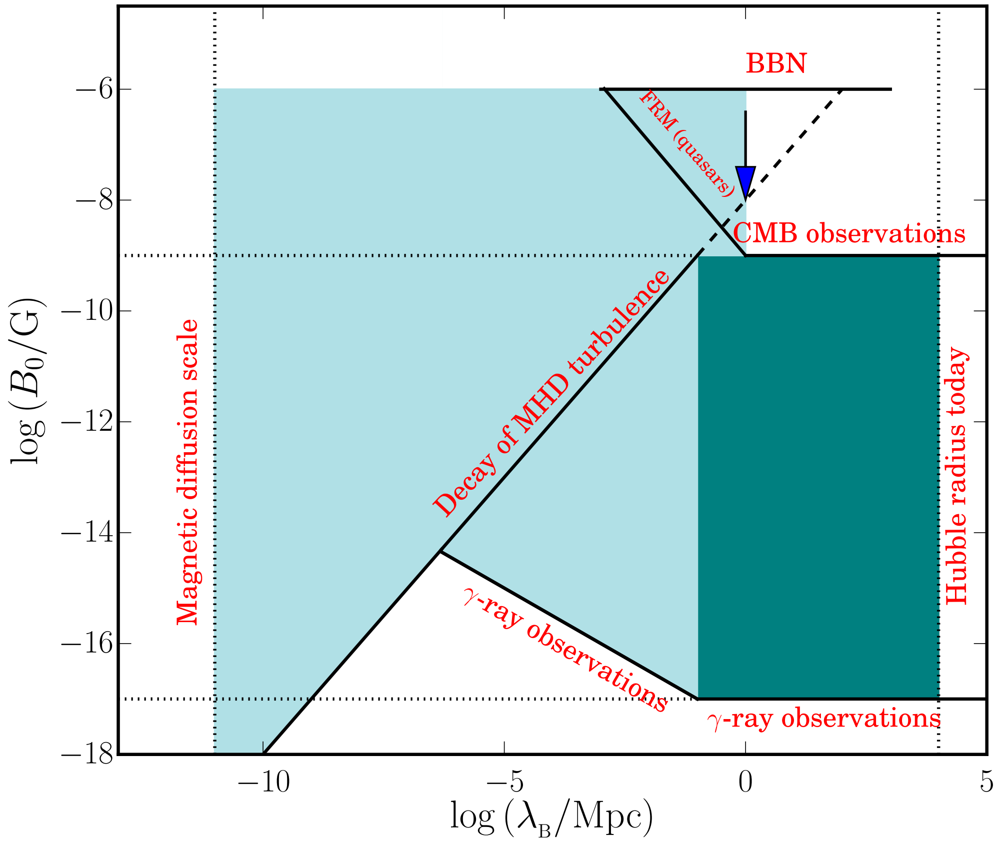

Figure 1.3: We have illustrated the theoretical and observational bounds on the current strengths of the magnetic field B_0 as a function of the coherence length scale λ_{B}. As we have discussed in the text, the constraints from BBN suggest that $B_0 < 10^{-6}\,\mathrm{G}$ over $10^{-3} < \lambda_{\mathrm{B}} < 1\,\mathrm{Mpc}$. The CMB and the observations of γ-ray blazars lead to the upper and lower bounds of $10^{-9}\,\mathrm{G}$ and $10^{-17}\,\mathrm{G}$, respectively, over the coherent scales $10^{-1} < \lambda_{\mathrm{B}} < 10^{4}\,\mathrm{Mpc}$ (indicated in teal). The γ-ray observations and the decay due to the MHD turbulence lead to constraints on scales smaller than $\lambda_{\mathrm{B}} < 10^{-1}\,\mathrm{Mpc}$ (indicated in powder blue). We have also delineated the largest and the smallest scales of interest, viz. the Hubble scale today (i.e. $10^{4}\,\mathrm{Mpc}$) and the scale of magnetic diffusion (i.e. $10^{-12}\,\mathrm{Mpc}$). Note that the other regions (in white) are excluded observationally.

Correlation length (λ_{B})	Present day amplitude (B_0
$-1 \leq \log\left(\frac{\lambda_{\mathrm{B}}}{\mathrm{Mpc}}\right) \leq 4$	$-17 \leq \log\left(\frac{B_0}{\mathrm{G}}\right) \leq -9$
$-6.3 \leq \log\left(\frac{\lambda_{\mathrm{B}}}{\mathrm{Mpc}}\right) \leq -1$	$-17.5 - 0.5\log\left(\frac{\lambda_{\mathrm{B}}}{\mathrm{Mpc}}\right) \leq \log\left(\frac{B_0}{\mathrm{G}}\right) \leq -8 + \log\left(\frac{\lambda_{\mathrm{B}}}{\mathrm{Mpc}}\right)$
$-9 \leq \log\left(\frac{\lambda_{\mathrm{B}}}{\mathrm{Mpc}}\right) \leq -6.3$	$-8 + \log\left(\frac{\lambda_{\mathrm{B}}}{\mathrm{Mpc}}\right) \leq \log\left(\frac{B_0}{\mathrm{G}}\right) <$ no upper bound

Table 1.1: We have listed the theoretical and observational constraints on the magnetic fields today, corresponding to different coherence length scales.

for magnetic fields with long correlation lengths (i.e. $\lambda_{\mathrm{B}} > 1\,\mathrm{Mpc}$) and $B_0 > 10^{-14}\,\mathrm{G}$ for magnetic fields of the cosmological origin present in the voids in the IGM [142]. We have illustrated these different observational bounds in Fig. 1.3.

Let us now turn to discuss the theoretical bounds on the PMFs over very small scales. The evolution of these fields is affected due to their coupling with the primordial plasma as the generation of PMFs causes turbulence in the plasma. For instance, if small scale magnetic fields are generated during the EW or QCD phase transitions, their amplitudes will decay with time until they reach the boundary of the largest possible region associated with the causal MHD processes [150]. Because of the non-linear processes affecting the evolution of the magnetic fields due to the turbulence in MHD, there is a transfer of energy from small scales to large scales (see, for instance, Refs. [41, 92, 151]). As a result, the correlation length of these fields increase, and it may reach a length scale of astrophysical interest. The locus of such points where the evolution of the amplitude and correlation length of the magnetic fields finally terminate, behave in a linear fashion, which can be seen in Fig. 1.3. It has been noticed that the amplitude of magnetic fields generated during the QCD phase transition with present-day coherence length of $50\,\mathrm{Kpc}$ could reach $10^{-9}\,\mathrm{G}$ and the fields which are generated during the EW phase transition with coherence length of about $0.3\,\mathrm{Kpc}$ could reach $10^{-10}\,\mathrm{G}$ after decay due to the MHD processes [89].

Along with the constraints on the magnetic fields, it is essential to understand the bounds on the correlation lengths λ_{B}. The upper bound on the correlation length is of the order of $\lambda_{\mathrm{B}} < 10^4\,\mathrm{Mpc}$. It arises owing to the non-observation of magnetic fields with correlation lengths larger than the Hubble radius today. The lower bound on the correlation length is established from the fact that the resistive magnetic diffusion timescale must not be larger than the age of the universe [1]. In Tab. 1.1, we have presented a summary of the theoretical and observational bounds on the magnetic fields today [8, 10, 81, 142].

1.9 ORGANISATION OF THE THESIS

In this section, we shall conclude the chapter with a brief outline of the thesis. The thesis consists of three pieces of research related to the generation of PMFs in non-standard inflationary scenarios and the evolution of the quantum states of non-helical as well as helical electromagnetic fields during inflation.

In Chap. 2, we shall consider the generation of magnetic fields in single field inflationary models involving deviations from slow roll inflation. We shall specifically discuss the challenges posed due to such departures from slow roll on generating spectra of magnetic fields with observable strengths and shapes. In Chap 3, we shall describe the manner in which the challenges encountered in magnetogenesis in single field models permitting departures from slow roll can be overcome with the aid of two field models of inflation. In addition, we shall also discuss the imprints of the PMFs generated in certain two field models on the angular power spectra (of both temperature and polarization) of the CMB. In Chap. 4, we shall discuss the quantum origin of the PMFs and study the evolution of the quantum states associated with the Fourier modes of the electromagnetic fields using different tools from the theory of quantum information. We shall particularly focus on the behaviour of these quantum measures in the case of helical electromagnetic fields. Lastly, in Chap. 5, after a quick overview of the thesis, we shall briefly outline the problems that can be further investigated in these contexts.

There is one point we would like to mention before we proceed. In the following chapters, to make it convenient while reading, we shall repeat some of the primary equations (such as actions, equations, and potentials) and some of the essential discussions.

CHAPTER 2

CHALLENGES IN THE CHOICE OF THE NON-CONFORMAL COUPLING FUNCTION IN INFLATIONARY MAGNETOGENESIS

2.1 INTRODUCTION

Large-scale magnetic fields are observed in galaxies, galaxy clusters and in the intergalactic voids (for reviews on magnetic fields, see Refs. [1–10]). The Fermi/LAT and HESS observations of TeV blazars suggest that the strength of magnetic fields in the intergalactic medium is of the order of 10^{-15} G [21–23, 152–155]. Also, magnetic fields of strength of the order of 10^{-6} G are observed within galaxies (for a recent discussion of the various observational constraints, see, for instance, Refs. [10, 149]). It seems challenging to explain the presence of magnetic fields of such strengths, specifically in the voids in the IGM, on the basis of astrophysical phenomena alone [3, 4]. Hence, it is believed that these magnetic fields may have a cosmological origin and they could have been generated during the inflationary epoch in the early universe (for reviews in this context, see Refs. [5, 6, 8–10]).

Recall that the standard electromagnetic action is conformally invariant. Therefore, the energy density of the magnetic fields generated in such a theory will be rapidly washed away during inflation. We should clarify that this is strictly true only in the case of the spatially flat FLRW universe, which is conformally flat globally. The FLRW universes with non-vanishing spatial curvature are conformally flat only locally and, as a result, the adiabatic evolution of magnetic fields in such scenarios can be affected (see Refs. [156, 157]; however, for further discussions in this context, see Refs. [158–160]). As we mentioned, in this thesis, we shall focus on the spatially flat FLRW universe. The spectrum of magnetic fields generated in the conformally invariant theory will be strongly scale-dependent, inconsistent with the recent constraints from the CMB [50]. The simplest way to generate magnetic fields of observable strengths today seems to break the conformal invariance of the electromagnetic action (in this context, see, for example, Refs. [93–95, 104, 107, 161–164]). Often, this is achieved by coupling the electromagnetic field to either the scalar field that drives inflation [81, 95, 161, 165, 166] or to the Ricci scalar describing the background [104, 107, 162, 164]. In fact, it has also been discovered that the addition of a parity violating term in the electromagnetic action can significantly enhance the amplitude of magnetic fields generated during inflation [97, 99, 167–173]. It can be shown that, for certain choices of the coupling function, the spectrum of magnetic fields generated can be nearly scale invariant consistent with the current constraints over a wide range of scales (see, for instance, Refs. [50, 174–177]).

The CMB observations point to a nearly scale invariant primordial scalar power spectrum as is generated in models of slow roll inflation [52]. Nevertheless, there has been a constant interest in the literature to examine if there exist features in the scalar power spectrum. During the last decade or two, the possibility of features in the inflationary power spectrum has been often examined with the aim of improving the fit to the CMB and the LSS data (in this context, see, for instance, Refs. [178–190]). More recently, with the detection of gravitational waves from merging binary black holes [191], there has been a tremendous interest in investigating whether such black holes could have a primordial origin [192–195]. In this context, a variety of inflationary models generating increased power on small scales (compared to the COBE normalized power on the CMB scales) which can lead to an enhanced formation of primordial black holes (PBHs) have been investigated (see, for instance, Refs. [196–203]). These features in the scalar power spectrum—both on the large as well as the small scales—are usually generated due to deviations from slow roll inflation. We mentioned above that the spectrum of the magnetic field depends on the choice of the function that couples the electromagnetic field to either the inflaton or the Ricci scalar. These coupling functions are often chosen such that the power spectrum of the magnetic field is nearly scale invariant in slow roll inflation (actually, the background is often assumed to be of the de Sitter or power law forms). However, if there arise departures from slow roll, the non-trivial dynamics can influence the behaviour of the coupling functions and thereby affect the spectrum of the magnetic field. In other words, the mechanism that generates features in the scalar power spectrum can also induce features in the spectrum of the magnetic field depending on the nature of the coupling that breaks the conformal invariance of the electromagnetic action or induces violation of parity.

In this chapter, we shall investigate the effects of deviations from slow roll inflation on the power spectra of the electromagnetic fields. While there have been some earlier attempts to understand the effects of transitions during inflation (in this context, see, for instance, Refs. [97, 98, 117, 204]; for some recent efforts, see Refs. [205, 206]), we find that there does not seem to have been any effort to systematically examine the imprints of departures from slow roll inflation on the spectra of the electromagnetic fields. We find that coupling the electromagnetic field to the scalar curvature poses certain difficulties even in slow roll inflation. We consider specific inflationary models that lead to features in the scalar power spectrum. We choose functions that are coupled to the inflaton which lead to nearly scale invariant spectra for the magnetic field either in the absence of departures from slow roll or over large scales (which are constrained by the CMB observations) and examine the effects due to the deviations from slow roll inflation. We show that, in these cases, unless the non-minimal coupling function is designed in a specific manner and is extremely fine-tuned, it is impossible to avoid features in the spectra of electromagnetic fields. Moreover, we notice that, in some cases, the strengths of the magnetic fields can be considerably suppressed over large scales. We believe that exploring the observational signatures of such features can help us understand the nature of the non-conformal coupling that is required to generate magnetic fields of observable strengths.

This chapter is organized as follows. In the next section, we shall discuss the spectra of electromagnetic fields generated during inflation, when the fields are coupled to either the inflaton or the scalar curvature. We shall arrive at the spectra of electromagnetic fields generated in de Sitter inflation when the field is coupled to the inflaton. We shall also evaluate the spectra in the presence of an additional term in the action that induces the violation of parity. We shall point out that, even in slow roll inflation, there arise specific challenges when considering the coupling of the electromagnetic field to the scalar curvature. In Sec. 2.3, we shall construct specific non-minimal coupling functions that lead to nearly scale invariant power spectra for the magnetic fields in some of the popular models of slow roll inflation. In Sec. 2.4, we shall introduce a few inflationary models that lead to features over large, intermediate and small scales in the scalar power spectrum. In Sec. 2.5, we shall examine the effects of deviations from slow roll inflation on the spectra of the electromagnetic fields. In certain cases, we shall support our numerical computations with analytical estimates of the amplitude and shape of the electromagnetic power spectra. In Sec. 2.6, with the help of an example, we shall illustrate that, given an inflationary model leading to features in the scalar power spectra, a suitably designed non-minimal coupling function can largely undo the sharp features generated in the spectra of the electromagnetic fields. Finally, we shall conclude with a summary in Sec. 2.7. We shall relegate some of the details to App. A.

2.2 GENERATION OF MAGNETIC FIELDS DURING INFLATION

In this section, we shall quickly summarize the essential aspects related to the generation of electromagnetic fields during inflation. We shall outline the spectra that arise in situations wherein a coupling function is introduced to break the conformal invariance of the action describing the electromagnetic fields.

2.2.1 The non-helical case

As is often done, we shall first consider a coupling between the electromagnetic field and the inflaton to break the conformal invariance of the standard action describing electromagnetism. We shall assume that the electromagnetic field is described by the action (see, for example, Refs. [5, 95])

$$S[A^\mu] = -\frac{1}{16\,\pi} \int \mathrm{d}^4x \sqrt{-g}\, J^2(\phi)\, F_{\mu\nu}\, F^{\mu\nu}, \tag{2.1}$$

where $J(\phi)$ denotes the coupling function and the field tensor $F_{\mu\nu}$ is expressed in terms of the vector potential A_μ as $F_{\mu\nu} = (\partial_\mu\, A_\nu - \partial_\nu\, A_\mu)$. On working in the Coulomb gauge wherein $A_\eta = 0$ and $\partial_i\, A^i = 0$, one finds that the Fourier modes, say, $\bar{A}_k$, describing the vector potential satisfy the differential equation (see, for example Refs. [95, 207]):

$$\bar{A}_k'' + 2\,\frac{J'}{J}\,\bar{A}_k' + k^2\,\bar{A}_k = 0. \tag{2.2}$$

If we write $\bar{A}_k = \mathcal{A}_k/J$, then this equation reduces to

$$\mathcal{A}_k'' + \left(k^2 - \frac{J''}{J}\right)\,\mathcal{A}_k = 0. \tag{2.3}$$

The power spectra associated with the magnetic and electric fields are defined to be [5, 95]

$$\mathcal{P}_{_{\mathrm{B}}}(k) = \frac{k^5}{2\,\pi^2}\,\frac{J^2}{a^4}\,\vert\bar{A}_k\vert^2 = \frac{k^5}{2\,\pi^2\,a^4}\,\vert\mathcal{A}_k\vert^2, \tag{2.4a}$$

$$\mathcal{P}_{_{\mathrm{E}}}(k) = \frac{k^3}{2\,\pi^2}\,\frac{J^2}{a^4}\,\vert\bar{A}_k'\vert^2 = \frac{k^3}{2\,\pi^2\,a^4}\,\left\vert\mathcal{A}_k' - \frac{J'}{J}\,\mathcal{A}_k\right\vert^2. \tag{2.4b}$$

The initial conditions on the quantity $\mathcal{A}_k$ can be imposed in the domain wherein $k \gg \sqrt{J''/J}$ and the spectra associated with the electromagnetic fields can be evaluated in the limit when $k \ll \sqrt{J''/J}$.

Let us now arrive at the power spectra of the electromagnetic fields in de Sitter inflation wherein the scale factor is given by $a(\eta) = -1/(H_{_{\mathrm{I}}}\,\eta)$, with $H_{_{\mathrm{I}}}$ denoting the constant Hubble parameter. Typically, the coupling function J is assumed to depend on the scale factor as follows (see, for instance, Refs. [5, 95]):

$$J(\eta) = \left[\frac{a(\eta)}{a(\eta_{\mathrm{e}})}\right]^n = \left(\frac{\eta}{\eta_{\mathrm{e}}}\right)^{-n}, \tag{2.5}$$

where η_{e} denotes the conformal time at the end of inflation. Note that we have chosen the overall constant so that the coupling function reduces to unity at the end of inflation. We should stress here that the parameter n is a real number and is not necessarily an integer. In such a case, the Bunch-Davies initial conditions on the electromagnetic modes $\mathcal{A}_k$ can be imposed in the limit $k \gg \sqrt{J''/J}$, which, for the above choice of the coupling function, corresponds to the modes being in the sub-Hubble domain at early times. For the coupling function (2.5), the solution to Eq. (2.3) that satisfies the Bunch-Davies initial conditions is given by

$$\mathcal{A}_k(\eta) = \sqrt{-\frac{\pi\,\eta}{4}}\, \mathrm{e}^{i\,(n+1)\,\pi/2}\, H_\nu^{(1)}(-k\,\eta), \tag{2.6}$$

where $\nu = n + (1/2)$, and $H_\nu^{(1)}(z)$ denotes the Hankel function of the first kind.

The spectra of the electromagnetic fields can be evaluated in the limit $k \ll \sqrt{J''/J}$, which corresponds to the super-Hubble limit in de Sitter inflation for our choice of the coupling function. In the limit $(-k\,\eta_\mathrm{e}) \ll 1$, the spectra of the magnetic and electric fields $\mathcal{P}_{_\mathrm{B}}(k)$ and $\mathcal{P}_{_\mathrm{E}}(k)$ can be obtained to be [5, 95]

$$\mathcal{P}_{_\mathrm{B}}(k) = \frac{H_{_\mathrm{I}}^4}{8\,\pi}\, \mathcal{F}(m)\, (-k\,\eta_\mathrm{e})^{2\,m+6}, \tag{2.7a}$$

$$\mathcal{P}_{_\mathrm{E}}(k) = \frac{H_{_\mathrm{I}}^4}{8\,\pi}\, \mathcal{G}(m)\, (-k\,\eta_\mathrm{e})^{2\,m+4}, \tag{2.7b}$$

where, recall that, η_e denotes the conformal time at the end of inflation. The quantities $\mathcal{F}(m)$ and $\mathcal{G}(m)$ are given by

$$\mathcal{F}(m) = \frac{1}{2^{2\,m+1}\cos^2(m\,\pi)\,\Gamma^2(m+3/2)}, \tag{2.8a}$$

$$\mathcal{G}(m) = \frac{1}{2^{2\,m-1}\cos^2(m\,\pi)\,\Gamma^2(m+1/2)}, \tag{2.8b}$$

with

$$m = \begin{cases} n, & \text{for } n < -\frac{1}{2}, \\ -n-1, & \text{for } n > -\frac{1}{2}. \end{cases} \tag{2.9}$$

in the case of $\mathcal{P}_{_\mathrm{B}}(k)$, and with

$$m = \begin{cases} n, & \text{for } n < \frac{1}{2}, \\ 1-n, & \text{for } n > \frac{1}{2}. \end{cases} \tag{2.10}$$

in the case of $\mathcal{P}_{_\mathrm{E}}(k)$. Note that the spectral indices for the magnetic and electric fields, say, n_{B} and n_{E}, can be written as

$$n_{\mathrm{B}} = \begin{cases} 2\,n+6, & \text{for } n < -\frac{1}{2}, \\ 4-2\,n, & \text{for } n > -\frac{1}{2}, \end{cases} \tag{2.11}$$

and

$$n_{\mathrm{E}} = \begin{cases} 2\,n+4, & \text{for } n < \frac{1}{2}, \\ 6-2\,n, & \text{for } n > \frac{1}{2}. \end{cases} \tag{2.12}$$

To be consistent with observations, the magnetic field is expected to be nearly scale invariant and, evidently, this is possible when $n \simeq -3$ or when $n \simeq 2$. In these cases, it is clear that $n_{\mathrm{E}} \simeq -2$ and $n_{\mathrm{E}} \simeq 2$, respectively. At late times, $n_{\mathrm{E}} \simeq -2$ implies that the energy density in the electric field is significant leading to a large backreaction. In order to avoid such an issue, one often considers the $n = 2$ case to lead to a scale invariant magnetic field with negligible backreaction due to the electric field. Note that, in these cases, the power spectra reduce to the following simple forms

$$\mathcal{P}_{\mathrm{B}}(k) = \frac{9\,H_{\mathrm{I}}^4}{4\,\pi^2}, \quad \mathcal{P}_{\mathrm{E}}(k) = \frac{H_{\mathrm{I}}^4}{4\,\pi^2}\,(-k\,\eta_{\mathrm{e}})^2. \tag{2.13}$$

2.2.2 The helical case

Recall that, we had considered the action (2.1) to break the conformal invariance of the electromagnetic field. The action can be extended to include a parity violating term as follows (in this context, see, for instance, Refs. [97, 99, 167–169, 204]):

$$S[A^\mu] = -\frac{1}{16\,\pi}\int \mathrm{d}^4x\,\sqrt{-g}\,\left[J^2(\phi)\,F_{\mu\nu}\,F^{\mu\nu} - \frac{\gamma}{2}\,I^2(\phi)\,F_{\mu\nu}\,\widetilde{F}^{\mu\nu}\right], \tag{2.14}$$

where $\widetilde{F}^{\mu\nu} = (\epsilon^{\mu\nu\alpha\beta}/\sqrt{-g})\,F_{\alpha\beta}$, with $\epsilon^{\mu\nu\alpha\beta}$ being the completely anti-symmetric Levi-Civita tensor, and γ is a constant. In such a case, the modes of the electromagnetic field can be decomposed in a suitable helical basis. Also, we can work in the Coulomb gauge as we had done in the non-helical case. In such a case, it is found that the second term in the above action amplifies the electromagnetic modes associated with one of the polarizations when compared to the other, thereby violating parity or, equivalently, inducing helicity [99, 168, 169, 172, 173].

When we decompose the electromagnetic field in the helical basis, the Fourier modes of the field, say, $\bar{A}_k^\sigma$, are found to satisfy the differential equation

$$\bar{A}_k^{\sigma\,\prime\prime} + 2\,\frac{J'}{J}\,\bar{A}_k^{\sigma\,\prime} + \left(k^2 + \frac{\sigma\,\gamma\,k}{J^2}\,\frac{\mathrm{d}I^2}{\mathrm{d}\eta}\right)\bar{A}_k^\sigma = 0, \tag{2.15}$$

where $\sigma = \pm 1$ represents positive and negative helicity. Let us define $\bar{A}_k^\sigma = \mathcal{A}_k^\sigma/J$ as we had done in the non-helical case. In terms of the new variable $\mathcal{A}_k^\sigma$, the above equation reduces to

$$\mathcal{A}_k^{\sigma\,\prime\prime} + \left(k^2 + \frac{2\,\sigma\,\gamma\,k\,I\,I'}{J^2} - \frac{J''}{J}\right)\mathcal{A}_k^\sigma = 0. \tag{2.16}$$

We shall restrict ourselves to the simplest of scenarios wherein $I = J$. In such a case, the above equation simplifies to

$$\mathcal{A}_k^{\sigma\,\prime\prime} + \left(k^2 + \frac{2\,\sigma\,\gamma\,k\,J'}{J} - \frac{J''}{J}\right)\mathcal{A}_k^\sigma = 0. \tag{2.17}$$

The power spectra of the magnetic and electric fields can be expressed in terms of the modes $\bar{A}_k^\sigma$ and the coupling function J as follows [97, 99, 167, 169]:

$$\begin{aligned}
\mathcal{P}_{\mathrm{B}}(k) &= \frac{k^5}{4\,\pi^2}\,\frac{J^2}{a^4}\,\left[\left|\bar{A}_k^+\right|^2 + \left|\bar{A}_k^-\right|^2\right] \\
&= \frac{k^5}{4\,\pi^2\,a^4}\,\left[\left|\mathcal{A}_k^+\right|^2 + \left|\mathcal{A}_k^-\right|^2\right], \qquad (2.18\mathrm{a}) \\
\mathcal{P}_{\mathrm{E}}(k) &= \frac{k^3}{4\,\pi^2}\,\frac{J^2}{a^4}\,\left[\left|\bar{A}_k^{+\prime}\right|^2 + \left|\bar{A}_k^{-\prime}\right|^2\right] \\
&= \frac{k^3}{4\,\pi^2\,a^4}\,\left[\left|\mathcal{A}_k^{+\prime} - \frac{J'}{J}\mathcal{A}_k^+\right|^2 + \left|\mathcal{A}_k^{-\prime} - \frac{J'}{J}\mathcal{A}_k^-\right|^2\right]. \qquad (2.18\mathrm{b})
\end{aligned}$$

For the form of the coupling function given by Eq. (2.5), the solutions to the electromagnetic modes satisfying the differential equation (2.17) and the Bunch-Davies initial conditions can be written as follows (for a recent discussion, see, for example, Ref. [169]):

$$\mathcal{A}_k^\sigma(\eta) = \frac{1}{\sqrt{2\,k}}\,\mathrm{e}^{\pi\,\sigma\,\xi/2}\,W_{-i\,\sigma\,\xi,\nu}(2\,i\,k\,\eta), \tag{2.19}$$

where $\nu = n + (1/2)$, $\xi = -n\,\gamma$, and $W_{\lambda,\mu}(z)$ denotes the Whittaker function. In the domain $z \ll 1$, the Whittaker function $W_{\lambda,\mu}(z)$ behaves as [208, 209]

$$W_{\lambda,\mu}(z) \to \frac{\Gamma(-2\,\mu)}{\Gamma(\frac{1}{2} - \lambda - \mu)}\,z^{(1/2)+\mu} + \frac{\Gamma(2\,\mu)}{\Gamma(\frac{1}{2} - \lambda + \mu)}\,z^{(1/2)-\mu}. \tag{2.20}$$

Upon using this result and the expression (4.96a), we find that the spectrum of the magnetic field evaluated in the limit $(-k\,\eta_{\mathrm{e}})\ll 1$ is given by [99, 169]

$$\mathcal{P}_{_{\mathrm{B}}}(k) \;=\; \frac{H_{_{\mathrm{I}}}^4}{8\,\pi^2}\,\frac{\Gamma^2(|2\,n+1|)}{|\Gamma(\frac{1}{2}+i\,n\,\gamma+|n+\frac{1}{2}|)|^2}\,\left(\frac{\cosh\,(n\,\pi\,\gamma)}{2^{|2\,n+1|-2}}\,(-k\,\eta_{\mathrm{e}})^{5-|2\,n+1|}\right). \tag{2.21}$$

Let us now turn to the evaluation of the spectrum of the electric field. In the calculation of the spectrum, the following relation for the derivative of the Whittaker function [208, 209]:

$$\frac{\mathrm{d}W_{\lambda,\mu}(z)}{\mathrm{d}z} = \left(\frac{1}{2}-\frac{\lambda}{z}\right)\,W_{\lambda,\mu}(z)-\frac{1}{z}\,W_{1+\lambda,\mu}(z) \tag{2.22}$$

and the following recursion relation:

$$W_{\lambda,\mu}(z) = \sqrt{z}\,W_{\lambda-\frac{1}{2},\mu-\frac{1}{2}}(z)+\left(\frac{1}{2}-\lambda+\mu\right)\,W_{\lambda-1,\mu}(z) \tag{2.23}$$

prove to be helpful. On using the above relations and the behaviour (2.20) of the Whittaker function, we can obtain the spectrum of the electric field in the helical case [as defined in Eq. (4.96b)] in the limit $(-k\,\eta_{\mathrm{e}})\ll 1$ to be

$$\mathcal{P}_{_{\mathrm{E}}}(k) = \frac{H_{_{\mathrm{I}}}^4}{4\,\pi^2}\,\frac{\Gamma^2(2\,|n|)}{|\Gamma(|n|+i\,n\,\gamma)|^2}\,\left(\frac{\gamma^2}{1+\gamma^2}\right)\,\left[\frac{\cosh\,(n\,\pi\,\gamma)}{2^{2\,|n|-2}}\right]\,(-k\,\eta_{\mathrm{e}})^{4-2\,|n|} \tag{2.24}$$

with the factor $\gamma^2/(1+\gamma^2)$ arising *only* for positive values of the index n. Evidently, the spectral indices for the magnetic and electric fields—viz. $n_{_{\mathrm{B}}}$ and $n_{_{\mathrm{E}}}$—are given by

$$n_{_{\mathrm{B}}} = 5-|2\,n+1|\,,\quad n_{_{\mathrm{E}}} = 4-2\,|n|. \tag{2.25}$$

As in the non-helical case, we find that the spectrum of the magnetic field is scale invariant when $n=-3$ and $n=2$. Interestingly, in the helical case, the spectrum of the electric field is also scale invariant when $n=2$, whereas, when $n=-3$, the spectrum has the same tilt (i.e. $n_{_{\mathrm{E}}}=-2$) as in the non-helical case.

In our later discussion, we shall be focusing on the $n=2$ case. When $n=2$, we find that the spectra of the helical magnetic and electric fields [evaluated in the limit $(-k\,\eta_{\mathrm{e}})\ll 1$] can be written as [209]

$$\mathcal{P}_{_{\mathrm{B}}}(k) \;=\; \frac{9\,H_{_{\mathrm{I}}}^4}{4\,\pi^2}\,f(\gamma), \tag{2.26a}$$

$$\mathcal{P}_{_{\mathrm{E}}}(k) \;=\; \frac{9\,H_{_{\mathrm{I}}}^4}{4\,\pi^2}\,f(\gamma)\,\biggl[\gamma^2-\frac{\sinh^2(2\,\pi\,\gamma)}{3\,\pi\,\left(1+\gamma^2\right)\,f(\gamma)}\,(-k\,\eta_{\mathrm{e}}) +\frac{1}{9}\,\left(1+23\,\gamma^2+40\,\gamma^4\right)\,\left(-k\,\eta_{\mathrm{e}}\right)^2\biggr], \tag{2.26b}$$

where the function $f(\gamma)$ is given by

$$f(\gamma) = \frac{\sinh(4\,\pi\,\gamma)}{4\,\pi\,\gamma\,(1+5\,\gamma^2+4\,\gamma^4)}. \tag{2.27}$$

We will soon clarify the reason for retaining the second and third terms within the square brackets [despite the fact that we are considering the $(-k\,\eta_{\mathrm{e}}) \ll 1$ limit] in the above expression for $\mathcal{P}_{_{\mathrm{E}}}(k)$. There are two related points that we need to highlight regarding the results we have arrived at above. Firstly, note that, as $\gamma \to 0$, $f(\gamma) \to 1$, and these spectra reduce to the non-helical results (2.13), as required. Secondly, in the above spectrum for the electric field, the first two terms go to zero in the limit of vanishing helicity (i.e. as $\gamma \to 0$). In other words, even a small amount of helicity modifies the spectrum of the electric field considerably, making it scale invariant. It is only in the case of extremely small helicity—to be precise, when $\gamma \ll (-k\,\eta_{\mathrm{e}}) \simeq k/k_{\mathrm{e}}$, where k_{e} is the wave number that leaves the Hubble radius at the end of inflation—that the third term becomes dominant leading to the behaviour that we had encountered in the non-helical case.

2.2.3 Coupling to the scalar curvature

Let us now turn to the case of the electromagnetic field that is coupled to the scalar curvature R and is described by the following action [93, 104, 107]:

$$S[A^\mu] = -\frac{1}{16\,\pi}\int \mathrm{d}^4x\,\sqrt{-g}\,J^2(R)\,F_{\mu\nu}\,F^{\mu\nu}, \tag{2.28}$$

where $F_{\mu\nu}$ is the electromagnetic field tensor defined earlier. Evidently, in such a case, one can work in the Coulomb gauge and the Fourier modes of the electromagnetic vector potential $\bar{A}_k$ and the quantity $\mathcal{A}_k = J\,\bar{A}_k$ would continue to be governed by the differential equations (2.2) and (2.3). Therefore, if the coupling function $J(R)$ is chosen so that it depends on the conformal time as in Eq. (2.5), then we can expect scale invariant spectra for the magnetic field when $n = -3$ and $n = 2$.

Earlier, while considering the coupling function (2.5), we had assumed the background to be that of de Sitter. Note that the scalar curvature R associated with the FLRW line-element (1.2) can be expressed as

$$R = 6\,\frac{a''}{a^3} = 6\,H^2\,(2-\epsilon_1) \tag{2.29}$$

and we should emphasize that this expression is exact. In a de Sitter universe wherein

H is a constant and ϵ_1 vanishes, the above relation implies that the scalar curvature is time-independent. Therefore, we cannot work in the de Sitter limit. Since we are interested in potentials which typically lead to slow roll inflation, we can assume the scale factor to be of the slow roll form. In such a case, it can be shown that the scalar curvature behaves in terms of the conformal time as $R \propto \eta^{2\,\epsilon_1}$. This suggests that we can possibly work with a coupling function of the form

$$J(R) = \left[\frac{R(\eta)}{R(\eta_{\rm e})}\right]^{\alpha}, \tag{2.30}$$

where $R(\eta_{\rm e})$ denotes the scalar curvature at the end of inflation. In slow roll inflation, such a coupling will behave in terms of the conformal time coordinate as follows:

$$J(\eta) \simeq \left(\frac{\eta}{\eta_{\rm e}}\right)^{2\,\epsilon_1\,\alpha}, \tag{2.31}$$

which reduces to our original form of the coupling function, as given by Eq. (2.5), if we choose $\alpha = -n/(2\,\epsilon_1)$. Also, we can expect to arrive at a scale invariant spectrum for the magnetic field without any backreaction in the case of $n = 2$.

But, there arises a challenge, which, in fact, proves to be a rather serious one. When considering a non-conformal coupling of the form $J(R)$, we find that, in the literature, the scale factor describing the FLRW background is often assumed to be of a power law form. Such an assumption works well in power law inflationary scenarios wherein the first slow roll parameter ϵ_1 is strictly a constant, but poses difficulties in realistic slow roll models of inflation wherein ϵ_1 evolves towards unity and inflation ends naturally. Note that, since ϵ_1 is rather small at early times in slow roll inflation (in order to be consistent with the constraints on the tensor-to-scalar ratio r over the CMB scales; for the latest constraints, see Refs. [52, 210]), the index $\alpha = -1/\epsilon_1$ (for $n = 2$) turns out to be large in magnitude, typically of the order of 10^2 or larger. The fact that the index α has a large magnitude is not surprising and can be easily understood. In slow roll inflation, $R \simeq 12\,H^2$ and hence it hardly changes during the initial stages of inflation. Therefore, one has to raise the scalar curvature to an adequately large power to achieve the desired time-dependence of the coupling function. Moreover, since, in any realistic slow roll model of inflation, ϵ_1 is *not* a constant, one has to work with an α that is determined by, say, the value of ϵ_1 when the pivot scale leaves the Hubble radius. However, because ϵ_1 is time-dependent, we are not guaranteed a scale invariant spectrum for the magnetic field. In order to illustrate this point, in Fig. 2.1, we have

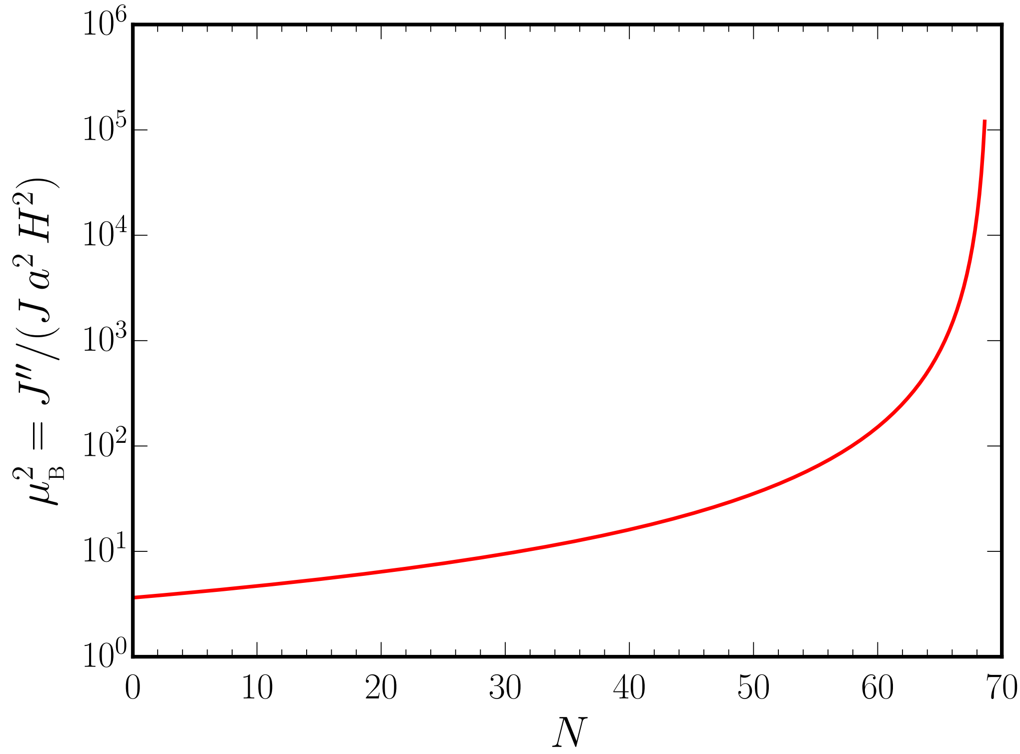

Figure 2.1: The evolution of the quantity $\mu_{\rm B}^2 = J''/(J\,a^2\,H^2)$, with J being given by the coupling function (2.30), as it occurs in the case of slow roll inflation driven by the quadratic potential (in this context, see Sec. 2.3), has been plotted as a function of e-folds N. We have set $\alpha = -1/\epsilon_{1*} \simeq -10^2$, where ϵ_{1*} is the value of the first slow roll parameter when the pivot scale k_* leaves the Hubble radius. For the value of the parameter m (describing the quadratic potential) and the initial conditions we have worked with, we find that the pivot scale k_* leaves the Hubble radius at the e-fold of $N = 18.63$. We find that $\mu_{\rm B}^2 \simeq 6$ near $N \simeq 18$, which is necessary to result in a scale invariant spectrum for the magnetic field. However, since the first slow roll parameter ϵ_1 is not a constant, $\mu_{\rm B}^2$ changes with time and, actually, grows to a large value towards the end of inflation. Apart from affecting the shape of the spectra of the electromagnetic fields, we find that, a large value of α also leads to exceedingly large values of the electromagnetic vector potential at either the early or the late stages of inflation.

plotted the quantity $\mu_{\rm B}^2 = J''/(J\,a^2\,H^2)$ in a slow roll inflationary model described by the quadratic potential [which we shall introduce later, see Eq. (2.39)]. We have chosen the parameter α so that $\mu_{\rm B}^2 \simeq 6$ when the pivot scale leaves the Hubble radius, which is required to lead to a nearly scale invariant spectrum for the magnetic field. But, since ϵ_1 changes with time, the quantity $\mu_{\rm B}^2$ grows to large values at later times. Such a behaviour of $\mu_{\rm B}^2$ not only affects the shape of the spectra of the electromagnetic fields, it influences their amplitude as well. Importantly, we find that, in general, a large value for α leads to rather large values for the electromagnetic vector potential at either early or late times.

Phenomenologically, the only way out of this difficulty is to choose the index α in $J(R)$ [cf. Eq. (2.30)] to be dependent on time. In order to arrive at a scale invariant power spectrum for the magnetic field, one may work with a coupling function of the following form:

$$J = \left(\frac{R}{6\,H_{\rm e}^2}\right)^{\alpha(N)} = \left[\frac{H^2\,(2-\epsilon_1)}{H_{\rm e}^2}\right]^{\alpha(N)} \tag{2.32}$$

and choose $\alpha(N)$ to be

$$\alpha(N) = \frac{2\,(N-N_{\rm e})}{\ln\left[H^2\,(2-\epsilon_1)/H_{\rm e}^2\right]}, \tag{2.33}$$

where $H_{\rm e}$ and $N_{\rm e}$ denote the Hubble parameter and the e-fold at the end of inflation. Such a choice essentially leads to $J(R) \propto a^2$, thereby guaranteeing a scale invariant spectrum for the magnetic field. However, the action (2.28) of the electromagnetic field described by the coupling function (2.30) with an α that depends on time will not be invariant under general coordinate transformations. A theory which breaks general covariance seems unattractive and is also quite likely to be unviable.

2.2.4 Strength of magnetic fields at the present epoch

The spectrum of magnetic fields evaluated at the end of inflation allows us to arrive at their strengths at the present epoch. In the conventional picture, the epoch of reheating is supposed to succeed inflation. During reheating, when the energy from the inflaton is being transferred to the particles constituting matter, the universe is expected to be filled with a plasma of charged particles. The creation of charged particles results in a rapid rise in the conductivity of the plasma during reheating and, as a result, the electric fields are shorted out, i.e. they decay exponentially. Thereafter, the magnetic fields are supposed to evolve adiabatically with the expansion of the universe due to the fact that the fluxes freeze in the highly conducting plasma (for a discussion on these points, see, for instance, Refs. [5, 8]).

Let us consider the simple scenario wherein reheating occurs instantaneously at the termination of inflation. In such a case, the spectrum of the magnetic field today, say, $\mathcal{P}_{_{\rm B}}^0(k)$, can be related to the spectrum $\mathcal{P}_{_{\rm B}}(k)$ at the end of inflation as follows:

$$\mathcal{P}_{_{\rm B}}^0(k) \simeq \mathcal{P}_{_{\rm B}}(k)\,\left(\frac{a_{\rm e}}{a_0}\right)^4, \tag{2.34}$$

where $a_{\rm e}$ is the scale factor at the end of inflation, while a_0 denotes the scale factor today. The ratio $a_{\rm e}/a_0$ can be determined from the conservation of entropy, i.e. the constancy of the quantity $g_{\rm s}\, T^3\, a^3$ from the end of inflation until today, where T is the temperature of radiation at a given epoch and $g_{\rm s}$ represents the effective relativistic degrees of freedom that contribute to the entropy. As a result, we can write

$$\frac{a_0}{a_{\rm e}} = \left(\frac{g_{\rm s,e}}{g_{\rm s,0}}\right)^{1/3} \frac{T_{\rm e}}{T_0}, \tag{2.35}$$

where $(T_{\rm e}, g_{\rm s,e})$ and $(T_0, g_{\rm s,0})$ denote the temperature and the effective number of relativistic degrees of freedom at the onset of the radiation dominated epoch and today, respectively. The quantity $T_{\rm e}$ can be determined using the fact that, in the case of instantaneous reheating, the energy density at the end of inflation equals that of radiation at the epoch, leading to $\rho_{_{\rm I}} \simeq 3\, H_{_{\rm I}}^2\, M_{_{\rm Pl}}^2 \simeq g_{\rm r,e}\, (\pi^2/30)\, T_{\rm e}^4$, where $g_{\rm r}$ denotes the effective number of relativistic degrees that contribute to the energy density of radiation. For simplicity, if we assume that $g_{\rm r} \simeq g_{\rm s}$, upon using the above relation, we can arrive at

$$\frac{a_0}{a_{\rm e}} \simeq \left(\frac{g_{\rm e}}{g_0}\right)^{1/3} \left(\frac{90\, H_{_{\rm I}}^2\, M_{_{\rm Pl}}^2}{g_{\rm e}\, \pi^2\, T_0^4}\right)^{1/4}. \tag{2.36}$$

If we consider $g_{\rm e} = 106.75$, since $g_0 = 3.36$ and $T_0 = 2.725\,{\rm K}$, we obtain that

$$\frac{a_0}{a_{\rm e}} \simeq 2.8 \times 10^{28} \left(\frac{H_{_{\rm I}}}{10^{-5}\, M_{_{\rm Pl}}}\right)^{1/2}. \tag{2.37}$$

Given the scale invariant spectrum (2.26a) for the magnetic field at the end of inflation in the $n = 2$, helical case, upon substituting the above expression for $a_0/a_{\rm e}$ in Eq. (2.34), we can estimate the present day strength of the magnetic field, say, B_0 (at any scale), to be

$$B_0 \simeq 4.5 \times 10^{-12} \left(\frac{H_{_{\rm I}}}{10^{-5}\, M_{_{\rm Pl}}}\right) f^{1/2}(\gamma)\ {\rm G}, \tag{2.38}$$

where the function $f(\gamma)$ is given by Eq. (2.27). Recall that, in the non-helical case, since $\gamma = 0$, we have $f(\gamma) = 1$. Therefore, when parity is conserved, if inflation occurs over energy scales such that $10^{-10} \lesssim H_{_{\rm I}}/M_{_{\rm Pl}} \lesssim 10^{-5}$, then inflationary magnetogenesis can be expected to lead to magnetic fields of strength in the range $10^{-17} \lesssim B_0 \lesssim 10^{-11}\,{\rm G}$ today. As we shall discuss later, to avoid backreaction due to the generated electromagnetic fields, the helicity parameter γ is constrained to be less than about 2.5. We find that, when parity is violated, the above-mentioned strengths of the magnetic fields today are amplified by a factor of about 34 when $\gamma \simeq 1$ and by a factor of about 4.4×10^3 when $\gamma \simeq 2$.

2.3 COUPLING FUNCTION IN SLOW ROLL INFLATIONARY MODELS

Before we go on to discuss inflationary models leading to features in the scalar power spectrum, we shall evaluate the spectra of electromagnetic fields generated in slow roll inflation. Specifically, we shall discuss the forms of the coupling function $J(\phi)$ that are required to generate nearly scale invariant magnetic fields in slow roll inflation. This simple exercise proves to be instructive when we later consider situations involving departures from slow roll.

Note that, in terms of e-folds, the coupling function (2.5) is given by $J(N) = \exp\left[n\,(N - N_{\mathrm{e}})\right]$, where N_{e} denotes the e-fold at the end of inflation. Since the evolution of the field $\phi(N)$ will depend on the inflationary potential, it should be evident that a specific function $J(\phi)$ will not lead to the above-mentioned form of $J(N)$ in all the models. We shall now construct the coupling functions $J(\phi)$ that result in the required $J(N)$ in some of the popular inflationary models that permit slow roll inflation. For these choices of the coupling functions, assuming $n = 2$, we shall also numerically evaluate the power spectra of the electromagnetic fields in these potentials. We shall impose the initial conditions on the electromagnetic modes when $k \simeq 10^2\,\sqrt{J''/J}$, evolve the modes until late times and evaluate the spectra at the end of inflation.

We shall consider three forms for the potential $V(\phi)$. The first model we shall consider is the popular quadratic potential given by

$$V(\phi) = \frac{m^2}{2}\,\phi^2. \tag{2.39}$$

(For convenience, we shall refer to the model as QP in the figures.) In such a potential, it is well known that, under the slow roll approximation, the evolution of the field can be expressed as

$$\phi^2(N) \simeq \phi_{\mathrm{e}}^2 + 4\,\left(N_{\mathrm{e}} - N\right) M_{_{\mathrm{Pl}}}^2, \tag{2.40}$$

where $\phi_{\mathrm{e}} \simeq \sqrt{2}\,M_{_{\mathrm{Pl}}}$ denotes the value of the field at the end of inflation. Clearly, we can arrive at the form of $J(N)$ that we desire if we choose $J(\phi)$ to be (in this context, see Refs. [165, 166])

$$J(\phi) = \exp\left[-\frac{n}{4\,M_{_{\mathrm{Pl}}}^2}\,\left(\phi^2 - \phi_{\mathrm{e}}^2\right)\right]. \tag{2.41}$$

Recall that, COBE normalization determines the value of the parameter m, and we find that we need to choose $m = 7.18 \times 10^{-6}\,M_{_{\mathrm{Pl}}}$ to arrive at the observed scalar amplitude at the pivot scale [52]. To evolve the background, we shall choose the initial values of the field and the first slow roll parameter to be $\phi_{\mathrm{i}} = 16.5\,M_{_{\mathrm{Pl}}}$ and $\epsilon_{1\mathrm{i}} = 7.346 \times 10^{-3}$, respectively. In such a case, we find that inflation lasts for 68.6 e-folds in the model.

The second example we shall consider is the small field model described by the potential

$$V(\phi) = V_0\,\left[1 - \left(\frac{\phi}{\mu}\right)^q\right] \tag{2.42}$$

and we shall focus on the case wherein $q = 2$. (We shall refer to the model as SFM in the figures.) On working in the slow roll approximation, the evolution of the field in such a model can be written as

$$\mu^2\,\ln\left(\frac{\phi}{\phi_{\rm e}}\right) - \frac{1}{2}\,\left(\phi^2 - \phi_{\rm e}^2\right) \simeq 2\,(N - N_{\rm e})\,M_{_{\rm Pl}}^2, \tag{2.43}$$

with $\phi_{\rm e}$ again denoting the value of the field at the end of inflation. Hence, we can arrive at the $J(N)$ of our interest if we choose the coupling function $J(\phi)$ to be

$$J(\phi) \simeq \left(\frac{\phi}{\phi_{\rm e}}\right)^{n\,\mu^2/2M_{_{\rm Pl}}^2}\,\exp\left[-\frac{n}{4\,M_{_{\rm Pl}}^2}\,(\phi^2 - \phi_{\rm e}^2)\right]. \tag{2.44}$$

If we assume that $\mu \gg M_{_{\rm Pl}}$, then we find that $\phi_{\rm e} \simeq \mu$. We shall choose $\mu = 10\,M_{_{\rm Pl}}$. We find that COBE normalization leads to $V_0 = 5.38 \times 10^{-10}\,M_{_{\rm Pl}}^4$. We have set the initial values of the field and the first slow roll parameter to be $\phi_{\rm i} = 1.6\,M_{_{\rm Pl}}$ and $\epsilon_{1{\rm i}} = 5.39 \times 10^{-4}$, which lead to about 68.4 e-folds of inflation.

The third case that we shall consider is the Starobinsky model described by the potential

$$V(\phi) = V_0\,\left[1 - \exp\left(-\sqrt{\frac{2}{3}}\,\frac{\phi}{M_{_{\rm Pl}}}\right)\right]^2. \tag{2.45}$$

As we shall consider another model due to Starobinsky later, we shall refer to this potential as the first Starobinsky model (or, simply as SM1 in the figures). In this model, the evolution of the field in the slow roll approximation is described by the expression

$$N - N_{\rm e} \simeq -\frac{3}{4}\left[\exp\left(\sqrt{\frac{2}{3}}\,\frac{\phi}{M_{_{\rm Pl}}}\right) - \exp\left(\sqrt{\frac{2}{3}}\,\frac{\phi_{\rm e}}{M_{_{\rm Pl}}}\right) - \sqrt{\frac{2}{3}}\,\left(\frac{\phi}{M_{_{\rm Pl}}} - \frac{\phi_{\rm e}}{M_{_{\rm Pl}}}\right)\right], \tag{2.46}$$

where the value of the field at the end of inflation, viz. $\phi_{\rm e}$, is determined by the relation $\exp\,[\sqrt{(2/3)}\,\phi_{\rm e}/M_{_{\rm Pl}}] \simeq 1 + 2/\sqrt{3}$. Therefore, to achieve the desired dependence of the coupling function on the scale factor, we can choose $J(\phi)$ in the model to be

$$J(\phi) = \exp\left\{-\frac{3\,n}{4}\left[\exp\left(\sqrt{\frac{2}{3}}\,\frac{\phi}{M_{_{\rm Pl}}}\right) - \exp\left(\sqrt{\frac{2}{3}}\,\frac{\phi_{\rm e}}{M_{_{\rm Pl}}}\right) - \sqrt{\frac{2}{3}}\,\left(\frac{\phi}{M_{_{\rm Pl}}} - \frac{\phi_{\rm e}}{M_{_{\rm Pl}}}\right)\right]\right\}. \tag{2.47}$$

Again, COBE normalization fixes the overall amplitude of the potential to be $V_0 =$

$1.43 \times 10^{-10}\, M_{_{\rm Pl}}^4$. We have chosen the initial values of the field and the first slow roll parameter to be $\phi_{\rm i} = 5.6\, M_{_{\rm Pl}}$ and $\epsilon_{1\rm i} = 1.453 \times 10^{-4}$. We find that, for the above-mentioned value of V_0, these initial conditions lead to about 69.5 e-folds before inflation ends.

Let us now try to understand the amplitude and shape of the spectra of the electromagnetic fields that arise in these models. Evidently, to arrive at a nearly scale invariant spectrum for the magnetic field, we shall choose to work with $n = 2$. Since the inflationary models introduced above will lead to a scale factor of the slow roll form (rather of the de Sitter type), clearly, we can expect the spectrum of the magnetic field in both the non-helical and helical cases to exhibit a small tilt. Moreover, in these situations, the spectrum of the electric field can be expected to be nearly scale invariant (as the spectrum of the magnetic field) in the helical case, while it can be expected to behave nearly as k^2 in the non-helical case. In Fig. 2.2, we have plotted the spectra arising in the three slow roll models that we discussed above. Interestingly, we find that, while the power spectrum for the non-helical magnetic field arising in the case of the quadratic potential has a small red tilt, the spectral tilt happens to be slightly blue in the cases of the small field and the Starobinsky models. One may have naively imagined that, in such situations, it would be possible to express the spectral tilts $n_{_{\rm B}}$ and $n_{_{\rm E}}$ *completely* in terms of the slow roll parameters. This would have indeed been true had we assumed that $J \propto a^n$ and worked with the slow roll expression for the scale factor (in this context, see App. A). However, our choices for the coupling functions [viz. Eqs. (2.41), (2.44) and (2.47)] do not *exactly* mimic the behaviour of $J \propto a^n$, but contain small departures from it. As a result of these deviations, we find that the spectral indices depend on the parameters describing the potential apart from the slow roll parameters. In App. A, we show that, a simple analytical estimate of the spectral indices indeed match the results we have numerically obtained in all these three cases.

Let us now estimate the amplitude of the electromagnetic spectra in the slow roll models. Let us first consider the non-helical case. It can be easily shown that, when $n = 2$, the amplitude of the spectra of the magnetic and electric fields at the pivot scale $k_\ast$ can be expressed as [cf. Eqs. (2.13)]

$$\frac{\mathcal{P}_{_{\rm B}}(k)}{M_{_{\rm Pl}}^4} \simeq \frac{9\,\pi^2}{16}\,(r\,A_{\rm s})^2\,, \tag{2.48a}$$

$$\frac{\mathcal{P}_{_{\rm E}}(k)}{M_{_{\rm Pl}}^4} \simeq \frac{\mathcal{P}_{_{\rm B}}(k)}{9\,M_{_{\rm Pl}}^4}\,\left(\frac{k_\ast}{k_{\rm e}}\right)^2 \simeq \frac{\mathcal{P}_{_{\rm B}}(k)}{9\,M_{_{\rm Pl}}^4}\,{\rm e}^{-100}. \tag{2.48b}$$

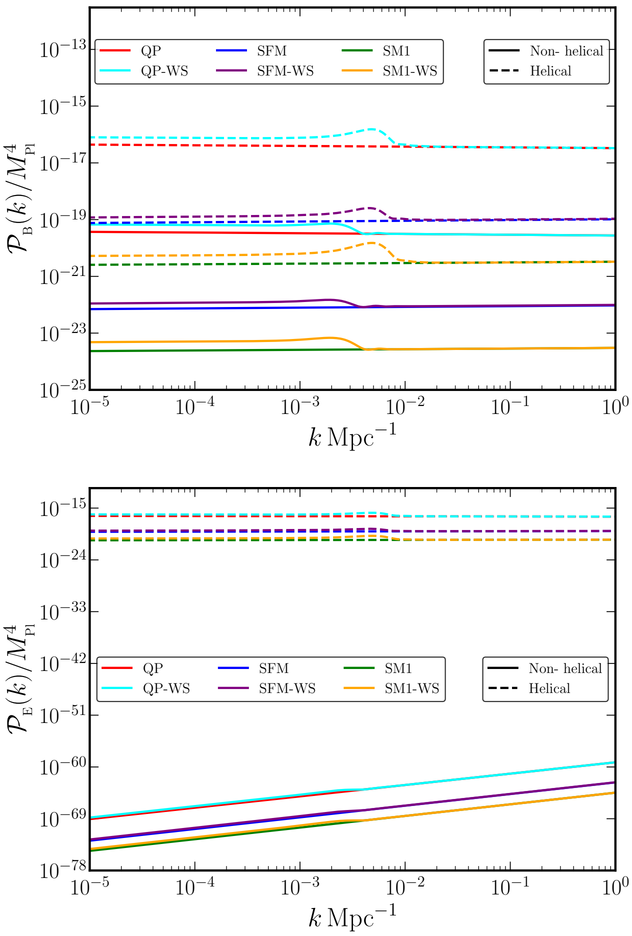

Figure 2.2: The spectra of the magnetic (on top) and electric (at the bottom) fields arising in the three slow roll inflationary models, viz. the quadratic potential (QP, in red), the small field model (SFM, in blue) and the first Starobinsky model (SM1, in green), have been plotted over the CMB scales. We have also plotted the corresponding spectra when a step has been introduced in these potentials (QP-WS, in cyan; SFM-WS, in purple; and SM1-WS, in orange, respectively), a scenario we shall discuss later in Subsec. 2.5.1. Moreover, we have plotted the spectra in both the non-helical (as solid lines) and helical (as dashed lines) cases. We have worked with the parameters mentioned in the text and we have set $n = 2$ in arriving at the spectra. In the helical case, we have set $\gamma = 1$. We should mention that the shapes and amplitudes of these numerically evaluated spectra roughly match the analytical estimates discussed in the text. For instance, the spectrum of the magnetic field is nearly scale invariant in all the models (and in both the non-helical and helical cases), modulo a small step-like feature that arises when a step is introduced in the potential. Also, the spectrum of the electric field behaves as k^2 in the non-helical case and it is scale invariant and matches the amplitude of the magnetic field in the helical case, as we had discussed. Further, clearly, the amplitude of the spectra of the helical magnetic fields are about 10^3 larger than the amplitude of the non-helical fields, as expected when $\gamma = 1$.

In these expressions, $A_{\rm s} = 2.1 \times 10^{-9}$ denotes the observed amplitude of the scalar power spectrum at the pivot scale and r represents the tensor-to-scalar ratio [52, 210]. Note that, we have set $k_{\rm e} \simeq -1/\eta_{\rm e}$, where, as we have indicated earlier, $k_{\rm e}$ is the wave number that leaves the Hubble radius at the end of inflation. Also, in arriving at the final equality in the above expression for $\mathcal{P}_{_{\rm E}}(k)$, we have assumed that the pivot scale leaves the Hubble radius 50 e-folds before the end of inflation, as we have done in the numerical evaluation of the electromagnetic spectra plotted in Fig. 2.2. In the three slow roll inflationary models of our interest, viz. the quadratic potential, the small field model and the Starobinsky model, the tensor-to-scalar ratio can be easily estimated to be $r \simeq (1.6 \times 10^{-1}, 5.79 \times 10^{-2}, 4.8 \times 10^{-3})$. The above expressions then suggest that these models will generate non-helical magnetic fields of amplitudes $\mathcal{P}_{_{\rm B}}(k) \simeq (6.27 \times 10^{-19}, 8.21 \times 10^{-20}, 5.64 \times 10^{-22})\, M_{_{\rm Pl}}^4$. Moreover, according to expressions above, $\mathcal{P}_{_{\rm B}}(k) \simeq 10^{-20}\, M_{_{\rm Pl}}^4$ implies that $\mathcal{P}_{_{\rm E}}(k) \simeq 10^{-66}\, M_{_{\rm Pl}}^4$. These estimates roughly match the results we have arrived at numerically and have illustrated in Fig. 2.2. Further, since $\mathcal{P}_{_{\rm B}}(k) \gg \mathcal{P}_{_{\rm E}}(k)$ in the non-helical case, clearly, most of the energy in the generated electromagnetic fields is in the magnetic field. Lastly, since $\mathcal{P}_{_{\rm B}}(k)/M_{_{\rm Pl}}^4 \simeq (H_{_{\rm I}}/M_{_{\rm Pl}})^4 \lesssim 10^{-20}$ in these models, we have $\mathcal{P}_{_{\rm B}}(k)/M_{_{\rm Pl}}^4 \ll \rho_{_{\rm I}}/M_{_{\rm Pl}}^4 \sim H_{_{\rm I}}^2/M_{_{\rm Pl}}^2$, where, recall that, $\rho_{_{\rm I}}$ is the energy density of the inflaton. This suggests that the energy density in the generated electromagnetic field is smaller than the background energy density and hence these scenarios do not suffer from the backreaction problem (for an early discussion in this context, see Ref. [166], for more recent discussions, see Ref. [81, 211]).

Let us now turn to case of the helical electromagnetic fields. In the helical case, when $n = 2$, the amplitude of the spectra of the magnetic and electric fields can be expressed as [cf. Eqs. (2.26)]

$$\frac{\mathcal{P}_{_{\rm B}}(k)}{M_{_{\rm Pl}}^4} \simeq \frac{9\,\pi^2}{16}\, (r\, A_{\rm s})^2\, f(\gamma), \tag{2.49a}$$

$$\frac{\mathcal{P}_{_{\rm E}}(k)}{M_{_{\rm Pl}}^4} \simeq \frac{\mathcal{P}_{_{\rm B}}(k)}{M_{_{\rm Pl}}^4}\, \gamma^2, \tag{2.49b}$$

where $f(\gamma)$ is given by Eq. (2.27). Note that, in contrast to the non-helical case, the energy density in the electric field is now comparable to that of the magnetic field and, in fact, the contribution due to electric fields dominates when $\gamma > 1$. Therefore, if we need to avoid backreaction due to the helical electromagnetic fields which have been generated, we require that $\mathcal{P}_{_{\rm B}}(k) + \mathcal{P}_{_{\rm E}}(k) \ll \rho_{_{\rm I}}$. Since we are considering inflationary models wherein $H_{_{\rm I}}/M_{_{\rm Pl}} \lesssim 10^{-5}$, on using the above expressions for the spectra of the electromagnetic fields, we find that the condition for avoiding backreaction leads to

$f(\gamma)\,(1+\gamma^2) \lesssim 10^{10}$. This limits the value of γ to be $\gamma \lesssim 2.5$. In Fig. 2.2, assuming $\gamma = 1$, we have also plotted the spectra of the helical electromagnetic fields in the three inflationary models discussed above. When $\gamma = 1$, we find that $f(\gamma) \simeq 10^3$. As should be evident from the figure, the spectra of the helical magnetic fields are indeed amplified by the factor of 10^3 when compared to the non-helical case in all the models. Also, it should be clear that, the spectra of the helical electric and magnetic fields are comparable, as expected.

2.4 INFLATIONARY MODELS LEADING TO FEATURES IN THE SCALAR POWER SPECTRUM

In this section, we shall discuss specific examples wherein deviations from slow roll inflation lead to features in the scalar power spectrum. In due course, we shall discuss the effects of such deviations on the spectra of the electromagnetic fields. When departures from slow roll occur, in general, the background and the modes describing the scalar perturbations prove to be difficult to evaluate analytically, and one resorts to numerics. We shall begin by recalling a few essential points regarding the evaluation of the scalar power spectrum.

Recall that f_k denote the Fourier mode functions associated with the curvature perturbation. As we had discussed in the last chapter, the mode functions f_k satisfy the differential equation (see, for instance, the reviews [63, 64, 71, 73, 212–218])

$$f_k'' + 2\,\frac{z'}{z}\,f_k' + k^2\,f_k = 0, \tag{2.50}$$

where the quantity z is given by $z = \sqrt{2\,\epsilon_1}\,M_{_{\rm Pl}}\,a$, with $\epsilon_1 = -\dot{H}/H^2$ being the first slow roll parameter. Moreover, in terms of the Mukhanov-Sasaki variable $v_k = f_k\,z$, the above equation reduces to

$$v_k'' + \left(k^2 - \frac{z''}{z}\right)\,v_k = 0. \tag{2.51}$$

The standard Bunch-Davies initial conditions are imposed on the variable v_k at very early times when $k \gg \sqrt{z''/z}$, which corresponds to the modes being in sub-Hubble regime. As we had seen earlier, the scalar power spectrum is defined as

$$\mathcal{P}_{_{\rm S}}(k) = \frac{k^3}{2\,\pi^2}\,\vert f_k\vert^2 = \frac{k^3}{2\,\pi^2}\,\frac{\vert v_k\vert^2}{z^2}. \tag{2.52}$$

The mode functions f_k are evolved from the Bunch-Davies initial conditions and the power spectra are evaluated in the super-Hubble regime at late times, i.e. when $k \ll \sqrt{z''/z}$. Since the modes oscillate in the sub-Hubble domain and the amplitude of the scalar modes are known to freeze on super-Hubble scales, numerically, one often finds that it is sufficient to evolve the modes from $k \simeq 10^2 \sqrt{z''/z}$ and evaluate the power spectrum when $k \simeq 10^{-5} \sqrt{z/''z}$ (in this context, see, for instance, Ref. [219]).

2.4.1 Potentials with a step

The first scenario leading to features in the scalar power spectrum that we shall consider are inflationary potentials wherein a step has been introduced by hand. Given an inflationary model described by the potential $V(\phi)$, we shall introduce a step in the potential as follows (for an early discussion, see Ref. [220]):

$$V_{\rm step}(\phi) = V(\phi)\, \left[1 + \alpha \tanh\left(\frac{\phi - \phi_0}{\Delta\phi}\right)\right], \tag{2.53}$$

where, evidently, ϕ_0, α and $\Delta\phi$ denote the location, the height and the width of the step. For the original potential $V(\phi)$, we shall consider the three models admitting slow roll we had discussed in the previous section. (We shall refer to these models with a step in their potentials as QP-WS, SFM-WS and SM1-WS in the figures.) Also, as far as the parameters regarding the original potential is concerned, we shall work with the values we had mentioned earlier. Moreover, we shall work with the following values of the three parameters describing the step: $(\phi_0, \alpha, \Delta\phi) = (14.6616\, M_{_{\rm Pl}}, 1.55177 \times 10^{-3}, 2.60584 \times 10^{-2}\, M_{_{\rm Pl}}), (2.14\, M_{_{\rm Pl}}, -0.1153 \times 10^{-3}, 0.0070\, M_{_{\rm Pl}})$ and $(5.3052\, M_{_{\rm Pl}}, 5.0 \times 10^{-5}, 5.0 \times 10^{-3}\, M_{_{\rm Pl}})$ in the cases of the quadratic potential, the small field model and the first Starobinsky model, respectively.

As we described above, to arrive at the scalar power spectrum, we impose the initial conditions on the modes when $k \simeq 10^2 \sqrt{z''/z}$ and evaluate the power spectrum when $k \simeq 10^{-5} \sqrt{z''/z}$. Moreover, in these three models, we shall assume that the pivot scale of $k_\ast = 0.05\, {\rm Mpc}^{-1}$ leaves the Hubble radius 50 e-folds before the end of inflation. The scalar power spectrum that arises with the introduction of the step in the quadratic potential is illustrated in Fig. 2.3. As one would expect, the introduction of the step in the potential leads to a short period of deviation from slow roll as the field crosses the step. The deviation from slow roll, in turn, generates a short burst of oscillations in the scalar power spectrum over wave numbers that leave the Hubble radius during the period of departure from slow roll. It is known that such features in the power spectrum can improve the fit to the CMB data to a certain extent [183, 184].

2.4.2 Suppressing power on large scales

Since the advent of the WMAP data, it has been known that a suppression in power on large scales comparable to the Hubble radius today leads to an improvement in the fit to the CMB data (for earlier discussions, see Refs. [178–182, 185, 186]; for a recent discussion, see Ref. [189]). In this subsection, we shall discuss two models that have often been considered in this context.

The first example that we shall consider is a model due to Starobinsky, which is governed by the potential [221]

$$V(\phi) = \begin{cases} V_0 + A_+\,(\phi - \phi_0), & \text{for } \phi > \phi_0, \\ V_0 + A_-\,(\phi - \phi_0), & \text{for } \phi < \phi_0. \end{cases} \tag{2.54}$$

To distinguish from the Starobinsky model (2.45) which permits slow roll inflation that we had discussed earlier, we shall refer to the above potential as the second Starobinsky model (or, simply as SM2 in the figures). Evidently, the model consists of a linear potential with a sudden change in its slope at the point ϕ_0. If we assume that the constant term V_0 in the potential is dominant, then the first slow roll parameter remains small and the scale factor can be described by the de Sitter form. Under this condition, it is possible to arrive at analytical solutions for the evolution of the background [221, 222]. We shall discuss the evolution of the field later, when we consider the coupling between the inflaton and the electromagnetic field. It is found that, as the field crosses ϕ_0, while the first slow roll parameter remains small, the second and the third slow roll parameters turn large leading to a departure from slow roll. Also, notice that the second derivative of the potential is described by a Dirac delta function with its peak at ϕ_0. It is the Dirac delta function that dominates the behaviour of the quantity z''/z that appears in the Mukhanov-Sasaki equation (2.51). Working in the de Sitter approximation to describe the scale factor as well as the scalar mode functions f_k, the deviation from slow roll could be accounted for by essentially considering the effects due to the Dirac delta function. In fact, under these conditions, it is possible to arrive at an analytical form for the power spectrum [189, 221, 222]. We shall instead arrive at the scalar power spectrum numerically. In order to permit numerical analysis, we shall modify

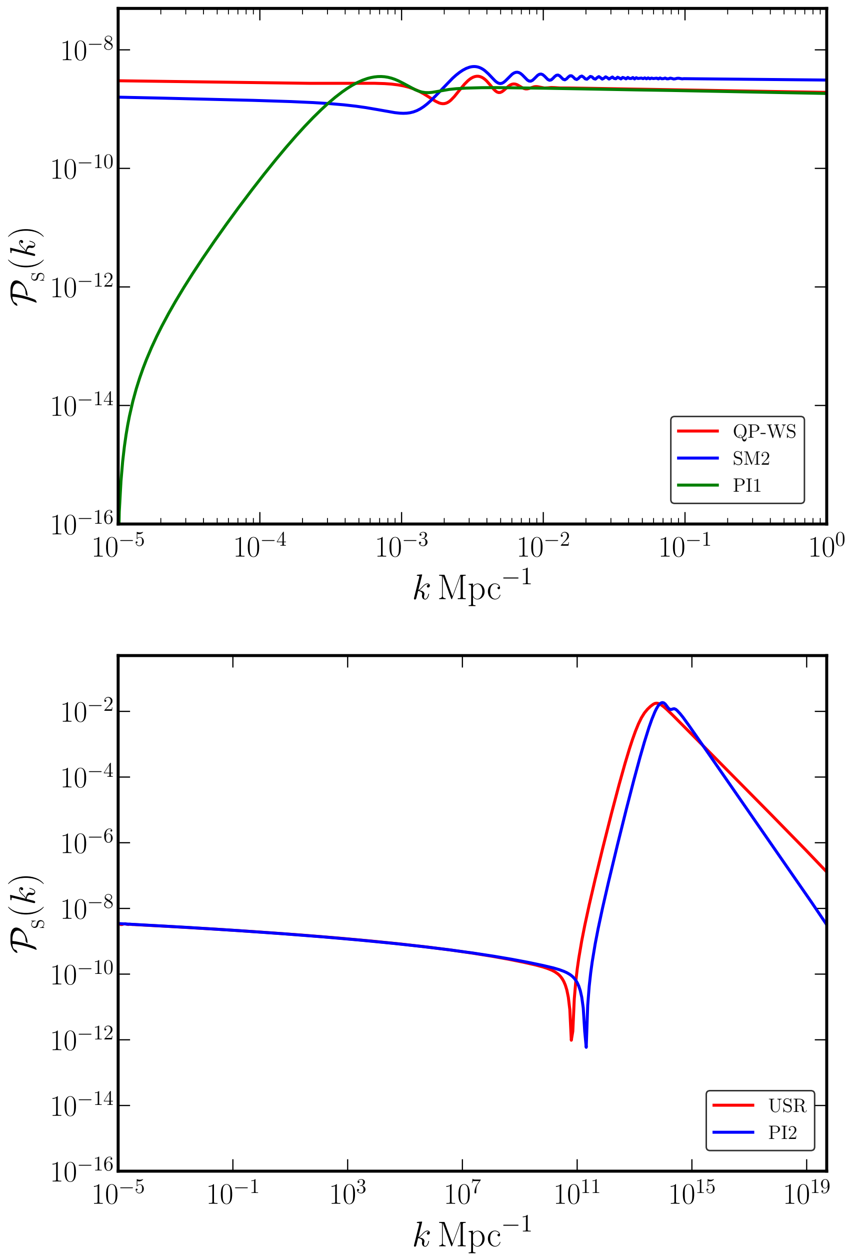

Figure 2.3: The scalar power spectra with features over the CMB and smaller scales have been plotted in some of the inflationary models that we have considered. We have plotted the scalar spectra with features over the CMB scales (on top) in the cases of the quadratic potential with a step (QP-WS, in red), the second Starobinsky model described by the linear potential with a sharp change in its slope (SM2, in blue), and the first punctuated inflation model (PI1, in green). We have also plotted the scalar power spectra with a peak in power at small scales (at the bottom) that are generated in the ultra slow roll (USR, in red) and the second punctuated (PI2, in blue) inflation models. As we shall point out later, the scalar spectra with a sharp rise in power on small scales are often considered to produce significant amount of PBHs.

the potential so that the change in the slope is smooth and not abrupt. We shall assume that the potential is given by

$$\begin{aligned} V(\phi) &= V_0 + \frac{1}{2}\left(A_+ + A_-\right)\left(\phi - \phi_0\right) \\ &\quad + \frac{1}{2}\left(A_+ - A_-\right)\left(\phi - \phi_0\right)\tanh\left(\frac{\phi - \phi_0}{\Delta\phi}\right), \end{aligned} \tag{2.55}$$

and work with the following values of the parameters involved: $V_0 = 2.98 \times 10^{-9}\, M_{_{\rm Pl}}^4$, $A_+ = 4.35881 \times 10^{-10}\, M_{_{\rm Pl}}^3$, $A_- = 2.499 \times 10^{-10}\, M_{_{\rm Pl}}^3$, $\phi_0 = 5.628\, M_{_{\rm Pl}}$ and $\Delta\phi = 10^{-4}\,\phi_0$. We shall choose the initial value of the field and the first slow roll parameter to be $\phi_{\rm i} = 8.4348\, M_{_{\rm Pl}}$ and $\epsilon_{1{\rm i}} = 10^{-4}$.

The second model that we shall consider is the so-called punctuated inflationary model described by the potential (in this context, see Refs. [181, 182, 189])

$$V(\phi) = \frac{m^2}{2}\,\phi^2 - \frac{2\,m^2}{3\,\phi_0}\,\phi^3 + \frac{m^2}{4\,\phi_0^2}\,\phi^4. \tag{2.56}$$

It is easy to see that this potential contains a point of inflection at ϕ_0. The point of inflection leads to two epochs of slow roll sandwiching a brief period of departure from inflation, which has led to the name of punctuated inflation. As we shall consider another model of punctuated inflation which leads to enhanced power at small scales in the following subsection, we shall refer to the above potential as the first model of punctuated inflation (or, simply as PI1 in the figures). In this case, we shall work with the following values of the parameters involved: $m = 7.17 \times 10^{-8}\, M_{_{\rm Pl}}$ and $\phi_0 = 1.9654\, M_{_{\rm Pl}}$. We shall choose the initial values of the field and the first slow roll parameter to be $\phi_{\rm i} = 12.0\, M_{_{\rm Pl}}$ and $\epsilon_{1{\rm i}} = 2 \times 10^{-3}$.

The drawback of these two models is that they lead to much longer epochs of inflation than the nominally required 60 odd e-folds [189]. In the Starobinsky model (2.54), we stop the evolution by hand after 72 e-folds, and assume that the pivot scale leaves the Hubble radius about 44.5 e-folds earlier. In the case of the punctuated inflationary model (2.56), inflation ends naturally after nearly 110.5 e-folds and the pivot scale is assumed to exit the Hubble radius about 91 e-folds before the termination of inflation. The departure from slow roll in these two potentials leads to a step-like feature in the scalar power spectrum, as illustrated in Fig. 2.3.

2.4.3 Enhancing power on small scales

Over the last few years, there has been a considerable interest in examining models of inflation that lead to enhanced power on scales much smaller than the CMB scales (in this context, see, for example, Refs. [196–200, 202, 203]). Apart from leading to copious production of PBHs, these models can also generate secondary gravitational waves of considerable strengths, which can possibly be detected by the current and forthcoming gravitational wave observatories. Most of these inflationary models contain a point of inflection (just as the model of punctuated inflation we discussed in the previous subsection), which permits a brief period wherein the first slow roll parameter decreases exponentially. Such a period of ultra slow roll proves to be responsible for enhancing the power on small scales in these models.

We shall consider two potentials that lead to enhanced power on small scales. The first model that we shall consider, which leads to a brief period of ultra slow roll, is described by the potential [199]

$$V(\phi) = V_0 \left\{\tanh\left(\frac{\phi}{\sqrt{6}\,M_{_{\mathrm{Pl}}}}\right) + A\,\sin\left[\frac{1}{f_\phi}\tanh\left(\frac{\phi}{\sqrt{6}\,M_{_{\mathrm{Pl}}}}\right)\right]\right\}^2. \tag{2.57}$$

(We shall refer to the model as USR in the figures.) We shall choose to work with the following values of the parameters involved: $V_0 = 2\times 10^{-10}\,M_{_{\mathrm{Pl}}}^4$, $A = 0.130383$ and $f_\phi = 0.129576$. For these values of the parameters, the point of inflection in the potential is located at $\phi_0 = 1.05\,M_{_{\mathrm{Pl}}}$ [202]. Also, if we choose the initial value of the field to be $\phi_{\mathrm{i}} = 6.1\,M_{_{\mathrm{Pl}}}$, with $\epsilon_{1\mathrm{i}} = 10^{-4}$, we obtain about 66 e-folds of inflation in the model. Moreover, we shall assume that the pivot scale exits the Hubble radius about 56.2 e-folds prior to the termination of inflation.

The second model that we shall consider which permits punctuated inflation is described by the potential [199, 203]

$$\begin{aligned} V(\phi) \;=\; V_0 \Biggl[&c_0 + c_1\,\tanh\left(\frac{\phi}{\sqrt{6}\,M_{_{\mathrm{Pl}}}}\right) + c_2\,\tanh^2\left(\frac{\phi}{\sqrt{6}\,M_{_{\mathrm{Pl}}}}\right) \\ &+ c_3\,\tanh^3\left(\frac{\phi}{\sqrt{6}\,M_{_{\mathrm{Pl}}}}\right)\Biggr]^2. \end{aligned} \tag{2.58}$$

(We shall refer to the model as PI2 in the figures.) In this case, we shall work with the following values for the parameters involved: $V_0 = 2.1\times 10^{-10}\,M_{_{\mathrm{Pl}}}^4$, $c_0 = 0.16401$, $c_1 = 0.3$, $c_2 = -1.426$ and $c_3 = 2.20313$. As in the previous model, this potential also contains a point of inflection. For the above values for the parameters, the point of inflection is located at $\phi_0 = 0.53\,M_{_{\mathrm{Pl}}}$. If we set the initial value of the field to be

$\phi_{\rm i} = 7.4\, M_{_{\rm Pl}}$ and choose $\epsilon_{1{\rm i}} = 10^{-3}$, for the above choice of parameters, we find that inflation is terminated after about 67.8 e-folds. Also, we shall assume that the pivot scale leaves the Hubble radius about 54.5 e-folds before the end of inflation.

The scalar power spectra that arise in the above two potentials are illustrated in Fig. 2.3. Note that the power spectra exhibit a sharp rise in power on small scales in these models. As has been repeatedly emphasized in the literature, it is the period of ultra slow roll, with its rather small value for the first slow roll parameter ϵ_1, that turns out to be responsible for the increased power in the scalar power spectrum on small scales (in this context, see, for instance, Ref. [223]).

2.5 EFFECTS OF DEVIATIONS FROM SLOW ROLL ON THE ELECTROMAGNETIC POWER SPECTRA

Let us now turn to understand the effects of deviations from slow roll on the power spectra of electric and magnetic fields.

2.5.1 In potentials with a step

As we discussed earlier and illustrated in Fig. 2.3, the introduction of the step in a potential which otherwise admits only slow roll inflation leads to a short burst of oscillations in the scalar power spectrum. In Sec. 2.3, we had constructed coupling functions $J(\phi)$ [as given by Eqs. (2.41), (2.44) and (2.47)] in the three slow roll models (2.39), (2.42) and (2.45) so that they lead to nearly scale invariant spectra for the magnetic field when $n = 2$. Even after the introduction of the step, we have chosen to work with the above mentioned coupling functions $J(\phi)$ that we had constructed in the slow roll approximation. In Fig. 2.2, we have plotted the resulting spectra of the magnetic and electric fields arrived at numerically in both the non-helical and helical cases. As should be clear from the figure, the step in the inflationary potential only has a small effect on the spectra of the electromagnetic fields. It essentially generates a small step-like feature in the power spectra. This is not surprising since, for the choices of the parameters we have worked with, the step in the potential leads to only a small and brief departure from slow roll inflation.

2.5.2 In models leading to suppression of power on large scales

In this context, we shall first consider the second Starobinsky model described by the potential (2.54). As we had mentioned earlier, in the model, the field rolls slowly until it reaches ϕ_0 where the slope of the potential changes from A_+ to $A-$. In the slow roll approximation, the evolution of the field prior to it crossing ϕ_0 can be determined to be [221, 222]

$$\phi_+(N) \simeq -\left(\frac{V_0}{A_+} - \phi_0\right) + \left[\left(\phi_{\rm i} - \phi_0 + \frac{V_0}{A_+}\right)^2 - 2\, M_{_{\rm Pl}}^2\, N\right]^{1/2}, \tag{2.59}$$

where $\phi_{\rm i}$ is the initial value of the field (i.e. at $N = 0$). If we choose to work with a suitably large value of V_0 so that it dominates the potential, then the above expression simplifies to be

$$\phi_+(N) \simeq \phi_{\rm i} - \frac{A_+\, M_{_{\rm Pl}}^2}{V_0}\, N. \tag{2.60}$$

Evidently, once the field has crossed ϕ_0 and slow roll has been restored, the evolution of the field can be expressed as

$$\phi_-(N) \simeq -\left(\frac{V_0}{A_-} - \phi_0\right) + \left[\left(\frac{V_0}{A_-}\right)^2 - 2\, M_{_{\rm Pl}}^2\, (N - N_0)\right]^{1/2}, \tag{2.61}$$

where N_0 denotes the e-fold when the field crosses ϕ_0. If we again assume that V_0 is dominant, then the above expression reduces to

$$\phi_-(N) \simeq \phi_0 - \frac{A_-\, M_{_{\rm Pl}}^2}{V_0}\, (N - N_0). \tag{2.62}$$

We should clarify here that, in arriving at the above expressions for the evolution of the field after it has crossed ϕ_0, we have ignored the effects that arise due to the change in the slope. As we had described, the change in the slope causes a brief period of departure from slow roll. If we take into account the effects due to the deviation from slow roll, the evolution of the field after it has crossed ϕ_0 can be obtained to be [221, 222]

$$\phi_-(N) \simeq \phi_0 + \frac{\Delta A\, M_{_{\rm Pl}}^2}{3\, V_0}\, \left[1 - {\rm e}^{-3\,(N - N_0)}\right] - \frac{A_-\, M_{_{\rm Pl}}^2}{V_0}\, (N - N_0), \tag{2.63}$$

where $\Delta A = (A_- - A_+)$. Upon comparing the above two equations, it should be obvious that it is the intermediate term that accounts for the departure from slow roll which occurs as the field crosses ϕ_0. On using the above expressions describing the behaviour of the field, one can show that, while the first slow roll parameter remains small, the second and the third slow roll parameters turn large as the field crosses ϕ_0.

Let us now turn to constructing the coupling function $J(\phi)$ for the second Starobinsky model. As we had done in the case of the models discussed in Sec. 2.3, we can choose to work with the solutions for the field in the slow roll approximation. If we choose to do so, we are left with two choices, viz. the slow roll solutions (2.59) and (2.61) for the field before and after the transition. In other words, we can work with either of the following choices for the coupling function:

$$\begin{aligned} J_+(\phi) &= J_{0+}\exp\left\{-\frac{n}{2\,M_{_{\rm Pl}}^2}\left[\left(\phi_+ - \phi_0 + \frac{V_0}{A_+}\right)^2\right.\right. \\ &\quad \left.\left. -\left(\phi_{\rm i} - \phi_0 + \frac{V_0}{A_+}\right)^2\right]\right\}, \end{aligned} \tag{2.64a}$$

$$\begin{aligned} J_-(\phi) &= J_{0-}\exp\left\{-\frac{n}{2\,M_{_{\rm Pl}}^2}\left[\left(\phi_- - \phi_0 + \frac{V_0}{A_-}\right)^2\right.\right. \\ &\quad \left.\left. -\left(\frac{V_0}{A_-}\right)^2 - 2\,N_0\,M_{_{\rm Pl}}^2\right]\right\}, \end{aligned} \tag{2.64b}$$

where the constants $J_{0\pm}$ are to be chosen suitably so that $J_\pm(\phi_{\rm e}) = 1$, i.e. the value of J is unity at the end of inflation.

The power spectra of the magnetic field for the two coupling functions $J_\pm(\phi)$ for the case of $n = 2$ are plotted in Fig. 2.4 for both the non-helical and helical cases. A few points needs to be emphasized regarding the spectra we have obtained. Firstly, the spectra are scale invariant only over either large or small scales. Let k_0 be the mode which leaves the Hubble radius when the field crosses ϕ_0. Then, clearly, for the choice of the coupling functions $J_+(\phi)$ and $J_-(\phi)$, the magnetic field spectra are scale invariant only over $k < k_0$ and $k > k_0$, respectively. This should not come as a surprise as the coupling functions $J_\pm(\phi)$ have been constructed based on the behaviour of the field in the slow roll approximation before and after it crosses ϕ_0. Secondly, when $n = 2$, for the coupling function $J_+(\phi)$, the spectral index of the magnetic field for $k > k_0$ can be estimated to be $n_{_{\rm B}} = -4\,\Delta A/A_+$, while for the function $J_-(\phi)$ the index over large scales can be determined to be $n_{_{\rm B}} = 4\,\Delta A/A_-$. Since $\Delta A = (A_- - A_+) < 0$, $n_{_{\rm B}} > 0$ (i.e. the spectrum is blue) in the first case and $n_{_{\rm B}} < 0$ (i.e. the spectrum is red) in the second. These estimates are indeed corroborated by the numerical results we have plotted in Fig. 2.4. Thirdly, while the amplitude of the magnetic field is considerably suppressed over large scales if we work with the coupling function $J_+(\phi)$, it is considerably enhanced over these scales in the case of $J_-(\phi)$. In fact, for the choice $J_-(\phi)$, the strength of the electromagnetic fields on large scales are

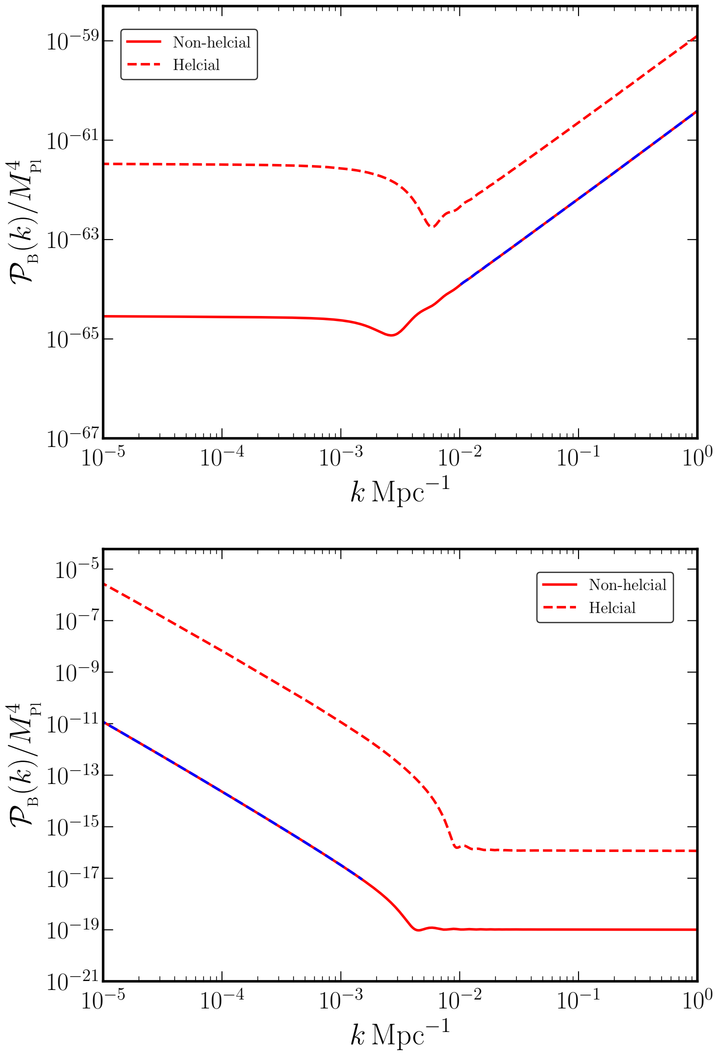

Figure 2.4: The power spectra of the magnetic field arising in the second Starobinsky model for the two choices of coupling functions $J_{+}(\phi)$ (on top) and $J_{-}(\phi)$ (at the bottom) [cf. Eqs. (2.64)] have been plotted for $n = 2$ in the non-helical (in solid red) as well as the helical (in dashed red) cases. A linear fit (indicated in dashed blue) to the non-helical power spectra over the small and the large scales (on the left and the right) lead to the spectral indices $n_{\rm B} = 1.75$ and $n_{\rm B} = -2.72$, respectively. For the values of the parameters we have worked with, the analytical estimates for these indices prove to be $n_{\rm B} = 1.71$ and $n_{\rm B} = -2.98$, which are close to the numerically determined values. As in Fig. 2.2, we have set the helicity parameter γ to be unity. Moreover, note that, for $\gamma = 1$, the spectra of the magnetic field over the scale invariant domain is about 10^3 times larger in the helical case when compared to the non-helical one, as we had estimated earlier. Lastly, we should add that, when the coupling function is given by $J_{-}(\phi)$, the strength of the magnetic fields generated is fairly large and hence the scenario will lead to a significant backreaction.

considerable and hence they will lead to a significant backreaction.

Let us now turn to the first punctuated inflation model described by the potential (2.56). It proves to be difficult to obtain an analytical solution for the evolution of the background scalar field in such a potential. Therefore, we shall solve for the background numerically to first arrive at $\phi(N)$. We then choose a quadratic function of the form $N(\phi) = a_1\,(\phi^2/M_{_{\rm Pl}}^2) + b_1\,(\phi/M_{_{\rm Pl}}) + c_1$ to fit the numerical solution we have obtained in the initial slow roll regime. When doing so, for the specific values of the parameters of the potential and the initial conditions that we have worked with, we obtain the values of the three dimensionless fitting parameters to be $(a_1, b_1, c_1) = (-0.104, -0.0408, 15.949)$. Finally, to evaluate the spectra of the electromagnetic fields, we shall work with a coupling function of the form

$$J(\phi) = \exp\left\{n\,\left[a_1\,\left(\frac{\phi^2-\phi_{\rm e}^2}{M_{_{\rm Pl}}^2}\right) + b_1\,\left(\frac{\phi-\phi_{\rm e}}{M_{_{\rm Pl}}}\right)\right]\right\} \tag{2.65}$$

and, note that, $J(\phi)$ reduces to unity at $\phi_{\rm e}$, as required. In Fig. 2.5, we have plotted the spectra of the resulting magnetic and electric fields in both the non-helical and helical cases for $n = 2$. We need to highlight a few points regarding the figure. The spectra of the electric and magnetic fields in the helical case and the spectrum of the magnetic field in the non-helical case are scale invariant over large scale modes that leave the Hubble radius during the initial stages of slow roll. Also, over the scale invariant domain, the helical amplitudes are 10^3 times larger than the non-helical amplitudes, as expected for $\gamma = 1$. For the choice of the coupling function that we have worked with, we find that, the spectra of both the magnetic and electric fields behave as k^4 (in the absence as well as in the presence of helicity) over the small scale modes which leave the Hubble radius at later stages. As we shall discuss in more detail in the following section, when the field approaches the point of inflection in the potential and enters a phase of ultra slow roll inflation, the coupling function J hardly changes. This implies that $J''/J \simeq 0$, which is responsible for the k^4 behaviour of the spectra at small scales. We should also point out that this behaviour significantly suppresses the scale invariant amplitude of the magnetic field over large scales.

The two examples discussed in this subsection point to the fact that unless the coupling function is suitably chosen, strong departures from slow roll inflation result in spectra of magnetic fields that contain significant deviations from scale invariance.

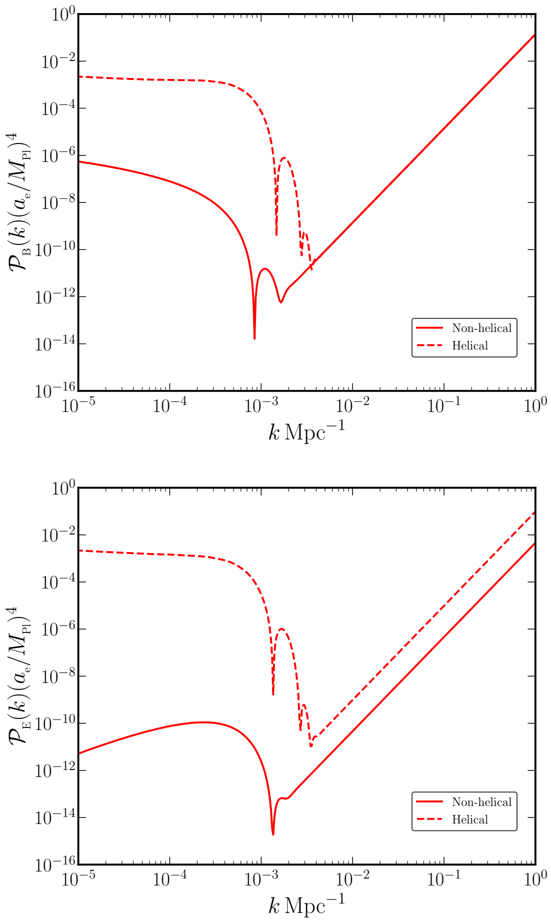

Figure 2.5: The spectra of the magnetic (on top) and electric (at the bottom) fields arising in the case of the first punctuated inflation model (2.56) have been plotted for both the non-helical (in solid red) and helical (in dashed red) cases. In arriving at these spectra, we have worked with the coupling function (2.65) and, as earlier, we have set the helicity parameter γ to be unity. As expected, over the large scales, when the modes leave the Hubble radius during the initial stages of slow roll inflation, the spectra of the magnetic as well as the electric fields in the helical case are nearly scale invariant and also have roughly the same amplitude. Moreover, the strengths of the helical magnetic fields are 10^3 times greater in amplitude than the non-helical fields over the scale invariant domain, as one may have guessed. Further, note that the spectra behave as k^4 over small scales. This behaviour can be attributed to the fact that, as the background scalar field approaches the point the inflection, leading to an epoch of ultra slow roll inflation, the non-minimal coupling function J hardly evolves. We should point out that, in the above plots, we have multiplied the spectra of the electromagnetic fields by the factor of by $a_{\rm e}^4$ (in contrast to the other figures) since their amplitudes turn out to be extremely small otherwise. As will be evident from the discussion in the following subsection, the rather small amplitudes in these cases can be attributed to a very early onset of the ultra slow roll epoch required to suppress the scalar power on the largest scales.

2.5.3 In models leading to enhanced power on small scales

Let us now turn to the two models described by the potentials (2.57) and (2.58) that lead to enhanced scalar power on small scales. As in the case of the first punctuated inflation model we discussed in the previous subsection, these models too lead to an epoch of ultra slow roll inflation wherein the first slow roll parameter decreases exponentially over a short period before it starts rising leading to the end of inflation. It is the sharp decrease in the first slow roll parameter that is responsible for the rise in the scalar power in such models (in this context, see Refs. [196–200, 202, 203]).

In these models, one chooses the parameters of the background potential as well as the initial conditions such that there occurs an extended period of slow roll inflation which generates scalar and tensor power spectra that are consistent with the CMB observations on large scales. If we require a nearly scale invariant spectrum of the magnetic field over the CMB scales, then, evidently, we need to choose a coupling function $J(\phi)$ that is based on the evolution of the field during the long initial epoch of slow roll inflation. Since the potentials (2.57) and (2.58) do not seem to admit simple analytical solutions, we repeat the exercise we had carried out in the case of the first punctuated inflation model. Utilizing the numerical solution, we arrive at $N(\phi)$ and fit a polynomial to describe the function. We find that we can fit fourth and sixth order polynomials to describe the $N(\phi)$ in the potentials (2.57) and (2.58). The coupling functions that we shall work with in these two cases can be expressed as

$$\begin{aligned} J(\phi) &= \exp\left\{n\left[a_2\left(\frac{\phi^4-\phi_{\mathrm{e}}^4}{M_{_{\mathrm{Pl}}}^4}\right)+b_2\left(\frac{\phi^3-\phi_{\mathrm{e}}^3}{M_{_{\mathrm{Pl}}}^3}\right)\right.\right.\\ &\quad\left.\left.+c_2\left(\frac{\phi^2-\phi_{\mathrm{e}}^2}{M_{_{\mathrm{Pl}}}^2}\right)+d_2\left(\frac{\phi-\phi_{\mathrm{e}}}{M_{_{\mathrm{Pl}}}}\right)\right]\right\}, \qquad (2.66a)\\ J(\phi) &= \exp\left\{n\left[a_3\left(\frac{\phi^6-\phi_{\mathrm{e}}^6}{M_{_{\mathrm{Pl}}}^6}\right)+b_3\left(\frac{\phi^5-\phi_{\mathrm{e}}^5}{M_{_{\mathrm{Pl}}}^5}\right)\right.\right.\\ &\quad+c_3\left(\frac{\phi^4-\phi_{\mathrm{e}}^4}{M_{_{\mathrm{Pl}}}^4}\right)+d_3\left(\frac{\phi^3-\phi_{\mathrm{e}}^3}{M_{_{\mathrm{Pl}}}^3}\right)\\ &\quad\left.\left.+e_3\left(\frac{\phi^2-\phi_{\mathrm{e}}^2}{M_{_{\mathrm{Pl}}}^2}\right)+f_3\left(\frac{\phi-\phi_{\mathrm{e}}}{M_{_{\mathrm{Pl}}}}\right)\right]\right\}, \qquad (2.66b)\end{aligned}$$

with the dimensionless fitting parameters being given by $(a_2, b_2, c_2, d_2) = (-0.184, 1.822, -7.040, 10.676)$ and $(a_3, b_3, c_3, d_3, e_3, f_3) = (-1.53 \times 10^{-3}, 2.37 \times 10^{-2}, -0.158, 0.439, -0.459, -0.778)$, respectively.

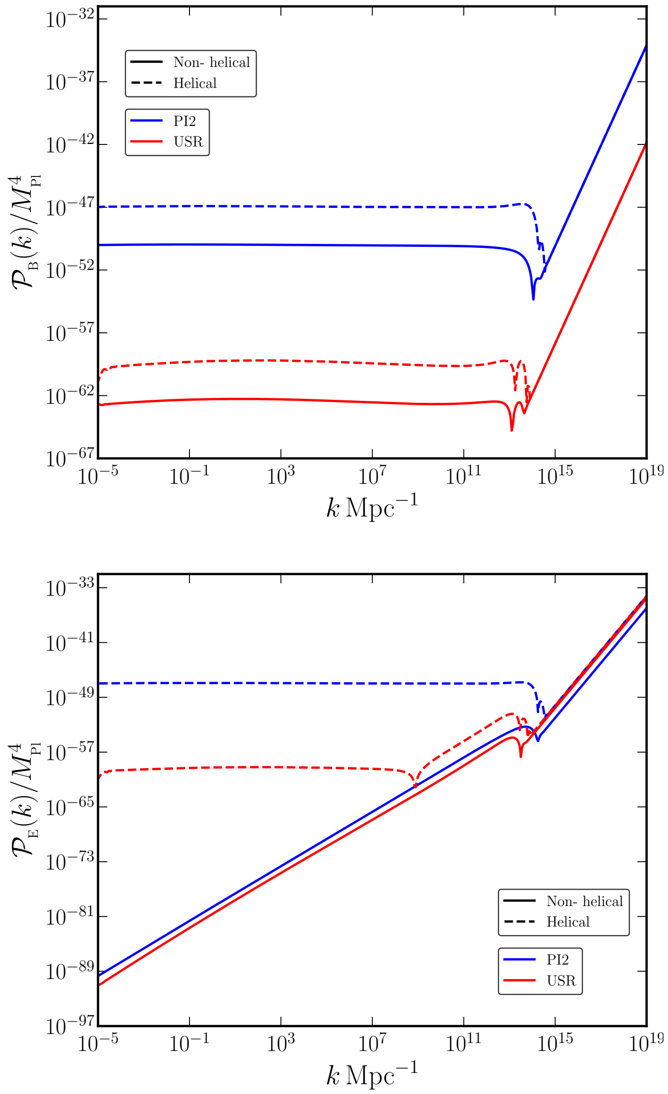

Figure 2.6: The spectra of the magnetic (on top) and electric (at the bottom) fields arising in the ultra slow roll inflationary model (2.57) (USR, in red) and the second punctuated inflationary model (2.58) (PI2, in blue) have been plotted in the non-helical (as solid lines) and helical (as dashed lines) cases, respectively. Note that we have worked with the coupling functions (2.66) to arrive at these spectra. Also, we have chosen $n = 2$ and set $\gamma = 1$, as we have done earlier. Clearly, the spectra of the electromagnetic fields in both the non-helical and helical cases are along expected lines, as we have discussed in the text. In particular, we should point out that the spectra in the two models behave as k^4 at large wave numbers. This behaviour arises due to the fact the the coupling functions cease to evolve as the field approaches the point of inflection in these models. In such a situation, the electromagnetic modes effectively behave as in the conformally invariant case, leading to the k^4 behaviour. We should also add that, apart from changing the shape of the spectra at small scales, the background evolution significantly suppresses the power in the spectra on large scales.

In Fig. 2.6, we have plotted the spectra of the electromagnetic fields that arise for the above choices of the coupling functions in the two models of our interest. We should mention that, in arriving at the spectra, we have set $n = 2$ and $\gamma = 1$, as we have done before. The following points are clear from the figure. Note that the spectra of the magnetic fields in both the non-helical and helical cases are nearly scale invariant over large scales. This is because the coupling functions have been determined by the slow roll behaviour of the field. Also, as we have seen earlier, the magnitude of the helical magnetic field is about 10^3 larger than the non-helical field over the scale invariant domain. Moreover, over large scales, as expected, the spectrum of the electric field behaves as k^2 in the non-helical case and is nearly scale invariant with an amplitude comparable to the spectrum of the magnetic field in the helical case. Further, at small scales, all the spectra behave as k^4 for the same reasons as we had encountered in the case of the first punctuated inflation model (2.56). When the background scalar field approaches the point of inflection in these models, the coupling functions J hardly evolve (in this context, see Fig. 2.7) and the electromagnetic modes effectively behave as in the conformally invariant case leading to the k^4 behaviour. Lastly, we should mention that such a background behaviour not only changes the shape of the spectra of the electromagnetic fields at small scales, it also suppresses the scale invariant amplitudes of the spectra at large scales.

2.5.4 An analytical estimate

In this subsection, we shall analytically arrive at the power spectra of the electromagnetic fields in models which permit ultra slow roll inflation and lead to enhanced scalar power on small scales.

A simple approximation

Recall that, in these scenarios, we had constructed the coupling function $J(\phi)$ so that we obtain a scale invariant spectrum for the magnetic field on large scales [cf. Eqs. (2.66); also see Eq. (2.65)]. In order to achieve such a scale invariant spectrum, during the initial stage of slow roll inflation, let us assume that $J(\eta) \propto a^2$. Note that, in these models, for our choices of the dependence of the coupling function on the field, we find that J freezes when the epoch of ultra slow roll sets in. This is evident from Fig. 2.7 wherein we have plotted the evolution of the coupling function in the first and second models of punctuated inflation [cf. Eqs. (2.56) and (2.58)] as well as in the model of ultra slow roll inflation [cf. Eq. (2.57)]. Therefore, we can assume that, after a time, say, η_1, $J(\eta) \simeq \mathrm{constant}$. In such a case, during the initial stage, the electromagnetic modes $\mathcal{A}_k$ can be easily obtained to be

$$\mathcal{A}_k^{\mathrm{I}}(\eta) = \frac{1}{\sqrt{2\,k}}\,\left(1 - \frac{3\,i}{k\,\eta} - \frac{3}{k^2\,\eta^2}\right)\,\mathrm{e}^{-i\,k\,\eta}. \tag{2.67}$$

It should be evident that, after η_1, the electromagnetic modes can be written as

$$\mathcal{A}_k^{\mathrm{II}}(\eta) = \frac{1}{\sqrt{2\,k}}\,\left(\alpha_k\,\mathrm{e}^{-i\,k\,\eta} + \beta_k\,\mathrm{e}^{i\,k\,\eta}\right). \tag{2.68}$$

The coefficients α_k and β_k are to be determined by imposing the matching conditions on the modes at the transition at η_1.

Since $J' \simeq -2\,\eta_1^2/\eta^3$ prior to η_1 and $J' \simeq 0$ after, there is a discontinuity in J' at η_1. This leads to a Dirac delta function in the behaviour of J''/J at the transition at η_1. As a result, the modes in the two domains are related by the matching conditions

$$\begin{aligned} \mathcal{A}_k^{\mathrm{I}}(\eta_1) &= \mathcal{A}_k^{\mathrm{II}}(\eta_1), & (2.69\mathrm{a})\\ \mathcal{A}_k^{\mathrm{II}\prime}(\eta) - \mathcal{A}_k^{\mathrm{I}\prime}(\eta) &= \frac{2}{\eta_1}\,\mathcal{A}_k^{\mathrm{I}}(\eta_1). & (2.69\mathrm{b}) \end{aligned}$$

These conditions lead to the following expressions for the coefficients α_k and β_k:

$$\begin{aligned} \alpha_k &= 1 + \frac{2\,i\,k_1}{k} - \frac{3\,k_1^2}{2\,k^2}, & (2.70\mathrm{a})\\ \beta_k &= \left(\frac{i\,k_1}{k} - \frac{3\,k_1^2}{2\,k^2}\right)\,\mathrm{e}^{2\,i\,k/k_1}, & (2.70\mathrm{b}) \end{aligned}$$

where we have set $k_1 = -1/\eta_1$, i.e. the wave number which leaves the Hubble radius at the onset of the ultra slow roll epoch. The power spectra of the magnetic and electric fields at late times [i.e. in the limit $(-k\,\eta_\mathrm{e}) \ll 1$] can be evaluated to be

$$\begin{aligned} \mathcal{P}_{_\mathrm{B}}(k) &= \frac{H_{_\mathrm{I}}^4}{4\,\pi^2}\,(-k\,\eta_\mathrm{e})^4\,|\alpha_k + \beta_k|^2, & (2.71\mathrm{a})\\ \mathcal{P}_{_\mathrm{E}}(k) &= \frac{H_{_\mathrm{I}}^4}{4\,\pi^2}\,(-k\,\eta_\mathrm{e})^4\,|\alpha_k - \beta_k|^2. & (2.71\mathrm{b}) \end{aligned}$$

For large k such that $k/k_1 \gg 1$, we find that $\alpha_k \to 1$ and $\beta_k \to 0$ [cf. Eqs. (2.70)]. Therefore, in such a limit, both the above power spectra behave as k^4, which is what we observe numerically (see Figs. 2.5 and 2.6). It can be shown that, in the limit $k/k_1 \ll 1$,

$$|\alpha_k + \beta_k|^2 = \frac{9\,k_1^4}{k^4}, \quad |\alpha_k - \beta_k|^2 = \frac{16\,k_1^2}{k^2}, \tag{2.72}$$

so that the above spectra reduce to the following forms:

$$\mathcal{P}_{\mathrm{B}}(k) \simeq \frac{9\,H_{\mathrm{I}}^4}{4\,\pi^2}\left[\frac{a(\eta_1)}{a(\eta_{\mathrm{e}})}\right]^4, \tag{2.73a}$$

$$\mathcal{P}_{\mathrm{E}}(k) \simeq \frac{H_{\mathrm{I}}^4}{4\,\pi^2}\left(\frac{4\,k}{k_1}\right)^2\left[\frac{a(\eta_1)}{a(\eta_{\mathrm{e}})}\right]^4. \tag{2.73b}$$

In other words, on the large scales, we obtain spectral shapes that are expected to occur when the coupling function behaves as $J \simeq a^2$ [cf. Eqs. (2.13)]. This should not come as a surprise since these modes leave during the initial slow roll regime. However, note that the factor $[a(\eta_1)/a(\eta_{\mathrm{e}})]^4$ considerably suppresses the amplitudes of the electromagnetic spectra on large scales. In fact, the earlier the onset of the ultra slow roll regime, the larger is the suppression. It is for this reason that the electromagnetic spectra in the first punctuated inflation model had substantially small amplitudes on large scales (see Fig. 2.5).

Let us now examine the corresponding situation in the helical case. In the case of the helical field, during the initial stage of slow roll inflation, when $n = 2$, the electromagnetic modes $\mathcal{A}_k^\sigma$ are given by [cf. Eq. (2.19)]

$$\mathcal{A}_k^{\sigma\mathrm{I}}(\eta) = \frac{1}{\sqrt{2\,k}}\,\mathrm{e}^{-\pi\,\sigma\,\gamma}\,W_{2\,i\,\sigma\,\gamma,\frac{5}{2}}(2\,i\,k\,\eta). \tag{2.74}$$

Since the coupling function J hardly evolves after the onset of ultra slow roll, the electromagnetic modes during the second stage, say, $\mathcal{A}_k^{\sigma\mathrm{II}}$, can be expressed just as in Eq. (2.68) for the non-helical case. Moreover, the matching conditions continue to be given by Eqs. (2.69). However, we should clarify that the coefficients α_k and β_k now depend on the polarization σ. The power spectra of the magnetic and electric fields at late times, i.e. when $(-k\,\eta_{\mathrm{e}}) \ll 1$, can be obtained to be

$$\mathcal{P}_{\mathrm{B}}(k) = \frac{H_{\mathrm{I}}^4}{8\,\pi^2}\,(-k\,\eta_{\mathrm{e}})^4\,\left(|\alpha_k^+ + \beta_k^+|^2 + |\alpha_k^- + \beta_k^-|^2\right), \tag{2.75a}$$

$$\mathcal{P}_{\mathrm{E}}(k) = \frac{H_{\mathrm{I}}^4}{8\,\pi^2}\,(-k\,\eta_{\mathrm{e}})^4\,\left(|\alpha_k^+ - \beta_k^+|^2 + |\alpha_k^- - \beta_k^-|^2\right). \tag{2.75b}$$

On matching the modes at η_1, we obtain the coefficients α_k^σ and β_k^σ to be

$$\alpha_k^\sigma = -\frac{\mathrm{e}^{-i\,k/k_1}\,\mathrm{e}^{-\pi\,\sigma\,\gamma}}{2\,(k/k_1)}\,\Big[2\,(i+\sigma\,\gamma)\,W_{2\,i\,\sigma\,\gamma,\frac{5}{2}}(-2\,i\,k/k_1)$$

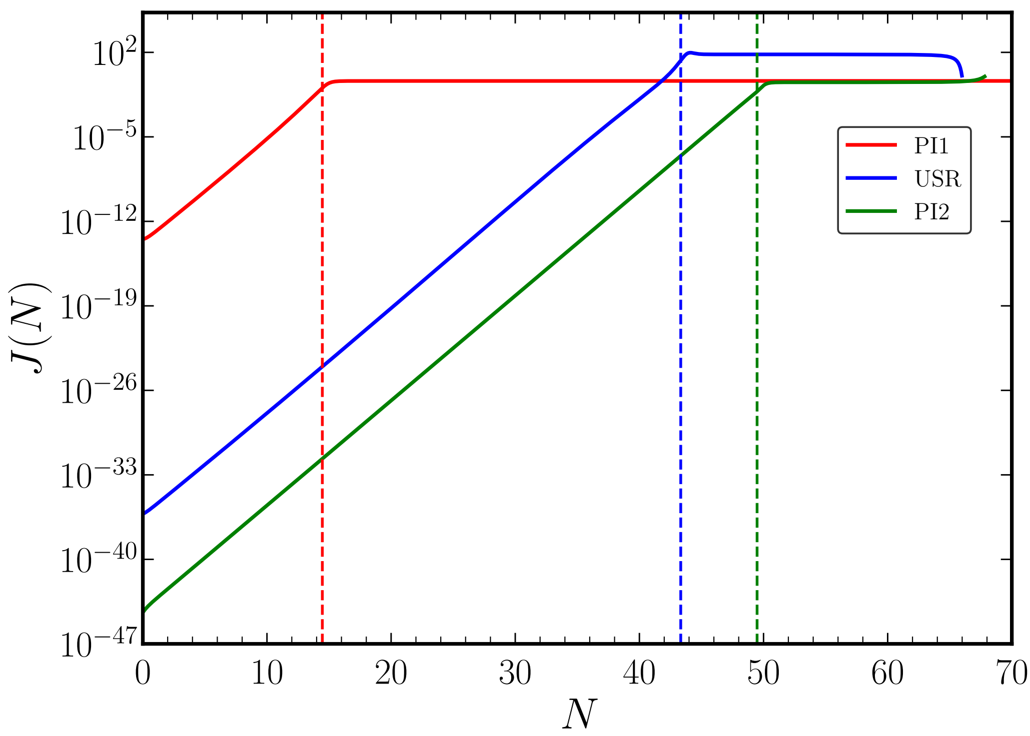

Figure 2.7: The evolution of the non-minimal coupling function J [as given by Eqs. (2.65) and (2.66)] that we had considered in the models described by the potentials (2.56), (2.57) and (2.58) has been plotted (PI1, in solid red; USR, in blue; and PI2, in green, respectively) as a function of the e-fold N. The onset of the ultra slow roll phase corresponds to the time when the first slow roll parameter starts to decrease rapidly. We have indicated the beginning of the ultra slow roll epoch (as dashed vertical lines of the corresponding color) in all these cases. Recall that, we had constructed coupling functions $J(\phi)$ so that they behave as a^2 during the initial slow roll phase. For such choices of $J(\phi)$, the coupling function does not seem to change appreciably (until very close to the end of inflation) after ultra slow has set in.

$$- i\, W_{1+2\,i\,\sigma\,\gamma,\frac{5}{2}}(-2\,i\,k/k_1)\Big], \tag{2.76a}$$

$$\beta_k^\sigma = -\frac{\mathrm{e}^{i\,k/k_1}\,\mathrm{e}^{-\pi\,\sigma\,\gamma}}{2\,(k/k_1)}\left[2\,\left(-i-\frac{k}{k_1}-\sigma\,\gamma\right)\,W_{2\,i\,\sigma\,\gamma,\frac{5}{2}}(-2\,i\,k/k_1)\right.$$
$$\left. + i\, W_{1+2\,i\,\sigma\,\gamma,\frac{5}{2}}(-2\,i\,k/k_1)\right], \tag{2.76b}$$

where, as earlier, we have set $k_1 = -1/\eta_1$. In the limit $k/k_1 \gg 1$, we find that $\alpha_k^\sigma \to 1$ and $\beta_k^\sigma \to 0$, as in the non-helical case. This suggests that the power spectra of both the electric and magnetic fields behave as k^4 in such a limit, which is indeed what we obtain numerically (see Figs. 2.5 and 2.6). Whereas, in the limit $k/k_1 \ll 1$, we find that [209]

$$
\begin{aligned}
|\alpha_k^\sigma + \beta_k^\sigma|^2 &= \frac{9\,(1-\mathrm{e}^{-4\,\pi\,\sigma\,\gamma})}{4\,\pi\,\sigma\,\gamma\,(1+5\,\gamma^2+4\,\gamma^4)}\,\left(\frac{k}{k_1}\right)^{-4}, \qquad (2.77)\\
|\alpha_k^\sigma - \beta_k^\sigma|^2 &= \frac{9\,\sigma\,\gamma^2\,(1-\mathrm{e}^{-4\,\pi\,\sigma\,\gamma})}{4\,\pi\,\gamma\,(1+5\,\gamma^2+4\,\gamma^4)}\,\left(\frac{k}{k_1}\right)^{-4}, \qquad (2.78)
\end{aligned}
$$

and hence the spectra (2.75) reduce to the following forms:

$$
\begin{aligned}
\mathcal{P}_{_\mathrm{B}}(k) &\simeq \frac{9\,H_{_\mathrm{I}}^4}{4\,\pi^2}\,f(\gamma)\,\left[\frac{a(\eta_1)}{a(\eta_\mathrm{e})}\right]^4, \qquad (2.79\mathrm{a})\\
\mathcal{P}_{_\mathrm{E}}(k) &\simeq \frac{9\,H_{_\mathrm{I}}^4}{4\,\pi^2}\,f(\gamma)\,\gamma^2\,\left[\frac{a(\eta_1)}{a(\eta_\mathrm{e})}\right]^4, \qquad (2.79\mathrm{b})
\end{aligned}
$$

where, recall that, $f(\gamma)$ is given by Eq. (2.27). Clearly, over large scales, the spectra of both the electric and magnetic fields are scale invariant as is expected in the helical case when $J \simeq a^2$ and the modes cross the Hubble radius during a regime of slow roll. Moreover, note that, as in the non-helical case, the onset of the ultra slow roll epoch leads to a suppression in the amplitudes of the power spectra on large scales by the factor of $[a(\eta_1)/a(\eta_\mathrm{e})]^4$.

We have been able to understand the shape of the electromagnetic spectra arising in models involving an epoch of ultra slow roll inflation using analytical arguments. Let us now compare the numerical results for the amplitudes of the spectra over large scales with the analytical estimates in both the non-helical and helical cases. In the case of the ultra slow roll model described by the potential (2.57), we find that, when the pivot scale leaves the Hubble radius, the value of the Hubble parameter is $H_{_\mathrm{I}} = 9.05\times 10^{-6}\,M_{_\mathrm{Pl}}$. The epoch of ultra slow roll inflation can be said to begin when the first slow roll parameter ϵ_1 attains the maximum value (prior to the end of inflation) and begins to decrease rapidly thereafter. We find that, in the model of our interest here, ultra slow roll sets in about 22.4 e-folds before the end of inflation. Also, the value of the wave number that equals $\sqrt{|J''/J|}$ at the onset of ultra slow roll inflation proves to be $k_1 = 2.2\times 10^{13}\,\mathrm{Mpc}^{-1}$. For these values, in the non-helical case, the analytical estimates we have obtained above lead to $\mathcal{P}_{_\mathrm{B}}(k) \simeq 10^{-60}\,M_{_\mathrm{Pl}}^4$ and $\mathcal{P}_{_\mathrm{E}}(k) \simeq 10^{-89}\,M_{_\mathrm{Pl}}^4$ at the pivot scale. Numerically, we have obtained the corresponding values to be $\mathcal{P}_{_\mathrm{B}}(k) \simeq 10^{-63}\,M_{_\mathrm{Pl}}^4$ and $\mathcal{P}_{_\mathrm{E}}(k) \simeq 10^{-84}\,M_{_\mathrm{Pl}}^4$. In the helical case, for $\gamma = 1$, the analytical estimates lead to $\mathcal{P}_{_\mathrm{B}}(k) = \mathcal{P}_{_\mathrm{E}}(k) \simeq 10^{-57}\,M_{_\mathrm{Pl}}^4$ at the pivot scale. The corresponding numerical values turn out to be $\mathcal{P}_{_\mathrm{B}}(k) = \mathcal{P}_{_\mathrm{E}}(k) \simeq 10^{-60}\,M_{_\mathrm{Pl}}^4$.

Similarly, in the case of the second model of punctuated inflation described by the potential (2.58), we find that the value of the Hubble parameter at the time when the pivot scale exits the Hubble radius is $H_{_{\rm I}} = 1.01 \times 10^{-5}\, M_{_{\rm Pl}}$. Moreover, the onset of the ultra slow roll epoch occurs about 18.3 e-folds prior to the end of inflation, which implies that $k_1 \simeq 1.6 \times 10^{14}\,{\rm Mpc}^{-1}$. According to the analytical estimates, in the non-helical case, these values lead to $\mathcal{P}_{_{\rm B}}(k) \simeq 10^{-53}\, M_{_{\rm Pl}}^4$ and $\mathcal{P}_{_{\rm E}}(k) \simeq 10^{-84}\, M_{_{\rm Pl}}^4$ at the pivot scale. Numerically, we obtain the corresponding values to be $\mathcal{P}_{_{\rm B}}(k) \simeq 10^{-50}\, M_{_{\rm Pl}}^4$ and $\mathcal{P}_{_{\rm E}}(k) \simeq 10^{-83}\, M_{_{\rm Pl}}^4$. In the case of the helical fields, when $\gamma = 1$, the analytical estimates suggest that $\mathcal{P}_{_{\rm B}}(k) = \mathcal{P}_{_{\rm E}}(k) \simeq 10^{-50}\, M_{_{\rm Pl}}^4$ at the pivot scale, while the corresponding numerical values turn out to be $\mathcal{P}_{_{\rm B}}(k) = \mathcal{P}_{_{\rm E}}(k) \simeq 10^{-47}\, M_{_{\rm Pl}}^4$.

While the analytical estimates broadly match the numerical results, there arise differences of the order of 10^3–10^5 in the values for the power spectra of the electromagnetic fields. These differences can be attributed to the coarseness of the analytical modeling and the fact that J evolves to a certain extent as one approaches the end of inflation.

A closer look at the evolution of the modes at late times

In Fig. 2.7, we had plotted the evolution of the non-minimal coupling function in the ultra slow roll model and the two punctuated inflation models we have considered. We had found that, once the epoch of ultra slow roll begins, the coupling function J hardly evolves. Based on such a behaviour, we had assumed that J' and J'' were zero and had arrived at the analytical form for the modes $\mathcal{A}_k$ and, eventually, the power spectra of the electromagnetic fields. While the coupling function J is almost a constant, one can show that it is not correct to set J' and J'' to zero in these scenarios. In Fig. 2.8, we have plotted the evolution of $|J''/J|$ in the three models. It is clear from the figure that the quantity does not vanish once ultra slow begins, as we have assumed earlier. Therefore, it seems that we need to revise our previous discussion.

One can expect that, since J as well as J''/J behave as a^2 during the initial slow roll phase, the power spectra over modes that leave the Hubble radius—to be precise, when $k = \sqrt{|J''/J|}$—will be scale invariant. However, in the ultra slow roll and the second punctuated inflation models, once the epoch of ultra slow roll comes to an end, J''/J behaves as $a^{5/2}$ (as illustrated in Fig. 2.8), while J is a constant. Let us now focus on large wave numbers in these models over which, numerically, we find that the power spectra of the magnetic as well as electric fields behave as k^4. In these cases, at suitably early times when $k \gg \sqrt{|J''/J|}$, the Fourier modes of the non-helical vector potential

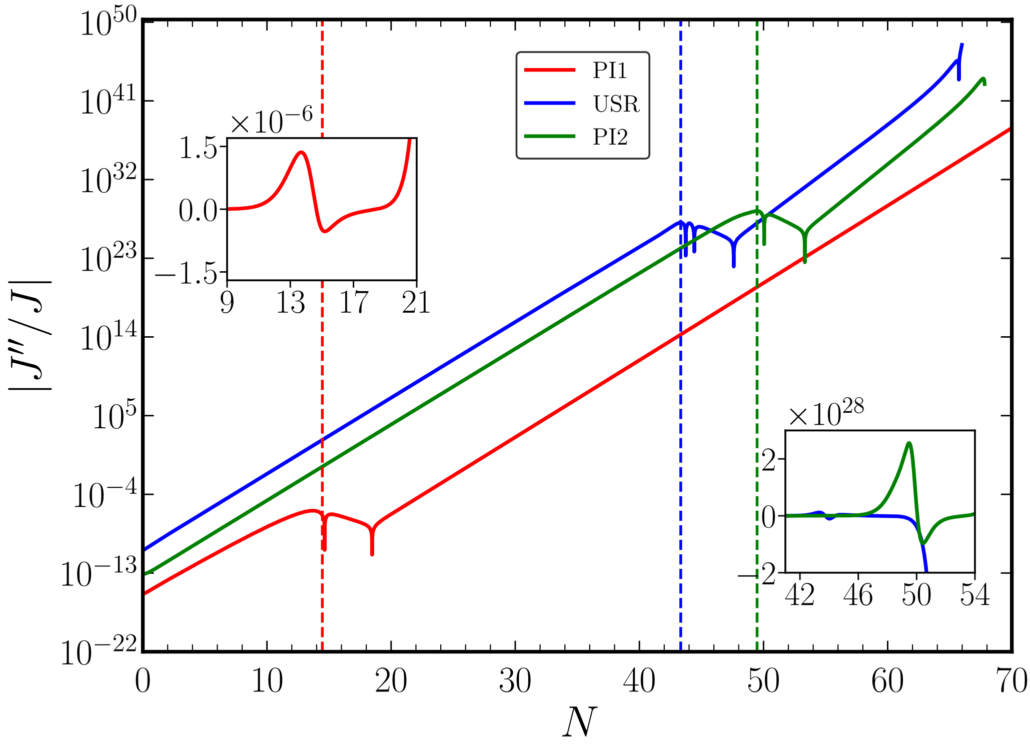

Figure 2.8: The evolution of the quantity J''/J corresponding to the three coupling functions we had illustrated in the previous figure has been plotted as a function of the e-fold N (with the same choice of colors). The insets highlight the behaviour of the quantity around the onset of the epoch of ultra slow roll. We find that $J''/J \propto \mathrm{e}^{2\,N}$ during the initial slow roll phase, as expected. It is clear J''/J does not vanish once ultra slow roll inflation begins (indicated by the vertical lines). In fact, the quantity is almost a constant during the period of ultra slow roll and it actually grows (either as $\mathrm{e}^{2\,N}$ in the case of the first punctuated inflation model or as $\mathrm{e}^{5\,N/2}$ in the other two models) when the phase of ultra slow roll is complete and the first slow roll parameter begins to rise. We should also mention the fact that J''/J can turn negative during these latter stages.

[governed by Eq. (2.3)] can be written as

$$\mathcal{A}_k^{\mathrm{I}}(\eta) = \frac{1}{\sqrt{2\,k}}\,\mathrm{e}^{-i\,k\,\eta}. \tag{2.80}$$

Also, since, J is a constant, at late times when $k \ll \sqrt{|J''/J|}$, we can express the non-helical electromagnetic modes as

$$\mathcal{A}_k^{\mathrm{II}}(\eta) = \frac{1}{\sqrt{2\,k}}\,\left[\alpha_k + \beta_k\,\eta\right], \tag{2.81}$$

where the coefficients α_k and β_k are to be determined by matching the above solutions and their derivatives at the time η_k corresponding to $k = \sqrt{|J''/J|}$. The coefficients α_k and β_k can be easily obtained to be

$$\alpha_k = (1 + i\,k\,\eta_k)\,\mathrm{e}^{-i\,k\,\eta_k}, \quad \beta_k = -i\,k\,\eta_k\,\mathrm{e}^{-i\,k\,\eta_k}, \tag{2.82}$$

and hence, at late times, we have

$$\mathcal{A}_k^{\mathrm{II}}(\eta) = \frac{1}{\sqrt{2\,k}}\,\left[1 - i\,k\,(\eta - \eta_k)\right]\,\mathrm{e}^{-i\,k\,\eta_k}. \tag{2.83}$$

Since J is constant, this implies that the quantity $\sqrt{k}\,\bar{A}_k$ will have the same value at late times [i.e. when $(-k\,\eta_{\mathrm{e}}) \ll 1$] for large wave numbers provided $(k\,\eta_k)$ is small. We shall see below that $(k\,\eta_k)$ is indeed small in the models of our interest. In Fig. 2.9, we have plotted the evolution of the electromagnetic modes at late times in the case of the ultra slow roll inflation model (2.57) for a range of wave numbers. It is clear from the figure that, over large enough wave numbers for which η_k occurs after the epoch of ultra slow roll, the quantity $\sqrt{k}\,|\bar{A}_k|$ has the same amplitude at late times. This, in turn, implies that the power spectrum of the magnetic field will behave as k^4, which is what we obtain numerically.

Note that, because of the fact that the first slow roll parameter remains small until we approach close to the end of inflation, the de Sitter expression for the scale factor remains valid. As a result, on using the above form for the electromagnetic modes, we obtain the spectra of the magnetic and electric fields in the limit $(-k\,\eta_{\mathrm{e}}) \ll 1$ to be

$$\mathcal{P}_{_{\mathrm{B}}}(k) = \frac{H_{_{\mathrm{I}}}^4}{4\,\pi^2}\,(-k\,\eta_{\mathrm{e}})^4\,\left(1 + k^2\,\eta_k^2\right), \tag{2.84a}$$

$$\mathcal{P}_{_{\mathrm{E}}}(k) = \frac{H_{_{\mathrm{I}}}^4}{4\,\pi^2}\,(-k\,\eta_{\mathrm{e}})^4. \tag{2.84b}$$

While $\mathcal{P}_{_{\mathrm{E}}}(k)$ is independent of η_k and evidently behaves as k^4 over large wave numbers, we need to determine η_k in order to understand the shape of $\mathcal{P}_{_{\mathrm{B}}}(k)$. Since $J''/J \propto a^{5/2}$ at late times, on using the behaviour of the scale factor in de Sitter, based on dimensional grounds, we can write $J''/J = (k_{\mathrm{t}}\,\eta^5)^{-1/2}$, where k_{t} is a wave number. The quantity k_{t} needs to be determined from the numerical value of J''/J at the end of the ultra slow roll phase. Hence, the condition $k^2 = J''/J = (k_{\mathrm{t}}\,\eta_k^5)^{-1/2}$ leads to $k^2\,\eta_k^2 = (k/k_{\mathrm{t}})^{2/5}$. In the ultra slow roll and the second punctuated inflation models, we find that, for our choices of the coupling functions, $k_{\mathrm{t}} \simeq 10^{23}\,\mathrm{Mpc}^{-1}$, whereas the largest wave number of our interest is $k \simeq 10^{19}\,\mathrm{Mpc}^{-1}$. These imply that $(k^2\,\eta_k^2) \lesssim 10^{-2}$. Therefore, we can

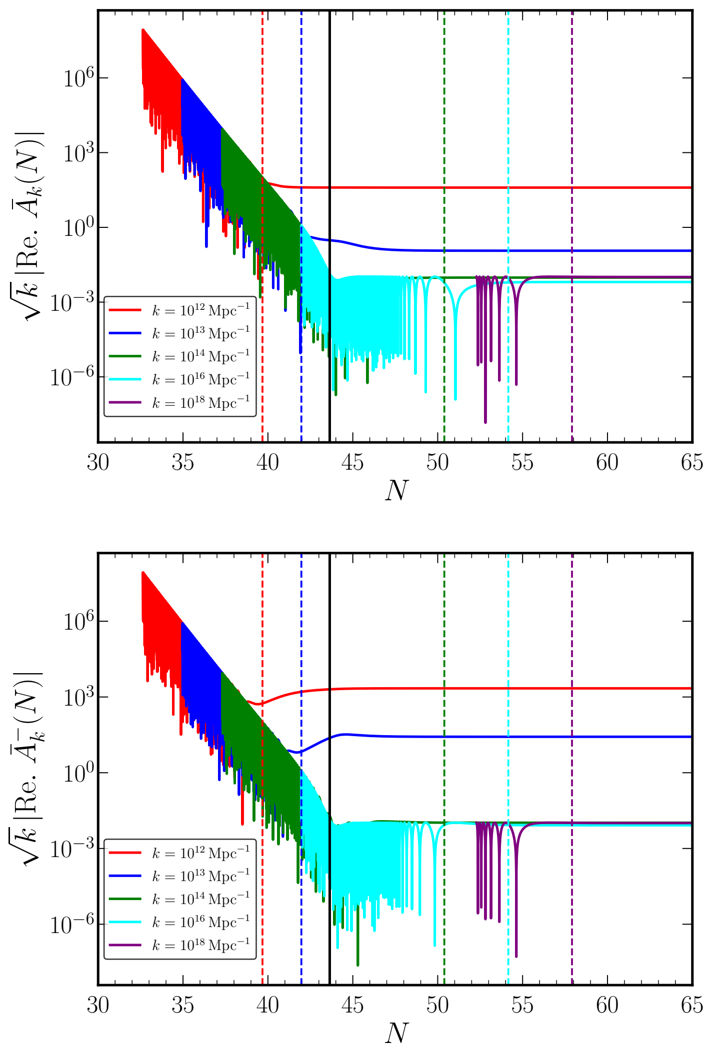

Figure 2.9: The evolution of the electromagnetic modes in the case of the ultra slow roll inflation model (2.57) has been plotted for the five choices of the wave numbers $k = (10^{12}, 10^{13}, 10^{14}, 10^{16}, 10^{18})\ \mathrm{Mpc}^{-1}$ (in red, blue, green, cyan, and purple), respectively. We have worked with the coupling function (2.66a) and have plotted the evolution of the dominant real part of the quantity $\sqrt{k}\,|\bar{A}_k|$ in the non-helical case (on top) and the quantity $\sqrt{k}\,|\bar{A}_k^-|$ in the helical case (at the bottom). We have also indicated the onset of the ultra slow roll epoch (as the solid vertical line in black) and the e-folds corresponding to the time η_k, i.e. when $k^2 = |J''/J|$, for the different wave numbers (as dashed vertical lines, with the same choice of colors as the modes). It is clear that the amplitude of the electromagnetic modes freeze at late times. Importantly, we find that, for $k \gtrsim 10^{13}\,\mathrm{Mpc}^{-1}$, the late time values of the quantities $\sqrt{k}\,|\bar{A}_k|$ and $\sqrt{k}\,|\bar{A}_k^-|$ are the same for the different wave numbers, which points to the k^4 behaviour for the spectrum of the magnetic field over small scales.

expect $\mathcal{P}_{\rm B}(k)$ to behave as k^4 over the wave numbers $10^{15}\,{\rm Mpc}^{-1} \lesssim k \lesssim 10^{19}\,{\rm Mpc}^{-1}$, which is what we observe numerically.

In retrospect, it should be clear that the approaches in the last two subsections yielded similar results for the behaviour of the spectra at large wave numbers because of the fact that the modes $\mathcal{A}_k^{\rm II}$ as given by Eqs. (2.68) and (2.81) have the same amplitudes at late times.

2.6 CAN THE FEATURES BE IRONED OUT?

It is now interesting to examine whether the features in the spectra of the electromagnetic fields can be ironed out so that we arrive at nearly scale invariant spectra for the magnetic field. In this section, we shall discuss this possibility in the second Starobinsky model [cf. Eqs. (2.54) and (2.55)] that leads to features in the scalar power spectrum over the large scales.

Earlier, we had arrived at the spectra of the magnetic field in this model assuming that the coupling function was given by either $J_+(\phi)$ or $J_-(\phi)$ described by Eqs. (2.64). In order to remove the strong features that arise in the spectrum of the magnetic field, it seems reasonable to stitch together these two coupling functions in the following fashion:

$$\begin{aligned} J(\phi) \;=\; & \frac{J_1}{2\,J_{0+}}\left[1+\tanh\left(\frac{\phi-\phi_0}{\Delta\phi_1}\right)\right]\,J_+(\phi) \\ & +\frac{J_1}{2\,J_{0-}}\left[1-\tanh\left(\frac{\phi-\phi_0}{\Delta\phi_1}\right)\right]\,J_-(\phi), \end{aligned} \tag{2.85}$$

where J_1 is constant which is determined by the condition that $J(\phi)$ reduces to unity at the end of inflation and $\Delta\phi_1$ is another constant which we shall choose suitably. Note that, for a small enough $\Delta\phi_1$, the quantities within the square brackets (involving the hyperbolic tangent functions) in the above expression behave as step functions. It should then be evident that the above coupling function has been constructed in such a fashion that it is essentially described by $J_+(\phi)$ when $\phi>\phi_0$ and $J_-(\phi)$ when $\phi<\phi_0$. In Fig. 2.10, we have plotted the resulting spectra for the magnetic as well as electric fields obtained numerically in the non-helical and helical cases. As can be seen from the figure, there arise two nearly scale invariant regions in the power spectra of the magnetic field (and in the case of the helical electric field), with a burst of oscillations in between. Clearly, the scale invariant parts correspond to the evolution of the field over the two linear parts of the potential and the oscillations arise as the deviations from slow roll occur when the field crosses ϕ_0. Thus, in a model involving a strong departure from slow roll, with a suitable choice of the coupling function, we have been able to arrive at electromagnetic spectra that do not lead to significant backreaction and can also be largely consistent with the current constraints. However, we should stress the fact that it has been achieved only at the severe cost of an extremely fine-tuned non-minimal coupling function.

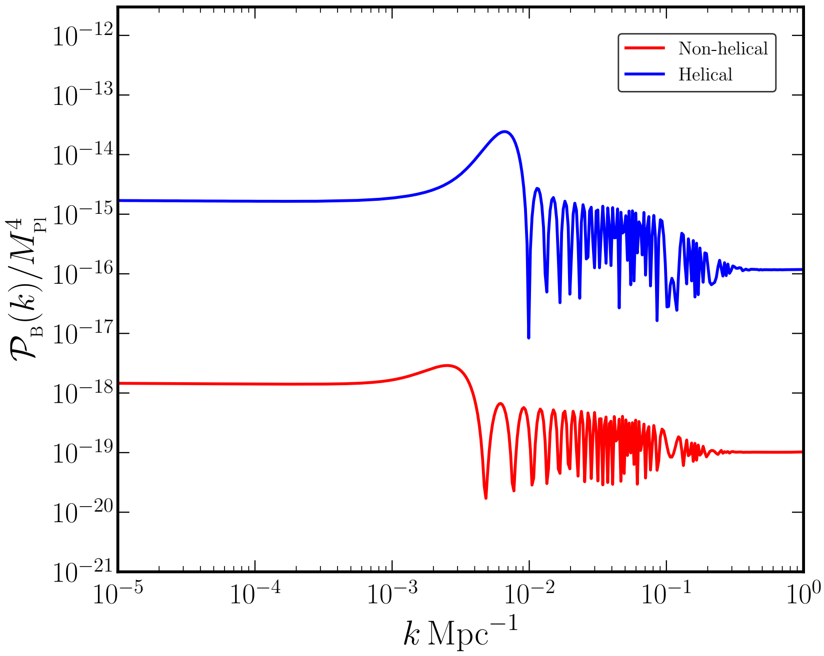

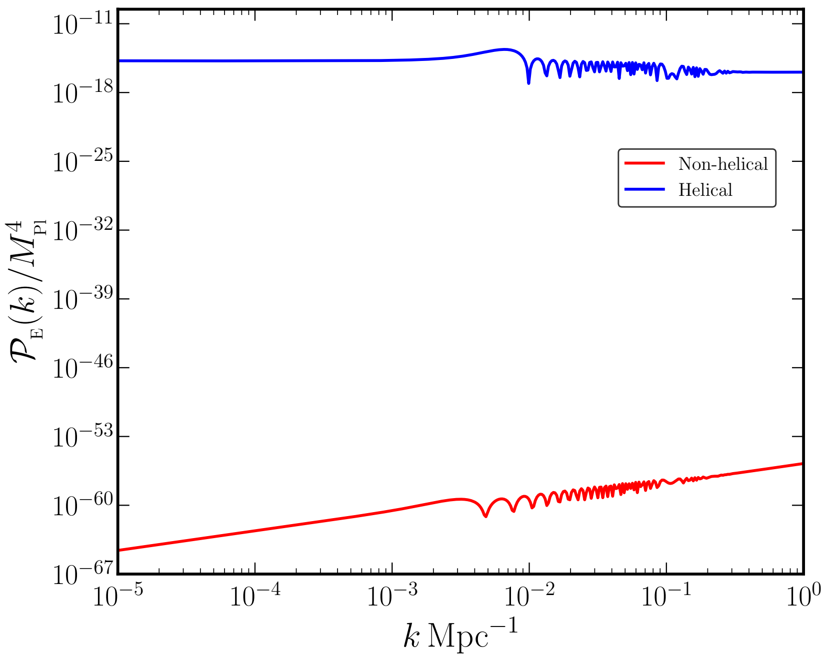

Figure 2.10: The spectra of the magnetic (on top) and electric (at the bottom) fields arising for the choice of the coupling function (2.85) in the second Starobinsky model (2.55) have been plotted for both the non-helical (in red) and helical (in blue) cases. As before, we have set $n = 2$ and $\gamma = 1$ when computing the spectra. Note that, with the new coupling function, the strong features have disappeared and we are left with relatively smaller features that can be expected to be consistent with the current constraints. Evidently, the burst of oscillations that remain in the spectra occurs because of the departure from slow roll as the field crosses the point ϕ_0.

2.7 CONCLUSIONS

A nearly scale invariant primordial scalar power spectrum, as is generated in slow roll inflationary models, is remarkably consistent with the CMB data [52, 210]. However, it has been repeatedly noticed that certain features in the scalar power spectrum can improve the fit to the data. Such features are often generated by considering potentials that induce departures from slow roll inflation [178–190].

Magnetic fields are generated during inflation by breaking the conformal invariance of the electromagnetic action. In this chapter, we have investigated the effects of deviations from slow roll on the spectra of the electromagnetic fields generated during inflation. Specifically, we have considered a class of inflationary models which allow transient deviations from slow roll and, as a result, generate localized features in the scalar power spectrum. When the electromagnetic fields are coupled to the scalar curvature, we found that it proves to be challenging to obtain nearly scale invariant magnetic fields of the desired shapes and strengths even in slow roll inflation. In contrast, this is easy to achieve when the electromagnetic field is coupled non-minimally to the inflaton, provided we work with model-dependent coupling functions. Therefore, we focused on situations wherein the electromagnetic field is coupled to the inflaton and evaluated the spectra of non-helical as well as helical electromagnetic fields in non-trivial scenarios involving deviations from slow roll. We found that, when strong departures from slow roll arise, apart from generating features in the scalar power spectrum, quite generically, these deviations also led to features in the spectra of electromagnetic fields. Moreover, in certain scenarios, it is also possible that the strengths of the magnetic fields are considerably suppressed on large scales. While it seems possible to remove the strong features in the spectra of the electromagnetic fields allowing us to arrive at nearly scale invariant spectra of required strengths, it is achieved at the terrible cost of extreme fine-tuning. In summary, if future observations confirm the presence of strong features in the primordial scalar power spectrum and, if the electromagnetic fields are to be generated by coupling them to the inflaton that is responsible for these features, then there seems to arise a severe challenge in being able to produce magnetic fields of the desired shape and strength in single field models of inflation. We are currently exploring possible ways of overcoming the challenge.

There are a couple of related points we wish to clarify before we conclude this chapter. As we have stressed earlier, in this chapter, we have focused on a domain wherein backreaction due to the electromagnetic fields is negligible [81, 166]. Another interesting aspect of generating electromagnetic fields during inflation is that they can induce non-adiabatic pressure perturbations which can source the adiabatic scalar perturbations on super-Hubble scales (in this context, see, for instance, Refs. [81, 117, 224]). This additional contribution can lead to distinguishable features in the CMB both at the level of the power spectrum as well as non-Gaussianities. However, for most of the models we have considered in this chapter, since the strength of generated magnetic fields over CMB scales is relatively weak, the effects arising from the induced curvature perturbations can be expected to be negligible. Nevertheless, it seems important to investigate these effects more closely in non-trivial scenarios involving departures from slow roll inflation. We are presently examining such issues.

CHAPTER 3

CIRCUMVENTING THE CHALLENGES IN THE CHOICE OF THE NON-CONFORMAL COUPLING FUNCTION IN INFLATIONARY MAGNETOGENESIS

3.1 INTRODUCTION

Magnetic fields are ubiquitous in the universe. They are observed at different strengths over a wide range of scales, ranging from planets [$\mathcal{O}(0.5\,\mathrm{G})$] and stars [$\mathcal{O}(1\,\mathrm{G})$] to galaxies and clusters of galaxies [$\mathcal{O}(10^{-6}\,\mathrm{G})$] (for reviews on magnetic fields, see Refs. [1–10]). The Fermi/LAT, HESS and MAGIC observations of TeV blazars over the last decade indicate that even the voids in the IGM may contain magnetic fields [$\mathcal{O}(10^{-15}\,\mathrm{G})$] [21–23, 142, 152–155]. While astrophysical processes involving the battery mechanism may be sufficient to explain the origin of magnetic fields in galaxies and clusters of galaxies (in this regard, see, for example, Refs. [3, 4]), one may have to turn to a cosmological phenomenon to explain the magnetic fields observed in voids (in this context, see the reviews [5, 6, 8–10]).

Without any doubt, the inflationary scenario is presently the most attractive paradigm to explain the origin of perturbations in the early universe. Hence, it seems natural to turn to inflation for the generation of the PMFs. However, since the standard electromagnetic action is conformally invariant and the FLRW universe is conformally flat, the strengths of minimally coupled electromagnetic fields are diluted considerably by the end of inflation. Therefore, it becomes necessary to break the conformal invariance of the action governing the electromagnetic field in order to generate magnetic fields of observed strengths today.

As we have discussed earlier, the conformal invariance of the electromagnetic action is typically broken by coupling the electromagnetic field to either the scalar curvature or the scalar field driving inflation (see, for example, Refs. [81, 93–95, 98, 104, 107, 117, 161–166, 204]; for discussions on effects due to the addition of a parity violating term, see Refs. [97, 99, 167–173, 211]). It can be easily established that, if the non-conformal coupling function, say, J, behaves as $\mathrm{e}^{2\,N}$, then one can arrive at a nearly scale invariant spectrum for the magnetic field with a strength that is dependent on the fourth power of the Hubble scale during inflation. In the previous chapter, we had argued that while the coupling to the scalar curvature, say, R, works satisfactorily in power law inflation, it poses a problem in slow roll inflation [225]. The reason being that, since the scalar curvature hardly varies during slow roll inflation, one has to raise R to a very high power in order to achieve the desired variation in the coupling function which leads to magnetic fields with nearly scale invariant spectra. In contrast, it is relatively easy to achieve the desired evolution of the coupling function (i.e. $J \propto e^{2N}$) when the electromagnetic field is coupled to the inflaton. However, there exists no universal form for the coupling function (in terms of the dependence on the inflaton) and its form has to be chosen depending on the inflationary model being considered.

There has been a constant interest in the literature towards examining whether specific features in the inflationary scalar power spectrum improve the fit to the CMB and the LSS data (in this context, see, for instance, Refs. [178–190, 226]). Moreover, over the last few years, there has been an interest in investigating the non-trivial signatures of strong features at small scales which can lead to enhanced levels of formation of PBHs and also generate secondary gravitational waves of possibly detectable amplitudes (for a short list of efforts in this regard, see Refs. [196–200, 202, 203, 227]). Such features are often achieved by considering inflationary potentials that lead to departures from slow roll inflation. In our recent work [225], we had shown that, unless the form of the non-conformal coupling function is extremely fine-tuned, the deviations from slow roll inflation that lead to features in the scalar power spectrum inevitably lead to features in the spectra of the electromagnetic fields as well. For instance, in the case of single field models of inflation that permit a brief phase of ultra slow roll, the spectrum of the magnetic field has a strong scale dependence on small scales. Moreover, the amplitude of the magnetic fields is strongly suppressed on large scales depending on the time of onset of the ultra slow roll epoch.

In this chapter, we shall examine whether these challenges can be circumvented in two field models of inflation (for some recent discussions on generating features in two field models at large and small scales, see, for example, Refs. [228–233]). The presence of the additional field permits a richer dynamics in the two field models, and one can possibly utilize the second field to overcome the challenges faced in single field models. As we shall see, with suitable choices for the non-conformal coupling function, we are able to generate magnetic fields of desired strengths even in situations wherein there arises an intermediate period of ultra slow roll. However, it seems difficult to avoid the presence of features in the spectra of the electromagnetic fields. In order to understand the viability of such electromagnetic spectra, we shall consider two specific inflationary models with suitable couplings, and roughly compare the smoothed strengths of the generated magnetic fields with the constraints from the CMB data [50]. Moreover, for one of the two models that we consider, we shall also evaluate the imprints of the PMFs on the angular power spectra of the CMB using the publicly available codes

CAMB [234] and MagCAMB [174].

This chapter is organized as follows. In Sec. 3.2, we shall briefly review the challenges that arise in single field inflationary models and explore possible non-conformal coupling functions that can help us overcome the challenges. In Sec. 3.3, we introduce the two field models of inflation that we shall consider. We shall focus on two models that lead either to a suppression in power on large scales or to an enhancement in power on small scales. Thereafter, we shall go on to construct suitable non-conformal coupling functions that allow us to arrive at magnetic fields of desired strengths over the CMB scales. We shall discuss the cases of non-helical as well as helical magnetic fields. As we shall illustrate, despite the presence of the additional field, it seems impossible to completely iron out the features that arise in the spectra of the electromagnetic fields. In Sec. 3.4, we shall first examine if the amplitudes of the magnetic fields that we obtain in the two inflationary models are broadly consistent with the constraints on the PMFs from the CMB data. Then, focusing on the non-helical case, using MagCAMB, we shall compute the angular power spectra of the CMB generated by the so-called passive and compensated magnetic modes [174]. We shall carry out such an exercise for one of the two models which leads to a nearly scale invariant spectrum for the magnetic field over large scales. We shall also approximately calculate the spectrum of the curvature perturbations induced by the magnetic field during inflation [131, 224], and compute the corresponding angular power spectra of the CMB using CAMB [234]. We shall compare these quantities with the contributions due to the primary scalar and tensor power spectra generated from the Bunch-Davies vacuum. We shall conclude this chapter in Sec. 3.5 with a summary of the results obtained. We shall relegate some of the related discussions to the Apps. B, C and D.

3.2 CHALLENGES IN SINGLE FIELD MODELS

In this section, we shall briefly highlight the challenges one faces in certain single field inflationary models to generate magnetic fields of the desired amplitudes and spectral shapes. Before we go on to describe these challenges, in order for this chapter to be self-contained, let us quickly recall a few essential points that we will require later for our discussion.

3.2.1 Electromagnetic modes and power spectra

We shall consider electromagnetic fields described by the action [81, 95, 97, 99, 161, 165–173]

$$S[A^\mu] = -\frac{1}{16\,\pi} \int \mathrm{d}^4x\,\sqrt{-g}\,J^2(\phi)\left[F_{\mu\nu}\,F^{\mu\nu} - \frac{\gamma}{2}\,F_{\mu\nu}\,\widetilde{F}^{\mu\nu}\right], \tag{3.1}$$

where $J(\phi)$ denotes the non-conformal coupling function and γ is a constant. As usual, the field tensor $F_{\mu\nu}$ is expressed in terms of the vector potential A_μ as $F_{\mu\nu} = (\partial_\mu\,A_\nu - \partial_\nu\,A_\mu)$, while the dual field tensor $\widetilde{F}^{\mu\nu}$ is defined as $\widetilde{F}^{\mu\nu} = (\epsilon^{\mu\nu\alpha\beta}/\sqrt{-g})\,F_{\alpha\beta}$, with $\epsilon^{\mu\nu\alpha\beta}$ being the completely anti-symmetric Levi-Civita tensor. The second term in the above action leads to violation of parity and, during inflation, this term amplifies the electromagnetic modes associated with one of the two states of polarization compared to the other [97, 99, 167–173].

In the spatially flat FLRW background of our interest, to arrive at the solutions describing the electromagnetic field, it proves to be convenient to work in the Coulomb gauge wherein $A_\eta = 0$ and $\partial_i\,A^i = 0$. We shall denote the Fourier modes of the three-vector potential A^i as $\bar{A}_k$, where the subscript k represents the wave number. If we write $\bar{A}_k = \mathcal{A}_k/J$, then, in the Coulomb gauge, the mode functions $\mathcal{A}_k$ are found to satisfy the differential equation [97, 99, 167–173]

$$\mathcal{A}_k^{\sigma\,\prime\prime} + \left(k^2 + \frac{2\,\sigma\,\gamma\,k\,J'}{J} - \frac{J''}{J}\right)\mathcal{A}_k^\sigma = 0, \tag{3.2}$$

where $\sigma = \pm$ corresponds to the two helicities. The power spectra of the magnetic and electric fields, viz. $\mathcal{P}_{\mathrm{B}}(k)$ and $\mathcal{P}_{\mathrm{E}}(k)$, are defined as (see, for example, Refs. [5, 95])

$$\mathcal{P}_{\mathrm{B}}(k) = \frac{\mathrm{d}\langle\hat{\rho}_{\mathrm{B}}\rangle}{\mathrm{d}\ln k}, \quad \mathcal{P}_{\mathrm{E}}(k) = \frac{\mathrm{d}\langle\hat{\rho}_{\mathrm{E}}\rangle}{\mathrm{d}\ln k}, \tag{3.3}$$

where ρ_{B} and ρ_{E} are the energy densities associated with the magnetic and electric fields, respectively, while the expectation values are to be evaluated in the Bunch-Davies vacuum. It is also useful to note here that we shall define the spectral index n_{B} of the magnetic field as $n_{\mathrm{B}} = (\mathrm{d}\ln\mathcal{P}_{\mathrm{B}}(k)/\mathrm{d}\ln k)$, and we shall refer to the case wherein $n_{\mathrm{B}} = 0$ as a scale invariant spectrum. The power spectra $\mathcal{P}_{\mathrm{B}}(k)$ and $\mathcal{P}_{\mathrm{E}}(k)$ can be expressed in terms of the mode functions $\mathcal{A}_k$ and their time derivatives $\mathcal{A}_k'$ as follows [5, 95, 225]:

$$\mathcal{P}_{\mathrm{B}}(k) = \frac{k^5}{4\,\pi^2\,a^4}\left[\left|\mathcal{A}_k^+\right|^2 + \left|\mathcal{A}_k^-\right|^2\right], \tag{3.4a}$$

$$\mathcal{P}_{\mathrm{E}}(k) = \frac{k^3}{4\,\pi^2\,a^4}\,\left[\left|\mathcal{A}_k^{+\prime} - \frac{J'}{J}\mathcal{A}_k^{+}\right|^2 + \left|\mathcal{A}_k^{-\prime} - \frac{J'}{J}\mathcal{A}_k^{-}\right|^2\right]. \tag{3.4b}$$

In a de Sitter universe, one often chooses the non-conformal coupling function to be of the form $J(\eta) = [a(\eta)/a(\eta_{\mathrm{e}})]^2$, where η_{e} denotes the conformal time coordinate towards the end of inflation. Such a choice for the coupling function leads to a scale invariant spectrum for the magnetic field (in this context, see, for example, Refs [5, 9, 95]). In models allowing slow roll inflation, there exists no universal or model independent form of $J(\phi)$ that leads to the above-mentioned behaviour in terms of the scale factor. However, given a model of inflation that permits slow roll, based on the evolution of the scalar field, it is easy to construct a function $J(\phi)$ that approximates the desired behaviour of $J \propto a^2$ fairly well. As we had discussed in the previous chapter, for such a choice of the non-conformal coupling function, the power spectra of the electromagnetic fields, evaluated at late times, i.e. as $(k\,\eta_{\mathrm{e}}) \to 0$, can be expressed as (see, for instance, Ref. [225])

$$\frac{\mathcal{P}_{\mathrm{B}}(k)}{M_{\mathrm{Pl}}^4} = \frac{9\,H_{\mathrm{I}}^4}{4\,\pi^2}\,f(\gamma) = \frac{9\,\pi^2}{16}\,\left(r\,A_{\mathrm{s}}\right)^2\,f(\gamma), \tag{3.5a}$$

$$\begin{aligned}\frac{\mathcal{P}_{\mathrm{E}}(k)}{M_{\mathrm{Pl}}^4} &= \frac{\mathcal{P}_{\mathrm{B}}(k)}{M_{\mathrm{Pl}}^4}\,\left[\gamma^2 - \frac{\sinh^2(2\,\pi\,\gamma)}{3\,\pi\,(1+\gamma^2)\,f(\gamma)}\,(-k\,\eta_{\mathrm{e}})\right.\\ &\quad\left. + \frac{1}{9}\,\left(1 + 23\,\gamma^2 + 40\,\gamma^4\right)\,(-k\,\eta_{\mathrm{e}})^2\right],\end{aligned} \tag{3.5b}$$

where H_{I} represents the Hubble scale during inflation, $A_{\mathrm{s}} = 2.1 \times 10^{-9}$ denotes the observed amplitude of the scalar power spectrum at the pivot scale, and r represents the tensor-to-scalar ratio [52, 210]. Also, the function $f(\gamma)$ is given by [225]

$$f(\gamma) = \frac{\sinh\left(4\,\pi\,\gamma\right)}{4\,\pi\,\gamma\,\left(1 + 5\,\gamma^2 + 4\,\gamma^4\right)}, \tag{3.6}$$

and we should be point out that $f(\gamma)$ reduces to unity in the limit of vanishing γ.

We shall now make a few clarifying remarks regarding the results we have quoted above. Let us first discuss the shape of the electromagnetic spectra in slow roll inflation before we turn to comment on their amplitudes. In the case of helical fields (i.e. when the parameter γ is non-zero), it is the first term within the square brackets in the expression (3.5b) for $\mathcal{P}_{\mathrm{E}}(k)$ that dominates, and hence one finds that the power spectra of both the magnetic and electric fields are scale invariant, with their amplitudes being determined by the tensor-to-scalar ratio r (or, equivalently, H_{I}) and the function $f(\gamma)$. When γ vanishes (i.e. in the case of non-helical fields), the function $f(\gamma)$ reduces to unity and one finds that the spectrum of the magnetic field $\mathcal{P}_{\rm B}(k)$ continues to remain scale invariant. However, in such a limit, it is the last term within the square brackets in the expression for $\mathcal{P}_{\rm E}(k)$ that survives, indicating that the power spectrum of the electric field behaves as k^2.

Let us now understand the amplitudes of the spectra in slow roll inflation. Clearly, in the helical case, for $\gamma \simeq \mathcal{O}(1)$, the strengths of the scale invariant spectra of the magnetic and electric fields are comparable and are primarily determined by the tensor-to-scalar ratio r. But, in the non-helical case, due to the k^2 dependence, the spectrum of the electric field is considerably suppressed over large scales when compared to the scale invariant amplitude of the magnetic field. We find that, for $10^{-12} \lesssim r \lesssim 10^{-2}$, upon assuming instantaneous reheating, inflationary magnetogenesis leads to non-helical magnetic fields of strength in the range of $10^{-17} \lesssim B_0 \lesssim 10^{-11}\,{\rm G}$ *today*. It should be clear that the function $f(\gamma)$ grows exponentially with γ [see Eq. (3.6)]. As a result, the amplitude of the helical fields can be considerably enhanced at late times when compared to the non-helical case. It can be shown that, for inflationary models wherein $r \simeq 10^{-2}$, if the backreaction due to the helical electromagnetic fields has to be negligible, then one has to work with $\gamma \lesssim 2.5$ [225]. When considering helical fields, we shall work with $\gamma = 0.25$. For $\gamma = 0.25$, we find that $f(0.25) \simeq 3$, which implies that the strengths of the helical magnetic fields will be higher by such a factor when compared to the non-helical case.

3.2.2 Difficulty in ultra slow roll inflation

We had mentioned above that, in models permitting slow roll inflation, based on the evolution of the field arrived at in the slow roll approximation, it is possible to construct a function $J(\phi)$ so that the desired behaviour of $J \propto a^2$ is achieved. Now, consider situations wherein there arise deviations from slow roll. In single field models of inflation involving the canonical scalar field, typically, departures from slow roll occur because of features in the inflationary potential, such as a step, a bump, a dip, a burst of oscillation, or a point of inflection. If the deviations from slow roll are small, then one can work with the form of $J(\phi)$ that is constructed using the slow roll approximation in the absence of the feature in the potential. Under such conditions, in the last chapter, we had shown that the departures from slow roll inflation generate features in the spectra of the electromagnetic fields in much the same manner as they produce features in the scalar power spectrum [225]. The small deviations from slow roll induce brief departures from scale invariance in the spectrum of the magnetic field. However, we had found that, for a given choice of the coupling function $J(\phi)$, say, chosen based on the slow roll evolution at early or late times, strong departures from slow roll inflation generically lead to prominent features in the spectra of the electromagnetic fields.

Strong departures from slow roll inflation are usually considered in two contexts. They are invoked either to suppress the scalar power over large scales in order to explain the lack of power observed at the low multipoles [178, 181, 182, 185, 186, 189] or to boost the power over small scales leading to enhanced formation of PBHs [196–200, 202, 203, 227]. These features are often achieved with the aid of an epoch of ultra slow roll inflation during which the first slow roll parameter decreases exponentially [235, 236]. While the first slow roll parameter remains small during this period, the second and higher order slow roll parameters prove to be large resulting in a violation of the slow roll conditions. In single field models of inflation driven by the canonical scalar field, a period of ultra slow roll, in turn, seems guaranteed, if there is a point of inflection in the potential. In the last chapter, we had seen that, in models which permit a period of ultra slow roll inflation, the non-conformal coupling function hardly evolves during the phase of ultra slow roll [225]. Due to this reason, the spectra of both the magnetic and electric fields behave as k^4 for wave numbers that leave the Hubble radius after the onset of ultra slow roll inflation. Moreover, the amplitude of the spectra on large scales are suppressed by the factor of $\mathrm{e}^{-4\,(N_\mathrm{e}-N_1)}$, where N_1 and N_e represent the e-folds at the onset of the epoch of ultra slow roll and the end of inflation, respectively. In arriving at these spectra, we had considered coupling functions that are based on the behaviour of the scalar field during the initial slow roll regime. One may wonder if it is possible to arrive at the desired non-minimal coupling function (i.e. one wherein $J(\phi) \propto a^2$) by fitting for the entire evolution of the scalar field. As we have illustrated in Fig. 3.1, we find that this is indeed difficult to achieve. This primarily occurs due to the fact that, generically, the scalar field virtually ceases to evolve once the epoch of ultra slow roll begins, until the very end of inflation. As we shall discuss in this chapter, due to the additional degree of freedom available, it is possible to circumvent such a challenge in the case of two field models.

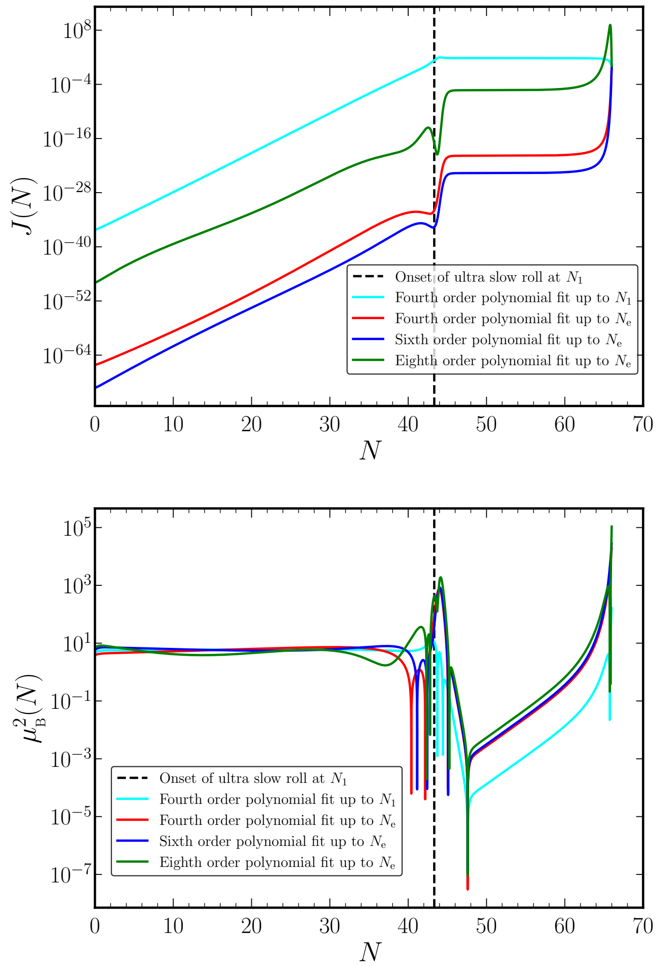

Figure 3.1: The evolution of the non-conformal coupling function J (on top) and the quantity $\mu_{\mathrm{B}}^2 = J''/(J\, a^2\, H^2)$ (at the bottom) in a model involving a single, canonical scalar field that leads to an epoch of ultra slow roll inflation—the potential (2.57) in the previous chapter [225]—have been plotted as functions of e-folds N. These plots illustrate the challenge faced in such scenarios. In the previous chapter, we had worked with a coupling function $J(\phi)$ that was arrived at by fitting the numerical solution for the scalar field with a fourth order polynomial *until* the onset of the ultra slow roll regime (plotted here in cyan). Apart from such a choice for the coupling function, we have plotted the coupling function $J(\phi)$ as well as the quantity μ_{B}^2 wherein the entire evolution of the field (i.e. from the initial time until the end of inflation) has been fit to fourth, sixth and eighth order polynomials (in red, blue and green, respectively). Note that $J \propto \mathrm{e}^{2\,N}$ and $\mu_{\mathrm{B}}^2 \simeq 6$ until the onset of the ultra slow roll regime (indicated by the vertical dashed black lines in the two figures), which are required to lead to a scale invariant spectrum for the magnetic field. However, it seems impossible to achieve such a behaviour for J and μ_{B}^2 after the onset of ultra slow roll. This can be primarily attributed to the fact that the field hardly evolves during this period.

3.3 CIRCUMVENTING THE CHALLENGES IN TWO FIELD MODELS

In this section, we shall illustrate the manner in which the challenges with the epochs of ultra slow roll inflation can be circumvented in two field models. We shall begin by introducing the inflationary models of our interest before we go on to discuss the choice of the non-conformal coupling functions and the resulting spectra of electromagnetic fields.

3.3.1 Models of interest

We shall consider a system of two scalar fields, say, ϕ and χ, that are described by the action [237]

$$S[\phi,\chi]=\int \mathrm{d}^4x\,\sqrt{-g}\left[-\frac{1}{2}\,\partial_\mu\phi\,\partial^\mu\phi-\frac{f(\phi)}{2}\,\partial_\mu\chi\,\partial^\mu\chi-V(\phi,\chi)\right]. \tag{3.7}$$

Clearly, while ϕ is a canonical scalar field, χ is a non-canonical scalar field due to the presence of the function $f(\phi)$ in the term describing its kinetic energy. We shall work with potentials $V(\phi,\chi)$ that are separable. As a result, the two fields essentially interact through the function $f(\phi)$, which we shall assume to be of the form $f(\phi)=\mathrm{e}^{2\,b(\phi)}$.

The equations of motion describing the evolution of the scalar fields are given by [237]

$$\begin{aligned}\ddot{\phi}+3\,H\,\dot{\phi}+V_\phi &= b_\phi\,\mathrm{e}^{2\,b}\,\dot{\chi}^2, && (3.8\mathrm{a})\\ \ddot{\chi}+(3\,H+2\,b_\phi\,\dot{\phi})\,\dot{\chi}+\mathrm{e}^{-2\,b}\,V_\chi &= 0, && (3.8\mathrm{b})\end{aligned}$$

where the subscripts ϕ and χ denote differentiation of the potential $V(\phi,\chi)$ and the function $b(\phi)$ with respect to the corresponding fields. Also, it is useful to note that the Hubble parameter and its time derivative are governed by the following equations:

$$H^2 = \frac{1}{3\,M_{_{\mathrm{Pl}}}^2}\left(\frac{\dot{\phi}^2}{2}+\mathrm{e}^{2\,b}\,\frac{\dot{\chi}^2}{2}+V\right), \tag{3.9}$$

$$\dot{H} = -\frac{1}{2\,M_{_{\mathrm{Pl}}}^2}\left(\dot{\phi}^2+\mathrm{e}^{2\,b}\,\dot{\chi}^2\right). \tag{3.10}$$

Let us now discuss the specific models that we shall consider.

Suppression of power on large scales

The first of the two models that we shall consider leads to a suppression of power on large scales. In our earlier work, we had discussed the so-called punctuated inflationary models which result in a suppression of power over large scales that are comparable to the Hubble radius today. We had also mentioned that such models can mildly improve the fit to the CMB data (for early discussions in this context, see Refs. [178–182, 185, 186]; for a recent discussion, see Ref. [189]). We had shown that the punctuated inflationary models leave strong imprints on the spectra of the electromagnetic fields. In particular, we had found that the strengths of the magnetic fields on large scales are considerably suppressed and their spectra behave as k^4 on small scales. Our aim in this section is to investigate whether such challenges can be overcome in inflationary models involving two fields.

To achieve a suppression in the spectrum of curvature perturbations on the largest scales, we shall consider a simple quadratic potential for the field ϕ and a KKLTI-like potential for the field χ [238], so that the complete potential is given by [228]

$$V(\phi,\chi) = \frac{m_\phi^2}{2}\,\phi^2 + V_0\,\frac{\chi^2}{\chi_0^2+\chi^2}. \tag{3.11}$$

(For convenience, we shall refer to the model as TFM1 in the figures.) Moreover, we shall assume that $b(\phi) = \bar{b}\,\phi$, where $\bar{b}$ is a constant. We shall work with the following two sets of values of the parameters involved: $(m_\phi/M_{_{\rm Pl}}, V_0/M_{_{\rm Pl}}^4, \chi_0/M_{_{\rm Pl}}, \bar{b}\,M_{_{\rm Pl}}) = (1.672\times 10^{-5}, 2.6\times 10^{-10}, \sqrt{3}, 1.0)$ and $(1.688\times 10^{-5}, 2.65\times 10^{-10}, \sqrt{3}, 2.0)$. We shall choose the initial values of the fields to be $\phi_{\rm i} = 8.8\,M_{_{\rm Pl}}$, $\chi_{\rm i} = 5.76\,M_{_{\rm Pl}}$, and set $\epsilon_{1{\rm i}} = 2.47\times 10^{-2}$, for both these sets of parameters. In fact, we shall choose a very small value of $\dot{\chi}$ so that χ does not evolve at all during the initial phase. For these choices of the parameters and initial conditions, there arise two stages of inflation with distinct values of the first slow roll parameter ϵ_1. In Fig. 3.2, we have plotted the evolution of the two scalar fields and the first slow roll parameter in the model for the above sets of parameters and initial conditions. It should be clear from the figure that the first stage is driven by the field ϕ with $\epsilon_1 \simeq 10^{-2}$. The second stage begins when the field ϕ has reached the bottom of the quadratic potential and the field χ begins to drive the accelerated expansion. In other words, there arises a turning in field space. During the transition, the first slow roll parameter falls exponentially in a manner somewhat similar to the single field models that admit an epoch of ultra slow roll inflation. The

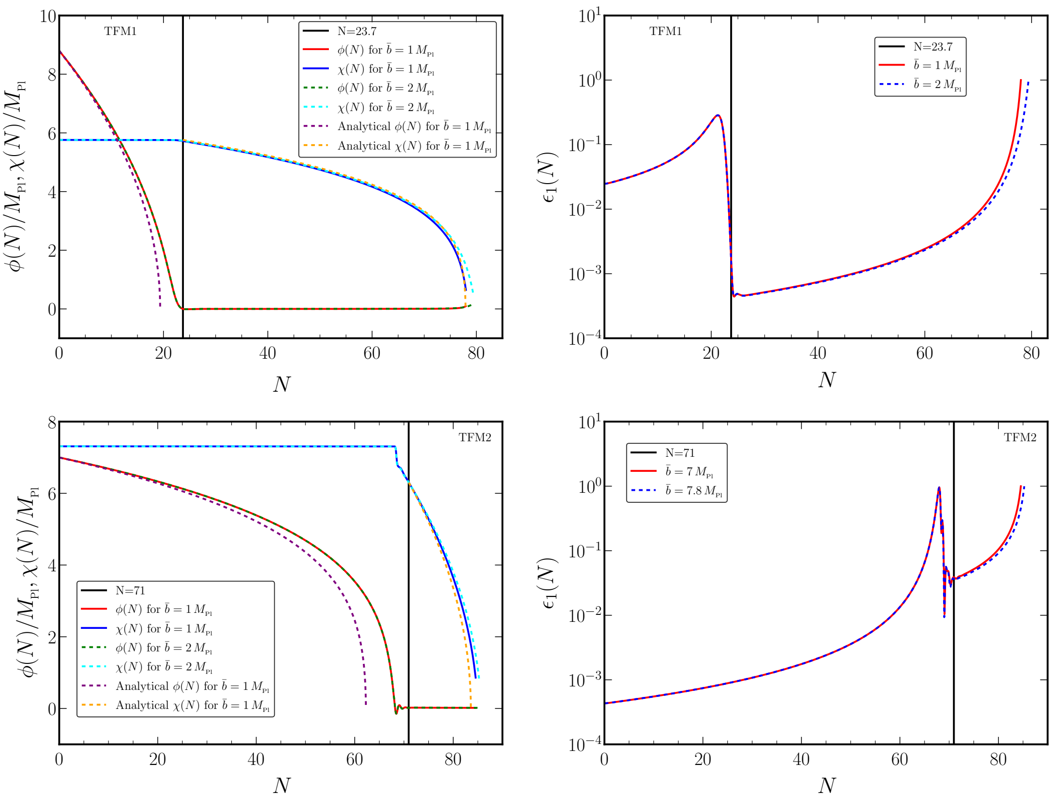

Figure 3.2: The evolution of the two scalar fields, viz. ϕ (in solid red and dashed green) and χ (in solid blue and dashed cyan), in the models described by the potentials (3.11) and (3.12) (say, TFM1 and TFM2) have been plotted (in the panels on the left, with TFM1 on top and TFM2 at the bottom, respectively) as functions of e-folds. We have plotted the results for two sets of values of the parameters involved (with the first set in solid lines and the second in dashed lines). We have also plotted the corresponding evolution of the first slow roll parameter (in solid red and dashed blue, on the right). Moreover, we have indicated the e-folds (as vertical black lines) when the transition from the first to the second stage of inflation occurs in the two models of our interest, viz. around $N \simeq 23.7$ in the first model (TFM1, on top) and $N \simeq 71$ in the second model (TFM2, at the bottom), respectively. Note that, for a given potential, the primary difference between the values of the two sets of parameters is the value of $\bar{b}$. However, it should be clear from the above plots that the difference in $\bar{b}$ does not lead to a significant difference in the evolution of the fields. In the figure, we have also indicated (as dotted curves) the analytical solutions for the fields ϕ (in purple) and χ (in orange) that can be arrived at in the slow roll approximation (for details, see App. B). It should be clear that the analytical solutions are a reasonably good approximation to the exact numerical results during the two slow roll regimes. As one would expect, the analytical solutions fail to capture the dynamics around the point of transition from the first to the second stage of inflation.

first slow roll parameter is very small (with $\epsilon_1 \simeq 10^{-3}$) during the early phase of the second stage and it slowly begins to rise leading to the end of inflation. We find that for the parameters and initial conditions that we have worked with, inflation lasts for 78–79 e-folds.

Enhancement of power on small scales

The second model we shall consider leads to enhanced power on small scales. As in the first model, this is achieved through a turning in field space, which briefly increases the strength of the coupling between the curvature and the isocurvature perturbations as well as induces a tachyonic instability. If the turning occurs at a sufficiently late stage of inflation, these two effects combine to lead to an enhancement in the spectrum of curvature perturbations on smaller scales [228–231].

To obtain a peak in the power spectrum at smaller scales, we interchange the potentials for the two fields we had considered earlier [see Eq. (3.11)]. In other words, we consider a model of inflation driven by a KKLTI-like potential for ϕ and a simple quadratic potential for χ, so that the complete potential is given by [231]

$$V(\phi, \chi) = V_0 \frac{\phi^2}{\phi_0^2 + \phi^2} + \frac{m_\chi^2}{2} \chi^2. \tag{3.12}$$

(We shall refer to the model as TFM2 in the figures.) We shall again assume that $b(\phi) = \bar{b}\, \phi$ and we shall work with the following two sets of values of the parameters: $(V_0/M_{\rm Pl}^4, \phi_0/M_{\rm Pl}, m_\chi/M_{\rm Pl}, \bar{b}\, M_{\rm Pl}) = (7.1\times 10^{-10}, \sqrt{6}, 1.19164\times 10^{-6}, 7.0)$ and $(7.31\times 10^{-10}, \sqrt{6}, 1.209\times 10^{-6}, 7.8)$. We assume that $\phi_{\rm i} = 7.0\, M_{\rm Pl}$, $\chi_{\rm i} = 7.31\, M_{\rm Pl}$ and $\epsilon_{1\rm i} = 4.32 \times 10^{-4}$. Also, as in the earlier model, we shall choose a small value of $\dot{\chi}$ so that χ hardly evolves during the first phase. With these choices of the parameters, we obtain about 84–85 e-folds of inflation. In Fig. 3.2, we have plotted the evolution of the two fields as well as the behaviour of the first slow roll parameter. Clearly, as in the previous case, there arise two stages of inflation, with the first stage again driven by the field ϕ and the second stage driven by the field χ. Moreover, at the transition, the first slow roll parameter ϵ_1 decreases briefly before increasing to unity leading to the termination of inflation. Further, we find that, in contrast to the single field case, the first slow roll parameter does not decrease to considerably low values [say, to $\mathcal{O}(10^{-9}$–$10^{-7})$] in order to lead to a significant enhancement in power.

3.3.2 Scalar and tensor power spectra

Let us now briefly discuss the spectra of curvature and isocurvature perturbations that arise in the two models we discussed above. Let us begin by recalling a few essential points regarding the scalar perturbations in two field models. As is well known, in two field models of inflation, the scalar perturbations can be decomposed into the so-called adiabatic (say, $\delta\sigma$) and entropy (say, δs) components [214, 237, 239]. In field space, while the adiabatic perturbations are parallel to the background trajectory, the entropy perturbations are orthogonal to it.

If $\delta\phi$ and $\delta\chi$ denote the perturbations in the two scalar fields, the adiabatic and entropic perturbations are defined as [237, 240]

$$\delta\sigma = \cos\theta\,\delta\phi + \mathrm{e}^{b}\,\sin\theta\,\delta\chi, \tag{3.13a}$$

$$\delta s = -\sin\theta\,\delta\phi + \mathrm{e}^{b}\,\cos\theta\,\delta\chi, \tag{3.13b}$$

where $\cos\theta = \dot{\phi}/\dot{\sigma}$, $\sin\theta = \dot{\chi}/\dot{\sigma}$, and $\dot{\sigma}^2 = \dot{\phi}^2 + \mathrm{e}^{2\,b}\,\dot{\chi}^2$. Upon using the background equations (3.8), one can arrive at the following equations that govern the adiabatic field σ and the angle θ:

$$\ddot{\sigma} + 3\,H\,\dot{\phi} + V_\sigma = 0, \tag{3.14a}$$

$$\dot{\theta} = -\frac{V_s}{\dot{\sigma}} - b_\phi\,\dot{\sigma}\,\sin\theta, \tag{3.14b}$$

where the quantities V_σ and V_s are given by

$$V_\sigma = \cos\theta\,V_\phi + \mathrm{e}^{-b}\,\sin\theta\,V_\chi, \tag{3.15a}$$

$$V_s = -\sin\theta\,V_\phi + \mathrm{e}^{-b}\,\cos\theta\,V_\chi. \tag{3.15b}$$

In the spatially flat gauge, the Mukhanov-Sasaki variables associated with the curvature and isocurvature perturbations are given by $v^\sigma = a\,\delta\sigma$ and $v^s = a\,\delta s$. The equations of motion describing the evolution of the Mukhanov-Sasaki variables can be obtained to be [228, 231, 237, 240]

$$v_k^{\sigma\prime\prime} + \left(k^2 - \frac{z''}{z}\right)\,v_k^\sigma = \frac{1}{z}\,(z\,\xi\,v_k^s)', \tag{3.16a}$$

$$v_k^{s\prime\prime} + \left(k^2 - \frac{a''}{a} + \mu_s^2\,a^2\right)\,v_k^s = -z\,\xi\,\left(\frac{v_k^\sigma}{z}\right)', \tag{3.16b}$$

where $z = a\,\dot{\sigma}/H$, $\xi = -2\,a\,V_s/\dot{\sigma}$, while μ_s^2 is given by

$$\begin{aligned}
\mu_s^2 &= V_{ss} - \left(\frac{V_s}{\dot{\sigma}}\right)^2 + b_\phi\,\left(1+\sin^2\theta\right)\,\cos\theta\,V_\sigma \\
&\quad + b_\phi\,\cos^2\theta\,\sin\theta\,V_s - \left(b_\phi^2 + b_{\phi\phi}\right)\,\dot{\sigma}^2, \qquad (3.17)
\end{aligned}$$

with V_{ss} being defined as

$$V_{ss} = \sin^2\theta\,V_{\phi\phi} - \mathrm{e}^{-b}\,\sin 2\,\theta\,V_{\phi\chi} + \mathrm{e}^{-2\,b}\,\cos^2\theta\,V_{\chi\chi}. \qquad (3.18)$$

As is done in the case of single field models, the Bunch-Davies initial conditions are imposed on the Fourier modes when they are sufficiently inside the Hubble radius, and the scalar and tensor power spectra are evaluated when the modes are well outside the Hubble radius. While computing the scalar power spectra numerically, we impose the initial conditions when $k \simeq 10^2\,\sqrt{z''/z}$ and evaluate the spectra at the end of inflation. To ensure that there are no correlations between the curvature and the isocurvature perturbations at early times, when the modes are inside the Hubble radius, the scalar perturbations are evolved from two sets of initial conditions [237, 239]. In the first set, the standard Bunch-Davies initial conditions are imposed on the Mukhanov-Sasaki variable v_k^σ, while the variable v_k^s is set to be zero. In the second set, the initial conditions on v_k^σ and v_k^s are interchanged. The curvature perturbation $\mathcal{R}_k$ and the isocurvature perturbation $\mathcal{S}_k$ are related to the Mukhanov-Sasaki variables as follows: $\mathcal{R}_k = v_k^\sigma/z$ and $\mathcal{S}_k = v_k^s/z$ [228, 231]. Let $(\mathcal{R}_{k1}, \mathcal{S}_{k1})$ and $(\mathcal{R}_{k2}, \mathcal{S}_{k2})$ denote the curvature and the isocurvature perturbations evolved from the two sets of initial conditions mentioned above. The spectra of curvature and isocurvature perturbations are evaluated from both these sets of solutions and are given by [228, 231, 237, 240]

$$\mathcal{P}_{_{\mathcal{R}}}(k) = \frac{k^3}{2\,\pi^2}\,\left(|\mathcal{R}_{k1}|^2 + |\mathcal{R}_{k2}|^2\right), \qquad (3.19a)$$

$$\mathcal{P}_{_{\mathcal{S}}}(k) = \frac{k^3}{2\,\pi^2}\,\left(|\mathcal{S}_{k1}|^2 + |\mathcal{S}_{k2}|^2\right). \qquad (3.19b)$$

In our discussion below, we shall focus on the spectrum of curvature perturbations $\mathcal{P}_{_{\mathcal{R}}}(k)$. Also, we should mention that the tensor power spectrum is evaluated in the same manner as in single field inflation.

The evolution of the scalar fields in the two models of our interest can be obtained by solving the background equations (3.8) numerically as discussed in the previous subsection. Recall that, we had illustrated the behaviour of the scalar fields and the first slow roll parameter as functions of e-folds in Fig. 3.2. In the case of the potential (3.11), the field ϕ slowly rolls down the potential until it reaches the bottom of the potential when $N \simeq 23.7$, while the field χ remains frozen during this period. At this point of transition, for the set of parameters we have worked with, the values of the fields ϕ and χ are $\phi_1 = 6.55 \times 10^{-4}\, M_{_{\rm Pl}}$ and $\chi_1 = 5.722\, M_{_{\rm Pl}}$, respectively. After the transition, while ϕ oscillates about the minimum of the potential, the field χ drives inflation until the end. Also, the first slow roll parameter ϵ_1 decreases exponentially soon after the transition, giving rise to a brief period of ultra slow roll, before it eventually rises to unity leading to the end of inflation. A similar behaviour of the fields and the slow roll parameter are observed in the case of the potential (3.12) as well, with the transition point occurring at a much later time, viz. at the e-fold $N \simeq 71$. In this case, we choose the point of transition to be when the oscillations of the field ϕ have substantially died down. At the transition point, the values of the fields ϕ and χ are found to be $\phi_1 = 1.694 \times 10^{-2}\, M_{_{\rm Pl}}$ and $\chi_1 = 6.3\, M_{_{\rm Pl}}$, respectively. In Fig. 3.3, we have presented the spectra of the curvature and tensor perturbations arising in the two models for the two sets of parameters we have considered. In the case of the potential (3.11), we obtain a suppression in power in the spectrum of curvature perturbations on the largest observable scales, while over the CMB and smaller scales, the scalar power spectrum is nearly scale invariant. The imprints of these scalar and tensor power spectra on the anisotropies in the CMB have been discussed earlier (in this context, see Ref. [228]). For the potential (3.12), we obtain nearly scale invariant scalar and tensor power spectra over the CMB scales, whereas there is a significant enhancement in scalar power on small scales. We find that, at the pivot scale of $k_\ast = 0.05\,{\rm Mpc}^{-1}$, the scalar spectral index and the tensor-to-scalar ratio turn out to be $n_{_{\rm S}} = 0.96$ and $r = 0.02$, which are consistent with the constraints from the CMB data [52]. As has been illustrated earlier in the literature, the turning in field space briefly increases the strength of the coupling between the isocurvature and the curvature perturbations. It also induces tachyonic instability. These two effects combine to lead to the increased scalar power on smaller scales over modes which leave the Hubble radius just prior to or during the turning in field space [228–231]. Earlier, we had seen that for a given potential, despite the difference in the values of the parameter $\bar{b}$, the evolution of background scalar fields were very similar (see Fig. 3.2). However, as should be clear from Fig. 3.3, the resulting inflationary scalar power spectra are considerably different. This can be attributed to the difference in μ_s^2 [cf. Eq. (3.17)] that arises due to the difference in the values of $\bar{b}$ and the resulting amplitude of the tachyonic instability that occurs due to the turning in field space (for a detailed discussion in this context, see Ref. [228]).

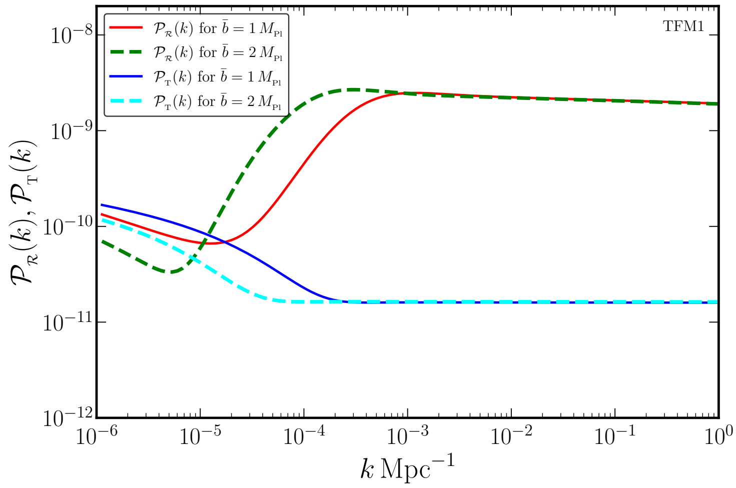

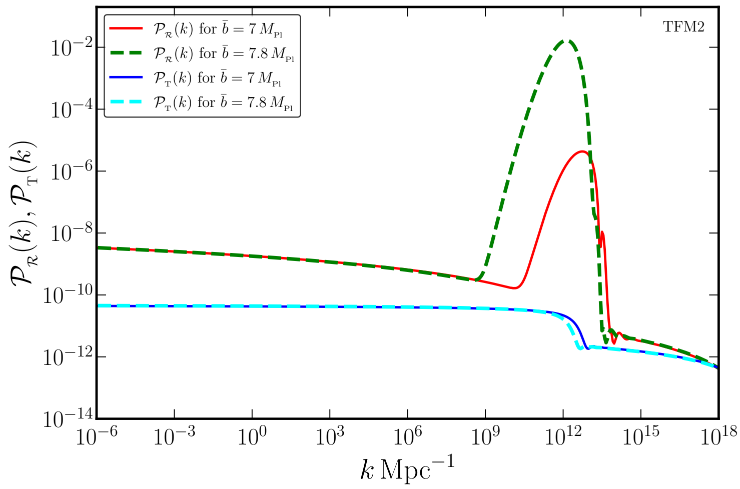

Figure 3.3: The spectra of curvature (in solid red and dashed green) and tensor (in solid blue and dashed cyan) perturbations, viz. $\mathcal{P}_{\mathcal{R}}(k)$ and $\mathcal{P}_{\rm T}(k)$, have been plotted for the two field inflationary models that we have considered. We have plotted the spectra with features over the CMB scales (on top) arising in the potential (3.11) (i.e. in TFM1) and with a peak in the scalar power at small scales (at the bottom) occurring in the potential (3.12) (i.e. in TFM2), for the two sets of parameters (as solid and dashed lines) we have mentioned earlier. In arriving at these spectra, we have assumed that the pivot scale $k_* = 0.05\,{\rm Mpc}^{-1}$ leaves the Hubble radius 50 e-folds before the end of inflation. It is the scalar spectra with a sharp rise in power on small scales that are often considered to produce a significant number of PBHs. Recall that, for a given potential, the two sets of parameters primarily differed in the value of $\bar{b}$. As we had seen in the previous figure, there was hardly any difference in the evolution of the background for the two sets of parameters. However, note that the spectra of curvature perturbations differ significantly for these two sets. This can be attributed to the tachyonic instability that arises for non-zero values of $\bar{b}$. It is found that, even small differences in $\bar{b}$ can significantly alter the evolution of the curvature perturbations, leading to very different scalar power spectra.

3.3.3 Construction of the non-conformal coupling function

Recall that, our main reason for considering two field models of inflation in this chapter is to circumvent the challenges that we face in single field models, especially those that permit an epoch of ultra slow roll inflation. Our goal is to overcome these hurdles and arrive at electromagnetic spectra of desired shapes and strengths. In the previous chapter, we had shown that, in slow roll inflation driven by a single field, say, ϕ, it is possible to construct analytical forms for the non-conformal coupling function $J(\phi)$ that lead to the required time dependence (viz. $J \propto a^2$) and therefore generate nearly scale invariant spectra for the magnetic field [225]. However, when strong departures from slow roll occur, we had to turn to a numerical approach to construct the coupling function. Since the dynamics in the two field models of our interest is fairly non-trivial, we shall adopt the numerical approach here as well. We shall now outline the procedure to construct the required $J(\phi, \chi)$. We should mention that, in App. B, we have discussed the construction of an analytical form for the coupling function $J(\phi, \chi)$ and the resulting power spectra of the electromagnetic fields that we obtain in such a case.

In fact, the procedure that needs to be adopted to construct the desired non-conformal coupling function $J(\phi, \chi)$ is fairly straightforward. In the two models of our interest, we have seen that, at any given time during inflation, one of the two slowly rolling fields largely determines the dynamics of the background. Essentially, we need to make use of the dominant field to construct the coupling function in a given domain. Thereafter, we can utilize the step function to stitch together the coupling functions in the two domains to arrive at the complete function. Let us, for instance, consider the model described by the potential (3.11). In the model, during the first domain, the field ϕ rolls down the potential largely determining the background dynamics, while the field χ remains frozen. After having solved the equations (3.8) numerically to arrive at $\phi(N)$, we assume an ansatz for the functional form of $N(\phi)$. We choose the functional form of $N(\phi)$ in the first regime to be given by the following fourth order polynomial:

$$N(\phi) = a_1 \frac{\phi^4}{M_{_{\mathrm{Pl}}}^4} + b_1 \frac{\phi^3}{M_{_{\mathrm{Pl}}}^3} + c_1 \frac{\phi^2}{M_{_{\mathrm{Pl}}}^2} + d_1 \frac{\phi}{M_{_{\mathrm{Pl}}}} + e_1. \tag{3.20}$$

We then determine the values of the constants $(a_1, b_1, c_1, d_1, e_1)$ by fitting the polynomial to the numerical solution for $\phi(N)$ during the initial regime, thereby arriving at $N(\phi)$. Similarly, after the transition, as the field χ starts to dominate the background dynamics, we choose $N(\chi)$ to be a fourth order polynomial of the following form:

$$N(\chi) = a_2 \frac{\chi^4}{M_{_{\mathrm{Pl}}}^4} + b_2 \frac{\chi^3}{M_{_{\mathrm{Pl}}}^3} + c_2 \frac{\chi^2}{M_{_{\mathrm{Pl}}}^2} + d_2 \frac{\chi}{M_{_{\mathrm{Pl}}}} + e_2. \tag{3.21}$$

We fit the polynomial to the solution $\chi(N)$ in the second regime to determine the constants $(a_2, b_2, c_2, d_2, e_2)$ and arrive at $N(\chi)$. We should clarify here that we have chosen to work with fourth order polynomials for $N(\phi)$ and $N(\chi)$ above since they seem sufficient to lead to the desired behaviour of J in the two slow roll regimes on either side of the transition. With the forms of $N(\phi)$ and $N(\chi)$ at hand, we can combine them to construct the complete non-conformal coupling function to be

$$\begin{aligned} J(\phi,\chi) &= \frac{J_0}{2}\left\{\left[1+\tanh\left(\frac{\chi-\chi_1}{\Delta\chi}\right)\right]\exp\left[n\,N(\phi)\right]\right. \\ &\quad \left.+\left[1-\tanh\left(\frac{\chi-\chi_1}{\Delta\chi}\right)\right]\,\exp\left[n\,N(\chi)\right]\right\}, \end{aligned} \tag{3.22}$$

where χ_1 is the value of the field χ at the transition (that we had mentioned earlier). Note that the quantity within the square brackets involving the hyperbolic tangent function in the above form for $J(\phi,\chi)$ essentially acts as a step function for a suitably small value of $\Delta\chi$. Evidently, it is the first and second terms in the above expression that contribute prior to and after the field crossing χ_1. Lastly, we should mention that we need to choose J_0 suitably so that $J(\phi,\chi)$ reduces to unity at the end of inflation. As we shall soon illustrate, for $n=2$, the above coupling function largely behaves as $J \propto a^2$.

Recall that, in each of the two models described by the potentials (3.11) and (3.12), we had worked with two sets of the parameters involved. Since the dynamics of the background fields for these two sets of parameters are not significantly different (in this context, see Fig. 3.2), we find that the coefficients characterizing the polynomial fitting functions $N(\phi)$ and $N(\chi)$ [cf. Eqs. (3.20) and (3.21)] largely prove to be the same. For the model described by the potential (3.11), we obtain the values of the fitting parameters to be $(a_1, b_1, c_1, d_1, e_1) = (2.7558\times 10^{-3}, -0.06, 0.227, -1.8556, 23.1717)$ and $(a_2, b_2, c_2, d_2, e_2) = (-0.0421, 5.47\times 10^{-3}, -0.2443, -0.4516, 78.3998)$. Similarly, in the case of the potential (3.12), we find that the fitting parameters are given by $(a_1, b_1, c_1, d_1, e_1) = (-0.01619, -0.1027, 0.3857, -2.0208, 69.4198)$ and $(a_2, b_2, c_2, d_2, e_2) = (2.7745\times 10^{-4}, -6.0702\times 10^{-3}, -0.2810, -0.2805, 85.0065)$. Moreover, we shall assume that the width of the step described by the hyperbolic tangent function is given by $\Delta\chi = 10^{-3}\,M_{_{\mathrm{Pl}}}$. In App. C, we have discussed the effects of modifying the transition point χ_1 and the width $\Delta\chi$ on the spectra of the electromagnetic fields. We find that the values of χ_1 and $\Delta\chi$ we shall work with are optimal, as they do not introduce spurious features in the spectra of the magnetic field.

In Fig. 3.4, we have plotted the evolution of the coupling function $J(\phi,\chi)$ as well

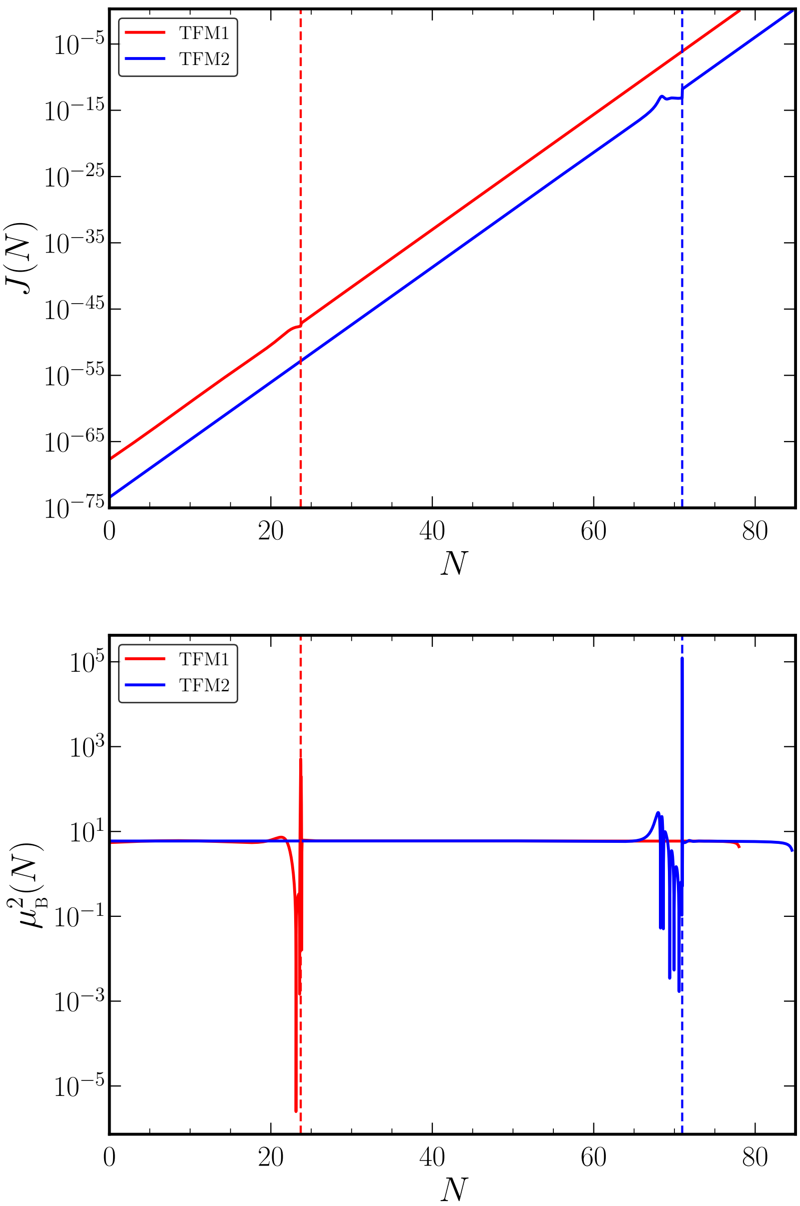

Figure 3.4: The evolution of the non-conformal coupling function $J(\phi, \chi)$ given by Eq. (3.22) (on top) and the quantity $\mu_{\rm B}^2$ (at the bottom) have been plotted as a function of e-folds for the two models described by the potentials (3.11) (i.e. in TFM1, in red) and (3.12) (i.e. in TFM2, in blue). Since the background evolution is very similar for the two sets of parameters we have worked with, the corresponding $J(N)$ prove to be essentially the same in both the models. The vertical lines (in corresponding colors) represent the points of transition at $N \simeq 23.7$ and $N \simeq 71$, respectively. It is clear from the figures that $J \propto a^2$ and $\mu_{\rm B}^2 \simeq 6$ for most of the evolution except for the domain near the transition. Recall that, in the single field case, it was impossible to achieve such a behaviour for J and $\mu_{\rm B}^2$ after the onset of ultra slow roll. Clearly, the presence of the additional field in the two field models allows us to circumvent this difficulty.

as the quantity $\mu_{\mathrm{B}}^2 = J''/(J\, a^2\, H^2)$ for the two potentials. In contrast to the single field case, where the coupling function almost ceased to evolve after the onset of ultra slow roll (see Fig. 3.1), we find that the J's we have constructed in the two field models grow as a^2 even after the transition. Moreover, clearly, $\mu_{\mathrm{B}}^2 \simeq 6$ for most of the evolution apart from the domain around the transition. This behaviour suggests that the spectrum of the magnetic field will remain scale invariant apart from the effects arising due to the transition. In Fig. 3.5, we have plotted the resulting spectra of the electromagnetic fields arising in the two models for the above choices of the coupling functions. In addition to the non-helical case, in Fig. 3.5, we have plotted the spectra in the helical case. It is evident that, in the helical case, the spectra of the magnetic and electric fields are nearly scale invariant and are of the same amplitude apart from the domain over wave numbers which leave the Hubble radius around the time of the turning in the field space. Around these wave numbers, the spectra exhibit a burst of oscillations. These oscillations occur over large scales in the first model described by the potential (3.11), whereas they occur over small scales in the second model governed by the potential (3.12). While we have been able to largely iron out very strong features in the power spectra of the electromagnetic fields, the oscillations are unavoidable unless we further fine tune the form of the non-minimal coupling function $J(\phi, \chi)$. We shall make some additional comments on this point in the concluding section.

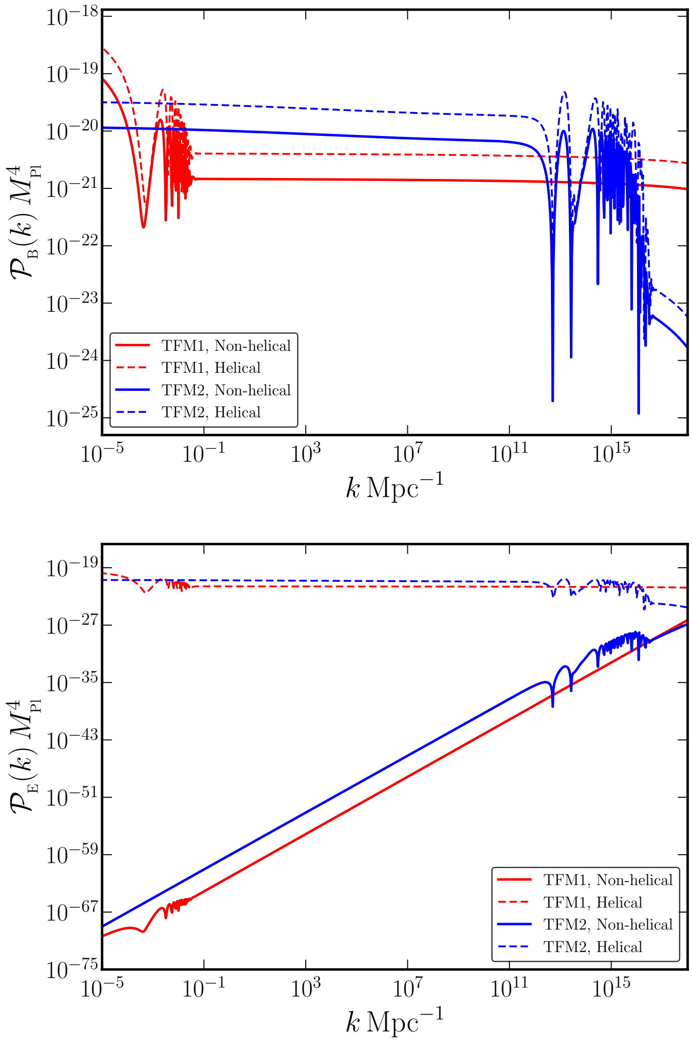

Figure 3.5: The power spectra of the magnetic (on top) and the electric (at the bottom) fields have been plotted in the cases of the models described by the potentials (3.11) (TFM1, in red) and (3.12) (TFM2, in blue) for the coupling function $J(\phi, \chi)$ given by Eq. (3.22). Apart from the non-helical case (plotted as solid curves), we have also plotted the results for the helical electromagnetic fields (as dashed curves) with $\gamma = 0.25$. The spectra of both the magnetic and electric fields are nearly scale invariant in the helical case. Also, in the non-helical case, while the spectra of the magnetic field are nearly scale invariant, the spectra of the electric field behave as k^2. Moreover, as expected, all the spectra exhibit bursts of oscillations over wave numbers which leave the Hubble radius around the time of the turning in the field space. This is because of the fact that the coupling function $J(\phi, \chi)$ contains deviations from the behaviour $J \propto a^2$ during the time of the transition. We should mention that we have worked with $\gamma = 0.25$ so that the amplitudes of the present day magnetic field generated in the two models of our interest are approximately consistent with the current constraints (see our discussion in Sec. 3.4). Note that, since $f(0.25) \simeq 3$, the scale invariant non-helical and helical amplitudes differ by a factor of three.

3.4 IMPRINTS ON THE CMB

In this section, we shall examine the observational imprints of the PMFs on the anisotropies in the CMB, which have been extensively discussed in the literature [8, 124, 130, 131, 174, 224, 241–245]. In what follows, we shall adopt the approach discussed earlier [131, 224] and make use of the publicly available packages CAMB [234] and MagCAMB [174] to calculate the angular power spectra of the anisotropies in the CMB generated by the PMFs.

Cosmological magnetic fields can be constrained via the measurement of the anisotropies in the temperature (T) and polarization (E and B modes) of the CMB (see Ref. [246]; for bounds from Planck, see Ref. [50]). We are specifically interested in the angular spectra of the CMB sourced by the PMFs in the epochs before and after neutrino decoupling. Recall that, neutrino decoupling takes place at an energy scale of about $1\,\mathrm{MeV}$, after which they start streaming freely. However, before that epoch, neutrinos are strongly bound to the photons and baryons. During this regime, the anisotropic stresses in the magnetic fields source the scalar and tensor perturbations, and these contributions are referred to as the passive magnetic modes [124, 224]. After the neutrinos decouple from the photons, they begin to stream freely and in the process, they can develop a non-zero anisotropic stress that compensates the anisotropic stress of the PMFs [245]. During this period, the PMFs generate the so-called compensated modes which are somewhat similar to the isocurvature perturbations [124, 224]. Apart from the passive and compensated modes, it has been shown that there arises a contribution to the angular power spectra of the CMB due to the curvature perturbations induced by the magnetic fields generated during inflation (in this context, see Refs. [81, 131]). The spectrum of these secondary curvature perturbations depend on the model being considered for the generation of the magnetic field. Also, we should clarify that the secondary curvature perturbations are induced in addition to the primary adiabatic perturbations generated during inflation. In our analysis below, we shall take into account the effects arising from all these contributions in the calculation of the angular power spectra of the anisotropies in the CMB. We should stress that, in this section, we shall confine our discussion to non-helical magnetic fields.

3.4.1 Contributions due to the passive and compensated modes

In order to evaluate the contributions due to the passive and compensated modes of the PMFs to the angular power spectra of the CMB, we shall make use of the publicly available package MagCAMB [174], which is a modification of CAMB [234]. Similar to CAMB, the package computes the multipole moments of the CMB, viz. the C_ℓ's, arising due to various contributions of the PMFs, for a given cosmological model. However, to reduce the computational complexity in estimating the integrals involved in arriving at the C_ℓ's, MagCAMB assumes a power law spectrum for the PMFs. In fact, we find that the power law form for the spectrum is hardcoded in the package. Note that, among the two inflationary models we have considered—viz. the models described by the potentials (3.11) and (3.12)—it is only the second potential which leads to a nearly scale invariant power law spectrum for the magnetic field over the CMB scales (see Fig. 3.5). Therefore, using MagCAMB, we shall explicitly compute the angular power spectra of the anisotropies in the CMB generated by the passive and the compensated modes for the case of the second potential (3.12). Moreover, since the potential (3.12) permits slow roll inflation during the early stages, as we shall discuss in the next subsection, it is also possible to approximately evaluate the angular power spectra of the CMB due to the curvature perturbations induced by the magnetic field. For the first model described by the potential (3.11), we find that it is challenging to carry out such an analysis, due to the complicated nature of the power spectrum for the magnetic field over large scales. Hence, in what follows, we shall only check if the strength of the magnetic field generated in this model is roughly compatible with the observational constraints.

Before going on to compute the angular power spectra of the CMB generated by the passive and compensated modes of the PMFs, let us examine if the magnetic fields generated in the two inflationary models of interest are broadly consistent with the current constraints. To do so, we need to evaluate the amplitude of the magnetic field, say, B_λ, that has been smoothed over a coherence scale λ [8, 174]. In practice, the quantity B_λ^2 is obtained by integrating the spectral energy density of the PMFs [i.e. the spectrum of the magnetic field, see Eq. (3.3)] with a Gaussian window function of width $\lambda = 1\,\mathrm{Mpc}$, and it is defined as

$$B_\lambda^2 = \int \frac{\mathrm{d}^3\boldsymbol{k}}{4\,\pi\,k^3}\,\mathrm{e}^{-\lambda^2\,k^2}\,\mathcal{P}_{_{\mathrm{B}}}(k). \tag{3.23}$$

For instantaneous reheating, the smoothed amplitude *today*, say, B_λ^0, is given by

$$B_\lambda^0 = B_\lambda\,\left(\frac{a_\mathrm{e}}{a_0}\right)^2, \tag{3.24}$$

where B_λ is the smoothed strength of the magnetic field generated during inflation, while a_e and a_0 denote the scale factors at the end of inflation and today, respectively.

The ratio of these scale factors is given by [225]

$$\frac{a_0}{a_{\rm e}} \simeq 2.8 \times 10^{28} \left(\frac{H_{\rm I}}{10^{-5}\, M_{\rm Pl}}\right)^{1/2}, \tag{3.25}$$

where $H_{\rm I}$ is the Hubble parameter during inflation.

Let us now evaluate the quantity B_λ^0 in the two inflationary models of our interest. In the case of the first potential (3.11), upon using the resulting power spectrum for the magnetic field (as illustrated in Fig. 3.5) and carrying out the integral (3.23) numerically over all scales (viz. $10^{-5} \lesssim k \lesssim 10^{19}\, {\rm Mpc}^{-1}$), we obtain that $B_\lambda^2 = 1.079 \times 10^{-20}\, M_{\rm Pl}^4$. Thereafter, upon using the relation (3.24), we obtain an estimate of the smoothed strength of the magnetic field today to be $B_\lambda^0 \simeq 2.77 \times 10^{-2}\, {\rm nG}$, corresponding to $H_{\rm I} \simeq 4.07 \times 10^{-6}\, M_{\rm Pl}$. We should mention that, to arrive at this result, we have used the conversion factors $1\, M_{\rm Pl} = 2.43 \times 10^{18}\, {\rm GeV}$ and $1\, {\rm G} = 6.91 \times 10^{-20}\, {\rm GeV}^2$. Similarly, in the case of the second potential (3.12), for the spectrum of the magnetic field illustrated in Fig. 3.5, we obtain that $B_\lambda^2 = 9.69 \times 10^{-21}\, M_{\rm Pl}^4$, which leads to the present day strength of $B_\lambda^0 \simeq 2.05 \times 10^{-1}\, {\rm nG}$, corresponding to $H_{\rm I} \simeq 5.26 \times 10^{-7}\, M_{\rm Pl}$. These estimates suggest that the spectra of the magnetic fields from the two inflationary models are broadly in agreement with the observational bound of $B_\lambda^0 \lesssim 1\, {\rm nG}$ on the strength of the magnetic field today (in this context, see, for instance, Ref. [81]).

Let us now turn to the explicit evaluation of the imprints of the passive and compensated modes induced by the PMFs on the CMB using MagCAMB. As we have already mentioned, in MagCAMB, the primordial power spectrum of the magnetic field is assumed to be of the power law form, say, $\mathcal{P}_{\rm B}(k) \propto k^{\bar{n}_{\rm B}}$, where $\bar{n}_{\rm B}$ is the spectral index. We find that the spectral index $n_{\rm B}$ we have defined [see our comments following Eq. (3.3)] is related to the spectral index $\bar{n}_{\rm B}$ of MagCAMB as $\bar{n}_{\rm B} = -3 + n_{\rm B}$. The quantities required to compute due to the PMFs using MagCAMB are the smoothed amplitude B_λ^0 that we discussed above and the spectral index $\bar{n}_{\rm B}$ [174]. As mentioned earlier, in the scenario described by the potential (3.11), since the magnetic power spectrum contains strong features over large scales, we are unable to use MagCAMB. For the model described by the potential (3.12), as the magnetic power spectrum is nearly scale invariant over large scales, we have provided MagCAMB with the smoothed amplitude B_λ^0 and the spectral index $\bar{n}_{\rm B}$ to arrive at the angular spectra of the CMB corresponding to the passive and compensated modes. We find that the spectral index over the CMB scales for the spectrum of the magnetic field illustrated in Fig. 3.5 is $n_{\rm B} = -0.0112$. So, we have supplied the following values of the parameters to MagCAMB: $B_\lambda^0 = 2.05 \times 10^{-1}\, {\rm nG}$, $\bar{n}_{\rm B} = -3.0112$, and set the pivot scale to be

$k_* = 0.05\,\mathrm{Mpc}^{-1}$. Using these parameters, we have computed the contributions of the PMFs to the angular power spectra of the CMB through the passive and compensated modes. We shall present and discuss the results in Subsec. 3.4.3.

3.4.2 Contributions due to the induced curvature perturbations

Next, we investigate the contributions to the angular power spectra of the CMB due to the curvature perturbations induced by the magnetic fields generated during inflation, which are often referred to as the inflationary magnetic modes [131, 224]. These modes are unique to inflationary magnetogenesis and are absent if the PMFs are generated after inflation. They remain unaffected by the behaviour of magnetic fields after the termination of inflation. Once again, to examine the imprints on the angular power spectrum of the CMB due to these modes, we restrict ourselves to the model described by the potential (3.12), as the sharp features in the spectrum arise only over small scales and we can work with the de Sitter approximation to compute the observables over the CMB scales.

In the slow roll approximation, the strength of the curvature perturbation, say $\mathcal{R}_k^{\mathrm{mag}}$, induced by the magnetic fields during inflation (for the case wherein $J \propto a^2$) can be written as [131, 224]

$$k^{3/2}\,\mathcal{R}_k^{\mathrm{mag}}(\eta_\mathrm{e}) = \frac{2\,H_{\mathrm{I}}^2}{3\,M_{\mathrm{Pl}}^2\,\epsilon_1}\,C_{\mathrm{EM}}(k)\,\ln\left(\frac{k}{k_\mathrm{e}}\right), \tag{3.26}$$

where ϵ_1 is the first slow roll parameter and k_e represents the wave number that leaves the Hubble radius at the end of inflation (i.e. at η_e), when the strength of the perturbations is evaluated. The quantity $C_{\mathrm{EM}}(k)$ is determined by the expression

$$\sqrt{\frac{k^3\,P_{\mathrm{EM}}(k)}{\rho_\phi^2}} = \frac{H_{\mathrm{I}}^2}{3\,M_{\mathrm{Pl}}^2}\,C_{\mathrm{EM}}(k), \tag{3.27}$$

where $P_{\mathrm{EM}}(k)$ is the power spectrum of the fluctuations in the energy density of a given mode of the electromagnetic field which is defined through the relation (D.1), and ρ_ϕ denotes the energy density of the scalar field(s) driving the inflationary background. In App. D, we have initially arrived at a generic expression for the power spectrum $P_{\mathrm{EM}}(k)$ and have then gone on to evaluate the quantity for the case wherein $J \propto a^2$, which leads to a scale invariant spectrum for the magnetic field $\mathcal{P}_{\mathrm{B}}(k)$. But, evidently, in the model described by the potential (3.12), there arise deviations from slow roll. Also, the resulting spectrum of the magnetic field is not scale invariant, as should be clear from Fig. 3.5. However, note that the departures from slow roll occur at late times and, due to this reason, the deviations from the nearly scale invariant behaviour arise only over very small scales. Moreover, the deviations from scale invariance are mostly in the form of oscillations. Therefore, *over the CMB scales*, we believe that the slow roll approximation leads to a reasonable estimate of the power spectrum of the curvature perturbations induced by the magnetic field. We can arrive at the strength of the induced curvature perturbation at late times, i.e. $\mathcal{R}_k^{\mathrm{mag}}(\eta_{\mathrm{e}})$, by using the result (D.4) for $P_{_{\mathrm{EM}}}(k)$ in Eqs. (3.26) and (3.27) and the fact that $\rho_\phi = 3\, H^2\, M_{_{\mathrm{Pl}}}^2$. The scalar power spectrum associated with the inflationary magnetic mode can be obtained to be

$$\mathcal{P}_{\mathcal{R}}^{\mathrm{mag}}(k) \simeq \frac{24}{\pi^3}\, \left(\mathcal{P}_{_{\mathrm{S}}}^0\right)^2\, \ln\left(\frac{k}{k_{\mathrm{min}}}\right)\, \left[\ln\left(\frac{k}{k_{\mathrm{e}}}\right)\right]^2, \tag{3.28}$$

where $\mathcal{P}_{_{\mathrm{S}}}^0 = H_{_{\mathrm{I}}}^2/(8\,\pi^2\,\epsilon_1)$ is the standard scalar power spectrum evaluated in the slow roll approximation.

Having obtained the spectrum of curvature perturbations induced by the magnetic field, we proceed to compute the corresponding contributions to the angular power spectrum of the CMB. We should stress that the contributions due to the inflationary magnetic mode arise *in addition* to the contributions due to the primary curvature perturbations generated from the quantum vacuum during inflation. This enables us to treat it in the same manner as the primary curvature perturbations and use the standard apparatus of CAMB to compute the corresponding angular power spectra. To evaluate the C_ℓ's, we make use of the scalar power spectrum obtained in Eq. (3.28). Since we are working with the de Sitter approximation over the CMB scales, the parameters that we require to compute the amplitude $\mathcal{P}_{_{\mathrm{S}}}^0$ are $H_{_{\mathrm{I}}}$ and ϵ_1, evaluated at the e-fold when the pivot scale exits the Hubble radius. Moreover, to obtain $\mathcal{P}_{\mathcal{R}}^{\mathrm{mag}}(k)$, we require k_{min} and k_{e}. We assume k_{min} to be $10^{-7}\,\mathrm{Mpc}^{-1}$. In the model of our interest [viz. the potential (3.12)], for the values of parameters we have worked with, we find that $k_{\mathrm{e}} \simeq 10^{19}\,\mathrm{Mpc}^{-1}$. We should further note that, since the electromagnetic field possesses anisotropic stress, apart from inducing secondary scalar perturbations, they will also generate secondary tensor perturbations (in this context, see, for example, Refs. [99, 247–252]). Such a tensor mode will also contribute to the B-mode polarization of the CMB, apart from the contributions to the temperature and E-mode polarizations. We should clarify that we have *not* calculated these contributions due to the induced tensor perturbations.

3.4.3 Angular power spectra of the CMB

In Fig. 3.6, we have illustrated all the contributions to the CMB angular spectra arising due to the PMFs for the model described by the potential (3.12) which generates enhanced scalar power on small scales. For reference, we have also plotted the standard CMB spectra obtained from CAMB, where there are no contributions from the PMFs. We should mention that these standard spectra of TT, TE, EE and BB are obtained by supplying the numerically computed scalar and tensor power spectra from our inflationary model (illustrated in Fig. 3.3) to CAMB. In arriving at these spectra, we have included the effects due to non-linear lensing. We have then presented the contributions due to the scalar inflationary magnetic mode, obtained using our modified setup of CAMB as described above. This mode contributes only to the CMB temperature and E-mode polarization spectra. We should clarify that, in computing these spectra, we have ignored the effects due to non-linear lensing. As is evident from the plots, this contribution is lower in amplitude when compared to the standard CMB spectra by $\mathcal{O}(10^4)$. We have further illustrated the contributions due to the passive and compensated modes to the angular power spectra of the CMB, which have been computed using MagCAMB. We have computed these contributions using the parameters obtained from the power spectrum of magnetic field arising in the model, viz. $B_\lambda^0 = 7.25 \times 10^{-1}\,\mathrm{nG}$ and $\bar{n}_{\rm B} = -3.0112$. As can be seen clearly, although the spectra due to the passive and compensated modes have different amplitudes, their shape is roughly similar to the standard CMB spectra. It is evident from the figure that the contributions to the CMB angular spectra due to the PMFs are substantially smaller in magnitude for the model we have considered. The largest contribution arises from the inflationary magnetic mode and it is still at least $\mathcal{O}(10^4)$ lesser in magnitude than the standard spectra.

Though we could not carry out a similar exercise for the model described by the potential (3.11), which leads to a suppression in the scalar power spectrum over large scales, the estimate of B_λ^0 in that case suggests that the corresponding contributions to C_ℓ's would be of amplitudes lesser than the case that we have discussed. Recall that, for these additional contributions, $C_\ell \propto (B_\lambda^0)^4$ and hence the overall amplitude of the passive and compensated contributions can be expected to be of lesser magnitude for the model (3.11) than in the model (3.12) wherein we have explicitly have computed these contributions. However, there can arise a difference in the shape of C_ℓ's at the lower multipoles due to the sharp features in $\mathcal{P}_{\rm B}(k)$ over large scales. In particular, the scalar

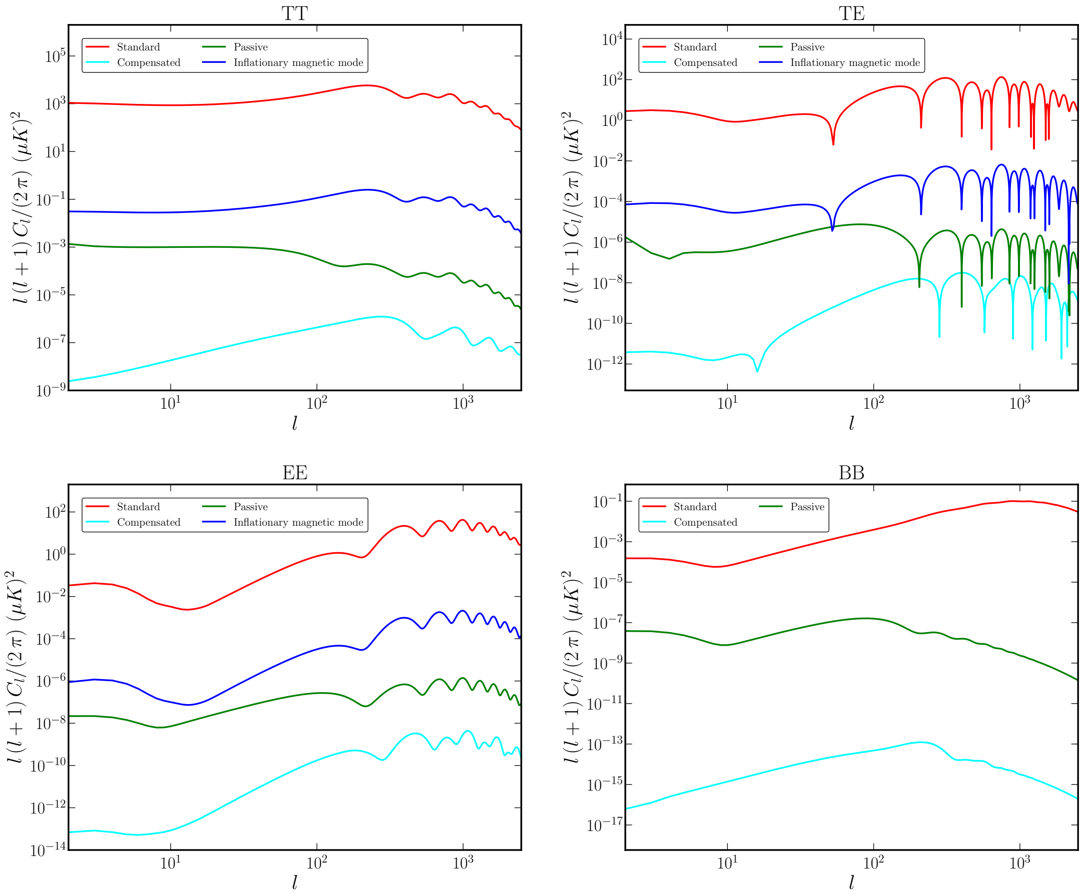

Figure 3.6: We have illustrated the contributions of the magnetic modes to the temperature and polarization angular power spectra of the CMB due to the total (i.e. scalar plus tensor) passive (in green) and the total compensated (in cyan) modes. We have arrived at these quantities using MagCAMB corresponding to a magnetic field with smoothed strength of $B^0_{1\,\mathrm{Mpc}} = 2.05 \times 10^{-1}\,\mathrm{nG}$ today and a spectral index of $\bar{n}_{\mathrm{B}} = -3.0112$. In addition, using CAMB, we have plotted the standard angular power spectra of the CMB (in red) induced by the primary scalar and tensor perturbations. Moreover, we have also presented the contribution due to the curvature perturbation induced by the magnetic field during inflation (i.e. the inflationary magnetic mode, in blue), which we have computed using CAMB. Note that, apart from the contributions due to the primary tensor perturbations to the angular power spectrum of the CMB (in particular, to the B-mode polarization, which we have illustrated in red in the plot on the bottom right corner), there will also arise a contribution due to the tensor perturbations induced by the magnetic fields during inflation. We should mention that we have *not* calculated this additional contribution.

power spectrum associated with the inflationary magnetic mode in this case can have interesting features, and being the largest of the contributions, it may leave discernible imprints on the total angular power spectrum of the CMB. But it is challenging to compute these contributions induced by the magnetic field using analytical methods for spectra with strong features. We would have to employ numerical procedures to compute the induced scalar spectra over large scales. This is a non-trivial exercise and we believe that it is beyond the scope of the current work.

3.5 CONCLUSIONS

In the previous chapter, we had shown that, in the case of single field models involving strong deviations from slow roll inflation, there arise certain challenges in obtaining nearly scale invariant power spectra for the magnetic field [225]. We had shown that even finely tuned non-conformal coupling functions may not help us avoid strong features generated in scenarios involving an epoch of ultra slow roll inflation. To overcome such challenges, in this chapter, we have examined two field models of inflation where a turning in the background trajectory in the field space gives rise to departures from slow roll. We have considered two field models where such deviations from slow roll lead to either a suppression in the scalar power over large scales or to an enhancement over small scales.

We have constructed model-dependent coupling functions numerically using the background dynamics of the two fields in these models. Using these coupling functions, we have been able to obtain the desired amplitude and a nearly scale invariant form for the power spectra of magnetic fields in the models of interest. While we have been able to mostly circumvent the challenges faced in single field models, we find that it is not entirely possible to remove the strong features over the range of scales that leave the Hubble radius during deviations from slow roll. For the potential that gives rise to an enhancement in scalar power over small scales, we obtain a power spectrum for the magnetic field which is nearly scale invariant over large scales, but contains a rapid burst of oscillations over small scales. Similarly, for the potential that generates a suppression in the scalar power over large scales, the power spectrum of the magnetic field exhibits strong oscillations over very large scales and turns scale invariant over smaller scales. In the first model, the oscillations have higher amplitude than the scale invariant part, whereas they have same amplitude in the second model. In both these models, we obtain amplitudes of the smoothed magnetic fields, which lie in the current range of observations, i.e. 10^{-16}–10^{-9} G.

Further, for the model that generates enhancement in scalar power over small scales, we have also computed the contributions of the PMFs to the anisotropies in the CMB using MagCAMB. Apart from calculating the contributions due to the passive and compensated modes, using CAMB, we have also evaluated the contribution due to the curvature perturbation induced by the magnetic field during inflation. These contributions to the angular power spectra of the CMB are of roughly similar shape as the standard spectrum, but are of lower amplitudes. Moreover, we find that, the corresponding value of the smoothed amplitude B^0_λ is well within the upper bound on the parameter obtained earlier (in this context, see Ref. [174]).

To summarize, using two field models, along with suitable choices of coupling functions, we have been able to largely overcome the challenges faced in the generation of PMFs in single field models of inflation permitting an epoch of ultra slow roll. Also, we have been able to approximately evaluate the imprints of the PMFs on the CMB in the second model that leads to a scale invariant spectrum for the magnetic field over large scales. But, clearly, there are some limitations to the approach we have adopted. For instance, it seems fair to assume that the small scale features in the power spectrum of the magnetic field are unlikely to affect the angular power spectra of the CMB. However, since there arise departures from slow roll at late times in the second model, the de Sitter approximation we have worked with to estimate the induced spectrum of curvature perturbations is likely to be inadequate. Moreover, as we mentioned, the first model which leads to features in the spectrum of the magnetic field over the CMB scales needs to be analyzed numerically to evaluate the induced spectrum of curvature perturbations and the corresponding imprints on the CMB. In addition, to compute the signatures of the passive and compensated modes in such models, MagCAMB needs to be suitably modified to take into account features in the power spectra of the electromagnetic fields. We are presently investigating such issues.

CHAPTER 4

AMPLIFYING QUANTUM DISCORD DURING INFLATIONARY MAGNETOGENESIS THROUGH VIOLATION OF PARITY

4.1 INTRODUCTION

Magnetic fields are observed over a wide range of scales in the universe (for reviews on magnetic fields, see Refs. [1–10]). They are observed in planets, stars, galaxies, clusters of galaxies and even in the IGM (for recent discussions of the various observational constraints, see, for example, Refs. [10, 149]). The magnetic fields observed in planets, stars and galaxies can be generated through astrophysical mechanisms such as batteries (in this context, see, for instance, Refs. [3, 4]). However, one may need to invoke a cosmological mechanism to explain the magnetic fields observed in the IGM [21–23, 152–155].

As is well known, the inflationary paradigm provides a simple and elegant mechanism for the origin of perturbations in the early universe (see, for example, the reviews [63, 64, 71, 73, 212–215, 217, 218]). The scalar and tensor perturbations arise due to quantum fluctuations when the Fourier modes are in the sub-Hubble domain during the early stages of inflation, and they are expected to turn classical as the modes emerge from the Hubble radius and evolve onto super-Hubble scales (for discussions in this regard, see, for instance, Refs. [253–262]). The magnetic fields can also be generated in a similar manner. However, since the standard electromagnetic action is conformally invariant, the strengths of the electromagnetic fields produced in such a case will be rapidly diluted (as a^{-2}, with a being the scale factor) during inflation. Therefore, the conformal invariance of the electromagnetic action has to be broken in order to generate magnetic fields of adequate strengths today (see, for example, Refs. [93–95, 104, 107, 161–164]). This can be efficiently achieved by coupling the electromagnetic field to one or more of the scalar fields that drive inflation [81, 95, 161, 165, 166, 225, 263]. Interestingly, it has been found that the addition of a parity violating term to the action can significantly enhance the strengths of the generated electromagnetic fields [97, 99, 167–173, 225, 263].

One of the open problems in cosmology today is to understand the quantum-to-classical transition of the perturbations generated during inflation. The main challenge in this regard is to identify observable signatures that can unequivocally point to the quantum origin of the perturbations. The evolution of the quantum state associated with the Fourier modes of the scalar and tensor perturbations during inflation has been studied extensively in the literature (for an intrinsically incomplete list of efforts on this topic, see Refs. [253–262, 264–267]; for related discussions in alternative scenarios such as bounces, see Refs. [268–270]). At the linear order in perturbation theory, these Fourier modes are described by time-dependent, quadratic Hamiltonians and, in such situations, the unitary evolution operator can be described in terms of what are known as the squeezing and rotation operators [271, 272]. The evolution of the quantum state of such systems is often tracked using the Wigner function, which is a quasi-probability distribution in phase space (in this regard, see, for example, Refs. [273, 274]). The so-called Wigner ellipse is a contour in phase space corresponding to a given value of the Wigner function. Usually, the perturbations are assumed to evolve from the ground state, in which case, the Wigner ellipse is initially a circle. As the nomenclature suggests, the squeezing and rotation operators typically squeeze the Wigner circle into an ellipse and rotate it around its center, as the system evolves [275, 276].

At the linear order in perturbation theory, the Fourier modes associated with the scalar or tensor perturbations corresponding to the different wave numbers evolve independently. However, interestingly, one finds that, for a given wave number, say, k, the Hamiltonian describing the scalar or the tensor perturbations contain a term that describes an interaction between Fourier modes with the opposite wave vectors $\boldsymbol{k}$ and $-\boldsymbol{k}$. As a result, the quantum state associated with these wave vectors prove to be entangled [262, 277]. Over the last decade, it has been realized that the notion of quantum discord can be utilized as a tool to describe the evolution of the perturbations in such situations [262, 277, 278]. Discord is a quintessentially quantum property, i.e. it can be shown to be zero for a classical system. Further, it is more ubiquitous than entanglement, and discordant systems contain entangled systems as a subset [279]. In other words, a system possessing entanglement will also have a non-zero quantum discord, but the converse is not true. Since it reflects the quantumness of a system, quantum discord has been made use of in cosmology to probe the quantum origin of the cosmological perturbations. The large quantum discord at the end of inflation has been used to argue that cosmological perturbations are indeed placed in a very quantum state [262].

While the evolution of the quantum state associated with the primordial scalar and tensor perturbations have been studied in considerable detail, we notice that there has only been limited efforts to understand the behaviour in the case of magnetic fields (in this context, see, for instance, Refs. [100, 280]). Though there are some similarities between the evolution of scalar or tensor perturbations and magnetic fields, there can be crucial differences as well. In this chapter, we shall examine the evolution of the quantum state of the Fourier modes of the non-conformally coupled and parity violating electromagnetic field during inflation. Using tools such as the Wigner ellipse, squeezing parameters and quantum discord, we shall, in particular, investigate the effects that arise due to the violation of parity. Apart from the standard case of slow roll inflation, we shall examine the behaviour of these measures when there arise departures from slow roll. Specifically, we shall show that the violation of parity amplifies the extent of squeezing and quantum discord associated with one of the two states of polarization.

This chapter is organized as follows. In the following section, we shall arrive at the action governing the Fourier modes of the electromagnetic field that is coupled non-conformally to the scalar field driving inflation. We shall also consider the effects of an additional term in the action that induces the violation of parity. In Sec. 4.3, we shall carry out the quantization of the electromagnetic modes in the Schrödinger picture. We shall also discuss the evolution of the quantum state during inflation. In Sec. 4.4, we shall introduce the different measures, such as the Wigner ellipse, squeezing parameters and entanglement entropy (or quantum discord), that allow us to describe the evolution of the quantum state of the electromagnetic field. In Sec. 4.5, we shall discuss the behaviour of these measures of the quantum state in specific inflationary models. In addition to discussing the results in models that permit slow roll inflation, we shall discuss the behaviour in single and two field models that lead to departures from slow roll. Finally, we shall conclude in Sec. 4.6 with a summary of the main results obtained. We shall discuss a few related points in Apps. E and F. In App. G, we shall discuss the similarity between the behaviour of the modes of a parity violating electromagnetic field and a charged scalar field in the presence of an electric field in a de Sitter background.

4.2 NON-CONFORMALLY COUPLED ELECTROMAGNETIC FIELDS

In this section, we shall describe the actions of our interest and express them in terms of the Fourier modes of the electromagnetic vector potential. Later, we shall utilize the reduced action to arrive at the corresponding Hamiltonian while discussing the quantization of the electromagnetic modes in the Schrödinger picture. As we mentioned, we shall be interested in examining a situation wherein the electromagnetic field is coupled non-conformally to the scalar field, say, ϕ, that drives inflation. It proves to be instructive to first discuss non-helical electromagnetic fields, before we go on to consider the helical case.

4.2.1 Non-helical electromagnetic fields

As we have seen, the action describing the non-helical electromagnetic field has the form

$$S[A^\mu] = -\frac{1}{16\,\pi} \int \mathrm{d}^4x\, \sqrt{-g}\, J^2(\phi)\, F_{\mu\nu}\, F^{\mu\nu}, \tag{4.1}$$

where $J(\phi)$ denotes the non-conformal coupling function and the field tensor $F_{\mu\nu}$ is expressed in terms of the vector potential A_μ as $F_{\mu\nu} = (\partial_\mu\, A_\nu - \partial_\nu\, A_\mu)$. In a spatially flat, FLRW universe, if we work in the Coulomb gauge wherein $A_\eta = 0$ and $\partial_i\, A^i = 0$, then the above action reduces to

$$S[A_i] = \frac{1}{4\,\pi} \int \mathrm{d}\eta \int \mathrm{d}^3\boldsymbol{x}\, J^2(\eta) \left(\frac{1}{2}\, A_i'\, A^{i\prime} - \frac{1}{4}\, F_{ij}\, F^{ij}\right), \tag{4.2}$$

with the spatial indices raised or lowered with the aid of δ^{ij} or δ_{ij}.

Let $\boldsymbol{k}$ denote the comoving wave vector and let $\hat{\boldsymbol{k}}$ be the corresponding unit vector. For each vector $\boldsymbol{k}$, we can define the right-handed orthonormal basis vectors $(\hat{\boldsymbol{\varepsilon}}_1^{\boldsymbol{k}}, \hat{\boldsymbol{\varepsilon}}_2^{\boldsymbol{k}}, \hat{\boldsymbol{k}})$ which satisfy the relations

$$\hat{\boldsymbol{\varepsilon}}_1^{\boldsymbol{k}} \cdot \hat{\boldsymbol{\varepsilon}}_1^{\boldsymbol{k}} = \hat{\boldsymbol{\varepsilon}}_2^{\boldsymbol{k}} \cdot \hat{\boldsymbol{\varepsilon}}_2^{\boldsymbol{k}} = 1,\ \hat{\boldsymbol{\varepsilon}}_1^{\boldsymbol{k}} \cdot \hat{\boldsymbol{\varepsilon}}_2^{\boldsymbol{k}} = 0, \tag{4.3a}$$

$$\hat{\boldsymbol{\varepsilon}}_1^{\boldsymbol{k}} \times \hat{\boldsymbol{\varepsilon}}_2^{\boldsymbol{k}} = \hat{\boldsymbol{k}},\ \hat{\boldsymbol{k}} \cdot \hat{\boldsymbol{\varepsilon}}_1^{\boldsymbol{k}} = \hat{\boldsymbol{k}} \cdot \hat{\boldsymbol{\varepsilon}}_2^{\boldsymbol{k}} = 0, \tag{4.3b}$$

$$\hat{\boldsymbol{\varepsilon}}_1^{-\boldsymbol{k}} = -\hat{\boldsymbol{\varepsilon}}_1^{\boldsymbol{k}},\ \hat{\boldsymbol{\varepsilon}}_2^{-\boldsymbol{k}} = \hat{\boldsymbol{\varepsilon}}_2^{\boldsymbol{k}}. \tag{4.3c}$$

Let us denote the components of the polarization vector as $\varepsilon_{\lambda i}^{\boldsymbol{k}}$, where $\lambda = \{1, 2\}$ represents the two states of polarization of the electromagnetic field. It can be shown that the components $\varepsilon_{\lambda i}^{\boldsymbol{k}}$ satisfy the condition

$$\sum_{\lambda=1}^{2} \varepsilon_{\lambda i}^{\boldsymbol{k}}\, \varepsilon_{\lambda j}^{\boldsymbol{k}} = \delta_{ij} - \frac{k_i\, k_j}{k^2} = \delta_{ij} - \hat{k}_i\, \hat{k}_j, \tag{4.4}$$

where $\hat{k}_i$ denotes the i-th component of unit vector $\hat{\boldsymbol{k}}$. In terms of the components $\varepsilon_{\lambda i}^{\boldsymbol{k}}$, we can Fourier decompose the vector potential $A_i(\eta, \boldsymbol{x})$ in the following manner:

$$A_i(\eta, \boldsymbol{x}) = \sqrt{4\,\pi} \int \frac{\mathrm{d}^3\boldsymbol{k}}{(2\,\pi)^{3/2}} \sum_{\lambda=1}^{2} \varepsilon_{\lambda i}^{\boldsymbol{k}}\, \bar{A}_{\boldsymbol{k}}^{\lambda}(\eta)\, \mathrm{e}^{i\,\boldsymbol{k}\cdot\boldsymbol{x}}. \tag{4.5}$$

Since $A_i(\eta, \boldsymbol{x})$ and $\varepsilon_{\lambda i}^{\boldsymbol{k}}$ are real, we obtain that

$$\varepsilon_{\lambda i}^{\boldsymbol{k}}\, \bar{A}_{\boldsymbol{k}}^{\lambda}(\eta) = \varepsilon_{\lambda i}^{-\boldsymbol{k}}\, \bar{A}_{-\boldsymbol{k}}^{\lambda *}(\eta) \tag{4.6}$$

and, upon using the properties in Eqs. (4.3), this condition for reality leads to

$$\bar{A}^1_{-\boldsymbol{k}} = -\bar{A}^{1*}_{\boldsymbol{k}}, \quad \bar{A}^2_{-\boldsymbol{k}} = \bar{A}^{2*}_{\boldsymbol{k}}. \tag{4.7}$$

In terms of the Fourier modes $\bar{A}^\lambda_{\boldsymbol{k}}$, we can express the action (4.2) as follows:

$$S[\bar{A}_{\boldsymbol{k}}] = \int \mathrm{d}\eta \int \mathrm{d}^3\boldsymbol{k} \sum_{\lambda=1}^{2} J^2(\eta) \left(\frac{1}{2}\,|\bar{A}^{\lambda\prime}_{\boldsymbol{k}}|^2 - \frac{k^2}{2}\,|\bar{A}^\lambda_{\boldsymbol{k}}|^2\right). \tag{4.8}$$

On varying this action, we obtain the equation of motion governing the modes $\bar{A}^\lambda_{\boldsymbol{k}}$ to be [95, 207]

$$\bar{A}^{\lambda\prime\prime}_{\boldsymbol{k}} + 2\,\frac{J'}{J}\,\bar{A}^{\lambda\prime}_{\boldsymbol{k}} + k^2\,\bar{A}^\lambda_{\boldsymbol{k}} = 0. \tag{4.9}$$

4.2.2 Helical electromagnetic fields

Let us now turn to the case of helical electromagnetic fields. As we have discussed, in general, the action describing helical electromagnetic fields has the form [97, 99, 167–173, 225, 263]

$$S[A^\mu] = -\frac{1}{16\,\pi}\int \mathrm{d}^4x\,\sqrt{-g}\,\left[J^2(\phi)\,F_{\mu\nu}\,F^{\mu\nu} - \frac{\gamma}{2}\,I^2(\phi)\,F_{\mu\nu}\widetilde{F}^{\mu\nu}\right], \tag{4.10}$$

where $I(\phi)$ represents another coupling function, while γ is a constant. The dual field tensor $\widetilde{F}^{\mu\nu}$ is defined as $\widetilde{F}^{\mu\nu} = \epsilon^{\mu\nu\alpha\beta}\,F_{\alpha\beta}$, with $\epsilon^{\mu\nu\alpha\beta} = (1/\sqrt{-g})\,\mathcal{A}^{\mu\nu\alpha\beta}$. The quantity $\epsilon^{\mu\nu\alpha\beta}$ is the totally antisymmetric Levi-Civita tensor and $\mathcal{A}^{\mu\nu\alpha\beta}$ is the corresponding tensor density with the convention that $\mathcal{A}^{0123} = 1$ [9]. In a spatially flat, FLRW universe, when working in the Coulomb gauge, the above action describing the helical electromagnetic field simplifies to

$$\begin{aligned} S[A_i] = \frac{1}{4\,\pi}\int \mathrm{d}\eta \int \mathrm{d}^3\boldsymbol{x}\,\Bigg[&J^2(\eta)\,\left(\frac{1}{2}\,A_i'\,A^{i\prime} - \frac{1}{4}\,F_{ij}\,F^{ij}\right) \\ &+ \gamma\,I^2(\eta)\,\epsilon^{ijl}\,A_i'\,(\partial_j A_l)\Bigg]. \end{aligned} \tag{4.11}$$

where, as before, the spatial indices are raised or lowered using δ^{ij} or δ_{ij}, and ϵ^{ijl} represents the totally anti-symmetric Levi-Civita tensor in three-dimensional Euclidean space.

The Fourier modes of the helical field will be coupled in the basis $(\hat{\boldsymbol{\varepsilon}}^{\boldsymbol{k}}_1, \hat{\boldsymbol{\varepsilon}}^{\boldsymbol{k}}_2, \hat{\boldsymbol{k}})$ that we had considered in the case of non-helical electromagnetic field. To decouple the modes, one can combine the two transverse directions $\hat{\varepsilon}_1^{\boldsymbol{k}}$ and $\hat{\varepsilon}_2^{\boldsymbol{k}}$ to form the so-called helicity basis [97, 99, 167–173, 225, 263]. In such a case, we can define an orthonormal basis of vectors $(\hat{\varepsilon}_+^{\boldsymbol{k}}, \hat{\varepsilon}_-^{\boldsymbol{k}}, \hat{\boldsymbol{k}})$, where the vectors $\hat{\varepsilon}_\pm^{\boldsymbol{k}}$ are defined as

$$\hat{\varepsilon}_\pm^{\boldsymbol{k}} = \frac{1}{\sqrt{2}}\,(\hat{\varepsilon}_1^{\boldsymbol{k}} \pm i\,\hat{\varepsilon}_2^{\boldsymbol{k}}). \tag{4.12}$$

Using Eqs. (4.3), one can show that these vectors satisfy the following properties:

$$\hat{\varepsilon}_+^{\boldsymbol{k}} \cdot \hat{\varepsilon}_+^{\boldsymbol{k}*} = 1,\ \hat{\varepsilon}_-^{\boldsymbol{k}} \cdot \hat{\varepsilon}_-^{\boldsymbol{k}*} = 1,\ \hat{\varepsilon}_+^{\boldsymbol{k}} \cdot \hat{\varepsilon}_-^{\boldsymbol{k}*} = 0, \tag{4.13a}$$

$$\hat{\varepsilon}_\pm^{\boldsymbol{k}*} = \hat{\varepsilon}_\mp^{\boldsymbol{k}},\ \hat{\varepsilon}_\pm^{-\boldsymbol{k}} = -\hat{\varepsilon}_\mp^{\boldsymbol{k}},\ i\,\hat{\boldsymbol{k}} \times \hat{\varepsilon}_\pm^{\boldsymbol{k}} = \pm\hat{\varepsilon}_\pm^{\boldsymbol{k}}. \tag{4.13b}$$

Let $\varepsilon_{\sigma i}^{\boldsymbol{k}}$ denote the components of the polarization vector, with $\sigma = \pm 1$ corresponding to the two helical polarizations in the transverse directions of the wave vectors. It can be established that

$$\sum_{\sigma=\pm} \varepsilon_{\sigma i}^{\boldsymbol{k}}\, \varepsilon_{\sigma j}^{\boldsymbol{k}*} = \delta_{ij} - \frac{k_i\,k_j}{k^2} = \delta_{ij} - \hat{k}_i\,\hat{k}_j. \tag{4.14}$$

In terms of the components $\varepsilon_{\sigma i}^{\boldsymbol{k}}$ of the polarization vector, we can decompose the electromagnetic vector potential in terms of the Fourier mode functions $\bar{A}_{\boldsymbol{k}}^\sigma$ as follows:

$$A_i(\eta, \boldsymbol{x}) = \sqrt{4\,\pi} \int \frac{\mathrm{d}^3\boldsymbol{k}}{(2\,\pi)^{3/2}} \sum_{\sigma=\pm} \varepsilon_{\sigma i}^{\boldsymbol{k}}\, \bar{A}_{\boldsymbol{k}}^\sigma(\eta)\, \mathrm{e}^{i\,\boldsymbol{k}\cdot\boldsymbol{x}}. \tag{4.15}$$

Note that $\bar{A}_{\boldsymbol{k}}^\sigma$ can be written in terms of $\bar{A}_{\boldsymbol{k}}^\lambda$ as

$$\bar{A}_{\boldsymbol{k}}^\sigma = \frac{1}{\sqrt{2}}\,\left(\bar{A}_{\boldsymbol{k}}^1 - i\,\sigma\,\bar{A}_{\boldsymbol{k}}^2\right) \tag{4.16}$$

so that the reality condition (4.7) becomes

$$\bar{A}_{-\boldsymbol{k}}^\sigma = -\bar{A}_{\boldsymbol{k}}^{\sigma*}. \tag{4.17}$$

In terms of the Fourier modes $\bar{A}_{\boldsymbol{k}}^\sigma$, the action (4.11) can be expressed as

$$\begin{aligned} S[\bar{A}_{\boldsymbol{k}}^\sigma] \;=\; & \int \mathrm{d}\eta \int \mathrm{d}^3\boldsymbol{k}\, \sum_{\sigma=\pm} J^2(\eta)\, \Biggl[\frac{1}{2}\,|\bar{A}_{\boldsymbol{k}}^{\sigma\prime}|^2 + \frac{\sigma\,\gamma\,k\,I^2}{2\,J^2}\,\left(\bar{A}_{\boldsymbol{k}}^{\sigma\prime}\,\bar{A}_{\boldsymbol{k}}^{\sigma*} + \bar{A}_{\boldsymbol{k}}^{\sigma\prime*}\,\bar{A}_{\boldsymbol{k}}^\sigma\right) \\ & - \frac{k^2}{2}\,|\bar{A}_{\boldsymbol{k}}^\sigma|^2\Biggr]. \end{aligned} \tag{4.18}$$

On varying this action, we obtain the equation of motion governing the Fourier modes $\bar{A}_{\boldsymbol{k}}^{\sigma}$ to be [97, 99, 167–173, 225, 263]

$$\bar{A}_{\boldsymbol{k}}^{\sigma\prime\prime} + 2\,\frac{J'}{J}\,\bar{A}_{\boldsymbol{k}}^{\sigma\prime} + \bar{\omega}^2\,\bar{A}_{\boldsymbol{k}}^{\sigma} = 0. \tag{4.19}$$

where the quantity $\bar{\omega}^2$ is given by

$$\bar{\omega}^2 = k^2 + \frac{2\,\sigma\,\gamma\,k\,I\,I'}{J^2}. \tag{4.20}$$

We should point out that, in contrast to the non-helical case, the two states of polarization in the helical case (corresponding to $\sigma = \pm 1$) satisfy different equations and hence evolve differently.

4.3 QUANTIZATION IN THE SCHRÖDINGER PICTURE

In this section, we shall discuss the quantization of the Fourier modes of the electromagnetic field in the Schrödinger picture.

4.3.1 Identifying the independent degrees of freedom

To proceed in a manner similar to the analysis of the scalar or the tensor perturbations described in terms of the associated Mukhanov-Sasaki variable, we define the quantity

$$\mathcal{A}_{\boldsymbol{k}}^{\sigma} = i\,J\,\bar{A}_{\boldsymbol{k}}^{\sigma}. \tag{4.21}$$

We should clarify that the i factor has been introduced so that the reality condition (4.17) becomes

$$\mathcal{A}_{-\boldsymbol{k}}^{\sigma} = \mathcal{A}_{\boldsymbol{k}}^{\sigma *}, \tag{4.22}$$

mirroring the relation for the Fourier components of the Mukhanov-Sasaki variable in the case of the scalar perturbations [262]. In terms of the quantities $\mathcal{A}_{\boldsymbol{k}}^{\sigma}$, the action (4.18) can be expressed as

$$S[\mathcal{A}_{\boldsymbol{k}}^{\sigma}] = \int \mathrm{d}\eta \int \mathrm{d}^3\boldsymbol{k}\,\sum_{\sigma=\pm}\left[\frac{1}{2}\,|\mathcal{A}_{\boldsymbol{k}}^{\sigma\prime}|^2 - \frac{\kappa}{2}\,\left(\mathcal{A}_{\boldsymbol{k}}^{\sigma\prime}\,\mathcal{A}_{\boldsymbol{k}}^{\sigma *} + \mathcal{A}_{\boldsymbol{k}}^{\sigma\prime *}\,\mathcal{A}_{\boldsymbol{k}}^{\sigma}\right) - \frac{\mu^2}{2}\,|\mathcal{A}_{\boldsymbol{k}}^{\sigma}|^2\right], \tag{4.23}$$

where the quantities μ^2 and κ are given by

$$\mu^2 \;=\; k^2 - \left(\frac{J'}{J}\right)^2 + \frac{2\,\sigma\,\gamma\,k\,I^2\,J'}{J^3}, \tag{4.24a}$$

$$\kappa \;=\; \frac{J'}{J} - \frac{\sigma\,\gamma\,k\,I^2}{J^2}. \tag{4.24b}$$

The above action has the same structure as the action describing the Fourier components of the Mukhanov-Sasaki variable associated with the scalar perturbations (in this context, see, for instance, Ref. [262]). But, note that, in the case of the electromagnetic field, the two values of σ lead to twice as many degrees of freedom for every $\boldsymbol{k}$. In the non-helical case (i.e. when $\gamma = 0$), the above action, in fact, reduces *exactly* to the form of the action describing the scalar perturbations (with the non-conformal coupling function J replaced by the scalar pump field z). However, in the helical case, there arises an important difference with the quantities μ^2 and κ turning out to be dependent on the combination $(\sigma\,\gamma\,k)$.

With the action describing the Fourier modes of the electromagnetic field at hand, we can construct the Hamiltonian associated with each of these modes. Using the Hamiltonian, we can carry out the quantization of the modes in the Schrödinger picture. However, note that the reality condition (4.22) implies that not all the Fourier modes $\mathcal{A}_{\boldsymbol{k}}^{\sigma}$ are independent. In order to focus on only the independent degrees of freedom, we divide the Fourier space into two parts (such that $\boldsymbol{k}$ and $-\boldsymbol{k}$ occur in different halves) and express the modes in one half in terms of the modes in the other half using the relation (4.22) (for a similar discussion in the case of scalar and tensor perturbations, see, for instance, Refs. [260, 262, 278, 281–283]). The division of the three-dimensional Euclidean space $\mathbb{R}^3$ into two can be carried out by any plane passing through the origin. Therefore, the resultant integral will be over one-half of the Fourier space (which we shall denote as $\mathbb{R}^3/2$) so that we have

$$S[\mathcal{A}_{\boldsymbol{k}}^{\sigma}] = \int \mathrm{d}\eta \int_{\mathbb{R}^3/2} \mathrm{d}^3\boldsymbol{k} \sum_{\sigma=\pm} \left[|\mathcal{A}_{\boldsymbol{k}}^{\sigma\prime}|^2 - \kappa\, \left(\mathcal{A}_{\boldsymbol{k}}^{\sigma}\, \mathcal{A}_{\boldsymbol{k}}^{\sigma\prime *} + \mathcal{A}_{\boldsymbol{k}}^{\sigma *}\, \mathcal{A}_{\boldsymbol{k}}^{\sigma\prime}\right) - \mu^2\, |\mathcal{A}_{\boldsymbol{k}}^{\sigma}|^2\right]. \tag{4.25}$$

Later, we shall be focusing on scenarios wherein $I = J$, with J'/J vanishing at early times. In such situations, due to the term involving $(\sigma\,\gamma\,k)$ in κ, the above action does not reduce to that of a free harmonic oscillator during the initial stages of inflation[1]. We remedy the issue by adding the following total time derivative term to the above action:

$$-\frac{\mathrm{d}}{\mathrm{d}\eta}\left[\frac{\sigma\,\gamma\,k\,I^2}{J^2}\,|\mathcal{A}_{\boldsymbol{k}}^{\sigma}|^2\right]. \tag{4.26}$$

[1]Though, we should hasten to clarify that the equation of motion governing $\mathcal{A}_{\boldsymbol{k}}^{\sigma}$ indeed reduces to that of a free harmonic oscillator at such times.

In such a case, the resulting action turns out to be

$$S[\mathcal{A}_{\boldsymbol{k}}^{\sigma}] = \int \mathrm{d}\eta \int_{\mathbb{R}^3/2} \mathrm{d}^3\boldsymbol{k} \sum_{\sigma=\pm} \left[|\mathcal{A}_{\boldsymbol{k}}^{\sigma\prime}|^2 - \frac{J'}{J}\left(\mathcal{A}_{\boldsymbol{k}}^{\sigma}\,\mathcal{A}_{\boldsymbol{k}}^{\sigma\prime *} + \mathcal{A}_{\boldsymbol{k}}^{\sigma *}\,\mathcal{A}_{\boldsymbol{k}}^{\sigma\prime}\right) - \bar{\mu}^2\,|\mathcal{A}_{\boldsymbol{k}}^{\sigma}|^2 \right], \tag{4.27}$$

where the quantity $\bar{\mu}^2$ is defined as

$$\bar{\mu}^2 = \bar{\omega}^2 - \left(\frac{J'}{J}\right)^2 \tag{4.28}$$

with $\bar{\omega}^2$ given by Eq. (4.20). In App. E, we shall discuss further the reasons for adding the total time derivative and working with the modified action.

But, since $\mathcal{A}_{\boldsymbol{k}}^{\sigma}$ is not a real variable, it will not lead to a Hermitian operator on quantization. Hence, we shall perform the quantization in terms of the real and imaginary parts of the variable. Let $\mathcal{A}_{\boldsymbol{k}\mathrm{R}}^{\sigma}/\sqrt{2}$ and $\mathcal{A}_{\boldsymbol{k}\mathrm{I}}^{\sigma}/\sqrt{2}$ denote the real and imaginary parts of $\mathcal{A}_{\boldsymbol{k}}^{\sigma}$ so that we have

$$\mathcal{A}_{\boldsymbol{k}}^{\sigma} = \frac{1}{\sqrt{2}}\left(\mathcal{A}_{\boldsymbol{k}\mathrm{R}}^{\sigma} + i\,\mathcal{A}_{\boldsymbol{k}\mathrm{I}}^{\sigma}\right). \tag{4.29}$$

In such a case, we find that the action (4.27) splits into two equivalent terms describing the real and imaginary parts, which implies that they evolve independently. These quantities are governed by the following Lagrangian density *in Fourier space*:

$$\mathcal{L} = \frac{1}{2}\,\mathcal{A}'^2 - \frac{J'}{J}\,\mathcal{A}'\,\mathcal{A} - \frac{\bar{\mu}^2}{2}\,\mathcal{A}^2. \tag{4.30}$$

where $\mathcal{A}$ stands for either $\mathcal{A}_{\boldsymbol{k}\mathrm{R}}^{\sigma}$ or $\mathcal{A}_{\boldsymbol{k}\mathrm{I}}^{\sigma}$.

4.3.2 Schrödinger equation and the Gaussian ansatz

Let us now quantize the system in the Schrödinger picture. Given the Lagrangian (4.30), the canonical conjugate momentum $\mathcal{P}$ is given by

$$\mathcal{P} = \mathcal{A}' - \frac{J'}{J}\,\mathcal{A}. \tag{4.31}$$

The corresponding Hamiltonian density *in Fourier space*, can be immediately obtained to be[2]

$$\mathcal{H} = \frac{\mathcal{P}^2}{2} + \frac{J'}{J}\,\mathcal{P}\,\mathcal{A} + \frac{1}{2}\,\bar{\omega}^2\,\mathcal{A}^2, \tag{4.32}$$

where $\bar{\omega}^2$ is given by Eq. (4.20). If $\Psi(\mathcal{A},\eta)$ is the wave function describing the system, then this Hamiltonian leads to the following Schrödinger equation governing the wave function:

$$i\,\frac{\partial\Psi}{\partial\eta} \;=\; -\frac{1}{2}\,\frac{\partial^2\Psi}{\partial\mathcal{A}^2} - \frac{i}{2}\,\frac{J'}{J}\left(\Psi + 2\,\mathcal{A}\,\frac{\partial\Psi}{\partial\mathcal{A}}\right) + \frac{1}{2}\,\bar{\omega}^2\mathcal{A}^2\,\Psi. \tag{4.33}$$

We shall assume that, at very early times, the Fourier modes are in the ground state, often referred to as the Bunch-Davies vacuum. To take into account such an initial condition, we shall assume that the wave function is described by the Gaussian ansatz (see, for instance, Refs. [260, 284–287])

$$\Psi(\mathcal{A},\eta) = \mathcal{N}(\eta)\,\exp\left[-\Omega(\eta)\,\mathcal{A}^2/2\right], \tag{4.34}$$

where $\mathcal{N}$ and Ω are, in general, complex quantities. The normalization of the wave function $\Psi(\mathcal{A},\eta)$, viz.

$$\int_{-\infty}^{\infty} \mathrm{d}\mathcal{A}\,|\Psi(\mathcal{A},\eta)|^2 = 1, \tag{4.35}$$

immediately leads to the following relation between the functions $\mathcal{N}(\eta)$ and $\Omega(\eta)$:

$$|\mathcal{N}| = \left(\frac{\Omega_{\rm R}}{\pi}\right)^{1/4}, \tag{4.36}$$

where $\Omega_{\rm R} = (\Omega + \Omega^*)/2$ denotes the real part of the function Ω. This implies that $\mathcal{N}$ can be determined (modulo an unimportant overall phase factor) if we can obtain Ω.

Upon substituting the ansatz (4.34) for the wave function $\Psi(\mathcal{A},\eta)$ in the Schrödinger equation (4.33), we find that the quantity Ω satisfies the differential equation

$$\Omega' = -i\,\Omega^2 - 2\,\frac{J'}{J}\,\Omega + i\,\bar{\omega}^2. \tag{4.37}$$

[2]As with the Lagrangian density $\mathcal{L}$ in Fourier space, we shall hereafter refer to $\mathcal{H}$ simply as the Hamiltonian. Also, the Hamiltonian $\mathcal{H}$ should not be confused with the conformal Hubble parameter, which is often denoted in the same manner. *We do not make use of the conformal Hubble parameter in this chapter.*

In order to solve such a differential equation, let us write

$$\Omega = -i\,\frac{g^*}{f^*}, \tag{4.38}$$

where

$$g = f' - \frac{J'}{J}\,f. \tag{4.39}$$

On substituting the above expression for Ω in Eq. (4.37), we arrive at the following equation governing f^*:

$$f^{*\prime\prime} + \omega^2\, f^* = 0, \tag{4.40}$$

where the quantity ω^2 is given by

$$\omega^2 = \mu^2 - \kappa' = \bar{\omega}^2 - \frac{J''}{J} = k^2 - \frac{J''}{J} + \frac{2\,\sigma\,\gamma\,k\,I\,I'}{J^2}. \tag{4.41}$$

The above differential equation for f^* is identical in form to the equation of motion that governs $\mathcal{A}$ [which can be arrived at by substituting the relation (4.21) between $\mathcal{A}_{\boldsymbol{k}}^{\sigma}$ and $\bar{A}_{\boldsymbol{k}}^{\sigma}$ in Eq. (4.19)]. In other words, if we know the classical solution for $\mathcal{A}$ (or, equivalently, f), then we can construct the wave function $\Psi(\mathcal{A},\eta)$ completely.

4.4 MEASURES THAT REFLECT THE EVOLUTION OF THE QUANTUM STATE

In this section, we shall discuss the ideas of the Wigner ellipse, squeezing parameters and entanglement entropy (or, equivalently, quantum discord), measures that help us understand the evolution of the wave function describing the system.

4.4.1 Wigner ellipse

Given a wave function $\Psi(\mathcal{A},\eta)$, the Wigner function $W(\mathcal{A},\mathcal{P},\eta)$ is defined as [273, 274]

$$W(\mathcal{A},\mathcal{P},\eta) = \frac{1}{\pi}\int_{-\infty}^{\infty} \mathrm{d}y\, \Psi(\mathcal{A}-y,\eta)\, \Psi^*(\mathcal{A}+y,\eta)\, \mathrm{e}^{2\,i\,\mathcal{P}\,y}. \tag{4.42}$$

For the Gaussian form of $\Psi(\mathcal{A},\eta)$ in Eq. (4.34), we can easily obtain the Wigner function to be

$$W(\mathcal{A},\mathcal{P},\eta) = \frac{1}{\pi}\exp\left[-\Omega_{\mathrm{R}}\,\mathcal{A}^2 - \frac{1}{\Omega_{\mathrm{R}}}\,(\mathcal{P} + \Omega_{\mathrm{I}}\,\mathcal{A})^2\right], \tag{4.43}$$

where $\Omega_{\rm I}$ is the imaginary part of Ω, i.e. $\Omega_{\rm I} = (\Omega - \Omega^*)/(2\,i)$. To visualize the evolution of the Wigner function in the phase space $\mathcal{A}$-$\mathcal{P}$, we can choose to plot the behaviour of the contour described by the condition

$$\Omega_{\rm R}\,\mathcal{A}^2 + \frac{1}{\Omega_{\rm R}}\,(\mathcal{P} + \Omega_{\rm I}\,\mathcal{A})^2 = 1, \tag{4.44}$$

which is often referred to as the Wigner ellipse [274–276].

At very early times, if we demand that the wave function $\Psi(\mathcal{A}, \eta)$ corresponds to the Bunch-Davies vacuum, then the function f is expected to behave as

$$f \simeq \frac{1}{\sqrt{2\,k}}\,{\rm e}^{-i\,k\,\eta}. \tag{4.45}$$

For a power law form of J (say, when $J \propto \eta^{-n}$, where n is a real number), we have, at early times (i.e. as $\eta \to -\infty$)

$$g = f' - \frac{J'}{J}\,f \simeq -i\,\sqrt{\frac{k}{2}}\,{\rm e}^{-i\,k\,\eta}. \tag{4.46}$$

It is useful to note that, for such an initial condition, the Wronskian associated with the functions f and g is given by

$$\mathcal{W} = f\,g^* - g\,f^* = i. \tag{4.47}$$

The above expressions for f and g lead to $\Omega_{\rm R} = k$ and $\Omega_{\rm I} = 0$. If we introduce the following canonical variables which have the same dimension:

$$\bar{\mathcal{A}} = \sqrt{k}\,\mathcal{A}, \quad \bar{\mathcal{P}} = \frac{\mathcal{P}}{\sqrt{k}}, \tag{4.48}$$

then the condition (4.44) reduces to

$$\bar{\mathcal{A}}^2 + \bar{\mathcal{P}}^2 = 1. \tag{4.49}$$

In other words, at early times, the Wigner ellipse is a circle with its centre located at the origin, as in the case of the scalar perturbations.

4.4.2 Squeezing parameters

The squeezing parameters can be related to the components of the so-called covariance matrix associated with the wave function. In terms of the conjugate variables $\mathcal{A}$ and $\mathcal{P}$, the covariance matrix is defined as (see, for example, Refs. [260, 285])

$$V = \begin{bmatrix} k\,\langle\hat{\mathcal{A}}^2\rangle & \langle\hat{\mathcal{A}}\,\hat{\mathcal{P}} + \hat{\mathcal{P}}\,\hat{\mathcal{A}}\rangle/2 \\ \langle\hat{\mathcal{A}}\,\hat{\mathcal{P}} + \hat{\mathcal{P}}\,\hat{\mathcal{A}}\rangle/2 & \langle\hat{\mathcal{P}}^2\rangle/k \end{bmatrix}, \tag{4.50}$$

where the expectation values are to be evaluated in the state described by the wave function $\Psi(\mathcal{A}, \eta)$ [cf. Eq. (4.34)]. The covariance matrix can be expressed in terms of the squeezing amplitude r and the squeezing angle φ as follows [272, 278, 281, 285]

$$V = \frac{1}{2}\begin{bmatrix} \cosh(2\,r) + \sinh(2\,r)\,\cos(2\,\varphi) & \sinh(2\,r)\,\sin(2\,\varphi) \\ \sinh(2\,r)\,\sin(2\,\varphi) & \cosh(2\,r) - \sinh(2\,r)\,\cos(2\,\varphi) \end{bmatrix}. \tag{4.51}$$

The shape and orientation of the Wigner ellipse has a one-to-one correspondence with the covariance matrix (in this regard, see Refs. [272, 278, 285]; in particular, see Ref. [288], App. A). Using the wave function (4.34) and the expressions for $\mathcal{N}$ and Ω in Eqs. (4.36) and (4.38), it can be shown that[3]

$$\langle\hat{\mathcal{A}}^2\rangle = |f|^2 = \frac{1}{2\,k}\,[\cosh(2\,r) + \sinh(2\,r)\,\cos(2\,\varphi)], \tag{4.52a}$$

$$\langle\hat{\mathcal{P}}^2\rangle = |g|^2 = \frac{k}{2}\,[\cosh(2\,r) - \sinh(2\,r)\,\cos(2\,\varphi)], \tag{4.52b}$$

$$\frac{1}{2}\,\langle\hat{\mathcal{A}}\,\hat{\mathcal{P}} + \hat{\mathcal{P}}\,\hat{\mathcal{A}}\rangle = \frac{1}{2}\,(f\,g^* + f^*\,g) = \frac{1}{2}\,\sinh(2\,r)\,\sin(2\,\varphi), \tag{4.52c}$$

which can be inverted to arrive at

$$\cosh(2\,r) = k\,|f|^2 + \frac{|g|^2}{k}, \tag{4.53a}$$

$$\cos(2\,\varphi) = \frac{1}{\sinh(2\,r)}\left(k\,|f|^2 - \frac{|g|^2}{k}\right), \tag{4.53b}$$

$$\sin(2\,\varphi) = \frac{1}{\sinh(2\,r)}\,(f\,g^* + f^*\,g)\,. \tag{4.53c}$$

In other words, if we know the solutions to the classical Fourier modes of the electromagnetic field, we can arrive at the squeezing amplitude r and squeezing angle φ that describe the evolution of the wave function of the quantum system. We should point out that, since, at early times, f and g are given by Eqs. (4.45) and (4.46), we have $\cosh(2\,r) = 1$, or, equivalently, $r = 0$. This essentially indicates that the electromagnetic mode is in its ground state at early times. Note that, in the same limit, the squeezing angle φ is undetermined.

[3]The squeezing amplitude r should not be confused with the tensor-to-ratio, which is also denoted using the same variable.

4.4.3 Entanglement entropy and quantum discord

We shall now derive the entanglement entropy and quantum discord that arises when we make a particular partition of our system of the non-conformally coupled electromagnetic field into two subsystems. It can be shown that, when the complete system is in a pure state, quantum discord coincides with the entanglement entropy (for a discussion in this regard, see, for instance, Refs. [279, 289]). Since our system consists only of the electromagnetic field, with the coupling to the inflaton being parametrized by time-dependent coefficients, the quantum state of the system is a pure state. Therefore, from now on, we shall discuss the entanglement entropy of the system and it is to be understood that it is the same as the quantum discord.

In Secs. 4.3.2, 4.4.1 and 4.4.2, we had carried out the analysis in terms of the real or imaginary parts of the variable $\mathcal{A}_{\boldsymbol{k}}^{\sigma}$ defined in Eq. (4.29). All these variables are decoupled and hence we could work with a fiducial variable representing all of them. In terms of these variables, if we start with an initially unentangled state, there will be no generation of quantum correlations between the different degrees of freedom and, hence, no generation of quantum discord. However, we can evaluate the entanglement entropy or quantum discord between the $\boldsymbol{k}$ and $-\boldsymbol{k}$ sectors, similar to what has been carried out earlier for the scalar perturbations [262, 277]. In this section, working in the Schrodinger picture, we shall explicitly derive the entanglement entropy of the system that has been partitioned in the same manner, i.e. into two sectors of $\boldsymbol{k}$ and $-\boldsymbol{k}$.

Challenges with the modified action

Recall that we had originally obtained the action (4.23) to describe the Fourier modes $\mathcal{A}_{\boldsymbol{k}}^{\sigma}$ of the electromagnetic field. In order for the action to reduce to that of a free, simple harmonic oscillator during the early stages of inflation, we had added the total time derivative (4.26) to eventually arrive at the action (4.27). In this section, we shall point out that there arises a challenge in working with the action (or, equivalently, the associated conjugate momentum) to calculate the entanglement entropy between the electromagnetic modes with wave vectors $\boldsymbol{k}$ and $-\boldsymbol{k}$.

Let us begin by first rewriting the action (4.27) using the relation (4.22) between $\mathcal{A}_{-\boldsymbol{k}}^{\sigma}$ and $\mathcal{A}_{\boldsymbol{k}}^{\sigma}$ as follows:

$$\begin{aligned} S[\mathcal{A}_{\boldsymbol{k}}^{\sigma}, \mathcal{A}_{-\boldsymbol{k}}^{\sigma}] \quad = \quad & \int \mathrm{d}\eta \int_{\mathbb{R}^3/2} \mathrm{d}^3\boldsymbol{k} \sum_{\sigma=\pm} \Bigg[\mathcal{A}_{\boldsymbol{k}}^{\sigma\prime}\, \mathcal{A}_{-\boldsymbol{k}}^{\sigma\prime} - \frac{J'}{J}\, \left(\mathcal{A}_{\boldsymbol{k}}^{\sigma\prime}\, \mathcal{A}_{-\boldsymbol{k}}^{\sigma} + \mathcal{A}_{-\boldsymbol{k}}^{\sigma\prime} \mathcal{A}_{\boldsymbol{k}}^{\sigma}\right) \\ & - \bar{\mu}^2\, \mathcal{A}_{\boldsymbol{k}}^{\sigma}\, \mathcal{A}_{-\boldsymbol{k}}^{\sigma}\Bigg]. \end{aligned} \qquad (4.54)$$

The Lagrangian density in Fourier space associated with this action is clearly given by

$$\mathcal{L} = \mathcal{A}_{\boldsymbol{k}}^{\sigma\prime}\, \mathcal{A}_{-\boldsymbol{k}}^{\sigma\prime} - \frac{J'}{J}\, \left(\mathcal{A}_{\boldsymbol{k}}^{\sigma\prime}\, \mathcal{A}_{-\boldsymbol{k}}^{\sigma} + \mathcal{A}_{-\boldsymbol{k}}^{\sigma\prime} \mathcal{A}_{\boldsymbol{k}}^{\sigma}\right) - \,\bar{\mu}^2\, \mathcal{A}_{\boldsymbol{k}}^{\sigma}\, \mathcal{A}_{-\boldsymbol{k}}^{\sigma}. \tag{4.55}$$

Therefore, the conjugate momenta, say, $\mathcal{P}_{\boldsymbol{k}}^{\sigma}$ and $\mathcal{P}_{-\boldsymbol{k}}^{\sigma}$, associated with the variables $\mathcal{A}_{\boldsymbol{k}}^{\sigma}$ and $\mathcal{A}_{-\boldsymbol{k}}^{\sigma}$ are given by

$$\begin{aligned} \mathcal{P}_{\boldsymbol{k}}^{\sigma} &= \frac{\partial \mathcal{L}}{\partial \mathcal{A}_{-\boldsymbol{k}}^{\sigma\prime}} = \mathcal{A}_{\boldsymbol{k}}^{\sigma\prime} - \frac{J'}{J}\, \mathcal{A}_{\boldsymbol{k}}^{\sigma}, && \text{(4.56a)} \\ \mathcal{P}_{-\boldsymbol{k}}^{\sigma} &= \frac{\partial \mathcal{L}}{\partial \mathcal{A}_{\boldsymbol{k}}^{\sigma\prime}} = \mathcal{A}_{-\boldsymbol{k}}^{\sigma\prime} - \frac{J'}{J}\, \mathcal{A}_{-\boldsymbol{k}}^{\sigma}. && \text{(4.56b)} \end{aligned}$$

These conjugate momenta satisfy the relation

$$\mathcal{P}_{-\boldsymbol{k}}^{\sigma} = \mathcal{P}_{\boldsymbol{k}}^{\sigma *}, \tag{4.57}$$

which is akin to the relation (4.22) between $\mathcal{A}_{\boldsymbol{k}}^{\sigma}$ and $\mathcal{A}_{-\boldsymbol{k}}^{\sigma}$. The Hamiltonian of the system containing the two subsystems $\boldsymbol{k}$ and $-\boldsymbol{k}$ can be obtained to be (for a similar discussion in the case of scalar perturbations, see, for instance, Ref. [262])

$$\mathcal{H} = \mathcal{P}_{\boldsymbol{k}}^{\sigma}\, \mathcal{P}_{-\boldsymbol{k}}^{\sigma} + \frac{J'}{J}\, \left(\mathcal{A}_{\boldsymbol{k}}^{\sigma}\, \mathcal{P}_{-\boldsymbol{k}}^{\sigma} + \mathcal{A}_{-\boldsymbol{k}}^{\sigma}\, \mathcal{P}_{\boldsymbol{k}}^{\sigma}\right) + \bar{\omega}^2 \mathcal{A}_{\boldsymbol{k}}^{\sigma}\, \mathcal{A}_{-\boldsymbol{k}}^{\sigma}, \tag{4.58}$$

where the quantity $\bar{\omega}^2$ is given by Eq. (4.20).

The conjugate variables $(\mathcal{A}_{\boldsymbol{k}}^{\sigma}, \mathcal{P}_{\boldsymbol{k}}^{\sigma})$ and $(\mathcal{A}_{-\boldsymbol{k}}^{\sigma}, \mathcal{P}_{-\boldsymbol{k}}^{\sigma})$ that appear in the above Hamiltonian are *not* real. Hence, they will not turn out to be Hermitian when they are elevated to be operators on quantization. Motivated by the approach that has been adopted in the case of the scalar perturbations (in this context, see Refs. [262, 282]), we can define the new quantities $(x_{\boldsymbol{k}}^{\sigma}, p_{\boldsymbol{k}}^{\sigma})$ in terms of $(\mathcal{A}_{\boldsymbol{k}}^{\sigma}, \mathcal{P}_{\boldsymbol{k}}^{\sigma})$ and $(\mathcal{A}_{-\boldsymbol{k}}^{\sigma}, \mathcal{P}_{-\boldsymbol{k}}^{\sigma})$ as follows:

$$\begin{aligned} x_{\boldsymbol{k}}^{\sigma} &= \frac{1}{2}\, \left(\mathcal{A}_{\boldsymbol{k}}^{\sigma} + \mathcal{A}_{-\boldsymbol{k}}^{\sigma}\right) + \frac{i}{2\,\bar{\omega}}\, \left(\mathcal{P}_{\boldsymbol{k}}^{\sigma} - \mathcal{P}_{-\boldsymbol{k}}^{\sigma}\right), && \text{(4.59a)} \\ p_{\boldsymbol{k}}^{\sigma} &= \frac{1}{2}\, \left(\mathcal{P}_{\boldsymbol{k}}^{\sigma} + \mathcal{P}_{-\boldsymbol{k}}^{\sigma}\right) - \frac{i\,\bar{\omega}}{2}\, \left(\mathcal{A}_{\boldsymbol{k}}^{\sigma} - \mathcal{A}_{-\boldsymbol{k}}^{\sigma}\right), && \text{(4.59b)} \end{aligned}$$

and quantize the system in terms of these new variables. Note that, in the non-helical case wherein $\gamma = 0$, the quantity $\bar{\omega}^2$ [cf. Eq. (4.20)] reduces to k^2, and hence the new variables are similar to those encountered in the scalar case (with the non-conformal coupling function J replaced by the pump field z). However, we find that, in the helical case, i.e. when γ is non-zero, the quantity $\bar{\omega}^2$ may not remain positive definite over some domains in time, and hence the quantity $\bar{\omega}$ may turn out to be imaginary. This implies that the quantities $(x_{\boldsymbol{k}}^{\sigma}, p_{\boldsymbol{k}}^{\sigma})$ will *not* remain real, and hence cannot be utilized for carrying out the quantization of the system[4]. Therefore, in what follows, we shall turn to the original action (4.23) for quantization and the evaluation of the entanglement entropy between the electromagnetic modes with wave vectors $\boldsymbol{k}$ and $-\boldsymbol{k}$.

Working with the original action

Note that the original action (4.25) can be expressed as

$$\begin{aligned} S[\mathcal{A}_{\boldsymbol{k}}^{\sigma}, \mathcal{A}_{-\boldsymbol{k}}^{\sigma}] &= \int \mathrm{d}\eta \int_{\mathbb{R}^3/2} \mathrm{d}^3\boldsymbol{k} \sum_{\sigma=\pm} \Big[\mathcal{A}_{\boldsymbol{k}}^{\sigma\prime}\, \mathcal{A}_{-\boldsymbol{k}}^{\sigma\prime} - \kappa\, \left(\mathcal{A}_{\boldsymbol{k}}^{\sigma\prime}\, \mathcal{A}_{-\boldsymbol{k}}^{\sigma} + \mathcal{A}_{-\boldsymbol{k}}^{\sigma\prime} \mathcal{A}_{\boldsymbol{k}}^{\sigma}\right) \\ &\quad - \mu^2\, \mathcal{A}_{\boldsymbol{k}}^{\sigma}\, \mathcal{A}_{-\boldsymbol{k}}^{\sigma}\Big] \end{aligned} \tag{4.60}$$

so that the associated Lagrangian density in Fourier space is given by

$$\mathcal{L} = \mathcal{A}_{\boldsymbol{k}}^{\sigma\prime}\, \mathcal{A}_{-\boldsymbol{k}}^{\sigma\prime} - \kappa\, \left(\mathcal{A}_{\boldsymbol{k}}^{\sigma\prime}\, \mathcal{A}_{-\boldsymbol{k}}^{\sigma} + \mathcal{A}_{-\boldsymbol{k}}^{\sigma\prime} \mathcal{A}_{\boldsymbol{k}}^{\sigma}\right) - \mu^2\, \mathcal{A}_{\boldsymbol{k}}^{\sigma}\, \mathcal{A}_{-\boldsymbol{k}}^{\sigma}. \tag{4.61}$$

The conjugate momenta associated with the variables $\mathcal{A}_{\boldsymbol{k}}^{\sigma}$ and $\mathcal{A}_{-\boldsymbol{k}}^{\sigma}$ can be easily obtained to be

$$\mathcal{P}_{\boldsymbol{k}}^{\sigma} = \frac{\partial \mathcal{L}}{\partial \mathcal{A}_{-\boldsymbol{k}}^{\sigma\prime}} = \mathcal{A}_{\boldsymbol{k}}^{\sigma\prime} - \kappa\, \mathcal{A}_{\boldsymbol{k}}^{\sigma}, \tag{4.62a}$$

$$\mathcal{P}_{-\boldsymbol{k}}^{\sigma} = \frac{\partial \mathcal{L}}{\partial \mathcal{A}_{\boldsymbol{k}}^{\sigma\prime}} = \mathcal{A}_{-\boldsymbol{k}}^{\sigma\prime} - \kappa\, \mathcal{A}_{-\boldsymbol{k}}^{\sigma}, \tag{4.62b}$$

which correspond to the conjugate momentum in Eq. (E.2). In such a case, we find that the Hamiltonian of the system can be expressed as

$$\mathcal{H} = \mathcal{P}_{\boldsymbol{k}}^{\sigma}\, \mathcal{P}_{-\boldsymbol{k}}^{\sigma} + \kappa\, \left(\mathcal{A}_{\boldsymbol{k}}^{\sigma}\, \mathcal{P}_{-\boldsymbol{k}}^{\sigma} + \mathcal{A}_{-\boldsymbol{k}}^{\sigma}\, \mathcal{P}_{\boldsymbol{k}}^{\sigma}\right) + \widetilde{\omega}^2\, \mathcal{A}_{\boldsymbol{k}}^{\sigma}\, \mathcal{A}_{-\boldsymbol{k}}^{\sigma}, \tag{4.63}$$

where the quantity $\widetilde{\omega}^2$ is given by

$$\widetilde{\omega}^2 = k^2\, \left(1 + \frac{\gamma^2\, I^4}{J^4}\right). \tag{4.64}$$

[4]One simple way to overcome this difficulty would be to replace $\bar{\omega}$ in Eqs. (4.59) by either k or $|\bar{\omega}|$. But, the resulting Hamiltonians turn out to be rather cumbersome to deal with. It would be worthwhile to examine if one can construct other canonical variables which remain real and can be utilized to quantize the system.

We should point out here that, in contrast to the quantity $\bar{\omega}^2$ [cf. Eq (4.20)] which we had encountered in the Hamiltonian (4.58) earlier, the quantity $\widetilde{\omega}^2$ that appears in the above Hamiltonian is clearly positive definite.

We can now make use of the transformations (4.59) with $\bar{\omega}$ replaced by $\widetilde{\omega}$ to arrive at the new set of real variables $(x^\sigma_{\boldsymbol{k}}, p^\sigma_{\boldsymbol{k}})$. In terms of these variables, the Hamiltonian (4.63) of the system turns out to be

$$\mathcal{H} = \frac{1}{2}\,\left(p^\sigma_{\boldsymbol{k}}\, p^\sigma_{\boldsymbol{k}} + p^\sigma_{-\boldsymbol{k}}\, p^\sigma_{-\boldsymbol{k}}\right) + \kappa\,\left(x^\sigma_{\boldsymbol{k}}\, p^\sigma_{-\boldsymbol{k}} + x^\sigma_{-\boldsymbol{k}}\, p^\sigma_{\boldsymbol{k}}\right) + \frac{\widetilde{\omega}^2}{2}\,\left(x^\sigma_{\boldsymbol{k}}\, x^\sigma_{\boldsymbol{k}} + x^\sigma_{-\boldsymbol{k}}\, x^\sigma_{-\boldsymbol{k}}\right). \quad (4.65)$$

For convenience, we shall hereafter refer to $x^\sigma_{\boldsymbol{k}}$ and $x^\sigma_{-\boldsymbol{k}}$ simply as x_1 and x_2. The Schrodinger equation describing the system can then be written as

$$i\,\frac{\partial\Psi}{\partial\eta} = -\frac{1}{2}\,\left(\frac{\partial^2\Psi}{\partial x_1^2} + \frac{\partial^2\Psi}{\partial x_2^2}\right) - i\,\kappa\,\left(x_1\,\frac{\partial\Psi}{\partial x_2} + x_2\,\frac{\partial\Psi}{\partial x_1}\right) + \frac{\widetilde{\omega}^2}{2}\,\left(x_1^2 + x_2^2\right)\Psi. \quad (4.66)$$

As we had done earlier [cf. Eq. (4.34)], we can consider the following Gaussian ansatz for the wave function describing the system:

$$\Psi(x_1, x_2, \eta) = \mathcal{N}(\eta)\,\exp\left[-\frac{1}{2}\,\Omega_1(\eta)\,\left(x_1^2 + x_2^2\right) - \Omega_2(\eta)\,x_1\,x_2\right], \quad (4.67)$$

where, evidently, $\mathcal{N}$ is a *new*, suitable, normalization factor. The normalization of the wave function leads to the condition

$$|\mathcal{N}| = \left(\frac{\Omega_{1\mathrm{R}}^2 - \Omega_{2\mathrm{R}}^2}{\pi^2}\right)^{1/4}, \quad (4.68)$$

where $\Omega_{1\mathrm{R}} = (\Omega_1 + \Omega_1^*)/2$ and $\Omega_{2\mathrm{R}} = (\Omega_2 + \Omega_2^*)/2$ are the real parts of the quantities Ω_1 and Ω_2.

On substituting the wave function (4.67) in the Schrödinger equation (4.66), we find that the quantities Ω_1 and Ω_2 satisfy the following differential equations:

$$\Omega_1' = -i\,\left(\Omega_1^2 + \Omega_2^2\right) - 2\,\kappa\,\Omega_2 + i\,\widetilde{\omega}^2, \quad (4.69a)$$

$$\Omega_2' = -2\,i\,\Omega_1\,\Omega_2 - 2\,\kappa\,\Omega_1. \quad (4.69b)$$

If we now define $\Omega_+ = \Omega_1 + \Omega_2$, upon combining the above equations for Ω_1 and Ω_2, it is easy to show that the quantity Ω_+ satisfies the equation

$$\Omega_+' = -i\,\Omega_+^2 - 2\,\kappa\,\Omega_+ + i\,\widetilde{\omega}^2, \quad (4.70)$$

where, recall that, the quantity $\widetilde{\omega}^2$ is given by Eq. (4.64). Hereafter, we shall restrict ourselves to the situations wherein $I = J$, in which case $\widetilde{\omega}^2 = k^2\,(1+\gamma^2)$, i.e. it reduces to a constant. In such situations, it is also straightforward to establish that, if we define $\Omega_- = \Omega_1 - \Omega_2$, then the above equations for Ω_1 and Ω_2 imply that $\Omega_- = \widetilde{\omega}^2/\Omega_+$. Note that the above equation satisfied by Ω_+ is the same as Eq. (E.5) that governs Ω. Therefore, if we use the definition (4.38) for Ω_+, with g given by Eq. (E.6), then f^* satisfies the equation of motion (4.40). In other words, as with the wave function $\Psi(\mathcal{A}, \eta)$ [cf. Eq. (4.34)] that describes the unentangled state associated with the wave number k, the wave function $\Psi(x_1, x_2, \eta)$ [cf. Eq. (4.67)] that carries information about the interaction between the wave vectors $\boldsymbol{k}$ and $-\boldsymbol{k}$ can also be completely expressed in terms of the classical solutions to the Fourier modes of the electromagnetic field. With Ω_+ and Ω_- at hand, we can obtain Ω_1 and Ω_2 using the relations

$$\Omega_1 = \frac{1}{2}\,(\Omega_+ + \Omega_-) = \frac{1}{2\,\Omega_+}\,(\Omega_+^2 + \widetilde{\omega}^2), \tag{4.71a}$$

$$\Omega_2 = \frac{1}{2}\,(\Omega_+ - \Omega_-) = \frac{1}{2\,\Omega_+}\,(\Omega_+^2 - \widetilde{\omega}^2), \tag{4.71b}$$

which, in turn, allow us to construct the wave function $\Psi(x_1, x_2, \eta)$.

Derivation of the entanglement entropy

Note that the *complete* wave function $\Psi(x_1, x_2, \eta)$ of the system of our interest describes a pure state and hence does not possess any entanglement entropy. We shall trace one of the two degrees of freedom to arrive at the reduced density matrix and evaluate the corresponding entanglement entropy[5]. The reduced density matrix, obtained by tracing out the degrees of freedom associated with the variable x_1, is defined as

$$\rho_{\rm red}(x_2, x_2', \eta) = \int_{-\infty}^{\infty} {\rm d}x_1\, \Psi(x_1, x_2, \eta)\, \Psi^*(x_1, x_2', \eta), \tag{4.72}$$

with the wave function $\Psi(x_1, x_2, \eta)$ given by Eq. (4.67). The Gaussian integral over x_1 can be easily evaluated to arrive at the reduced density matrix

$$\rho_{\rm red}(x_2, x_2', \eta) = |\mathcal{N}|^2\,\sqrt{\frac{\pi}{\Omega_{\rm 1R}}}\,\exp\left[-\frac{\alpha}{2}\,\left(x_2^2 + {x_2'}^2\right) + \beta\, x_2\, x_2'\right],$$

[5]As is well known, the entanglement entropy of a bipartite system proves to be the same, independent of which of the two parts of the system is traced over.

where $|\mathcal{N}|$ is given by Eq. (4.68), while α and β are *real* quantities which are given by the expressions

$$\alpha = \Omega_1 - \frac{\Omega_2^2}{2\,\Omega_{1\mathrm{R}}} = \frac{1}{2\,\Omega_{1\mathrm{R}}}\,\left[2\,\Omega_{1\mathrm{R}}^2 - \left(\Omega_{2\mathrm{R}}^2 - \Omega_{2\mathrm{I}}^2\right)\right], \tag{4.73a}$$

$$\beta = \frac{|\Omega_2|^2}{2\,\Omega_{1\mathrm{R}}}, \tag{4.73b}$$

with $\Omega_{2\mathrm{I}} = (\Omega_2 - \Omega_2^*)/(2\,i)$ denoting the imaginary part of Ω_2. It is also useful to note here that $(\alpha^2 - \beta^2) = \widetilde{\omega}^2$.

Our aim is to now calculate the entanglement entropy associated with the above reduced density matrix. Since the system of our interest behaves as a time-dependent oscillator, the entanglement entropy of the system, say, $\mathcal{S}$, can be expressed as

$$\mathcal{S} = -\sum_{n=0}^{\infty} p_n\,\ln\,p_n, \tag{4.74}$$

where p_n denotes the probability of finding the system in the n-th energy eigen state of the oscillator. Since the entanglement entropy is the same as the quantum discord for a pure state, we shall hereafter refer to $\mathcal{S}$ above as quantum discord δ, in the manner it is often done in the context of the scalar perturbations [262, 282]. The eigen values p_n of the reduced density matrix $\rho_{\mathrm{red}}(x_2, x_2', \eta)$ are determined by the relation (for an early discussion, see Ref. [290]; for a recent discussion in this context, see, for instance, Ref. [286, 287])

$$\int_{-\infty}^{\infty} \mathrm{d}x_2'\,\rho_{\mathrm{red}}(x_2, x_2', \eta)\,\psi_n(x_2', \eta) = p_n\,\psi_n(x_2). \tag{4.75}$$

The quantities $\psi_n(x)$ are the energy eigen states of the harmonic oscillator with unit mass and frequency $\widetilde{\omega}$, and are given by

$$\psi_n(x) = \frac{1}{2^n\,n!}\,\left(\frac{\widetilde{\omega}}{\pi}\right)^{1/4}\,H_n\left(\sqrt{\widetilde{\omega}}\,x\right)\,\mathrm{e}^{-\widetilde{\omega}\,x^2/2}, \tag{4.76}$$

where the function $H_n(z)$ denotes the Hermite polynomial. With the density matrix $\rho_{\mathrm{red}}(x_2, x_2', \eta)$ and the wave function $\psi_n(x)$ at hand [as given by Eqs. (4.73) and (4.76)], it is straightforward to carry out the integral (4.75) and determine the probability p_n to be [291]

$$p_n = (1 - \xi)\,\xi^n, \tag{4.77}$$

where ξ is given by

$$\xi = \frac{\beta}{\widetilde{\omega} + \alpha}. \tag{4.78}$$

With the help of the above expression for p_n, we can carry out the sum in the definition (4.74) of the entanglement entropy (or quantum discord) to arrive at the following result in terms of ξ (in this context, see, for example, Refs. [286, 287, 290]):

$$\delta = -\ln(1-\xi) - \frac{\xi}{1-\xi}\, \ln \xi. \tag{4.79}$$

An equivalent expression that is more convenient for later numerical evaluation in specific inflationary models is given by

$$\delta = \left(1 + \frac{y}{2}\right)\, \ln\left(1 + \frac{2}{y}\right) + \ln\left(\frac{y}{2}\right), \tag{4.80}$$

where y is related to ξ as follows:

$$y = \frac{2\,\xi}{1-\xi}. \tag{4.81}$$

Upon using Eqs. (4.71), (4.73), (4.78) and (4.81), we find that the quantity y can be expressed as

$$y = \frac{\left(\widetilde{\omega} - \Omega_{+\mathrm{R}}\right)^2 + \Omega_{+\mathrm{I}}^2}{2\,\widetilde{\omega}\,\Omega_{+\mathrm{R}}}, \tag{4.82}$$

where $\Omega_{+\mathrm{R}} = (\Omega_+ + \Omega_+^*)/2$ and $\Omega_{+\mathrm{I}} = (\Omega_+ - \Omega_+^*)/(2\,i)$ denote the real and imaginary parts of Ω_+. If we further use Eq. (4.38), we obtain that

$$y = \frac{\left(1 - 2\,\widetilde{\omega}\,|f|^2\right)^2 + \left(f\,g^* + g\,f^*\right)^2}{4\,\widetilde{\omega}\,|f|^2}, \tag{4.83}$$

with $\widetilde{\omega}^2$ given by Eq. (4.64) (recall that we have set $I = J$) and g being defined as in Eq. (E.6). Note that the quantities in the above expression for y depend on the non-conformal coupling function J and the solution f. In other words, we can evaluate the quantum discord δ if we know the classical solutions to the Fourier modes of the electromagnetic vector potential. In the following section, we shall use the expressions (4.80) and (4.83) to evaluate the quantum discord in different models of inflation. We should mention that, in App. F, we have provided an alternative derivation of the quantum discord, obtained from the covariance matrix of the system.

However, before we proceed to calculate the evolution of the different measures describing the state of the electromagnetic field in specific inflationary scenarios, we ought to make a few clarifying remarks. Earlier, when we had focused on a single wave number of the electromagnetic field (in Secs. 4.3.2, 4.4.1 and 4.4.2), we had worked with the modified action (4.27), which corresponds to working with the conjugate momenta (4.56) or (4.31). In contrast, when calculating the quantum discord between the electromagnetic modes with the wave vectors $\boldsymbol{k}$ and $-\boldsymbol{k}$, we have instead worked with the original action (4.23), which leads to the conjugate momenta (4.62) or (E.2). We have already described the reason for doing so, viz. the fact that the transformations (4.59) do not lead to real variables when $\bar{\omega}^2$ [given by Eq. (4.20)] proves to be negative. We should also caution that, when $\bar{\omega}^2$ turns negative, the derivation of the entanglement entropy we have outlined above—which is based on the wave function $\psi_n(x)$ describing the normal oscillator [cf. Eq. (4.76)]—may not apply.

There is yet another point that we need to make at this stage of our discussion. In the non-helical case, $\bar{\omega}$ reduces to the wave number k and hence the above-mentioned problems do not arise. Also, in such a situation, the actions (4.54) and (4.60) [and, hence, the corresponding conjugate momenta (4.56) and (4.62)] reduce to the same form and, in fact, exactly resemble the action describing the scalar perturbations, as we have already mentioned. Under this condition, on using the expressions (4.52) from the previous section, we find that the quantity y as defined in Eq. (4.83) can be written in terms of the squeezing amplitude r as follows:

$$y = \cosh{(2\,r)} - 1. \tag{4.84}$$

On substituting this relation in Eq. (4.80), we can readily obtain an expression for quantum discord δ in terms of the squeezing amplitude r in the non-helical case. In fact, at late times during inflation, since the squeezing amplitude r proves to be large, we have $y \propto \exp{(2\,r)}$ so that the quantum discord behaves as $\delta \propto 2\,r$ [cf. Eqs. (4.84) and (4.80)], as in the case of the scalar perturbations [262]. However, we should clarify here that, for the helical fields, we do not have an explicit expression that relates the quantum discord δ and the squeezing amplitude r. Therefore, we shall work with Eqs. (4.80) and (4.83) to evaluate quantum discord for the parity violating electromagnetic fields. In the next section, when we discuss the numerical results in specific inflationary models, we shall see that, even in the helical case, the quantum discord has a similar relation to the squeezing amplitude (i.e. $\delta \propto 2\,r$) at late times.

4.5 BEHAVIOUR IN DIFFERENT INFLATIONARY SCENARIOS

With various tools to describe the evolution of the quantum state of the electromagnetic modes at hand, let us examine the evolution of the state in some specific situations.

In the following sections, we shall examine the evolution of the quantum state in simple situations involving slow roll as well as in non-trivial scenarios permitting some departures from slow roll. We shall assume that $I = J$ and focus on the helical case. Evidently, the results for the non-helical case can be obtained by considering the limit wherein γ vanishes.

4.5.1 In de Sitter inflation

Let us first discuss the often considered de Sitter case as it permits analytical solutions. Evidently, we shall require a form of $J(\eta)$ in order to make progress. The non-conformal coupling function that breaks the conformal invariance of the standard electromagnetic action is typically assumed to be of the following form [5, 9, 169, 225, 263]:

$$J(\eta) = \left[\frac{a(\eta)}{a(\eta_{\rm e})}\right]^n, \tag{4.85}$$

where $\eta_{\rm e}$ is the conformal time at the end of inflation and the parameter n is a real number. Note that the non-conformal coupling function reduces to unity at the end of inflation. As is well known, in the de Sitter case, the above coupling function leads to a scale invariant spectrum of the magnetic field for $n = -3$ and $n = 2$. We shall restrict our discussion to $n = 2$ throughout this chapter in order to avoid the issue of backreaction (in this context, see, for instance, Refs. [81, 225]).

Recall that, in de Sitter inflation, the scale factor describing the FLRW universe is given by $a(\eta) = -1/(H_{_{\rm I}}\,\eta)$, where $H_{_{\rm I}}$ is the Hubble parameter which is a constant. In such a case, J is given by

$$J(\eta) = \left(\frac{\eta}{\eta_{\rm e}}\right)^{-n} \tag{4.86}$$

so that

$$\frac{J'}{J} = -\frac{n}{\eta}, \quad \frac{J''}{J} = \frac{n\,(n+1)}{\eta^2} \tag{4.87}$$

and, hence, the function f which describes the wave function $\Psi(\mathcal{A}, \eta)$ [cf. Eqs. (4.34), (4.38) and (4.40)] satisfies the differential equation

$$f'' + \left[k^2 - \frac{2\,\sigma\,\gamma\,k\,n}{\eta} - \frac{n\,(n+1)}{\eta^2}\right] f = 0. \tag{4.88}$$

As we had seen in Chap. 2, the solution to this differential equation which satisfies the Bunch-Davies initial conditions at early times can be written as follows (for recent discussions, see, for example, Refs. [169, 225]):

$$f(\eta) = \frac{1}{\sqrt{2\,k}}\, \mathrm{e}^{-\sigma\,\pi\,n\,\gamma/2}\, W_{i\,\sigma\,n\,\gamma,\nu}(2\,i\,k\,\eta), \tag{4.89}$$

where $\nu = n + (1/2)$ and $W_{\lambda,\nu}(z)$ denotes the Whittaker function [291]. We find that, as $(-k\,\eta) \to \infty$, the above function f and the quantity $g = f' - (J'/J)\,f$ reduce to the asymptotic forms in Eqs. (4.45) and (4.46), as required. We should mention that, for a range of values of the Hubble parameter $H_{\rm I}$, the parameter γ and $n \simeq 2$, the resulting spectrum of the magnetic field proves to be nearly scale invariant and consistent with the current constraints from observations [225, 263].

When $n = 2$, upon using the solution (4.89) for the mode function f in the expression (4.53a) for the squeezing amplitude r, we obtain that, at late times (i.e. as $\eta \to 0$)

$$\cosh{(2\,r)} \simeq \frac{9\,\mathrm{e}^{-2\,\pi\,\sigma\,\gamma}\sinh{(2\,\pi\,\sigma\,\gamma)}}{4\,\pi\,\sigma\,\gamma\,(1+4\,\gamma^2)}\,\left(\frac{1}{k\,\eta}\right)^4. \tag{4.90}$$

This result implies that, towards the end of inflation, the squeezing amplitude r behaves as (since r is large) $\exp{(2\,r)} \propto a^4$ or, equivalently, $r \propto 2\,N$. Actually, in the following sections, when we analyze the behaviour of the squeezing amplitude in specific inflationary models, we shall see that such a behaviour arises soon after the modes leave the Hubble radius. The above result can be inverted to express the squeezing amplitude r (for large r) as follows:

$$r \simeq \ln\left(\frac{3}{2}\right) - 2\,\ln\left(\frac{k}{k_{\rm e}}\right) - \pi\,\sigma\,\gamma + \frac{1}{2}\ln\left[\frac{\sinh{(2\,\pi\,\sigma\,\gamma)}}{\pi\,\sigma\,\gamma\,(1+4\,\gamma^2)}\right], \tag{4.91}$$

where $k_{\rm e}$ represents the wave number that leaves the Hubble radius at the end of inflation. It is useful to note that, for small γ, we find that r behaves as

$$r \simeq \ln\left(\frac{3}{2}\right) + \frac{1}{2}\,\ln\,2 - 2\,\ln\left(\frac{k}{k_{\rm e}}\right) - \pi\,\sigma\,\gamma, \tag{4.92}$$

which suggests that r is linear in γ in the limit. Also, we had earlier pointed out that, for large r, the quantum discord δ behaves linearly with r. Later, when we evaluate the quantum discord δ numerically in the helical case, we shall find that, for small γ, the quantum discord depends linearly on the helicity parameter γ.

To understand the behaviour of the squeezing angle, we can make use of

Eqs. (4.52) and write

$$\frac{\langle \hat{\mathcal{P}}^2 \rangle}{k^2\, \langle \hat{\mathcal{A}}^2 \rangle} = \frac{1 - \tanh\,(2\,r)\,\cos\,(2\,\varphi)}{1 + \tanh\,(2\,r)\,\cos\,(2\,\varphi)} = \frac{|g|^2}{k^2\,|f|^2}. \tag{4.93}$$

At late times, when the squeezing amplitude r is large, $\tanh\,(2\,r)$ tends to unity, and the above relation simplifies to the following expression for the squeezing angle φ:

$$\tan\varphi = \pm\frac{|g|}{k\,|f|}. \tag{4.94}$$

Upon using the solution (4.89) in the de Sitter case, we find that, at late times, the squeezing angle reduces to

$$\tan\varphi \simeq -\sigma\,\gamma. \tag{4.95}$$

This implies that, while the angle φ vanishes for the non-helical modes, it is non-zero in the helical case and is of opposite signs for the two states of polarization.

Until now, we have focused on the $n = 2$ case, which leads to a scale invariant spectrum for the magnetic field. It is now interesting to examine if there can occur a situation (say, for a specific value of the parameter n) wherein the squeezing amplitude over large scales is small. In other words, do there exist non-trivial coupling functions which lead to a small squeezing amplitude r over large scales so that the modes remain close to the initial vacuum state at late times? To understand this point, it proves to be helpful to express the squeezing amplitude in terms of the power spectra of the electromagnetic fields. Recall that the power spectra of the helical magnetic and electric fields, say, $\mathcal{P}_{\rm B}(k)$ and $\mathcal{P}_{\rm E}(k)$, are defined as follows [97, 99, 167, 169]:

$$\mathcal{P}_{\rm B}(k) = \mathcal{P}_{\rm B}^{+}(k) + \mathcal{P}_{\rm B}^{-}(k) = \frac{k^5}{4\,\pi^2\,a^4}\,\left[\left|\mathcal{A}_k^{+}\right|^2 + \left|\mathcal{A}_k^{-}\right|^2\right], \tag{4.96a}$$

$$\mathcal{P}_{\rm E}(k) = \mathcal{P}_{\rm E}^{+}(k) + \mathcal{P}_{\rm E}^{-}(k) = \frac{k^3}{4\,\pi^2\,a^4}\,\left[\left|\mathcal{A}_k^{+\prime} - \frac{J'}{J}\mathcal{A}_k^{+}\right|^2 + \left|\mathcal{A}_k^{-\prime} - \frac{J'}{J}\mathcal{A}_k^{-}\right|^2\right]. \tag{4.96b}$$

Of course, in the non-helical case, the contributions from the two polarizations to the power spectra become equal. The above expressions for the power spectra and Eq. (4.53a) suggest that we can express the squeezing amplitude r for a given polarization σ as follows:

$$\cosh\,(2\,r) = \frac{4\,\pi^2\,a^4}{k^4}\,\left[\mathcal{P}_{\rm B}^{\sigma}(k) + \mathcal{P}_{\rm E}^{\sigma}(k)\right]. \tag{4.97}$$

Let us first consider the non-helical case. For $n > 1/2$, we find that, at late times, we can express the squeezing amplitude as

$$\cosh(2\,r) \propto A_1\,k^{-2\,n} + B_1\,k^{2-2\,n}, \tag{4.98}$$

whereas for $n < -1/2$, we have

$$\cosh(2\,r) \propto A_2\,k^{2\,n+2} + B_2\,k^{2\,n}, \tag{4.99}$$

where (A_1, B_1, A_2, B_2) are constants [225, 263]. Under either of these conditions, one of the two terms in the above expressions dominates at small k suggesting a large squeezing amplitude. In the helical case, for either polarization and for a non-zero n, we have

$$\cosh(2\,r) \propto A_3\,k^{1-|2\,n+1|} + B_3\,k^{-2\,|n|}, \tag{4.100}$$

where (A_3, B_3) are constants. Again, for any $n \neq 0$, one of the two terms dominates at small k leading to a significant squeezing amplitude. The above discussion suggests that any non-trivial coupling function J leaves the large scale electromagnetic modes in a highly squeezed state.

4.5.2 In slow roll scenarios

Let us now turn to understand the behaviour of the Wigner ellipse, the squeezing amplitude r and quantum discord δ in specific inflationary models. We shall first illustrate the behaviour in slow roll inflation using the popular Starobinsky model. As we had discussed in Chap. 2, the Starobinsky model is described by the potential

$$V(\phi) = V_0\left[1 - \exp\left(-\sqrt{\frac{2}{3}}\,\frac{\phi}{M_{_{\rm Pl}}}\right)\right]^2, \tag{4.101}$$

where V_0 is a constant that is determined by the COBE normalization of the scalar perturbations. For $V_0 = 1.43 \times 10^{-10}\,M_{_{\rm Pl}}^4$, it is known that, at the pivot scale of $k_\ast = 5 \times 10^{-2}\,{\rm Mpc}^{-1}$ (often assumed to leave the Hubble radius about $N_\ast = 50$ e-folds *before* the end of inflation), the Starobinsky model leads to the scalar spectral index of $n_{_{\rm S}} = 0.965$ and the tensor-to-scalar ratio of $r \simeq 4.3 \times 10^{-3}$, which fit the data from the anisotropies in the CMB very well [52]. (The tensor-to-scalar ratio r should not be confused with the squeezing amplitude which is denoted in the same manner.) In the slow roll approximation, the evolution of the field can be described in terms of the e-folds N by the expression

$$N - N_{\rm e} \simeq -\frac{3}{4}\left[\exp\left(\sqrt{\frac{2}{3}}\,\frac{\phi}{M_{_{\rm Pl}}}\right) - \exp\left(\sqrt{\frac{2}{3}}\,\frac{\phi_{\rm e}}{M_{_{\rm Pl}}}\right) - \sqrt{\frac{2}{3}}\left(\frac{\phi}{M_{_{\rm Pl}}} - \frac{\phi_{\rm e}}{M_{_{\rm Pl}}}\right)\right], \tag{4.102}$$

where $\phi_{\rm e}$ is the value of the field at the e-fold $N_{\rm e}$ when inflation comes to an end.

As we mentioned, we require the non-conformal coupling function to behave as $J(\phi) \propto a^2$ in order to generate magnetic fields with a nearly scale invariant spectrum. Since the evolution of the field $\phi(N)$ differs from one model of inflation to another, to achieve $J(N) = \exp\left[2\,(N - N_{\rm e})\right]$, the form of $J(\phi)$ will depend on the model at hand [95, 225, 263]. In the Starobinsky model, we can choose the function $J(\phi)$ to be

$$J(\phi) = \exp\left\{-\frac{3}{2}\left[\exp\left(\sqrt{\frac{2}{3}}\,\frac{\phi}{M_{_{\rm Pl}}}\right) - \exp\left(\sqrt{\frac{2}{3}}\,\frac{\phi_{\rm e}}{M_{_{\rm Pl}}}\right) - \sqrt{\frac{2}{3}}\left(\frac{\phi}{M_{_{\rm Pl}}} - \frac{\phi_{\rm e}}{M_{_{\rm Pl}}}\right)\right]\right\}. \tag{4.103}$$

The equations governing the non-helical and helical electromagnetic modes corresponding to such a coupling function can be solved numerically to arrive at the power spectra of the magnetic and electric fields (in this regard, see Refs. [225, 263]). We should point that the above coupling function $J(\phi)$ leads to minor deviations from the desired behaviour of $J \propto a^2$ and, as a result, the spectrum of the magnetic field is *nearly* scale invariant rather than a *strictly* scale independent one [225].

With the numerical solutions to the electromagnetic modes $\mathcal{A}_{\boldsymbol{k}}^{\sigma}$ at hand, we can immediately evaluate the Wigner ellipse, the squeezing amplitude r and the quantum discord δ using the expressions (4.44) (4.53a) and (4.80) [with y determined by Eq. (4.83)]. In Fig. 4.1, we have illustrated the evolution of the Wigner ellipse for a typical large scale mode in the Starobinsky model for the non-helical as well as helical fields. In the figure, we have also included the classical trajectory in phase space associated with the real parts of the solution f and the corresponding conjugate momentum g [cf. Eqs. (4.40) and (4.39)] that determine the wave function $\Psi(\mathcal{A}, \eta)$. In Fig. 4.2, we have plotted the evolution of the quantities r and δ as a function of the e-folds N in the Starobinsky model for electromagnetic modes with two different wave numbers. In the figure, we have also plotted the 'spectra' $r(k)$ and $\delta(k)$, i.e. the

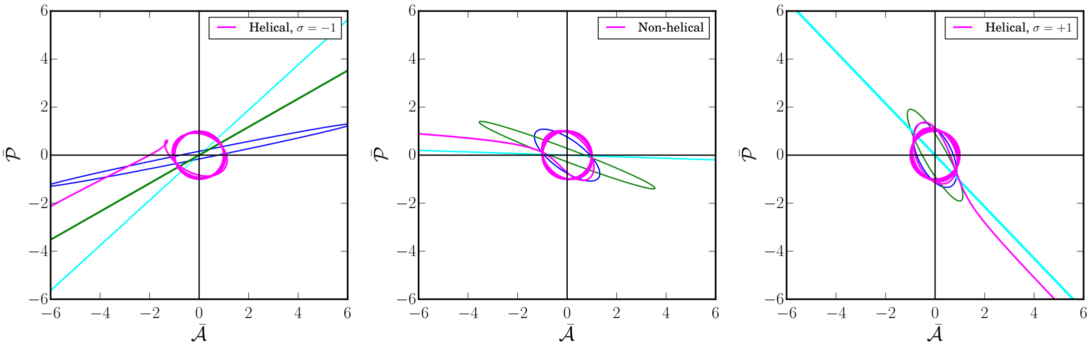

Figure 4.1: We have plotted the evolution of the Wigner ellipse (in red, blue, green and cyan) and the classical trajectory (in magenta) in the phase space $\bar{A}$-$\bar{\mathcal{P}}$ for the electromagnetic mode in the Starobinsky model with the wave number corresponding to the CMB pivot scale, i.e. $k_* = 0.05\,\mathrm{Mpc}^{-1}$. We have plotted these quantities for the non-helical (in the middle) as well as the helical cases (on the left and right for $\sigma = -1$ and $\sigma = +1$, respectively). The Wigner ellipses have been plotted at the following times: when the initial conditions are imposed on the mode in the sub-Hubble regime (in red, but hidden by the magenta curve), when $k = \sqrt{J''/J}$ (equivalent to the time of Hubble exit, in blue), on super-Hubble scales (in green) and closer to the end of inflation (in cyan). We have set the helicity parameter γ to be unity in plotting these figures. Clearly, the Wigner ellipse starts as a circle at early times and it is increasingly squeezed as time passes by. In the non-helical case, the major axis of the ellipse eventually orients itself along the $\bar{A}$ axis. However, in the helical case, at late times, the major axis of the ellipse orients itself along a straight line with a non-vanishing slope. As suggested by the condition (4.95), while the helical mode with the polarization state $\sigma = -1$ has a positive slope, the state with $\sigma = +1$ has a negative slope. Moreover, as the relation (4.94) suggests, we find that, at late times, the slope of the major axis of the ellipse is the same as that of the classical trajectory.

values of r and δ evaluated at the end of inflation for a wide range of wave numbers. In Fig. 4.3, we have plotted the dependence of the quantum discord δ on the helicity parameter γ for modes with the two different wave numbers. The following points are clear from these figures. Firstly, as expected, the Wigner ellipse starts as a circle and is increasingly squeezed with time. Also, as suggested by Eq. (4.94), we find that, at late times, the slope of the major axis of the Wigner ellipse matches that of the classical trajectory. Secondly, note that, on super-Hubble scales, the squeezing amplitude and the quantum discord associated with the $\sigma = -1$ helical modes have higher values when compared to the non-helical modes and the $\sigma = +1$ helical modes. In fact, as should be clear from the inset in Fig. 4.2, their values begin to differ even as they evolve in the sub-Hubble regime. Thirdly, as expected from the results in the case of de Sitter inflation

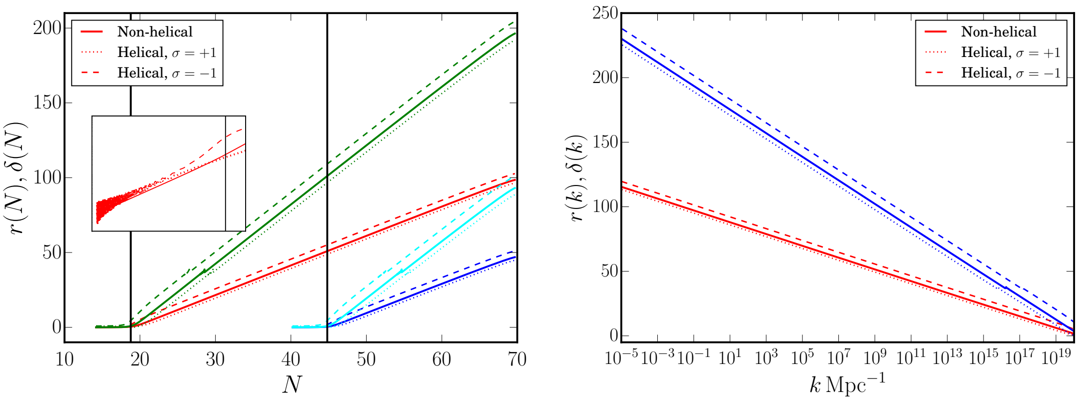

Figure 4.2: The evolution of the squeezing amplitude $r(N)$ (in red and blue) and quantum discord $\delta(N)$ (in green and cyan) have been plotted (on the left) for electromagnetic modes with two different wave numbers in the slow roll scenario admitted by the Starobinsky model. We have plotted the evolution for the CMB pivot scale of $k_* = 0.05\,\mathrm{Mpc}^{-1}$ (in red and green) and the small scale mode with the wave number $k = 10^{10}\,\mathrm{Mpc}^{-1}$ (in blue and cyan), which have been computed numerically. The vertical lines (in black, on the left) indicate the time when $k^2 = J''/J$, i.e. roughly the time when the two modes leave the Hubble radius (at $N = 18.75$ and $N = 44.72$). The inset (on the left, plotted on the log-linear scale) highlights the evolution of the squeezing amplitude associated with the pivot scale at early times. We have also plotted (on the right) the 'spectra' of the squeezing amplitude $r(k)$ and the quantum discord $\delta(k)$, evaluated at the end of inflation, for a wide range of wave numbers. Apart from the results for the non-helical case (which have been plotted as solid curves), we have plotted the results for the helical case (plotted as dotted and dashed lines, for $\sigma = +1$ and $\sigma = -1$, respectively). We have set $\gamma = 1$ in arriving at these figures. As we have discussed in the text, the evolution of the squeezing amplitude and the quantum discord as well as their spectra behave in the manner expected from the analytical results in de Sitter inflation discussed earlier.

discussed earlier, after the wave numbers have crossed the Hubble radius, $r(N)$ and $\delta(N)$ behave as $2\,N$ and $4\,N$, respectively, in all the cases. Fourthly, in the linear-log plot, the spectra $r(k)$ and $\delta(k)$ of the squeezing amplitude and quantum discord behave as $(k/k_{\mathrm{e}})^{-2}$ and $(k/k_{\mathrm{e}})^{-4}$, as we had discussed [cf. Eq. (4.91)]. Lastly, it is clear from Fig. 4.3 that quantum discord δ behaves linearly with the helicity parameter for small γ [cf. Eq. (4.92)].

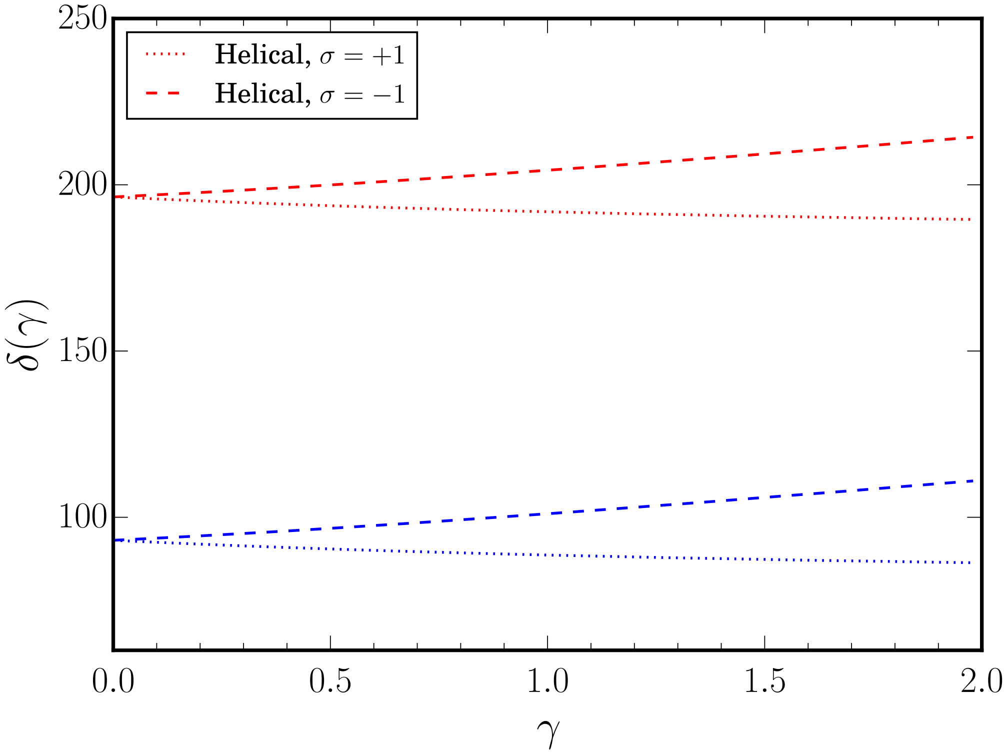

Figure 4.3: The quantum discord δ evaluated at the end of inflation in the case of the Starobinsky model has been plotted as a function of the helicity parameter γ. We have plotted the relation for two wave numbers, viz. the CMB pivot scale $k_* = 0.05\,\mathrm{Mpc}^{-1}$ (in red) and $k = 10^{10}\,\mathrm{Mpc}^{-1}$ (in blue), for the two helical modes with $\sigma = +1$ (as dotted lines) and $\sigma = -1$ (as dashed lines). Note that, for small γ, δ behaves linearly with γ.

4.5.3 In scenarios involving departures from slow roll

Let us now turn to understand the behaviour of the squeezing amplitude r and quantum discord δ in situations involving departures from slow roll. It is well known that specific features in the inflationary scalar power spectrum improve the fit to the CMB data, when compared to the nearly scale invariant power spectra that arise in slow roll scenarios (for a partial list of efforts in this regard, see Refs. [178, 180–190, 292]). Moreover, recently, there has been a considerable interest in the literature to study inflationary models that generate enhanced power on small scales and lead to the formation of a significant number of PBHs (in this context, see, for instance, Refs. [196–203, 293]). If such features are to be generated, then the inflationary potential should admit deviations from slow roll. In fact, the stronger the feature in the scalar power spectrum (as is, say, required to produce a considerable number of PBHs), the sharper should be the departures from slow roll inflation. Interestingly, in a recent work, we have illustrated that such deviations from slow roll inflation also lead to strong features in the spectra of magnetic fields [225] We have also shown that, while it is possible to restore scale invariance of the spectrum of the magnetic field in some situations, it is achieved at the cost of severe fine tuning [263]. In this section, we shall discuss the behaviour of the squeezing amplitude and quantum discord in single and two field models of inflation that permit *strong* departures from slow roll.

In single field models

We shall first consider two single field models that lead to sharp departures from slow roll inflation and hence to strong features in the scalar power spectra. The first model we shall consider is described by the potential [181, 182, 189]

$$V(\phi) = \frac{m^2}{2}\,\phi^2 - \frac{2\,m^2}{3\,\phi_0}\,\phi^3 + \frac{m^2}{4\,\phi_0^2}\,\phi^4, \tag{4.104}$$

and we shall work with the following values of the two parameters involved: $m = 7.17 \times 10^{-8}\,M_{_{\rm Pl}}$ and $\phi_0 = 1.9654\,M_{_{\rm Pl}}$. (As before, we shall refer to this model as PI1 in the figure below.) Also, we shall choose the initial values of the field and the first slow roll parameter to be $\phi_{\rm i} = 12.0\,M_{_{\rm Pl}}$ and $\epsilon_{1\rm i} = 2 \times 10^{-3}$. For these values of parameters and initial conditions, inflation lasts for about 110 e-folds in the model, which is much longer than the duration typically considered. However, if we assume that the pivot scale exits the Hubble radius about 91 e-folds before the termination of inflation, we find that the model leads to a suppression in the scalar power spectrum on the largest scales and thereby to a moderate improvement in the fit to the CMB data (in this context, see Ref. [189]). The second model that we shall consider is described by the potential [199]

$$V(\phi) = V_0 \left\{\tanh\left(\frac{\phi}{\sqrt{6}\,M_{_{\rm Pl}}}\right) + A\,\sin\left[\frac{1}{f_\phi}\,\tanh\left(\frac{\phi}{\sqrt{6}\,M_{_{\rm Pl}}}\right)\right]\right\}^2. \tag{4.105}$$

(We shall refer to this model as USR in the figure below.) We shall choose to work with the following values of the parameters: $V_0 = 2 \times 10^{-10}\,M_{_{\rm Pl}}^4$, $A = 0.130383$ and $f_\phi = 0.129576$. We find that, if we set the initial value of the field to be $\phi_{\rm i} = 6.1\,M_{_{\rm Pl}}$, with $\epsilon_{1\rm i} = 10^{-4}$, we obtain about 66 e-folds of inflation in the model. Moreover, we shall assume that the pivot scale exits the Hubble radius about 56.2 e-folds prior to the termination of inflation. This model generates enhanced power on small scales which results in the production of a significant number of PBHs. Both these models contain a point of inflection. It is located at $\phi_0 = 1.9654\,M_{_{\rm Pl}}$ in the first model and at $\phi_0 = 1.05\,M_{_{\rm Pl}}$ in the second [189, 202]. The point of inflection leads to an epoch of ultra slow roll inflation which is responsible for the sharp features in the power spectra (for a detailed discussion in this regard, see the recent review [293]).

Due to the strong departures from slow roll, in general, it proves to be challenging to arrive at analytical solutions for the background scalar field in these models. As we discussed, to arrive at a nearly scale invariant spectrum for the magnetic field, we need to choose the non-conformal coupling function to behave as $J \propto a^2$. Since there does not exist analytical solutions for the scalar field in the models of our interest, we are unable to construct an analytical form for $J(\phi)$ that leads to the desired behaviour, as we had done in the case of the Starobinsky model [cf. Eq. (4.103)]. Therefore, we have to resort to a numerical approach to arrive at a suitable non-conformal coupling function $J(\phi)$ (for discussions in this regard, see our recent efforts [225, 263]). However, because of the points of inflection, in these potentials, the non-conformal coupling function $J(\phi)$ hardly evolves as the field approaches the point of inflection and the epoch of ultra slow roll sets in. Such a behaviour generates magnetic fields with spectra that have a strong scale dependence. The resulting spectra of the magnetic field are scale invariant over large scales (i.e. over wave numbers that leave the Hubble radius prior to the onset of the epoch of ultra slow roll) and behave as k^4 on small scales (i.e. over wave numbers that leave the radius after ultra slow roll has set in). Moreover, it is found that the scale invariant amplitude of the magnetic field on large scales is strongly suppressed, with the amplitude being lower when the onset of ultra slow roll is earlier. In Fig. 4.4, we have plotted the spectra of the squeezing amplitude $r(k)$ and quantum discord $\delta(k)$ for the magnetic fields generated in the two inflationary models described above. Note that, on larger scales (corresponding to the scale invariant domain in the spectra of the magnetic field), the quantities $r(k)$ and $\delta(k)$ behave as in the slow roll case. However, over smaller scales wherein the spectra of the magnetic field behave as k^4, we find that $r(k)$ and $\delta(k)$ are rather small suggesting that the modes have not evolved significantly from the Bunch-Davies vacuum.

In two field models

We had pointed out above that, in the case of single field models permitting an epoch of ultra slow roll, the non-conformal coupling function $J(\phi)$ hardly evolves after the onset of ultra slow roll. Such a behaviour leads to magnetic field spectra which have strongly suppressed scale invariant amplitudes on larger scales and k^4 dependence on smaller scales. We have recently shown that these challenges can be circumvented in two field

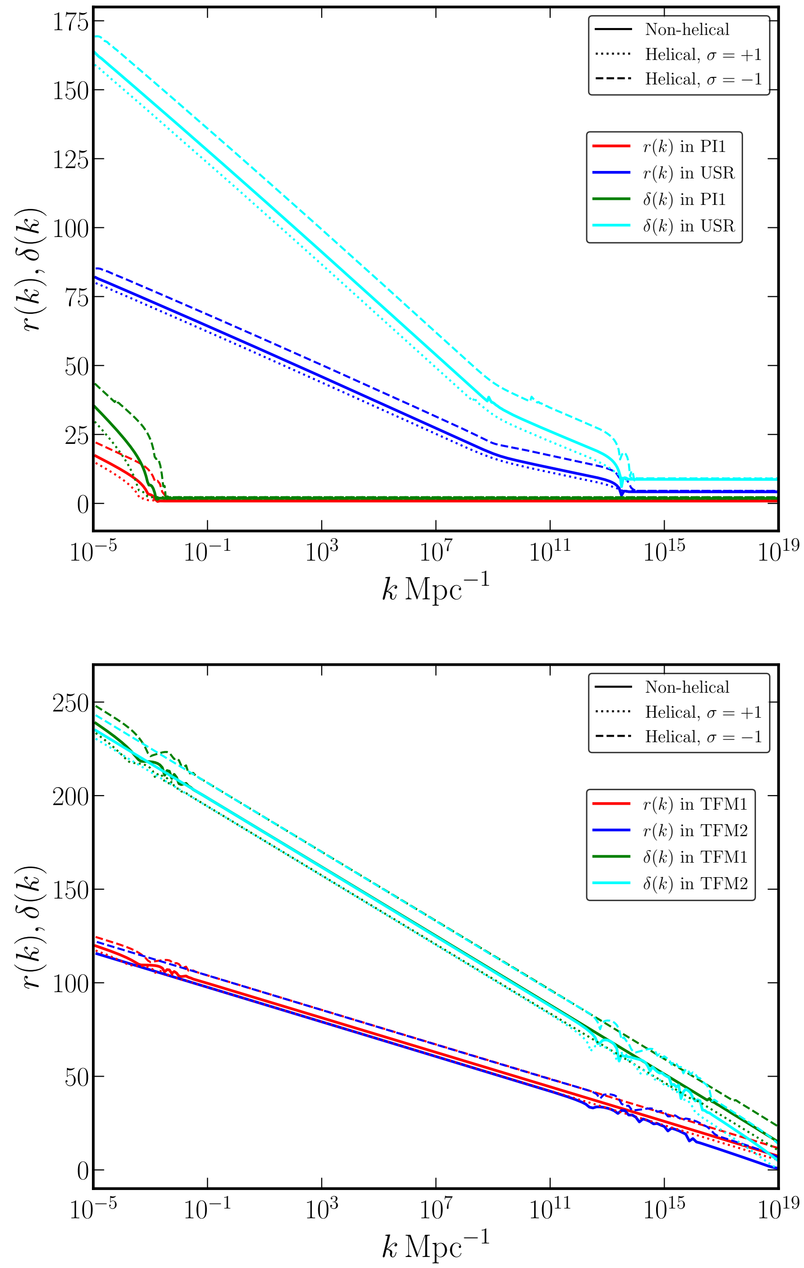

Figure 4.4: The 'spectra' of the squeezing amplitude $r(k)$ (in red and blue) and quantum discord $\delta(k)$ (in green and cyan) that arise in the single and two field inflationary models of our interest have been plotted (in PI1 and USR on top, and in TFM1 and TFM2 at the bottom, respectively) for a wide range of wave numbers. Note that, in the case of single field models, $r(k)$ and $\delta(k)$ (plotted on top) is rather small over wave numbers that leave the Hubble radius after the onset of ultra slow roll. However, in the case of the two field models, the quantities $r(k)$ and $\delta(k)$ behave virtually in the same manner as they do in the slow roll scenario. This behaviour has been achieved with the aid of the additional field available in the two field models.

models of inflation [263]. In models involving two fields, it is possible to construct inflationary scenarios that generate sharp features in the scalar power spectra (on either large or small scales) and design suitable non-conformal coupling functions that lead to nearly scale invariant spectra of magnetic fields with the desired amplitudes. We shall now discuss the behaviour of the squeezing amplitude r and the quantum discord δ in such models.

We shall consider two models, one which leads to a suppression in the spectrum of curvature perturbations on large scales and another which leads to an enhancement in the scalar power on small scales, models we had discussed in the previous chapter. The two field models are described by the action [228, 231]

$$S[\phi, \chi] = \int \mathrm{d}^4x \sqrt{-g}\left[-\frac{1}{2}\,\partial_\mu\phi\,\partial^\mu\phi - \frac{f(\phi)}{2}\,\partial_\mu\chi\,\partial^\mu\chi - V(\phi,\chi)\right], \tag{4.106}$$

where, evidently, while ϕ is a canonical scalar field, χ is a non-canonical scalar field due to the presence of the function $f(\phi)$ in the term describing its kinetic energy. We shall assume that $f(\phi) = \exp(2\,\bar{b}\,\phi)$, where $\bar{b}$ is a constant. The first model we shall consider is described by the potential [228]

$$V(\phi,\chi) = \frac{m_\phi^2}{2}\,\phi^2 + V_0\,\frac{\chi^2}{\chi_0^2+\chi^2}. \tag{4.107}$$

(As we did earlier, we have referred to this model as TFM1 in the figure above.) We shall work with the following set of values for the parameters involved: $(m_\phi/M_{\mathrm{Pl}}, V_0/M_{\mathrm{Pl}}^4, \chi_0/M_{\mathrm{Pl}}, \bar{b}\,M_{\mathrm{Pl}}) = (1.672\times10^{-5}, 2.6\times10^{-10}, \sqrt{3}, 1.0)$. Also, we shall choose the initial values of the fields to be $\phi_{\mathrm{i}} = 8.8\,M_{\mathrm{Pl}}$, $\chi_{\mathrm{i}} = 5.76\,M_{\mathrm{Pl}}$, and set $\epsilon_{1\mathrm{i}} = 2.47\times10^{-2}$. For these values of the parameters, we obtain about 78 e-folds of inflation. The second potential we shall investigate can be arrived at by interchanging the individual potentials for the two fields we considered above, and is given by [231]

$$V(\phi,\chi) = V_0\,\frac{\phi^2}{\phi_0^2+\phi^2} + \frac{m_\chi^2}{2}\,\chi^2. \tag{4.108}$$

(As before, we have referred to this model as TFM2 in the figure above.) We shall work with the following set of values for the parameters involved: $(V_0/M_{\mathrm{Pl}}^4, \phi_0/M_{\mathrm{Pl}}, m_\chi/M_{\mathrm{Pl}}, \bar{b}\,M_{\mathrm{Pl}}) = (7.1\times10^{-10}, \sqrt{6}, 1.19164\times10^{-6}, 7.0)$ and assume that $\phi_{\mathrm{i}} = 7.0\,M_{\mathrm{Pl}}$, $\chi_{\mathrm{i}} = 7.31\,M_{\mathrm{Pl}}$ and $\epsilon_{1\mathrm{i}} = 4.32\times10^{-4}$. For these parameters and initial conditions, we obtain about 84 e-folds of inflation in the model.

These models lead to two stages of slow roll inflation, with each stage being driven by one of the two fields. There arises a sharp turn in the field space as the transition from one stage to another occurs. The transition leads to a tachyonic instability and the isocurvature perturbations source the curvature perturbations associated with wave numbers which leave the Hubble radius during the turn in the field space [228, 231]. The first of the above two models leads to a suppression in scalar power on large scales [231], while the second leads to an enhancement in power on small scales [228]. In these models, we can construct non-conformal coupling functions that depend on the field driving slow roll inflation in each of the two stages. The two functions can then be combined together to arrive at a complete non-conformal coupling function $J(\phi, \chi)$ that largely leads to the desired behaviour of $J \propto a^2$, barring the period around the transition in the dependence of J on one field to the other (for a detailed discussion in this regard, see Ref. [263]). We should clarify that the non-conformal coupling function has to be fine tuned to a certain extent to avoid substantial deviations from the $J \propto a^2$ behaviour around the transition. The resulting non-conformal coupling function leads to a nearly scale invariant spectrum for the magnetic field which contains some features around the range of wave numbers which leave the Hubble radius around the time of the transition. In Fig. 4.4, we have plotted the spectra of the squeezing amplitude $r(k)$ and quantum discord $\delta(k)$ that arise in the two field models that we have introduced above. Clearly, the quantities $r(k)$ and $\delta(k)$ contain some small wiggles around the domain (in wave numbers) when the spectra of the magnetic field contain features (for the spectra of the magnetic field that arise in these cases, see Fig. 3.5 and Ref. [263]). Otherwise, the spectra of the squeezing amplitude and quantum discord behave in the same manner as in the slow roll scenario (cf. Fig. 4.2).

4.6 DISCUSSION

In this chapter, we have examined the evolution of the quantum state of non-helical as well as helical electromagnetic fields generated during inflation. We have tracked the evolution of the state of the electromagnetic field using measures such as the Wigner ellipse, squeezing amplitude and quantum discord. We find that, in a manner similar to the case of the scalar perturbations, the squeezing amplitude and quantum discord associated with the non-helical electromagnetic modes evolve linearly with e-folds on super-Hubble scales. Interestingly, in case of the helical electromagnetic field, the squeezing amplitude as well as the quantum discord of one of the two states of polarization ($\sigma = -1$) is enhanced when compared to the non-helical case, whereas they are suppressed for the other (i.e. for the polarization state with $\sigma = +1$). In fact, the enhancement (or suppression) occurs as the helical modes leave the Hubble radius and, on super-Hubble scales, the squeezing amplitude (and quantum discord) behave as a function of e-folds just as in the non-helical case. We find that, over the range of the values of the helicity parameter γ that we have considered, the enhancement of the squeezing amplitude and quantum discord is not very significant. We had limited ourselves to $\gamma \lesssim 2.5$ to avoid the issue of backreaction due to the helical modes on the background (in this context, see Ref. [225]).

On a related note, we find that there is a similarity between the effects on the electromagnetic field due to the violation of parity during inflation that we have discussed and the Schwinger effect associated with, say, a charged scalar field that arises when a constant electric field is present in the de Sitter spacetime (for relatively recent discussions on the Schwinger effect in the de Sitter spacetime, see, for instance, Refs. [294–297]). The electric field provides a direction breaking the isotropy of the FLRW universe. As a result, the modes of the charged field behave in a fashion akin to the helical electromagnetic field with the modes propagating along the direction of the electric field behaving differently from the modes traveling in the opposite direction. We have discussed these points in some detail in App. G.

Let us conclude by highlighting a few different directions in which further investigations need to be carried out. Firstly, it will be worthwhile to examine carefully (including backreaction) the effects due to helicity for larger values of γ [298]. Secondly, due to a technical difficulty, we had faced in the helical case (as described in Sec. 4.4.3), we have worked with two different conjugate momenta [given by Eqs. (4.31) and (E.2)] while calculating the squeezing amplitude r and the quantum discord δ. While we have been able to evaluate the squeezing amplitude r with the wave function starting in the Bunch-Davies vacuum (as described in Sec. 4.3.2), we have evaluated the quantum discord δ with the wave function beginning in a slightly squeezed initial state (arising due to the choice of the conjugate momentum; in this context, see the discussion in App. E). We need to overcome this challenge and evaluate the quantum discord of the system associated with the action (4.54). Thirdly, the effects due to parity violation we have encountered can also occur in the case of tensor perturbations described by modified theories such as the Chern-Simons theory of gravitation (in this regard, see, for example, Ref. [299]). It seems worthwhile to examine the effects of parity violation on the evolution of the quantum state in the case of tensor perturbations. Lastly, it has been pointed out that the quantum-to-classical transition of the primordial scalar perturbations can affect the extent of non-Gaussianities generated in the early universe [300]. It will be interesting to consider the effects that arise due to the decoherence of the scalar (or the tensor) perturbations and the magnetic fields on the cross-correlations between the magnetic fields and the curvature (or the tensor) perturbations [106, 134, 168, 207, 301, 302]. We are presently investigating some of these issues.

CHAPTER 5
SUMMARY AND OUTLOOK

5.1 SUMMARY

The main focus of this thesis has been to explore the generation and evolution of magnetic fields in non-trivial inflationary scenarios. We have considered inflationary models which give rise to features in the scalar power spectra over various length scales and computed the corresponding strengths of the magnetic fields generated in these models. Further, we have utilized different tools to study the evolution of the quantum state of the electromagnetic fields during inflation. In this section, we shall provide a concise summary of the key findings derived from our analyses.

In Chap. 2, we have investigated the origin of magnetic fields in inflationary models driven by a single, canonical scalar field that lead to features in the scalar power spectrum. These features are typically generated with the aid of brief departures from slow roll inflation. We have constructed model-dependent non-conformal coupling functions to examine whether nearly scale invariant magnetic fields of observable strengths can be produced in such scenarios. It proves to be difficult to solve the background equations analytically in some of the models that generate strong features in the scalar power spectrum. Hence, in these cases, we have solved the background equations numerically in the initial slowly rolling phase and have constructed coupling functions using a polynomial fit to the solutions. We have shown that such coupling functions lead to strong features in the power spectra of the electromagnetic fields. Specifically, in situations that permit a brief epoch of ultra slow roll inflation, we find that the electromagnetic spectra exhibit a suppression of power over large scales and a strong blue tilt over small scales. Although, in some models, it is possible to overcome the issue with a finely tuned coupling function, generically, the features in the electromagnetic power spectra seem unavoidable in models that permit non-trivial dynamics.

In Chap. 3, we have described the manner in which, using two field models, we can circumvent the challenges that arise in the generation of magnetic fields in single field inflationary models that permit non-trivial dynamics, in particular, a phase of ultra slow roll. The presence of a second field in inflationary models involving two fields provides a richer dynamics. In the two field models, the features in the scalar power spectrum are generated due to a turn in the field space. With the aid of the fields that are slowly rolling prior to and after the turn, we have been able to construct non-conformal coupling functions (using the method of a polynomial fit we alluded to above) that lead to the required behaviour and hence to magnetic fields of the desired shapes and strengths. We find that, while it is possible to generate nearly scale invariant spectra for the magnetic fields, the features can not be removed entirely. Moreover, in one of the models, we have proceeded to compute the contributions of the PMFs to the CMB anisotropies. We have utilized MagCAMB to calculate the imprints due to the so-called passive and compensated modes. Also, using an estimate for the power spectrum of the scalar perturbations induced by the magnetic field and CAMB, we have also evaluated the contributions to the angular power spectrum of the CMB due to the inflationary magnetic mode. We find that, in the inflationary model that we have considered, the contributions to the angular power spectra of the CMB due to the magnetic fields are considerably smaller in amplitude when compared to the contributions due to the primary scalar and tensor perturbations generated from the quantum vacuum.

In Chap. 4, working in the Schrodinger picture, we have utilized different measures to understand the evolution of the quantum state associated with the Fourier modes of the electromagnetic fields during inflation. We have examined the behaviour of the quantum state of the system using measures such as the Wigner function and the squeezing parameters. We have also evaluated the entanglement entropy (or, equivalently, the quantum discord in the situation of interest) associated with the system when it is partitioned into Fourier modes with opposite wave vectors. Interestingly, we have shown that, in the case of the helical electromagnetic fields, the squeezing amplitude and quantum discord are enhanced for one of the two states of polarization when compared to the other and also when compared to the non-helical case.

5.2 OUTLOOK

The main objective of this thesis has been to investigate the generation of PMFs in non-trivial inflationary scenarios. There are different directions in which these efforts can be extended. In what follows, we shall highlight some of the ideas that can be explored further.

We have worked with non-conformal coupling functions that avoid the issue of backreaction. However, the coupling functions we have constructed suffer from the strong coupling problem. There have been several attempts in the literature to construct coupling functions that avoid the backreaction as well as the strong coupling problems (in this context, see, for instance, Refs. [169, 303]). It will be worthwhile to construct such model-dependent coupling functions and examine inflationary magnetogenesis in these situations.

The imprints of the scalar and the tensor perturbations on the anisotropies in the CMB have been well investigated in the literature. It is equally important to study the contributions of the PMFs to the anisotropies in the CMB. To understand these effects, numerical codes such as MagCAMB (which we made use of to arrive at the results presented in Chap. 3) have been developed to compute the signatures of the PMFs on the temperature and polarization angular power spectra of the CMB through the passive and compensated modes [124]. A limitation with the numerical codes that compute the signatures of the PMFs on the CMB is that the power spectrum of the magnetic fields is assumed to be of the power law form (see, for instance, Refs. [131, 174, 304]). A power law is a good choice for describing the spectra of PMFs generated in slow roll inflation. However, when there are deviations from slow roll, there arise departures from such a form. It will be worthwhile to develop a code to compute the angular power spectra of the CMB induced by the PMFs generated in a generic inflationary scenario.

Another direction that is worth pursuing corresponds to non-Gaussianities involving the PMFs. There has been a continuing interest in calculating the cross-correlations between the scalar perturbations and the PMFs generated during inflation [106, 168]. The imprints of these cross-correlations on the CMB and the large scale structure have also been investigated [305]. However, we find that most of these effects have been examined only in the context of slow roll inflation. As we have discussed in this thesis, deviations from slow roll inflation can lead to significant features in the spectra of the magnetic fields. It seems timely to examine the non-Gaussianities involving the magnetic fields generated in non-trivial inflationary scenarios and their observational signatures.

When the anisotropies in the CMB are measured, they are treated as classical, stochastic correlations. However, they are expected to be imprints of the scalar and tensor perturbations as well as of the PMFs, which originate from quantum fluctuations during inflation. As we have mentioned earlier, the quantum-to-classical transition of the primordial perturbations is one of the fundamental, open problems in cosmology today. In this thesis, we have shown that measures such as the squeezing amplitude and quantum discord of helical magnetic fields are enhanced when compared to the non-helical fields. In the case of scalar and tensor perturbations, recently, other measures such as the violation of the Bell's inequality has been considered to understand if there are observable effects that can indicate the quantum origin of the primordial perturbations [306]. Motivated by these efforts, as a next step, we can examine the behaviour of Bell's inequalities in observables constructed out of the modes of the electromagnetic fields. The violation of parity can enhance the measures involved leading to a possibly observable effect. Another related aspect that is important to consider is the issue of decoherence. The impact of decoherence on the scalar power and bi-spectra due to additional degrees of freedom has been explored over the last couple of years [300, 307, 308]. It will be interesting to carry out similar analyses in the case of cross-correlations between the scalar or tensor perturbations and the magnetic fields.

APPENDIX A

THE ELECTROMAGNETIC SPECTRAL INDICES IN SLOW ROLL INFLATION

In this appendix, we shall derive the spectral indices of the non-helical magnetic and electric fields, viz. $n_{_{\rm B}}$ and $n_{_{\rm E}}$, in the slow roll approximation.

Given the form $J = [a(\eta)/a(\eta_{\rm e})]^n$ for the non-minimal coupling function [cf. Eq. (2.5)], one finds that

$$\frac{J''}{J} = \mathcal{H}^2\,\left(n^2 + n - n\,\epsilon_1\right), \tag{A.1}$$

where $\epsilon_1 = -\dot{H}/H^2$ is the first slow roll parameter, and we should emphasize that this relation is exact. Note that the quantity $\mathcal{H} = a'/a$ is the conformal Hubble parameter. As we had discussed earlier [cf. Eq. (1.36)], in the slow roll approximation, the conformal Hubble parameter can be written as [63, 64, 71, 73, 212–218]

$$\mathcal{H} = \frac{a'}{a} \simeq -\frac{1}{(1-\epsilon_1)\,\eta}. \tag{A.2}$$

so that, at the first order in the slow roll parameter ϵ_1, we have

$$\frac{J''}{J} \simeq \frac{1}{\eta^2}\,\left[n^2 + n + (2\,n^2 + n)\,\epsilon_1\right]. \tag{A.3}$$

In such a case, the solution to Eq. (2.3) that satisfies the Bunch-Davies initial conditions is given by

$$\mathcal{A}_k(\eta) = \sqrt{-\frac{\pi\,\eta}{4}}\,{\rm e}^{i\,[\nu+(1/2)]\,\pi/2}\,H_\nu^{(1)}(-k\,\eta), \tag{A.4}$$

where, as we had mentioned earlier, $H_\nu^{(1)}(z)$ is the Hankel function of the first kind. For $\epsilon_1 \ll 1$, at the first order in the slow roll parameter, the index ν is given by

$$\nu \simeq \left(n + \frac{1}{2}\right) + n\,\epsilon_1. \tag{A.5}$$

We should point out that, when $\epsilon_1 = 0$, the above solution reduces to the de Sitter solution (2.6), as required. Since we are eventually interested in the case $n = 2$, for convenience, we shall assume that $\nu > 1$. In such a case, we find that the power spectra of the magnetic and electric fields evaluated at late times can be expressed as

$$\mathcal{P}_{_{\rm B}}(k) \propto k^{5-2\,\nu}, \quad \mathcal{P}_{_{\rm E}}(k) \propto k^{7-2\,\nu}, \tag{A.6}$$

which correspond to the spectral indices of

$$n_{\rm B} = 4 - 2\,n\,(1+\epsilon_1), \quad n_{\rm E} = 6 - 2\,n\,(1+\epsilon_1). \tag{A.7}$$

For $n = 2$, these correspond to $n_{\rm B} = -4\,\epsilon_1$ and $n_{\rm E} = 2 - 4\,\epsilon_1$.

Since $0 < \epsilon_1 \ll 1$, the above results imply that, for $n = 2$, in the non-helical case, the spectrum of the magnetic field should be red in slow roll inflation. However, on closer inspection of Fig. 2.2, we find that the spectrum of the magnetic field is red in the case of the quadratic potential (2.39), but is mildly blue in the cases of the small field model (2.42) and the first Starobinsky model (2.45), which lead to slow roll inflation. This can be attributed to the fact that the coupling functions (2.41), (2.44) and (2.47) do not exactly mimic the coupling function $J = [a(\eta)/a(\eta_{\rm e})]^n$. In the case of the quadratic potential, for the choice of the coupling function (2.41), we find that the quantity J''/J can be expressed as

$$\begin{aligned}\frac{J''}{J} &= a^2\,H^2\left[\frac{n^2\,H^2}{m^2}\,(3\,\epsilon_1 - \epsilon_1^2) - n\,\epsilon_1\right.\\ &\left.\quad + \frac{n\,H}{m}\,\left(3\,\epsilon_1 - \epsilon_1^2\right)^{1/2}\left(1 - \epsilon_1 + \frac{\epsilon_2}{2}\right)\right].\end{aligned} \tag{A.8}$$

We should mention that no approximations have been made in arriving at this expression. It does not seem possible to express the quantity J''/J purely in terms of the slow roll parameters. For $n = 2$, if we make use of the expression (A.2) for the conformal Hubble parameter $\mathcal{H}$, we obtain that

$$\begin{aligned}\frac{J''}{J} &= \frac{1}{\eta^2}\left\{\frac{1}{(1-\epsilon_1)^2}\left[\frac{4\,H^2}{m^2}\,(3\,\epsilon_1 - \epsilon_1^2) - 2\,\epsilon_1\right.\right.\\ &\left.\left.\quad + \frac{2\,H}{m}\,\left(3\,\epsilon_1 - \epsilon_1^2\right)^{1/2}\left(1 - \epsilon_1 + \frac{\epsilon_2}{2}\right)\right]\right\}.\end{aligned} \tag{A.9}$$

We should clarify that, while the quantity within the square brackets in this expression is an exact one, the conformal Hubble parameter has been evaluated in the slow roll approximation. Clearly, in such a case, the solution to the electromagnetic vector potential can be written in terms of the Hankel function as in Eq. (A.4). The index ν can be determined by equating the quantity within the curly brackets in the above expression for J''/J to $\nu^2 - (1/4)$. At the time when the pivot scale leaves the Hubble radius, for the choice of the parameters we have worked with, we find that $\nu = 2.513$. Since $2\,\nu > 5$, the spectrum of the magnetic field exhibits a red tilt for our choice of the coupling function in the case of the quadratic potential [cf. Eq. (A.6)].

We find that, in general, the quantity J''/J can be expressed as

$$\frac{J''}{J} = a^2\, H^2\, \mu_{_{\rm B}}^2(N), \tag{A.10}$$

where $\mu_{_{\rm B}}(N)$ is given by

$$\mu_{_{\rm B}}^2(N) = \frac{J_{NN}}{J} + (1-\epsilon_1)\,\frac{J_N}{J}, \tag{A.11}$$

with $J_N = {\rm d}J/{\rm d}N$ and $J_{NN} = {\rm d}^2J/{\rm d}^2N$. If we make use of the conformal Hubble parameter in the slow roll approximation [cf. Eq. (A.2)], then, we can write

$$\frac{J''}{J} = \frac{1}{\eta^2}\,\frac{\mu_{_{\rm B}}^2(N)}{(1-\epsilon_1)^2}, \tag{A.12}$$

which implies that $\nu^2 - (1/4) = \mu_{_{\rm B}}^2/(1-\epsilon_1)^2$, with $\mu_{_{\rm B}}$ and ϵ_1 evaluated, say, when the pivot scale leaves the Hubble radius. Note that, one obtains a strictly scale invariant spectrum for the magnetic field when $\mu_{_{\rm B}}^2/(1-\epsilon_1)^2 = 6$, which corresponds to $2\,\nu = 5$. For our choice of the coupling function, in the case of the quadratic potential, at the time the pivot scale leaves the Hubble radius, we find that $\mu_{_{\rm B}}^2/(1-\epsilon_1)^2 = 6.068$, which leads to $\nu = 2.513$ that we mentioned above. In the cases of the small field and the first Starobinsky models, for the choices of the coupling functions (2.44) and (2.47), we find that, when the pivot scale exits the Hubble radius, $\mu_{_{\rm B}}^2/(1-\epsilon_1)^2 = 5.935$ and 5.939 which correspond to $\nu = 2.487$ and 2.488, respectively. Since, $2\,\nu < 5$, we obtain magnetic field spectra with blue tilts in these two cases.

APPENDIX B

ANALYTICAL CONSTRUCTION OF THE NON-CONFORMAL COUPLING FUNCTION

In this appendix, using the solutions for the fields ϕ and χ that can be arrived at in the slow roll approximation, we shall construct analytical forms for the non-conformal coupling function $J(\phi, \chi)$ in the two inflationary models we have considered. We shall then make use of the analytical forms for $J(\phi, \chi)$ to numerically compute the resulting spectra of the magnetic field and compare them with the spectra we have obtained earlier.

Let us first discuss the model described by the potential (3.11). As we have seen, in the two field models of our interest, there arise two stages of inflation, with each regime being driven by one of the two fields. In the case of inflation driven by the potential (3.11), during the first stage, the field ϕ rolls down the potential, while the field χ remains frozen. During this phase, the evolution of the field ϕ in the slow roll approximation can be expressed as [231]

$$\phi^2(N) = \phi_{\rm i}^2 - 4\, M_{_{\rm Pl}}^2\, N, \tag{B.1}$$

where we have assumed that $\phi = \phi_{\rm i}$ at $N = 0$. To achieve the desired behavior of $J \propto a^2$, in the first stage, we can assume that

$$J(\phi) \propto \exp\left[-\frac{1}{2}\left(\frac{\phi^2}{M_{_{\rm Pl}}^2} - \frac{\phi_{\rm i}^2}{M_{_{\rm Pl}}^2}\right)\right]. \tag{B.2}$$

The first stage dominated by the field ϕ eventually ends and, after a few damped oscillations, the field settles down at the value

$$\phi_{\rm min} \simeq \frac{1}{2\,\bar{b}}\, W\left(\frac{8\, V_0\, \bar{b}^2\, M_{_{\rm Pl}}^2\, \chi_0^4}{3\, m_\phi^2\, \chi_{\rm i}^6}\right), \tag{B.3}$$

where $W(z)$ is the so-called Lambert or the product logarithmic function [309]. The field χ drives the second stage of inflation and, during this period, the solution for the field in the slow roll approximation can be written as

$$\chi^2(N) \;=\; \left[\left(\chi_0^2 + \chi_{\rm i}^2\right)^2 - 8\, M_{_{\rm Pl}}^2\, \chi_0^2\, {\rm e}^{-2\,\bar{b}\,\phi_{\rm min}}\, (N - N_1)\right]^{1/2} - \chi_0^2, \tag{B.4}$$

where N_1 is the e-fold when $\phi = \phi_{\rm min}$. In a fashion similar to the first phase, to achieve $J \propto a^2$, we can choose the coupling function during the second stage of slow roll inflation to be

$$J(\chi) \;=\; \exp\left\{2\,N_1 - \frac{\mathrm{e}^{2\,\bar{b}\,\phi_{\rm min}}}{4\,M_{_{\rm Pl}}^2\,\chi_0^2}\,\left[\left(\chi^2+\chi_0^2\right)^2 - \,\left(\chi_{\rm i}^2+\chi_0^2\right)^2\right]\right\}. \tag{B.5}$$

Let us now turn to the second model described by the potential (3.12). During the first stage driven by the field ϕ, in the slow roll approximation, the evolution of the field can be expressed as

$$\phi^2(N) = \left[\left(\phi_{\rm i}^2+\phi_0^2\right)^2 - 8\,M_{_{\rm Pl}}^2\,\phi_0^2\,N\right]^{1/2} - \phi_0^2, \tag{B.6}$$

where we have assumed that the field is at $\phi_{\rm i}$ when $N = 0$. To achieve $J \propto a^2$, the coupling function can be chosen to be

$$J(\phi) \propto \exp\left\{-\frac{1}{4\,M_{_{\rm Pl}}^2\,\phi_0^2}\,\left[\left(\phi^2+\phi_0^2\right)^2 - \left(\phi_{\rm i}^2-\phi_0\right)^2\right]\right\}. \tag{B.7}$$

In between the two stages of inflation, ϕ behaves like a massive scalar field and undergoes damped oscillations around the minimum [231]. It seems difficult to obtain an analytical solution during this period since the Hubble parameter H and the field χ experience a jump. We find that ϕ eventually approaches a constant value $\phi_{\rm min}$, given by the minimum of its effective potential. The value of χ at the onset of this period can be written as $\chi_{1\rm i} = \chi_{\rm i} - \Delta\chi$, where $\Delta\chi$ is the jump in χ. During the second stage of slow roll inflation, the solution for χ can be written as

$$\chi^2(N) = \chi_{\rm i}^2 - 4\,\mathrm{e}^{-2\,\bar{b}\,[\phi_{\rm min}+\Delta\phi(N)]}\,M_{_{\rm Pl}}^2\,(N-N_1), \tag{B.8}$$

where $\phi_{\rm min} = \bar{b}\,M_{_{\rm Pl}}^2\,m_\chi^2\,\phi_0^2/(3\,V_0)$ and the quantity $\Delta\phi$ is governed by the equation

$$\frac{\mathrm{d}^2\Delta\phi}{\mathrm{d}N^2} + (3-\epsilon_1)\,\frac{\mathrm{d}\Delta\phi}{\mathrm{d}N} + \frac{m_{\Delta\phi}^2}{H^2}\,\Delta\phi = 0 \tag{B.9}$$

with $m_{\Delta\phi}^2$ being given by

$$m_{\Delta\phi}^2 = \frac{2\,V_0}{\phi_0^2} + \frac{4}{3}\,\bar{b}^2\,m_\chi^2\,\phi_0^2. \tag{B.10}$$

Therefore, the coupling function during the second stage can be chosen to be

$$J(\chi) = \exp\left\{2\,N_1 - \frac{1}{2}\,\mathrm{e}^{2\,\bar{b}\,[\phi_{\rm min}+\Delta\phi(N)]}\,\left(\frac{\chi^2}{M_{_{\rm Pl}}^2} - \frac{\chi_{\rm i}^2}{M_{_{\rm Pl}}^2}\right)\right\}. \tag{B.11}$$

With the solutions of the coupling functions in the two stages at hand, we can combine them [in a manner similar to Eq. (3.22)] to arrive at the following coupling function:

$$\begin{aligned} J(\phi,\chi) &= J_0\left\{\frac{1}{2}\left[1+\tanh\left(\frac{\chi-\chi_1}{\Delta\chi}\right)\right]\, J(\phi)\right. \\ &\quad \left.+\frac{1}{2}\left[1-\tanh\left(\frac{\chi-\chi_1}{\Delta\chi}\right)\right]\, J(\chi)\right\}, \end{aligned} \tag{B.12}$$

where χ_1 is the value of χ around the e-fold when the transition from the the first stage of slow roll region to the second stage occurs. Since we require J to reduce to unity at the end of inflation, we have

$$\begin{aligned} J_0 &= \left\{\frac{1}{2}\left[1+\tanh\left(\frac{\chi_{\mathrm{e}}-\chi_1}{\Delta\chi}\right)\right]\, J(\phi_{\mathrm{e}})\right. \\ &\quad \left.+\frac{1}{2}\left[1-\tanh\left(\frac{\chi_{\mathrm{e}}-\chi_1}{\Delta\chi}\right)\right]\, J(\chi_{\mathrm{e}})\right\}^{-1}, \end{aligned} \tag{B.13}$$

where ϕ_{e} and χ_{e} denote the values of the fields at the end of inflation.

Earlier, in Fig. 3.2, we had compared the analytical solutions for the background scalar fields we have obtained above with the exact numerical results. Clearly, while the analytical solutions are a good approximation to the exact numerical results in the two domains involving slow roll, they perform poorly around the transition. In Fig. B.1, we have plotted the non-conformal coupling function J we have arrived at analytically using the expression (B.12) for the two models of our interest. In the figure, we have also plotted the quantity $\mu_{_{\mathrm{B}}}^2 = J''/(J\, a^2\, H^2)$ and the resulting power spectra of magnetic fields $\mathcal{P}_{_{\mathrm{B}}}(k)$ for the two models. As should be evident, though the strengths of magnetic field roughly match the numerical results we had obtained earlier (plotted in Fig. 3.5), the shapes of the power spectra are fairly different. This can be attributed to the discontinuous behavior of the fields around the point of transition in the analytical case.

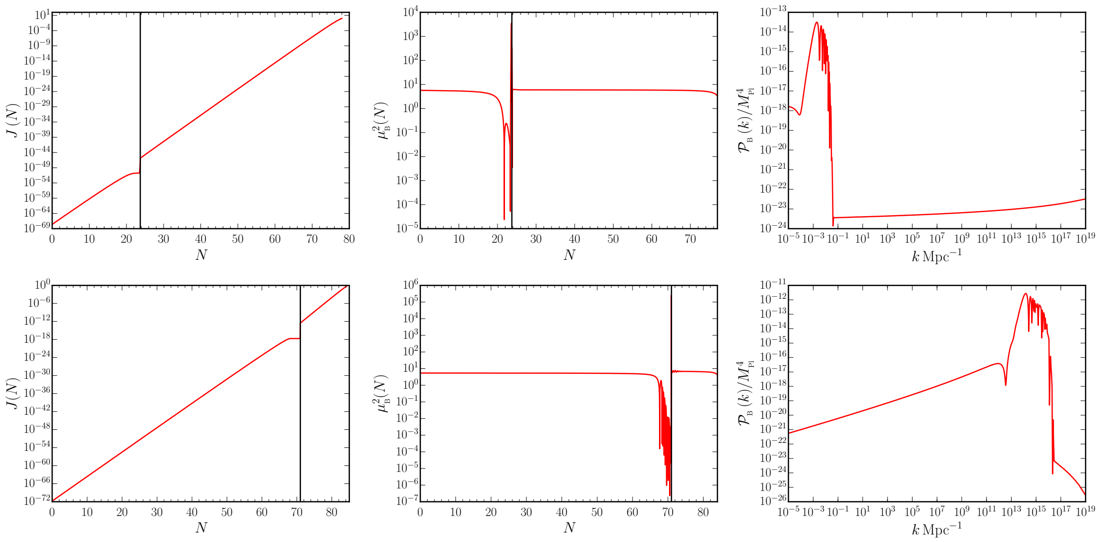

Figure B.1: The coupling functions $J(N)$ constructed analytically using Eq. (B.12) (on the left), along with the corresponding $\mu_{\rm B}^2(N)$ (in the middle), and the resulting spectra of the magnetic field (on the right) have been plotted for the models described by the potentials (3.11) (on top) and (3.12) (at the bottom). We have indicated the point of transition in the plots of $J(N)$ and $\mu_{\rm B}^2(N)$ (as vertical black lines). Note that the above spectra of the magnetic field differ from the spectra we had arrived at earlier in Fig. 3.5. The differences can be attributed to the inability of the analytical solutions to capture the dynamics of the fields around the point of transition from the first stage to the second stage of slow roll inflation.

APPENDIX C

IMPACT OF THE CHOICE OF THE PARAMETERS IN THE NON-CONFORMAL COUPLING FUNCTION

Recall that, the non-conformal coupling function $J(\phi, \chi)$ in Eq. (3.22) was constructed so that its evolution was determined by the field driving the background expansion at any given time. Such a construction had ensured that the function largely behaves in the manner that we desire, i.e. as $J(\phi, \chi) \propto a^2$ (see Fig. 3.4). The point at which $J(\phi, \chi)$ switches its dependence on the evolution of ϕ to that of χ is determined by χ_1. Also, the range over which this switch happens is determined by $\Delta\chi$. Earlier, while arriving at the power spectra of the electromagnetic fields due to such a coupling function, we had worked with specific values of these two parameters. In this appendix, we shall discuss the impact of the choice of these parameters on the power spectrum of the magnetic field.

It seems natural to choose the value of χ_1 to be the point at which the turn in the trajectory in the field space occurs (as marked in Fig. 3.2). The value of $\Delta\chi$ can be chosen to be that it roughly corresponds to the duration of the transition. However, we ought to consider the effects that may occur due to variation of these parameters and quantify the dependence of the features in the spectrum of the magnetic field on such variations. Evidently, we should be cautious so that, even as we try to capture the features that arise from the intrinsic dynamics of the fields, we do not end up introducing features from the very construction and parametrization of the coupling function.

We have analyzed the effects of the parameters χ_1 and $\Delta\chi$ on the spectrum of the magnetic field in the case of the first model described by the potential (3.11). We have presented the results of the exercise in Fig. C.1. Note that, in our analysis, while we vary χ_1 and $\Delta\chi$, we have retained the original values for parameters of the model and of the fitting functions $N(\phi)$ and $N(\chi)$ [cf. Eqs. (3.20) and (3.21)]. To begin with, we shall discuss the effects due to variation of $\Delta\chi$. The value of $\Delta\chi = 10^{-3}\, M_{_{\rm Pl}}$ which we have used earlier, seems to be an appropriate choice since, for such a value, we are able to achieve the desired behavior of $J(\phi, \chi) \propto a^2$ without considerable deviations during the transition. However, for larger values of the parameter, say that lie in the range $10^{-3}\, M_{_{\rm Pl}} \leq \Delta\chi < 10^{-1}\, M_{_{\rm Pl}}$, we observe that, prior to the transition, the coupling function $J(\phi, \chi)$ turns to be a constant. This essentially arises due to the smoothing of the hyperbolic tangent function that we had introduced to effect the transition between the two parts of $J(\phi, \chi)$. A smoother hyperbolic tangent function suppresses the contribution due to the evolution of ϕ before transition and that of χ after

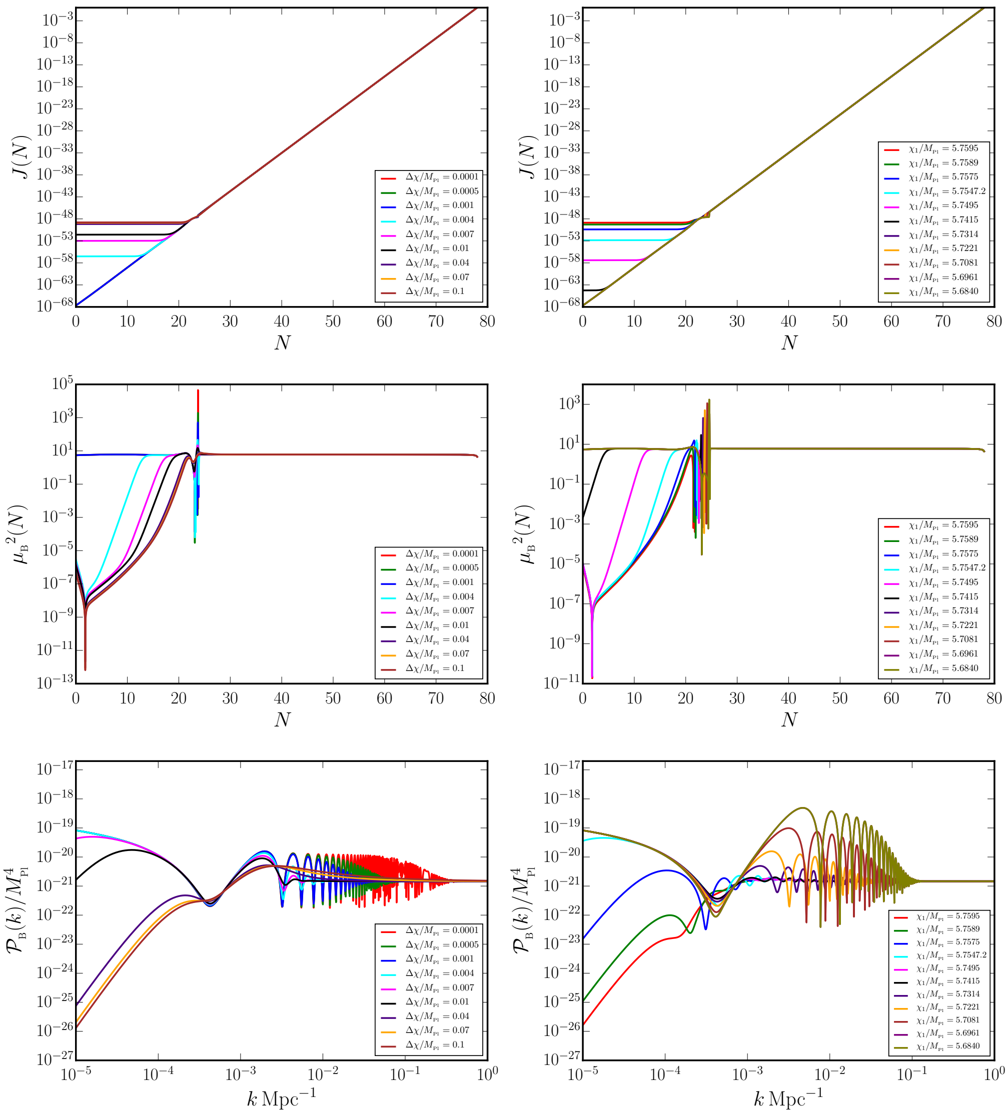

Figure C.1: We have presented the behavior of $J(\phi, \chi)$, $\mu_{\rm B}^2(N)$, and the corresponding power spectrum of the magnetic field $\mathcal{P}_{\rm B}(k)$ (on top, in the middle, and bottom rows, respectively) that arise due to the variation of the parameters $\Delta\chi$ (on the left column) and χ_1 (on the right column) in the case of the first model described by the potential (3.11). The parameters have been varied around the values of $\Delta\chi = 10^{-3}\, M_{\rm Pl}$ and $\chi_1 = 5.722\, M_{\rm Pl}$ that we had considered earlier. We should mention that we have retained the original values of the other parameters in arriving at these results. For larger values of $\Delta\chi$, which lead to a smoother transition of $J(\phi, \chi)$, we find that $\mathcal{P}_{\rm B}(k) \propto k^4$ over large scales, whereas for smaller values of $\Delta\chi$, effecting a sharper transition, we obtain a nearly scale invariant spectrum in the asymptotic domains (in wave number) with oscillations that extend over a wider range of wave numbers. Moreover, while larger values of χ_1 lead to the $\mathcal{P}_{\rm B}(k) \propto k^4$ behavior over large scales, smaller values result in asymptotically (i.e. in wave numbers) scale invariant spectra with oscillations that are of higher amplitude over the intermediate domain.

the transition. Because of this reason, $J(\phi, \chi)$ settles to a constant over the smoothed regime. Such a behavior of $J(\phi, \chi)$ leads to extremely small values of J''/J, which invariably results in the spectrum of the magnetic field $\mathcal{P}_{_{\rm B}}(k)$ behaving as k^4 over large scales (as can seen in the plots in left column of Fig. C.1). Moreover, if we make the transition sharper, i.e. if we choose $\Delta\chi < 10^{-3}\, M_{_{\rm Pl}}$, though the spectrum of the magnetic field largely retains its shape, there arise oscillations over a wider window of wave numbers between the two domains of scale invariance. This is expected since a faster transition leads to a sharp peak in J''/J between the two regimes. Hence, we can conclude that, to avoid any artificial features such as either a suppressed power over large scales or a prolonged burst of oscillations in the spectrum of the magnetic field, the choice of $\Delta\chi = 10^{-3}\, M_{_{\rm Pl}}$ seems optimal.

Let us now turn to understanding the effects due to the variation in χ_1. Upon choosing the value of χ_1 to be greater than $5.722\, M_{_{\rm Pl}}$, we observe that the non-conformal coupling function $J(\phi, \chi)$ again turns constant during the initial epoch, and hence the spectrum of the magnetic field $\mathcal{P}_{_{\rm B}}(k)$ behaves as k^4 over large scales. This is due to the coupling function switching its dependence from ϕ to χ at an earlier time, before the turn in the trajectory in the field space occurs. Such a choice suppresses the dependence of $J(\phi, \chi)$ on ϕ during the initial regime and makes it follow the behavior of χ which is frozen during this epoch. As a result, J''/J drops to very small values and, as we have already discussed, it leads to the k^4 behavior of the spectrum of the magnetic field over large scales. For $\chi_1 \leq 5.722\, M_{_{\rm Pl}}$, we find that the spectrum regains its near scale invariance in the two asymptotic domains, but the amplitude of oscillations over the intermediate domain in wave numbers prove to be larger. Therefore, the ideal value of χ_1 proves to be around $5.722\, M_{_{\rm Pl}}$, where the turn occurs in the trajectory in the field space. Otherwise, one may introduce either a suppression or oscillations with large amplitudes, which are clearly artifacts induced by a non-optimal value of χ_1.

APPENDIX D

POWER SPECTRUM OF FLUCTUATIONS IN THE ENERGY DENSITY OF THE ELECTROMAGNETIC FIELD

Let $\hat{\rho}^{\boldsymbol{k}}_{_{\rm EM}}(\eta)$ denote the operator associated with the energy density corresponding to a given wave vector $\boldsymbol{k}$ of the electromagnetic field. The power spectrum of fluctuations in the energy density of the electromagnetic field for a given mode, say, $P_{_{\rm EM}}(k)$, is defined through the relation [131, 224]

$$\langle\hat{\rho}^{\boldsymbol{k}\dagger}_{_{\rm EM}}(\eta_{\rm e})\,\hat{\rho}^{\boldsymbol{k}'}_{_{\rm EM}}(\eta_{\rm e})\rangle\,-\,\langle\hat{\rho}^{\boldsymbol{k}\dagger}_{_{\rm EM}}(\eta_{\rm e})\rangle\,\langle\hat{\rho}^{\boldsymbol{k}'}_{_{\rm EM}}(\eta_{\rm e})\rangle=(2\,\pi)^3\,P_{_{\rm EM}}(k)\,\delta^{(3)}(\boldsymbol{k}-\boldsymbol{k}'), \tag{D.1}$$

where, as mentioned earlier, $\eta_{\rm e}$ denotes the conformal time coordinate close to the end of inflation. Note that the expectation values in the above expression are to be evaluated in the Bunch-Davies vacuum.

Recall that, in the non-helical case, for $J\propto a^2$, the energy density of the electric field is negligible at late times. Therefore, the total energy density of the electromagnetic field for a given mode can be expressed in terms of the Fourier modes of the magnetic field, say, $B_{i\boldsymbol{k}}$, as follows:

$$\rho^{\boldsymbol{k}}_{_{\rm EM}}(\eta)=\frac{J^2(\eta)}{8\,\pi}\int\frac{{\rm d}^3\boldsymbol{q}}{(2\,\pi)^{3/2}}\,B_{i\,\boldsymbol{q}}(\eta)\,B^i_{(\boldsymbol{k}-\boldsymbol{q})}(\eta), \tag{D.2}$$

where $B_i=\epsilon_{ijl}\,(\partial^j A^l)/a$, $B^i=g^{ij}\,B_j$, and $B_{i\,\boldsymbol{k}}$ denotes the Fourier modes associated with the magnetic field. For the case wherein the spectrum of the magnetic field is scale invariant [i.e. $\mathcal{P}_{_{\rm B}}(k)=9\,H_{_{\rm I}}^4/(4\,\pi^2)$, see Eq. (2.26a)], upon substituting Eq. (D.2) in Eq. (D.1) and using Wick's theorem, we find that the power spectrum $P_{_{\rm EM}}(k)$ can be expressed as

$$P_{_{\rm EM}}(k)\;=\;\frac{1}{2\,\pi^2}\left(\frac{3\,H_{_{\rm I}}^2}{4\,\pi}\right)^4\left[\int\frac{{\rm d}^3\boldsymbol{q}}{q^3\,\vert\boldsymbol{k}-\boldsymbol{q}\vert^3}+\int\frac{{\rm d}^3\boldsymbol{q}}{q^5\,\vert\boldsymbol{k}-\boldsymbol{q}\vert^5}\,\left[\boldsymbol{q}\cdot(\boldsymbol{k}-\boldsymbol{q})\right]^2\right]. \tag{D.3}$$

Upon carrying out the integrals over $\boldsymbol{q}$, we obtain that

$$k^3\,P_{_{\rm EM}}(k)=\frac{16}{3\,\pi}\,\left(\frac{3\,H_{_{\rm I}}^2}{4\,\pi}\right)^4\,\ln\left(\frac{k}{k_{\rm min}}\right), \tag{D.4}$$

where we have introduced the infrared cut-off $k_{\rm min}$ to regulate the integral. It is this result for $P_{_{\rm EM}}(k)$ that we have utilized to arrive at the power spectrum for the curvature perturbations induced by the magnetic field, viz. $\mathcal{P}^{\rm mag}_{\mathcal{R}}(k)$, in Eq. (3.28).

APPENDIX E

ON THE CHOICE OF CONJUGATE MOMENTUM

Recall that, initially, we had arrived the action (4.27) to describe the Fourier modes of the helical electromagnetic field. If we focus on the electromagnetic mode associated with a single wave number (as we did in Secs. 4.3.2, 4.4.1 and 4.4.2), the fiducial variable $\mathcal{A}$—which stands for either $\mathcal{A}^{\sigma}_{\boldsymbol{k}\mathrm{R}}$ or $\mathcal{A}^{\sigma}_{\boldsymbol{k}\mathrm{I}}$ [introduced in Eq. (4.29)]—is described by the following Lagrangian density in Fourier space:

$$\mathcal{L} = \frac{1}{2}\,\mathcal{A}'^2 - \kappa\,\mathcal{A}'\,\mathcal{A} - \frac{\mu^2}{2}\,\mathcal{A}^2. \tag{E.1}$$

In this appendix, we shall explain the reason for adding the total time derivative (4.26) to the original action (4.25) to arrive at the modified action (4.27) or, equivalently, the Lagrangian (4.30) for the variable $\mathcal{A}$.

E.1 CHOICES OF MOMENTA AND INITIAL CONDITIONS

Note that the conjugate momentum associated with the original Lagrangian (E.1) is given by

$$\mathcal{P} = \mathcal{A}' - \kappa\,\mathcal{A}. \tag{E.2}$$

The corresponding Hamiltonian can be obtained to be

$$\mathcal{H} = \frac{\mathcal{P}^2}{2} + \kappa\,\mathcal{P}\,\mathcal{A} + \frac{\widetilde{\omega}^2}{2}\,\mathcal{A}^2, \tag{E.3}$$

where the quantity $\widetilde{\omega}^2$ is given Eq. (4.64). The Schrödinger equation governing the wave function $\Psi(\mathcal{A},\eta)$ corresponding to the above Hamiltonian is given by

$$i\,\frac{\partial\Psi}{\partial\eta} = -\frac{1}{2}\,\frac{\partial^2\Psi}{\partial\mathcal{A}^2} - \frac{i\,\kappa}{2}\,\left(\Psi + 2\,\mathcal{A}\,\frac{\partial\Psi}{\partial\mathcal{A}}\right) + \frac{\widetilde{\omega}^2}{2}\,\mathcal{A}^2\,\Psi. \tag{E.4}$$

Upon using the Gaussian ansatz (4.34) for the wave function $\Psi(\mathcal{A},\eta)$ in this Schrödinger equation, we obtain that

$$\Omega' = -i\,\Omega^2 - 2\,\kappa\,\Omega + i\,\widetilde{\omega}^2. \tag{E.5}$$

If we now use the definition (4.38) of Ω in the above equation, but with g being given by

$$g = f' - \kappa\, f, \tag{E.6}$$

then we arrive at the same equation for f^* that we had obtained earlier, viz. Eq. (4.40). This should not come as a surprise since, classically, Lagrangians that differ by a total time derivative lead to the same equation of motion. Moreover, since the wave function is assumed to be of the same form, we obtain the same Wigner function as had obtained before, i.e. as in Eq. (4.43), but with $\mathcal{P}$ being the new conjugate momentum defined in Eq. (E.2). However, for $I = J$ and $J \propto \eta^{-n}$, we find that, at early times, while f behaves as in Eq. (4.45), g behaves as

$$g = f' - \kappa\, f \simeq -i\,\sqrt{\frac{k}{2}}\,(1 + i\,\sigma\,\gamma)\,\mathrm{e}^{-i\,k\,\eta}. \tag{E.7}$$

These f and g lead to the same Wronskian (4.47) that we had obtained earlier. Also, in such a case, we have $\Omega_{\mathrm{R}} = k$ and $\Omega_{\mathrm{I}} = \sigma\,\gamma\,k$, resulting in the following condition for the Wigner ellipse:

$$\bar{\mathcal{A}}^2 + \left(\mathcal{P} + \sigma\,\gamma\,\bar{\mathcal{A}}\right)^2 = 1. \tag{E.8}$$

Moreover, for the above initial conditions on f and g, from Eqs. (4.53), we obtain that $\cosh{(2\,r)} = 1 + (\gamma^2/2)$, while $\cos{(2\,\varphi)} = \pm\gamma/\sqrt{4+\gamma^2}$. These imply that, when γ is non-zero (i.e. in the helical case), at early times, the Wigner ellipse is not a circle. It starts as an ellipse with its major axis oriented at the angle φ with respect to the $\bar{\mathcal{A}}$ axis.

If we now instead add a different total time derivative to the original Lagrangian (E.1) as follows

$$\mathcal{L} = \frac{1}{2}\,\mathcal{A}'^2 - \kappa\,\mathcal{A}'\,\mathcal{A} - \frac{\mu^2}{2}\,\mathcal{A}^2 + \frac{\mathrm{d}}{\mathrm{d}\eta}\left(\frac{1}{2}\kappa\,\mathcal{A}^2\right), \tag{E.9}$$

then it simplifies to the form

$$\mathcal{L} = \frac{1}{2}\,\mathcal{A}'^2 - \frac{1}{2}\,\omega^2\,\mathcal{A}^2 \tag{E.10}$$

with ω^2 being given by Eq. (4.41). The corresponding conjugate momentum is given by

$$\mathcal{P} = \mathcal{A}' \tag{E.11}$$

and the associated Hamiltonian can be immediately obtained to be

$$\mathcal{H} = \frac{1}{2}\,\mathcal{P}^2 + \frac{1}{2}\,\omega^2\,\mathcal{A}^2. \tag{E.12}$$

The Schrödinger equation describing the wave function $\Psi(\mathcal{A},\eta)$ in such a case is given by

$$i\,\frac{\partial\Psi}{\partial\eta} = -\frac{1}{2}\,\frac{\partial^2\Psi}{\partial\mathcal{A}^2} + \frac{1}{2}\,\omega^2\,\mathcal{A}^2\,\Psi. \tag{E.13}$$

The Gaussian ansatz (4.34) for the wave function leads to the following equation for Ω:

$$\Omega' = -i\,\Omega^2 + i\,\omega^2. \tag{E.14}$$

Upon substituting the definition (4.38) of Ω in this differential equation, but with

$$g = f', \tag{E.15}$$

then we obtain Eq. (4.40) for f^*, as one would have expected. Note that, in such a situation, as with the Lagrangian (4.30), at early times, f and g reduce to the forms in Eqs. (4.45) and (4.46) implying that the initial Wigner ellipse is a circle. Also, as in the original case, we have, at early times, $\cosh{(2\,r)} = 1$, while $\cos{(2\,\varphi)}$ is undetermined.

In order to ensure that the system starts in the standard Bunch-Davies vacuum at early times with no squeezing involved, we have worked with the modified Lagrangian (4.30) instead of the Lagrangian (E.1). As we have discussed earlier, if we work in terms of the corresponding conjugate momentum $\mathcal{P}$ [cf. Eq. (4.31)], we obtain a Wigner ellipse which starts as a circle at early times, as desired [cf. Eq. (4.49)]. But, such a behavior of the Wigner ellipse and the squeezing parameters at early times is also encountered when the system is described by the Lagrangian (E.10)], as we discussed above. Could we have also worked with the Lagrangian (E.10)? It seems that the Lagrangian (4.30) is an appropriate choice. Let us illustrate this point with a simple example.

E.2 A SIMPLE EXAMPLE

To illustrate our point, we shall focus on the non-helical electromagnetic field (i.e. when $\gamma = 0$) and consider the case wherein $J = (\eta/\eta_{\rm e})^{-n}$. The trivial case, of course, corresponds to the conformally coupled field wherein $n = 0$. In such a case, all the momenta $\mathcal{P}$ we have encountered, i.e. those given by Eqs. (4.31), (E.2) and (E.11), turn out to be the same and the quantities f and g are given *exactly* by Eqs. (4.45) and (4.46) *at all times*. Therefore, $\cosh{(2\,r)} = 1$ forever, while $\cos{(2\,\varphi)}$ remains undetermined, and the Wigner ellipse remains a circle. This is not surprising.

Now, consider the *non-trivial*, $n = -1$ case. In such a situation, $J''/J = 0$, and hence the quantity f is given by Eq. (4.45) *at all times*. Since $\gamma = 0$, the momenta $\mathcal{P}$ defined in Eqs. (4.31) and (E.2) turn out to be the same. If we work with the momentum defined in Eq. (E.11), then the quantity g is given by Eq. (4.46) *at all times* so that the Wigner ellipse and the squeezing parameter behave as in the conformally invariant case. This seems strange. But, if we work with the conjugate momentum defined in Eq. (4.31) (as we have done in Secs. 4.3.2, 4.4.1 and 4.4.2), then we have

$$g = f' - \frac{J'}{J}\, f \simeq -i\,\sqrt{\frac{k}{2}}\,\left(1 - \frac{i}{k\,\eta}\right)\, \mathrm{e}^{-i\,k\,\eta}. \tag{E.16}$$

This implies that the Wigner ellipse starts as a circle at early times, while $\cosh\left(2\,r\right) = 1$. However, at late times, we have

$$\cosh\left(2\,r\right) \simeq \frac{1}{2}\,\left(1 + \frac{k_{\mathrm{e}}^2}{k^2}\right) \tag{E.17}$$

indicating a significant extent of squeezing for large scales. This example confirms that our choice for the conjugate momentum $\mathcal{P}$ as given by Eq. (4.31) to be an appropriate one.

APPENDIX F

ANOTHER DERIVATION OF QUANTUM DISCORD

A convenient method to calculate the quantum discord is to write down the covariance matrix of the canonically conjugate variables and arrive at the quantum discord using the submatrices of the covariance matrix [277, 288, 310]. But, one has to first choose an appropriate set of two pairs of canonically conjugate variables, such that tracing over one set will give us the correct quantum discord to match with the results in the earlier literature (i.e. one has to identify variables to represent the appropriate subsystem of the full system) [262, 277].

As we have described in Sec. 4.3.1, the action describing the modes $\mathcal{A}_{\boldsymbol{k}}^{\sigma}$ of the electromagnetic field is similar to the action that governs the Mukhanov-Sasaki variable characterizing the scalar perturbations. However, there are two differences. The first difference is that, due to the two states of polarization, the electromagnetic field contains twice as many degrees of freedom as the scalar perturbations. Secondly, in the helical case, due to the presence of the term that leads to the violation of parity, the modes corresponding to the two states of polarization evolve differently. Nevertheless, the two helical states of polarizations (with $\sigma = \pm 1$) evolve independently, and the method adopted in the case of the scalar perturbations can be used to characterize the quantum discord associated with either of the two states of the polarization of the electromagnetic field.

The quantum discord that we would like to calculate is when the system is divided into modes with wave vectors $\boldsymbol{k}$ and $-\boldsymbol{k}$, as in the case of the scalar perturbations [262, 277]. As we have explained in the main text, the correct variables to use are the conjugate variables $(x_{\boldsymbol{k}}^{\sigma}, p_{\boldsymbol{k}}^{\sigma})$ as defined in Eq. (4.59), but with $\bar{\omega}$ replaced by $\widetilde{\omega}$ [cf. Eq. (4.64)]. On using our convention of referring to $x_{\boldsymbol{k}}^{\sigma}$ and $x_{-\boldsymbol{k}}^{\sigma}$ as x_1 and x_2, the covariance matrix of the two pairs of canonically conjugate variables $(\hat{x}_1, \hat{p}_1, \hat{x}_2, \hat{p}_2)$ has the form

$$\boldsymbol{V} = \begin{bmatrix} \langle \hat{x}_1^2 \rangle & \frac{1}{2} \langle \hat{x}_1 \hat{p}_1 + \hat{p}_1 \hat{x}_1 \rangle & \langle \hat{x}_1 \hat{x}_2 \rangle & \langle \hat{x}_1 \hat{p}_2 \rangle \\ \frac{1}{2} \langle \hat{x}_1 \hat{p}_1 + \hat{p}_1 \hat{x}_1 \rangle & \langle \hat{p}_1^2 \rangle & \langle \hat{x}_2 \hat{p}_1 \rangle & \langle \hat{p}_1 \hat{p}_2 \rangle \\ \langle \hat{x}_1 \hat{x}_2 \rangle & \langle \hat{x}_2 \hat{p}_1 \rangle & \langle \hat{x}_2^2 \rangle & \frac{1}{2} \langle \hat{x}_2 \hat{p}_2 + \hat{p}_2 \hat{x}_2 \rangle \\ \langle \hat{x}_1 \hat{p}_2 \rangle & \langle \hat{p}_1 \hat{p}_2 \rangle & \frac{1}{2} \langle \hat{x}_2 \hat{p}_2 + \hat{p}_2 \hat{x}_2 \rangle & \langle \hat{p}_2^2 \rangle \end{bmatrix}. \tag{F.1}$$

To calculate quantum discord, first we define a scaled covariance matrix as

$$\boldsymbol{\sigma} = 2\,\boldsymbol{V}. \tag{F.2}$$

We next divide this (4×4) matrix in terms of (2×2) sub-blocks as follows:

$$\boldsymbol{\sigma} = \begin{bmatrix} \boldsymbol{\alpha} & \boldsymbol{\gamma} \\ \boldsymbol{\gamma}^T & \boldsymbol{\beta} \end{bmatrix}, \tag{F.3}$$

where $\boldsymbol{\alpha}$, $\boldsymbol{\beta}$ and $\boldsymbol{\gamma}$ are (2×2) matrices. Defining

$$B = \mathrm{det.}\, \boldsymbol{\beta}, \tag{F.4}$$

the entanglement entropy for the (x_2, p_2) subsystem, say, $\mathcal{S}_2(\sigma_{\mathbb{12}})$, can then be directly calculated to be (in this context, see Ref. [311])

$$\mathcal{S}_2(\sigma_{\mathbb{12}}) = F(\sqrt{B}), \tag{F.5}$$

with the function $F(x)$ being given by

$$F(x) = \left(\frac{x+1}{2}\right) \ln\left(\frac{x+1}{2}\right) - \left(\frac{x-1}{2}\right) \ln\left(\frac{x-1}{2}\right). \tag{F.6}$$

Using the wave function (4.67) and the relations (4.71), the elements of the matrix $\boldsymbol{\beta}$ can be evaluated to be

$$\langle \hat{x}_2^2 \rangle = \frac{\Omega_{1\mathrm{R}}}{2\,(\Omega_{1\mathrm{R}}^2 - \Omega_{2\mathrm{R}}^2)} = \frac{|\Omega_+|^2 + \widetilde{\omega}^2}{4\,\widetilde{\omega}^2\,\Omega_{+\mathrm{R}}}, \tag{F.7a}$$

$$\langle \hat{p}_2^2 \rangle = \widetilde{\omega}^2\,\langle \hat{x}_2^2 \rangle, \quad \frac{1}{2}\,\langle \hat{x}_2\,\hat{p}_2 + \hat{p}_2\,\hat{x}_2 \rangle = 0, \tag{F.7b}$$

where $\Omega_{+\mathrm{R}} = (\Omega_+ + \Omega_+^*)/2$ represents the real part of Ω_+. Therefore, the determinant of $\boldsymbol{\beta}$ becomes

$$B = 4\,\langle \hat{x}_2^2 \rangle\,\langle \hat{p}_2^2 \rangle - \langle \hat{x}_2\,\hat{p}_2 + \hat{p}_2\,\hat{x}_2 \rangle^2 = \frac{\left(|\Omega_+|^2 + \widetilde{\omega}^2\right)^2}{4\,\widetilde{\omega}^2\,\Omega_{+\mathrm{R}}^2}. \tag{F.8}$$

To connect with the results in the main text, we can use the expression (4.82) for y to obtain that

$$\sqrt{B} = y + 1. \tag{F.9}$$

On substituting this expression for B in Eq. (F.5), we can arrive at the result (4.80) for the quantum discord we had obtained earlier.

APPENDIX G

CHARGED SCALAR FIELD UNDER THE INFLUENCE OF AN ELECTRIC FIELD IN A DE SITTER UNIVERSE

In this appendix, we shall discuss the Schwinger effect in de Sitter spacetime by considering the evolution of a charged scalar field in the presence of a constant electric field (for earlier discussions in this regard, see, for instance, Refs. [294–297]). We should mention that the corresponding results in flat spacetime can be arrived at by considering the limit wherein the constant Hubble parameter in de Sitter vanishes.

G.1 EQUATION OF MOTION IN AN FLRW UNIVERSE

Consider a complex scalar field, say, ψ, evolving in a curved spacetime. In the presence of an electromagnetic field described by the vector potential A_μ, the action governing the complex scalar field is given by

$$S[\psi] = -\int \mathrm{d}^4x\, \sqrt{-g}\, \left[(D_\mu\psi)^*\, (D^\mu\psi) + m^2\, \psi\, \psi^*\right], \tag{G.1}$$

where $D_\mu = (\partial_\mu - i\, e\, A_\mu)$ and e denotes the electric charge. On varying the above action, we obtain the equation of motion governing the scalar field to be

$$\frac{1}{\sqrt{-g}}\, D_\mu \left(\sqrt{-g}\, g^{\mu\nu}\, D_\nu\right)\, \psi - m^2\, \psi = 0. \tag{G.2}$$

The strength E of the electric field can be expressed in terms of the field tensor $F_{\mu\nu}$ as

$$F^{\mu\nu}\, F_{\mu\nu} = -2\, E^2. \tag{G.3}$$

If we choose to work with the vector potential

$$A_\mu = [0, 0, 0, -A(\eta)], \tag{G.4}$$

then, in the FLRW universe, the electric field is oriented along the z-direction and its strength is given by

$$E = \frac{A'}{a^2}. \tag{G.5}$$

If we define the new variable

$$u(\eta, \boldsymbol{x}) = a(\eta)\, \psi(\eta, \boldsymbol{x}), \tag{G.6}$$

then, for the FLRW line-element (1.2) and the vector potential (G.4), the action (G.1) takes the form

$$S[u] = \int \mathrm{d}\eta \int \mathrm{d}^3\boldsymbol{x} \left\{ |u'|^2 - |\boldsymbol{\partial}_\perp u|^2 - |D_z u|^2 - \frac{a'}{a}\,(u\,u'^* + u^*\,u') - \left[m^2\,a^2 - \left(\frac{a'}{a}\right)^2\right] |u|^2 \right\}, \tag{G.7}$$

where $\boldsymbol{\partial}_\perp = (\partial_x, \partial_y)$ and $D_z = \partial_z + i\,e\,A(\eta)$. The symmetries of the FLRW metric and the fact that the vector potential A_μ depends only on the conformal time coordinate allows us to decompose the quantity $u(\eta, \boldsymbol{x})$ as follows:

$$u(\eta, \boldsymbol{x}) = \int \frac{\mathrm{d}^3\boldsymbol{k}}{(2\,\pi)^{3/2}}\, q_{\boldsymbol{k}}(\eta)\, \mathrm{e}^{i\,\boldsymbol{k}\cdot\boldsymbol{x}}. \tag{G.8}$$

We should point out that, since u is a complex field, we do *not* have a condition connecting the Fourier modes $q_{\boldsymbol{k}}$ and $q_{-\boldsymbol{k}}$ akin to Eq. (4.22). The action in Fourier space that governs the modes $q_{\boldsymbol{k}}$ can be obtained to be

$$S[q_{\boldsymbol{k}}] = \int \mathrm{d}\eta \int \mathrm{d}^3\boldsymbol{k} \left\{ |q_{\boldsymbol{k}}'|^2 - \frac{a'}{a}\,(q_{\boldsymbol{k}}\,q_{\boldsymbol{k}}'^* + q_{\boldsymbol{k}}'\,q_{\boldsymbol{k}}^*) - \mu_q^2\,|q_{\boldsymbol{k}}|^2 \right\}, \tag{G.9}$$

where the quantity μ_q^2 is given by

$$\mu_q^2(\eta) = k_\perp^2 + (k_z + e\,A)^2 + m^2\,a^2 - \left(\frac{a'}{a}\right)^2 \tag{G.10}$$

with $\boldsymbol{k}_\perp = (k_x, k_y)$ and $k_\perp = |\boldsymbol{k}_\perp|$. Thus, each mode with wave vector $\boldsymbol{k}$ evolves independently according to identical (though $\boldsymbol{k}$-dependent) actions.

Let us now express $q_{\boldsymbol{k}}$ as

$$q_{\boldsymbol{k}} = \frac{1}{\sqrt{2}}\,(q_{\boldsymbol{k}\mathrm{R}} + i\,q_{\boldsymbol{k}\mathrm{I}})\,, \tag{G.11}$$

where $q_{\boldsymbol{k}\mathrm{R}}$ and $q_{\boldsymbol{k}\mathrm{I}}$ are the real and imaginary parts of $q_{\boldsymbol{k}}$. The actions for $q_{\boldsymbol{k}\mathrm{R}}$ and $q_{\boldsymbol{k}\mathrm{I}}$ decouple and are identical in form. Therefore, the dynamics of the system can be analyzed using the following Lagrangian density in Fourier space:

$$\mathcal{L} = \frac{1}{2}\,q'^2 - \frac{a'}{a}\,q\,q' - \frac{1}{2}\,\mu_q^2\,q^2, \tag{G.12}$$

where q stands for either $q_{\boldsymbol{k}\mathrm{R}}$ or $q_{\boldsymbol{k}\mathrm{I}}$. The momentum conjugate to the variable q is given by

$$p_q = q' - \frac{a'}{a}\, q. \tag{G.13}$$

The Lagrangian (G.12) leads to following equation of motion for the Fourier mode q:

$$q'' + \omega_q^2\, q = 0, \tag{G.14}$$

where the quantity ω_q^2 is given by

$$\omega_q^2(\eta) = k_\perp^2 + (k_z + e\, A)^2 + m^2\, a^2 - \frac{a''}{a}. \tag{G.15}$$

G.2 SOLUTIONS IN DE SITTER AND THE BEHAVIOR OF THE SQUEEZING AMPLITUDE

Let us now discuss the solutions to the modes of the scalar field in the presence of a constant electric field in de Sitter spacetime and the behavior of the corresponding squeezing amplitude [294, 296]. Earlier, in Sec. 4.5.1, we had assumed that the scale factor in de Sitter inflation is given by $a(\eta) = -1/(H_{\rm I}\, \eta)$, where $H_{\rm I}$ is a constant. Instead, we shall now assume that the de Sitter spacetime is described by the scale factor

$$a(\eta) = \frac{1}{1 - H_{\rm I}\, \eta}, \tag{G.16}$$

where $-\infty < \eta < H_{\rm I}^{-1}$. We have chosen such a form since we can obtain the Minkowski spacetime as the limit $H_{\rm I} \to 0$. Since the strength of the electric field is given by $E = A'/a^2$ [see Eq. (G.5)], if we require E to be constant, then for the above choice of the scale factor, the vector potential $A(\eta)$ is given by

$$A(\eta) = \frac{E_0}{H_{\rm I}}\, [a(\eta) - 1]\,, \tag{G.17}$$

where E_0 is a constant and we have chosen the constant of integration to be $-E_0/H_{\rm I}$. Such a choice allows us to have a well behaved $H_{\rm I} \to 0$ limit of $A(\eta)$, which reduces to the usual choice of vector potential considered to examine the Schwinger effect in Minkowski spacetime.

Evidently, we can quantize the system described by the Lagrangian (G.12) in the same manner as we quantized the electromagnetic vector potential $\mathcal{A}$ in the Schrödinger picture in Sec. 4.3.2. For the above choices of the scale factor and the vector potential, we find that the function f that determines the wave function describing the system [given by Eqs. (4.34) and (4.38), and g defined as in Eq. (4.39), with the non-conformal coupling function J replaced by the scale factor a] satisfies the differential equation

$$\frac{\mathrm{d}^2 f}{\mathrm{d}\tau^2} + \left(\bar{k}^2 - \frac{2\,\zeta\,\bar{k}_z}{\tau} + \frac{\zeta^2 + \bar{m}^2 - 2}{\tau^2}\right) f = 0, \tag{G.18}$$

where $\bar{k}_z = k_z - (e\,E_0/H_{\rm I})$, $\bar{k}^2 = k_\perp^2 + \bar{k}_z^2$, $\zeta = e\,E_0/H_{\rm I}^2$, $\bar{m} = m/H_{\rm I}$ and $\tau = \eta - (1/H_{\rm I})$. We should point out here the similarity between the above differential equation and the equation (4.88) governing the evolution of the helical electromagnetic fields in de Sitter spacetime. Note that, for small $\bar{m}$ and ζ, their structure are very similar. Also, for a range of wave numbers, changing the sign of k_z (or the direction of the electric field E) is equivalent to considering the helical electromagnetic mode of opposite polarization.

Recall that, if the wave function describing the mode is to start from the ground state corresponding to the Bunch-Davies vacuum, then, as $(-k\,\eta) \to \infty$, we require that the function f behaves as $f \propto \exp\left(-i\,\bar{k}\,\eta\right)$. It is straightforward to show that the modes with such initial conditions are given by

$$f(\tau) = \frac{1}{\sqrt{2\,\bar{k}}}\,\mathrm{e}^{-\pi\,\zeta\,\bar{k}_z/(2\,\bar{k})}\,\mathrm{e}^{-i\,\bar{k}/H_{\rm I}}\,W_{i\,\zeta\,\bar{k}_z/\bar{k},\nu}(2\,i\,\bar{k}\,\tau), \tag{G.19}$$

where $W_{\lambda,\nu}(z)$ denotes the Whittaker function and $\nu^2 = (9/4) - \bar{m}^2 - \zeta^2$ [291]. Note that, when $\zeta = 0$ and $m = 0$, the above solution reduces to

$$f(\eta) = \frac{1}{\sqrt{2\,k}}\,\mathrm{e}^{-i\,k/H_{\rm I}}\,W_{0,3/2}(2\,i\,k\,\tau). \tag{G.20}$$

Since [291]

$$W_{0,3/2}(z) = \sqrt{\frac{z}{\pi}}\,K_{3/2}\left(\frac{z}{2}\right), \tag{G.21}$$

where $K_{3/2}(z)$ is the modified Bessel's function given by

$$K_{3/2}(z) = \sqrt{\frac{\pi}{2\,z}}\,\left(1 + \frac{1}{z}\right)\,\mathrm{e}^{-z}, \tag{G.22}$$

we find that the above function $f(\eta)$ can be expressed as

$$f(\eta) = \frac{1}{\sqrt{2\,k}}\,\left[1 - \frac{i}{k\,\eta - (k/H_{\rm I})}\right]\,\mathrm{e}^{-i\,k\,\eta}, \tag{G.23}$$

which is the well known solution describing a massless scalar field in de Sitter spacetime.

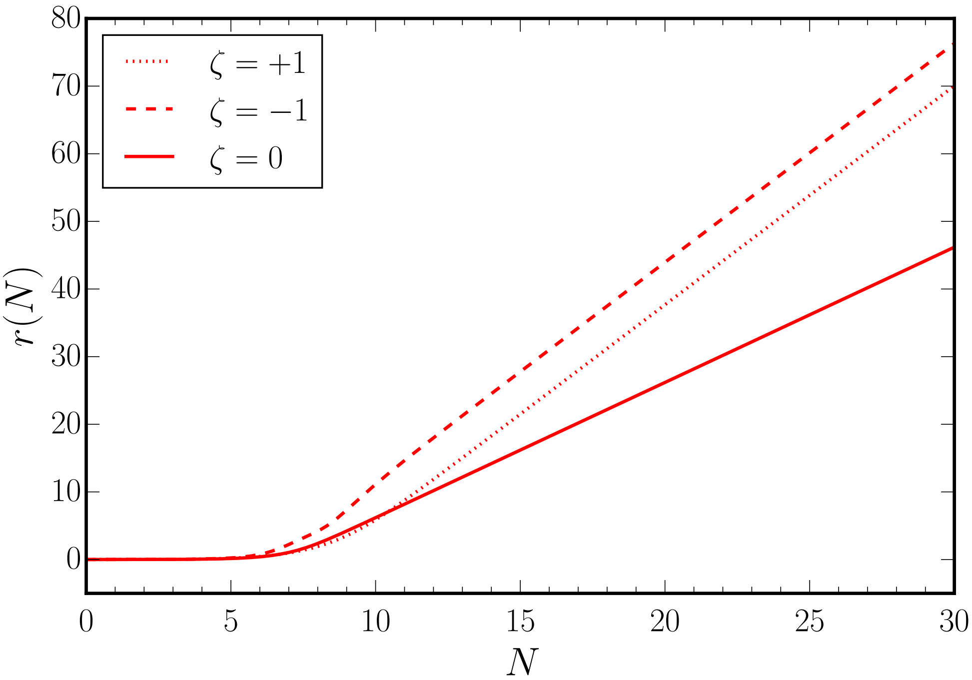

Figure G.1: The evolution of the squeezing amplitude $r(N)$ for a specific mode of a charged scalar field in de Sitter inflation has been plotted as a function of e-folds N for the following choices of the parameters: $(k_\perp, \bar{k}_z) = (0, 10^{-2})$, $\bar{m} = 0$ and $\zeta = (-1, 0, 1)$ (in dashed, solid and dotted red). Note that, in a manner similar to that of the $\sigma = -1$ helical electromagnetic mode, the squeezing amplitude r is larger when $\zeta = -1$ than the case wherein $\zeta = +1$. For the wave number we have worked with, we find that the modes can be said to leave Hubble radius around $N \simeq 7$.

The squeezing amplitude associated with the modes of the charged scalar field can be determined using the relation (4.53a), with f given by Eq. (G.19) and g defined as in Eq. (4.39), with J replaced by a. In Fig. G.1, we have plotted the evolution of the squeezing amplitude r (for a specific wave number) as a function of e-folds for two different sets of values of the parameters ζ, with $\bar{m}$ set to zero. We have also plotted for the case wherein ζ vanishes. It should be evident that the behavior of the squeezing amplitude for opposite signs of ζ is similar to the behavior of the two states of opposite polarization of the helical electromagnetic mode. In fact, because of the presence of the additional parameters (such as m), the evolution of the complex scalar field is considerably richer, but we have chosen to work with values so that the evolution closely resembles the behavior of the modes of the non-helical and helical electromagnetic fields.

REFERENCES

[1] D. Grasso and H. R. Rubinstein, Phys. Rept. **348**, 163 (2001), arXiv:astro-ph/0009061.

[2] M. Giovannini, Int. J. Mod. Phys. D **13**, 391 (2004), arXiv:astro-ph/0312614.

[3] A. Brandenburg and K. Subramanian, Phys. Rept. **417**, 1 (2005), arXiv:astro-ph/0405052.

[4] R. M. Kulsrud and E. G. Zweibel, **71**, 0046091 (2008), arXiv:0707.2783 [astro-ph].

[5] K. Subramanian, Astron. Nachr. **331**, 110 (2010), arXiv:0911.4771 [astro-ph.CO].

[6] A. Kandus, K. E. Kunze, and C. G. Tsagas, Phys. Rept. **505**, 1 (2011), arXiv:1007.3891 [astro-ph.CO].

[7] L. M. Widrow, D. Ryu, D. R. G. Schleicher, K. Subramanian, C. G. Tsagas, and R. A. Treumann, Space Sci. Rev. **166**, 37 (2012), arXiv:1109.4052 [astro-ph.CO].

[8] R. Durrer and A. Neronov, Astron. Astrophys. Rev. **21**, 62 (2013), arXiv:1303.7121 [astro-ph.CO].

[9] K. Subramanian, Rept. Prog. Phys. **79**, 076901 (2016), arXiv:1504.02311 [astro-ph.CO].

[10] T. Vachaspati 10.1088/1361-6633/ac03a9 (2020), arXiv:2010.10525 [astro-ph.CO].

[11] A. Brandenburg, D. Sokoloff, and K. Subramanian, Space Science Reviews **169**, 123 (2012).

[12] P. Olson, Physics Today **66**, 30 (2013), https://pubs.aip.org/physicstoday/article-pdf/66/11/30/10096858/30_1_online.pdf.

[13] P. Charbonneau, Annual Review of Astronomy and Astrophysics **52**, 251 (2014).

[14] D. H. Hathaway, Living reviews in solar physics **12**, 1 (2015).

[15] R. Beck, Space Science Reviews **99**, 243 (2001).

[16] T. D. Oswalt and G. Gilmore, *Planets, Stars and Stellar Systems: Volume 5: Galactic Structure and Stellar Populations* (Springer, 2013).

[17] C. Vogt and T. A. Ensslin, Astronomy & Astrophysics **434**, 67 (2005).

[18] F. Govoni and L. Feretti, International Journal of Modern Physics D **13**, 1549 (2004).

[19] M. L. Bernet, F. Miniati, S. J. Lilly, P. P. Kronberg, and M. Dessauges-Zavadsky, Nature **454**, 302 (2008).

[20] T. E. Clarke, P. P. Kronberg, and H. Böhringer, The Astrophysical Journal **547**, L111 (2001).

[21] A. Neronov and I. Vovk, Science **328**, 73 (2010), arXiv:1006.3504 [astro-ph.HE].

[22] K. Dolag, M. Kachelriess, S. Ostapchenko, and R. Tomas, Astrophys. J. Lett. **727**, L4 (2011), arXiv:1009.1782 [astro-ph.HE].

[23] F. Tavecchio, G. Ghisellini, L. Foschini, G. Bonnoli, G. Ghirlanda, and P. Coppi, Mon. Not. Roy. Astron. Soc. **406**, L70 (2010), arXiv:1004.1329 [astro-ph.CO].

[24] F. Tavecchio, G. Ghisellini, G. Bonnoli, and L. Foschini, Monthly Notices of the Royal Astronomical Society **414**, 3566 (2011).

[25] L. Biermann and A. Schlüter, Physical Review **82**, 863 (1951).

[26] L. Biermann, **29**, 274 (1951).

[27] E. W. Kolb and M. S. Turner, *The Early Universe*, Vol. 69 (1990).

[28] V. F. Mukhanov, *Physical foundations of cosmology* (Cambridge university press, 2005).

[29] S. Weinberg, *Cosmology* (OUP Oxford, 2008).

[30] D. H. Lyth and A. R. Liddle, *The primordial density perturbation: Cosmology, inflation and the origin of structure* (Cambridge university press, 2009).

[31] P. Peter and J.-P. Uzan, *Primordial cosmology* (Oxford University Press, 2009).

[32] H. Mo, F. Van den Bosch, and S. White, *Galaxy formation and evolution* (Cambridge University Press, 2010).

[33] D. Baumann and L. McAllister, *Inflation and string theory* (Cambridge University Press, 2015).

[34] S. Dodelson and F. Schmidt, *Modern cosmology* (Academic press, 2020).

[35] R. Durrer, *The cosmic microwave background* (Cambridge University Press, 2020).

[36] D. Scott, in *Cosmic Flows Workshop*, Vol. 201 (2000) p. 403.

[37] C. L. Bennett *et al.*, Astrophys. J. **436**, 423 (1994), arXiv:astro-ph/9401012.

[38] E. L. Wright, G. F. Smoot, C. L. Bennett, and P. M. Lubin, Astrophys. J. **436**, 443 (1994), arXiv:astro-ph/9401015.

[39] K. M. Gorski, **430**, L85 (1994), arXiv:astro-ph/9403066 [astro-ph].

[40] K. M. Gorski, G. Hinshaw, A. J. Banday, C. L. Bennett, E. L. Wright, A. Kogut, G. F. Smoot, and P. Lubin, arXiv preprint astro-ph/9403067 (1994).

[41] J. Dunkley, E. Komatsu, M. Nolta, D. Spergel, D. Larson, G. Hinshaw, L. Page, C. Bennett, B. Gold, N. Jarosik, *et al.*, The Astrophysical Journal Supplement Series **180**, 306 (2009).

[42] E. Komatsu, J. Dunkley, M. Nolta, C. Bennett, B. Gold, G. Hinshaw, N. Jarosik, D. Larson, M. Limon, L. Page, *et al.*, The Astrophysical Journal Supplement Series **180**, 330 (2009).

[43] D. Larson, J. Dunkley, G. Hinshaw, E. Komatsu, M. Nolta, C. Bennett, B. Gold, M. Halpern, R. Hill, N. Jarosik, *et al.*, The Astrophysical Journal Supplement Series **192**, 16 (2011).

[44] G. Hinshaw, D. Larson, E. Komatsu, D. N. Spergel, C. Bennett, J. Dunkley, M. Nolta, M. Halpern, R. Hill, N. Odegard, *et al.*, The Astrophysical Journal Supplement Series **208**, 19 (2013).

[45] C. L. Bennett *et al.* (WMAP), Astrophys. J. Suppl. **148**, 1 (2003), arXiv:astro-ph/0302207.

[46] C. Bennett, R. Hill, G. Hinshaw, D. Larson, K. Smith, J. Dunkley, B. Gold, M. Halpern, N. Jarosik, A. Kogut, *et al.*, The Astrophysical journal supplement series **192**, 17 (2011).

[47] C. L. Bennett, D. Larson, J. L. Weiland, N. Jarosik, G. Hinshaw, N. Odegard, K. Smith, R. Hill, B. Gold, M. Halpern, *et al.*, The Astrophysical Journal Supplement Series **208**, 20 (2013).

[48] P. A. R. Ade *et al.* (Planck), Astron. Astrophys. **594**, A13 (2016), arXiv:1502.01589 [astro-ph.CO].

[49] P. A. R. Ade *et al.* (Planck), Astron. Astrophys. **594**, A20 (2016), arXiv:1502.02114 [astro-ph.CO].

[50] P. A. R. Ade *et al.* (Planck), Astron. Astrophys. **594**, A19 (2016), arXiv:1502.01594 [astro-ph.CO].

[51] N. Aghanim *et al.* (Planck), Astron. Astrophys. **641**, A6 (2020), [Erratum: Astron.Astrophys. 652, C4 (2021)], arXiv:1807.06209 [astro-ph.CO].

[52] Y. Akrami *et al.* (Planck), Astron. Astrophys. **641**, A10 (2020), arXiv:1807.06211 [astro-ph.CO].

[53] H. Kodama and M. Sasaki, Progress of Theoretical Physics Supplement **78**, 1 (1984).

[54] V. F. Mukhanov, H. A. Feldman, and R. H. Brandenberger, Physics reports **215**, 203 (1992).

[55] J. E. Lidsey, A. R. Liddle, E. W. Kolb, E. J. Copeland, T. Barreiro, and M. Abney, Reviews of Modern Physics **69**, 373 (1997).

[56] A. Riotto, arXiv preprint hep-ph/0210162 (2002).

[57] W. H. Kinney, in *Techniques and Concepts of High-Energy Physics XII* (Springer, 2003) pp. 189–243.

[58] J. Martin, Inflationary Cosmology , 193 (2008).

[59] J. Martin, Planck Scale Effects in Astrophysics and Cosmology , 199 (2005).

[60] W. H. Kinney, arXiv preprint arXiv:0902.1529 (2009).

[61] D. Baumann, arXiv preprint arXiv:0907.5424 (2009).

[62] L. Sriramkumar, Current science , 868 (2009).

[63] L. Sriramkumar, On the generation and evolution of perturbations during inflation and reheating, in *Vignettes in Gravitation and Cosmology*, edited by L. Sriramkumar and T. R. Seshadri (World Scientific, Singapore, 2012).

[64] J. Martin, Astrophys. Space Sci. Proc. **45**, 41 (2016), arXiv:1502.05733 [astro-ph.CO].

[65] J. M. Maldacena, JHEP **05**, 013, arXiv:astro-ph/0210603.

[66] D. Seery and J. E. Lidsey, JCAP **06**, 003, arXiv:astro-ph/0503692.

[67] X. Chen, Phys. Rev. D **72**, 123518 (2005), arXiv:astro-ph/0507053.

[68] X. Chen, M.-x. Huang, S. Kachru, and G. Shiu, JCAP **01**, 002, arXiv:hep-th/0605045.

[69] D. Langlois, S. Renaux-Petel, D. A. Steer, and T. Tanaka, Phys. Rev. Lett. **101**, 061301 (2008), arXiv:0804.3139 [hep-th].

[70] J. Martin, Braz. J. Phys. **34**, 1307 (2004), arXiv:astro-ph/0312492.

[71] J. Martin, Lect. Notes Phys. **669**, 199 (2005), arXiv:hep-th/0406011.

[72] B. A. Bassett, S. Tsujikawa, and D. Wands, Reviews of Modern Physics **78**, 537 (2006).

[73] L. Sriramkumar, Curr. Sci. **97**, 868 (2009), arXiv:0904.4584 [astro-ph.CO].

[74] E. D. Stewart and D. H. Lyth, Physics Letters B **302**, 171 (1993).

[75] J. Martin and D. J. Schwarz, Physical Review D **62**, 103520 (2000).

[76] E. F. Bunn, A. R. Liddle, and M. J. White, Phys. Rev. D **54**, R5917 (1996), arXiv:astro-ph/9607038.

[77] M. Tristram *et al.*, Phys. Rev. D **105**, 083524 (2022), arXiv:2112.07961 [astro-ph.CO].

[78] P. Campeti and E. Komatsu, Astrophys. J. **941**, 110 (2022), arXiv:2205.05617 [astro-ph.CO].

[79] R. Davies, R. Booth, and A. Wilson, Nature **220**, 1207 (1968).

[80] M. Reid and E. Silverstein, Astrophysical Journal, Part 1 (ISSN 0004-637X), vol. 361, Oct. 1, 1990, p. 483-486. **361**, 483 (1990).

[81] T. Markkanen, S. Nurmi, S. Rasanen, and V. Vennin, JCAP **06**, 035, arXiv:1704.01343 [astro-ph.CO].

[82] C. J. Hogan, Phys. Rev. Lett. **51**, 1488 (1983).

[83] T. Vachaspati, Phys. Lett. B **265**, 258 (1991).

[84] K. Enqvist and P. Olesen, Phys. Lett. B **319**, 178 (1993), arXiv:hep-ph/9308270.

[85] G. Baym, D. Bodeker, and L. D. McLerran, Phys. Rev. D **53**, 662 (1996), arXiv:hep-ph/9507429.

[86] G. Sigl, A. V. Olinto, and K. Jedamzik, Phys. Rev. D **55**, 4582 (1997), arXiv:astro-ph/9610201.

[87] D. Grasso and A. Riotto, Phys. Lett. B **418**, 258 (1998), arXiv:hep-ph/9707265.

[88] A. G. Tevzadze, L. Kisslinger, A. Brandenburg, and T. Kahniashvili, Astrophys. J. **759**, 54 (2012), arXiv:1207.0751 [astro-ph.CO].

[89] T. Kahniashvili, A. G. Tevzadze, A. Brandenburg, and A. Neronov, Phys. Rev. D **87**, 083007 (2013), arXiv:1212.0596 [astro-ph.CO].

[90] Y. Zhang, T. Vachaspati, and F. Ferrer, Phys. Rev. D **100**, 083006 (2019), arXiv:1902.02751 [hep-ph].

[91] A. Brandenburg, K. Enqvist, and P. Olesen, Phys. Rev. D **54**, 1291 (1996), arXiv:astro-ph/9602031.

[92] R. Banerjee and K. Jedamzik, Phys. Rev. D **70**, 123003 (2004), arXiv:astro-ph/0410032.

[93] M. S. Turner and L. M. Widrow, Phys. Rev. D **37**, 2743 (1988).

[94] B. Ratra, Astrophys. J. Lett. **391**, L1 (1992).

[95] J. Martin and J. Yokoyama, JCAP **01**, 025, arXiv:0711.4307 [astro-ph].

[96] L. Campanelli, P. Cea, G. L. Fogli, and L. Tedesco, Phys. Rev. D **77**, 043001 (2008), arXiv:0710.2993 [astro-ph].

[97] R. Durrer, L. Hollenstein, and R. K. Jain, JCAP **03**, 037, arXiv:1005.5322 [astro-ph.CO].

[98] R. J. Ferreira, R. K. Jain, and M. S. Sloth, JCAP **10**, 004, arXiv:1305.7151 [astro-ph.CO].

[99] C. Caprini and L. Sorbo, JCAP **10**, 056, arXiv:1407.2809 [astro-ph.CO].

[100] L. Campanelli, Phys. Rev. Lett. **111**, 061301 (2013), arXiv:1304.6534 [astro-ph.CO].

[101] I. Agullo and J. Navarro-Salas, (2013), arXiv:1309.3435 [gr-qc].

[102] L. Campanelli, Eur. Phys. J. C **75**, 278 (2015), arXiv:1503.07415 [gr-qc].

[103] L. Parker, Phys. Rev. Lett. **21**, 562 (1968).

[104] K. Bamba and S. D. Odintsov, JCAP **04**, 024, arXiv:0801.0954 [astro-ph].

[105] K. E. Kunze, Physical Review D **81**, 043526 (2010).

[106] L. Motta and R. R. Caldwell, Phys. Rev. D **85**, 103532 (2012), arXiv:1203.1033 [astro-ph.CO].

[107] K. Bamba, E. Elizalde, S. D. Odintsov, and T. Paul, JCAP **04**, 009, arXiv:2012.12742 [gr-qc].

[108] K. Enqvist, A. Jokinen, and A. Mazumdar, JCAP **11**, 001, arXiv:hep-ph/0404269.

[109] M. Rees and M. Reinhardt, Astronomy and Astrophysics, Vol. 19, p. 189 (1972) **19**, 189 (1972).

[110] P. P. Kronberg and M. Simard-Normandin, Nature **263**, 653 (1976).

[111] P. P. Kronberg and J. J. Perry, Astrophysical Journal, Part 1, vol. 263, Dec. 15, 1982, p. 518-532. Research supported by the Natural Sciences and Engineering Research Council of Canada. **263**, 518 (1982).

[112] P. P. Kronberg, Rept. Prog. Phys. **57**, 325 (1994).

[113] P. Blasi, S. Burles, and A. V. Olinto, The Astrophysical Journal **514**, L79 (1999).

[114] P. Kronberg, M. Bernet, F. Miniati, S. Lilly, M. Short, and D. Higdon, The Astrophysical Journal **676**, 70 (2008).

[115] P. Bhat and K. Subramanian, Monthly Notices of the Royal Astronomical Society **429**, 2469 (2013).

[116] J. Adamek, R. Durrer, E. Fenu, and M. Vonlanthen, Journal of Cosmology and Astroparticle Physics **2011** (06), 017.

[117] R. J. Ferreira, R. K. Jain, and M. S. Sloth, JCAP **06**, 053, arXiv:1403.5516 [astro-ph.CO].

[118] D. Paoletti and F. Finelli, Journal of Cosmology and Astroparticle Physics **2019** (11), 028.

[119] F. Vazza, D. Paoletti, S. Banfi, F. Finelli, C. Gheller, S. O'Sullivan, and M. Brüggen, Monthly Notices of the Royal Astronomical Society **500**, 5350 (2021).

[120] P. P. Kronberg, Reports on Progress in Physics **57**, 325 (1994).

[121] R. Beck, arXiv preprint arXiv:1111.5802 (2011).

[122] J. D. Barrow, P. G. Ferreira, and J. Silk, Phys. Rev. Lett. **78**, 3610 (1997), arXiv:astro-ph/9701063.

[123] R. Durrer, New Astronomy Reviews **51**, 275 (2007).

[124] J. R. Shaw and A. Lewis, Phys. Rev. D **81**, 043517 (2010), arXiv:0911.2714 [astro-ph.CO].

[125] D. Paoletti and F. Finelli, Physical Review D **83**, 123533 (2011).

[126] J. R. Shaw and A. Lewis, Physical Review D **86**, 043510 (2012).

[127] D. Paoletti and F. Finelli, Physics Letters B **726**, 45 (2013).

[128] R. Durrer, P. G. Ferreira, and T. Kahniashvili, Phys. Rev. D **61**, 043001 (2000), arXiv:astro-ph/9911040.

[129] M. Giovannini and K. E. Kunze, Phys. Rev. D **77**, 063003 (2008), arXiv:0712.3483 [astro-ph].

[130] F. Finelli, F. Paci, and D. Paoletti, Phys. Rev. D **78**, 023510 (2008), arXiv:0803.1246 [astro-ph].

[131] C. Bonvin, C. Caprini, and R. Durrer, Phys. Rev. D **88**, 083515 (2013), arXiv:1308.3348 [astro-ph.CO].

[132] K. Subramanian, Astron. Nachr. **327**, 403 (2006), arXiv:astro-ph/0601570.

[133] R. Durrer, New Astron. Rev. **51**, 275 (2007), arXiv:astro-ph/0609216.

[134] R. K. Jain and M. S. Sloth, JCAP **02**, 003, arXiv:1210.3461 [astro-ph.CO].

[135] D. Grasso and H. R. Rubinstein, Phys. Lett. B **379**, 73 (1996), arXiv:astro-ph/9602055.

[136] B.-l. Cheng, A. V. Olinto, D. N. Schramm, and J. W. Truran, Phys. Rev. D **54**, 4714 (1996), arXiv:astro-ph/9606163.

[137] D. G. Yamazaki and M. Kusakabe, Phys. Rev. D **86**, 123006 (2012), arXiv:1212.2968 [astro-ph.CO].

[138] M. Kawasaki and M. Kusakabe, Phys. Rev. D **86**, 063003 (2012), arXiv:1204.6164 [astro-ph.CO].

[139] Y. Luo, T. Kajino, M. Kusakabe, and G. J. Mathews, Astrophys. J. **872**, 172 (2019), arXiv:1810.08803 [astro-ph.CO].

[140] A. Abramowski, F. Acero, F. Aharonian, A. Akhperjanian, G. Anton, S. Balenderan, A. Balzer, A. Barnacka, Y. Becherini, J. B. Tjus, *et al.*, Astronomy & Astrophysics **550**, A4 (2013).

[141] J. Yang, J. Wang, and J. Yang, Publications of the Astronomical Society of Japan **64**, 100 (2012).

[142] V. A. Acciari *et al.* (MAGIC), (2022), arXiv:2210.03321 [astro-ph.HE].

[143] F. Aharonian *et al.* (H.E.S.S., Fermi-LAT, H. E. S. S), Astrophys. J. Lett. **950**, L16 (2023), arXiv:2306.05132 [astro-ph.HE].

[144] A. Neronov and D. V. Semikoz, JETP Lett. **85**, 473 (2007), arXiv:astro-ph/0604607.

[145] A. Elyiv, A. Neronov, and D. Semikoz, Physical Review D **80**, 023010 (2009).

[146] K. Dolag, M. Kachelrieß, S. Ostapchenko, and R. Tomas, The Astrophysical Journal **703**, 1078 (2009).

[147] R. Plaga, Nature **374**, 430 (1995).

[148] K. Murase, K. Takahashi, S. Inoue, K. Ichiki, and S. Nagataki, Astrophys. J. Lett. **686**, L67 (2008), arXiv:0806.2829 [astro-ph].

[149] D. Paoletti and F. Finelli, JCAP **11**, 028, arXiv:1910.07456 [astro-ph.CO].

[150] D. Biskamp, *Magnetohydrodynamic turbulence* (Cambridge University Press, 2003).

[151] A. Brandenburg, T. Kahniashvili, and A. G. Tevzadze, Phys. Rev. Lett. **114**, 075001 (2015), arXiv:1404.2238 [astro-ph.CO].

[152] C. D. Dermer, M. Cavadini, S. Razzaque, J. D. Finke, J. Chiang, and B. Lott, Astrophys. J. Lett. **733**, L21 (2011), arXiv:1011.6660 [astro-ph.HE].

[153] I. Vovk, A. M. Taylor, D. Semikoz, and A. Neronov, Astrophys. J. Lett. **747**, L14 (2012), arXiv:1112.2534 [astro-ph.CO].

[154] A. Taylor, I. Vovk, and A. Neronov, Astron. Astrophys. **529**, A144 (2011), arXiv:1101.0932 [astro-ph.HE].

[155] K. Takahashi, M. Mori, K. Ichiki, and S. Inoue, Astrophys. J. Lett. **744**, L7 (2012), arXiv:1103.3835 [astro-ph.CO].

[156] J. D. Barrow and C. G. Tsagas, Phys. Rev. D **77**, 107302 (2008), [Erratum: Phys.Rev.D 77, 109904 (2008)], arXiv:0803.0660 [astro-ph].

[157] J. D. Barrow and C. G. Tsagas, Mon. Not. Roy. Astron. Soc. **414**, 512 (2011), arXiv:1101.2390 [astro-ph.CO].

[158] J. Adamek, C. de Rham, and R. Durrer, Mon. Not. Roy. Astron. Soc. **423**, 2705 (2012), arXiv:1110.2019 [gr-qc].

[159] Y. Shtanov and V. Sahni, JCAP **01**, 008, arXiv:1211.2168 [astro-ph.CO].

[160] D. Yamauchi, T. Fujita, and S. Mukohyama, JCAP **03**, 031, arXiv:1402.2784 [astro-ph.CO].

[161] K. Bamba and J. Yokoyama, Phys. Rev. D **69**, 043507 (2004), arXiv:astro-ph/0310824.

[162] K. Bamba and M. Sasaki, JCAP **02**, 030, arXiv:astro-ph/0611701.

[163] V. Demozzi, V. Mukhanov, and H. Rubinstein, JCAP **08**, 025, arXiv:0907.1030 [astro-ph.CO].

[164] K. Bamba, S. D. Odintsov, T. Paul, and D. Maity, (2021), arXiv:2107.11524 [gr-qc].

[165] M.-a. Watanabe, S. Kanno, and J. Soda, Phys. Rev. Lett. **102**, 191302 (2009), arXiv:0902.2833 [hep-th].

[166] S. Kanno, J. Soda, and M.-a. Watanabe, JCAP **12**, 009, arXiv:0908.3509 [astro-ph.CO].

[167] M. M. Anber and L. Sorbo, JCAP **10**, 018, arXiv:astro-ph/0606534.

[168] D. Chowdhury, L. Sriramkumar, and M. Kamionkowski, JCAP **10**, 031, arXiv:1807.07477 [astro-ph.CO].

[169] R. Sharma, K. Subramanian, and T. R. Seshadri, Phys. Rev. D **97**, 083503 (2018), arXiv:1802.04847 [astro-ph.CO].

[170] M. Giovannini, Class. Quant. Grav. **38**, 135018 (2021), arXiv:2012.14720 [gr-qc].

[171] M. Giovannini, (2021), arXiv:2106.14927 [hep-th].

[172] E. V. Gorbar, K. Schmitz, O. O. Sobol, and S. I. Vilchinskii, (2021), arXiv:2109.01651 [hep-ph].

[173] E. V. Gorbar, K. Schmitz, O. O. Sobol, and S. I. Vilchinskii, (2021), arXiv:2111.04712 [hep-ph].

[174] A. Zucca, Y. Li, and L. Pogosian, Phys. Rev. D **95**, 063506 (2017), arXiv:1611.00757 [astro-ph.CO].

[175] D. R. Sutton, C. Feng, and C. L. Reichardt, Astrophys. J. **846**, 164 (2017), arXiv:1702.01871 [astro-ph.CO].

[176] D. Paoletti, J. Chluba, F. Finelli, and J. A. Rubino-Martin, Mon. Not. Roy. Astron. Soc. **484**, 185 (2019), arXiv:1806.06830 [astro-ph.CO].

[177] T. Minoda, K. Ichiki, and H. Tashiro, JCAP **03**, 093, arXiv:2012.12542 [astro-ph.CO].

[178] C. R. Contaldi, M. Peloso, L. Kofman, and A. D. Linde, JCAP **07**, 002, arXiv:astro-ph/0303636.

[179] R. Sinha and T. Souradeep, Phys. Rev. D **74**, 043518 (2006), arXiv:astro-ph/0511808.

[180] B. A. Powell and W. H. Kinney, Phys. Rev. D **76**, 063512 (2007), arXiv:astro-ph/0612006.

[181] R. K. Jain, P. Chingangbam, J.-O. Gong, L. Sriramkumar, and T. Souradeep, JCAP **01**, 009, arXiv:0809.3915 [astro-ph].

[182] R. K. Jain, P. Chingangbam, L. Sriramkumar, and T. Souradeep, Phys. Rev. D **82**, 023509 (2010), arXiv:0904.2518 [astro-ph.CO].

[183] D. K. Hazra, M. Aich, R. K. Jain, L. Sriramkumar, and T. Souradeep, JCAP **10**, 008, arXiv:1005.2175 [astro-ph.CO].

[184] M. Benetti, Phys. Rev. D **88**, 087302 (2013), arXiv:1308.6406 [astro-ph.CO].

[185] D. K. Hazra, A. Shafieloo, G. F. Smoot, and A. A. Starobinsky, Phys. Rev. Lett. **113**, 071301 (2014), arXiv:1404.0360 [astro-ph.CO].

[186] D. K. Hazra, A. Shafieloo, G. F. Smoot, and A. A. Starobinsky, JCAP **08**, 048, arXiv:1405.2012 [astro-ph.CO].

[187] X. Chen, P. D. Meerburg, and M. Münchmeyer, JCAP **09**, 023, arXiv:1605.09364 [astro-ph.CO].

[188] X. Chen, C. Dvorkin, Z. Huang, M. H. Namjoo, and L. Verde, JCAP **11**, 014, arXiv:1605.09365 [astro-ph.CO].

[189] H. Ragavendra, D. Chowdhury, and L. Sriramkumar, (2020), arXiv:2003.01099 [astro-ph.CO].

[190] A. Antony and S. Jain, (2021), arXiv:2110.06837 [astro-ph.CO].

[191] R. Abbott *et al.* (LIGO Scientific, Virgo), Astrophys. J. Lett. **913**, L7 (2021), arXiv:2010.14533 [astro-ph.HE].

[192] V. De Luca, G. Franciolini, P. Pani, and A. Riotto, JCAP **06**, 044, arXiv:2005.05641 [astro-ph.CO].

[193] K. Jedamzik, JCAP **09**, 022, arXiv:2006.11172 [astro-ph.CO].

[194] K. Jedamzik, Phys. Rev. Lett. **126**, 051302 (2021), arXiv:2007.03565 [astro-ph.CO].

[195] G. Franciolini, V. Baibhav, V. De Luca, K. K. Y. Ng, K. W. K. Wong, E. Berti, P. Pani, A. Riotto, and S. Vitale, (2021), arXiv:2105.03349 [gr-qc].

[196] J. Garcia-Bellido and E. Ruiz Morales, Phys. Dark Univ. **18**, 47 (2017), arXiv:1702.03901 [astro-ph.CO].

[197] G. Ballesteros and M. Taoso, Phys. Rev. D **97**, 023501 (2018), arXiv:1709.05565 [hep-ph].

[198] C. Germani and T. Prokopec, Phys. Dark Univ. **18**, 6 (2017), arXiv:1706.04226 [astro-ph.CO].

[199] I. Dalianis, A. Kehagias, and G. Tringas, JCAP **01**, 037, arXiv:1805.09483 [astro-ph.CO].

[200] N. Bhaumik and R. K. Jain, JCAP **01**, 037, arXiv:1907.04125 [astro-ph.CO].

[201] A. Ashoorioon, A. Rostami, and J. T. Firouzjaee, JHEP **07**, 087, arXiv:1912.13326 [astro-ph.CO].

[202] H. V. Ragavendra, P. Saha, L. Sriramkumar, and J. Silk, Phys. Rev. D **103**, 083510 (2021), arXiv:2008.12202 [astro-ph.CO].

[203] I. Dalianis and K. Kritos, Phys. Rev. D **103**, 023505 (2021), arXiv:2007.07915 [astro-ph.CO].

[204] C. T. Byrnes, L. Hollenstein, R. K. Jain, and F. R. Urban, JCAP **03**, 009, arXiv:1111.2030 [astro-ph.CO].

[205] Y. Shtanov, JCAP **10**, 008, arXiv:1902.05894 [astro-ph.CO].

[206] Y. Shtanov and M. Pavliuk, JCAP **08**, 042, arXiv:2004.00947 [astro-ph.CO].

[207] D. Chowdhury, L. Sriramkumar, and M. Kamionkowski, JCAP **01**, 048, arXiv:1807.05530 [astro-ph.CO].

[208] I. S. Gradshteyn, I. M. Ryzhik, D. Zwillinger, and V. Moll, *Table of integrals, series, and products; 8th ed.* (Academic Press, Amsterdam, 2014).

[209] W. R. Inc., Mathematica, Version 12.3.1, champaign, IL, 2021.

[210] P. A. R. Ade *et al.* (BICEP/Keck), Phys. Rev. Lett. **127**, 151301 (2021), arXiv:2110.00483 [astro-ph.CO].

[211] K.-W. Ng, S.-L. Cheng, and W. Lee, Chin. J. Phys. **53**, 110105 (2015), arXiv:1409.2656 [astro-ph.CO].

[212] V. F. Mukhanov, H. A. Feldman, and R. H. Brandenberger, Phys. Rept. **215**, 203 (1992).

[213] J. Martin, Braz. J. Phys. **34**, 1307 (2004), arXiv:astro-ph/0312492.

[214] B. A. Bassett, S. Tsujikawa, and D. Wands, Rev. Mod. Phys. **78**, 537 (2006).

[215] D. Baumann and H. V. Peiris, Adv. Sci. Lett. **2**, 105 (2009), arXiv:0810.3022 [astro-ph].

[216] W. H. Kinney, (2009), arXiv:0902.1529 [astro-ph.CO].

[217] D. Baumann, in *Theoretical Advanced Study Institute in Elementary Particle Physics: Physics of the Large and the Small* (2009) arXiv:0907.5424 [hep-th].

[218] A. Linde, in *100e Ecole d'Ete de Physique: Post-Planck Cosmology* (2014) arXiv:1402.0526 [hep-th].

[219] D. K. Hazra, L. Sriramkumar, and J. Martin, JCAP **05**, 026, arXiv:1201.0926 [astro-ph.CO].

[220] J. A. Adams, B. Cresswell, and R. Easther, Phys. Rev. D **64**, 123514 (2001), arXiv:astro-ph/0102236.

[221] A. A. Starobinsky, JETP Lett. **55**, 489 (1992).

[222] J. Martin and L. Sriramkumar, JCAP **01**, 008, arXiv:1109.5838 [astro-ph.CO].

[223] C. T. Byrnes, P. S. Cole, and S. P. Patil, JCAP **06**, 028, arXiv:1811.11158 [astro-ph.CO].

[224] C. Bonvin, C. Caprini, and R. Durrer, Phys. Rev. D **86**, 023519 (2012), arXiv:1112.3901 [astro-ph.CO].

[225] S. Tripathy, D. Chowdhury, R. K. Jain, and L. Sriramkumar, Phys. Rev. D **105**, 063519 (2022), arXiv:2111.01478 [astro-ph.CO].

[226] M. Braglia, X. Chen, D. K. Hazra, and L. Pinol, (2022), arXiv:2210.07028 [astro-ph.CO].

[227] H. V. Ragavendra, Phys. Rev. D **105**, 063533 (2022), arXiv:2108.04193 [astro-ph.CO].

[228] M. Braglia, D. K. Hazra, L. Sriramkumar, and F. Finelli, JCAP **08**, 025, arXiv:2004.00672 [astro-ph.CO].

[229] G. A. Palma, S. Sypsas, and C. Zenteno, Phys. Rev. Lett. **125**, 121301 (2020), arXiv:2004.06106 [astro-ph.CO].

[230] J. Fumagalli, S. Renaux-Petel, J. W. Ronayne, and L. T. Witkowski, (2020), arXiv:2004.08369 [hep-th].

[231] M. Braglia, D. K. Hazra, F. Finelli, G. F. Smoot, L. Sriramkumar, and A. A. Starobinsky, JCAP **08**, 001, arXiv:2005.02895 [astro-ph.CO].

[232] S. Pi, Y.-l. Zhang, Q.-G. Huang, and M. Sasaki, JCAP **05**, 042, arXiv:1712.09896 [astro-ph.CO].

[233] M. Braglia, X. Chen, and D. K. Hazra, JCAP **03**, 005, arXiv:2012.05821 [astro-ph.CO].

[234] A. Lewis, A. Challinor, and A. Lasenby, Astrophys. J. **538**, 473 (2000), arXiv:astro-ph/9911177.

[235] N. C. Tsamis and R. P. Woodard, Phys. Rev. D **69**, 084005 (2004), arXiv:astro-ph/0307463.

[236] W. H. Kinney, Phys. Rev. D **72**, 023515 (2005), arXiv:gr-qc/0503017.

[237] Z. Lalak, D. Langlois, S. Pokorski, and K. Turzynski, JCAP **07**, 014, arXiv:0704.0212 [hep-th].

[238] R. Kallosh, A. Linde, and Y. Yamada, JHEP **01**, 008, arXiv:1811.01023 [hep-th].

[239] C. Gordon, D. Wands, B. A. Bassett, and R. Maartens, Phys. Rev. D **63**, 023506 (2000), arXiv:astro-ph/0009131.

[240] R. N. Raveendran and L. Sriramkumar, Phys. Rev. D **99**, 043527 (2019), arXiv:1809.03229 [astro-ph.CO].

[241] T. R. Seshadri and K. Subramanian, Phys. Rev. Lett. **87**, 101301 (2001), arXiv:astro-ph/0012056.

[242] A. Mack, T. Kahniashvili, and A. Kosowsky, Phys. Rev. D **65**, 123004 (2002), arXiv:astro-ph/0105504.

[243] A. Lewis, Phys. Rev. D **70**, 043011 (2004), arXiv:astro-ph/0406096.

[244] D. Paoletti, F. Finelli, and F. Paci, Mon. Not. Roy. Astron. Soc. **396**, 523 (2009), arXiv:0811.0230 [astro-ph].

[245] J. Adamek, R. Durrer, E. Fenu, and M. Vonlanthen, JCAP **06**, 017, arXiv:1102.5235 [astro-ph.CO].

[246] J. R. Shaw and A. Lewis, Phys. Rev. D **86**, 043510 (2012), arXiv:1006.4242 [astro-ph.CO].

[247] C. Caprini, R. Durrer, and T. Kahniashvili, Phys. Rev. D **69**, 063006 (2004), arXiv:astro-ph/0304556.

[248] M. Ballardini, F. Finelli, and D. Paoletti, JCAP **10**, 031, arXiv:1412.1836 [astro-ph.CO].

[249] R. Sharma, K. Subramanian, and T. R. Seshadri, Phys. Rev. D **101**, 103526 (2020), arXiv:1912.12089 [astro-ph.CO].

[250] S. Okano and T. Fujita, JCAP **03**, 026, arXiv:2005.13833 [astro-ph.CO].

[251] A. Brandenburg, Y. He, and R. Sharma, Astrophys. J. **922**, 192 (2021), arXiv:2107.12333 [astro-ph.CO].

[252] A. Brandenburg and R. Sharma, Astrophys. J. **920**, 26 (2021), arXiv:2106.03857 [astro-ph.CO].

[253] A. Albrecht, P. Ferreira, M. Joyce, and T. Prokopec, Phys. Rev. **D50**, 4807 (1994), arXiv:astro-ph/9303001 [astro-ph].

[254] D. Polarski and A. A. Starobinsky, Class. Quant. Grav. **13**, 377 (1996), arXiv:gr-qc/9504030 [gr-qc].

[255] C. Kiefer, D. Polarski, and A. A. Starobinsky, Int. J. Mod. Phys. **D7**, 455 (1998), arXiv:gr-qc/9802003 [gr-qc].

[256] C. Kiefer and D. Polarski, Annalen Phys. **7**, 137 (1998), arXiv:gr-qc/9805014.

[257] C. Kiefer, I. Lohmar, D. Polarski, and A. A. Starobinsky, Class. Quant. Grav. **24**, 1699 (2007), arXiv:astro-ph/0610700 [astro-ph].

[258] J. Martin, Lect. Notes Phys. **738**, 193 (2008), arXiv:0704.3540 [hep-th].

[259] C. Kiefer and D. Polarski, Adv. Sci. Lett. **2**, 164 (2009), arXiv:0810.0087 [astro-ph].

[260] J. Martin, V. Vennin, and P. Peter, Phys. Rev. **D86**, 103524 (2012), arXiv:1207.2086 [hep-th].

[261] J. Martin, *Proceedings, International Conference on Modern Perspectives of Cosmology and Gravitation (COSGRAV 12): Kolkata, India, 7?11 February 2012*, J. Phys. Conf. Ser. **405**, 012004 (2012), arXiv:1209.3092 [hep-th].

[262] J. Martin and V. Vennin, Phys. Rev. **D93**, 023505 (2016), arXiv:1510.04038 [astro-ph.CO].

[263] S. Tripathy, D. Chowdhury, H. V. Ragavendra, R. K. Jain, and L. Sriramkumar, (2022), arXiv:2211.05834 [astro-ph.CO].

[264] S. Choudhury and S. Panda, Universe **6**, 79 (2020), arXiv:1809.02905 [hep-th].

[265] S. Brahma, O. Alaryani, and R. Brandenberger, Phys. Rev. D **102**, 043529 (2020), arXiv:2005.09688 [hep-th].

[266] S. Choudhury, (2022), arXiv:2301.05203 [hep-th].

[267] S. Brahma, J. Calderón-Figueroa, M. Hassan, and X. Mi, (2023), arXiv:2302.13894 [hep-th].

[268] L. Battarra and J.-L. Lehners, Phys. Rev. D **89**, 063516 (2014), arXiv:1309.2281 [hep-th].

[269] D. J. Stargen, V. Sreenath, and L. Sriramkumar, Int. J. Mod. Phys. D **30**, 2150049 (2021), arXiv:1605.07311 [gr-qc].

[270] R. N. Raveendran and S. Chakraborty, (2023), arXiv:2302.02584 [astro-ph.CO].

[271] S. L. Braunstein and P. van Loock, Rev. Mod. Phys. **77**, 513 (2005), arXiv:quant-ph/0410100.

[272] C. Weedbrook, S. Pirandola, R. García-Patrón, N. J. Cerf, T. C. Ralph, J. H. Shapiro, and S. Lloyd, Rev. Mod. Phys. **84**, 621 (2012).

[273] M. Hillery, R. F. O'Connell, M. O. Scully, and E. P. Wigner, Phys. Rept. **106**, 121 (1984).

[274] W. B. Case, Am. J. Phys. **76**, 937 (2008).

[275] F. J. Narcowich, J. Math. Phys. **31**, 354 (1990).

[276] T. J. Hollowood and J. I. McDonald, Phys. Rev. **D95**, 103521 (2017), arXiv:1701.02235 [gr-qc].

[277] E. A. Lim, Phys. Rev. **D91**, 083522 (2015), arXiv:1410.5508 [hep-th].

[278] J. Martin, A. Micheli, and V. Vennin, JCAP **04** (04), 051, arXiv:2112.05037 [quant-ph].

[279] A. Bera, T. Das, D. Sadhukhan, S. S. Roy, A. S. De, and U. Sen, Reports on Progress in Physics **81**, 024001 (2017), arXiv:1703.10542 [quant-ph].

[280] D. Maity and S. Pal, Phys. Lett. B **835**, 137503 (2022), arXiv:2107.12793 [gr-qc].

[281] L. P. Grishchuk, Class. Quant. Grav. **10**, 2449 (1993), arXiv:gr-qc/9302036.

[282] J. Martin, Universe **5**, 92 (2019), arXiv:1904.00083 [quant-ph].

[283] I. Agullo, B. Bonga, and P. R. Metidieri, JCAP **09**, 032, arXiv:2203.07066 [gr-qc].

[284] A. H. Guth and S. Y. Pi, Phys. Rev. Lett. **49**, 1110 (1982).

[285] G. Cariolaro, *Quantum communications* (Springer, 2015).

[286] D. Katsinis, G. Pastras, and N. Tetradis, (2023), arXiv:2304.04241 [hep-th].

[287] K. Boutivas, G. Pastras, and N. Tetradis, JHEP **05**, 199, arXiv:2302.14666 [hep-th].

[288] R. N. Raveendran, K. Parattu, and L. Sriramkumar, Gen. Rel. Grav. **54**, 91 (2022), arXiv:2206.05760 [astro-ph.CO].

[289] A. Datta, A. Shaji, and C. M. Caves, Physical review letters **100**, 050502 (2008), arXiv:0709.0548 [quant-ph].

[290] M. Srednicki, Phys. Rev. Lett. **71**, 666 (1993), arXiv:hep-th/9303048.

[291] I. S. Gradshteyn and I. M. Ryzhik, *Table of Integrals, Series, and Products; 7th ed.* (Academic Press, 2007).

[292] M. Aich, D. K. Hazra, L. Sriramkumar, and T. Souradeep, Phys. Rev. D **87**, 083526 (2013), arXiv:1106.2798 [astro-ph.CO].

[293] H. V. Ragavendra and L. Sriramkumar, Galaxies **11**, 34 (2023), arXiv:2301.08887 [astro-ph.CO].

[294] M. B. Fröb, J. Garriga, S. Kanno, M. Sasaki, J. Soda, T. Tanaka, and A. Vilenkin, JCAP **04**, 009, arXiv:1401.4137 [hep-th].

[295] T. Kobayashi and N. Afshordi, JHEP **10**, 166, arXiv:1408.4141 [hep-th].

[296] R. Sharma and S. Singh, Phys. Rev. D **96**, 025012 (2017), arXiv:1704.05076 [gr-qc].

[297] M. Banyeres, G. Domènech, and J. Garriga, JCAP **10**, 023, arXiv:1809.08977 [hep-th].

[298] R. Durrer, O. Sobol, and S. Vilchinskii, (2023), arXiv:2303.04583 [gr-qc].

[299] Z.-Z. Peng, Z.-M. Zeng, C. Fu, and Z.-K. Guo, Phys. Rev. D **106**, 124044 (2022), arXiv:2209.10374 [gr-qc].

[300] A. Daddi Hammou and N. Bartolo, (2022), arXiv:2211.07598 [astro-ph.CO].

[301] R. K. Jain and M. S. Sloth, Phys. Rev. D **86**, 123528 (2012), arXiv:1207.4187 [astro-ph.CO].

[302] R. K. Jain, P. J. Sai, and M. S. Sloth, JCAP **03**, 054, arXiv:2108.10887 [hep-th].

[303] C. Cecchini and M. Rinaldi, Phys. Dark Univ. **40**, 101212 (2023), arXiv:2301.07699 [astro-ph.CO].

[304] Y. Guan and A. Kosowsky, Phys. Rev. D **106**, 063505 (2022), arXiv:2205.05241 [astro-ph.CO].

[305] K. E. Kunze, Phys. Rev. D **87**, 103005 (2013), arXiv:1301.6105 [astro-ph.CO].

[306] J. Martin, A. Micheli, and V. Vennin, EPL **142**, 18001 (2023), arXiv:2211.10114 [quant-ph].

[307] J. Martin and V. Vennin, JCAP **06**, 037, arXiv:1805.05609 [astro-ph.CO].

[308] C. P. Burgess, R. Holman, G. Kaplanek, J. Martin, and V. Vennin, JCAP **07**, 022, arXiv:2211.11046 [hep-th].

[309] R. M. Corless, G. H. Gonnet, D. E. Hare, D. J. Jeffrey, and D. E. Knuth, Advances in Computational mathematics **5**, 329 (1996).

[310] G. Adesso and A. Datta, Physical review letters **105**, 030501 (2010).

[311] A. Serafini, F. Illuminati, and S. De Siena, J. Phys. B **37**, L21 (2004), arXiv:quant-ph/0307073.

CURRICULUM VITAE

PERSONAL INFORMATION

Name: Sagarika Tripathy
Date of Birth: April 3, 1994
Gender: Female
Nationality: Indian
Post: Department of Physics, Indian Institute of Technology Madras, Chennai 600036
E-mail: sagarika@physics.iitm.ac.in
Personal e-mail: sagarikatripathy093@gmail.com
Mobile: +91-82-4948-3516

ACADEMIC HISTORY

- **Ph.D. Physics**, Indian Institute of Technology Madras, Chennai, 2017–Present
- **M.Sc. Physics**, Savitribai Phule Pune University, Pune, 2014–2016
- **B.Sc. Physics**, B. J. B. Autonomous College, Bhubaneswar, 2011–2014

DOCTORAL COMMITTEE

Guide

Prof. L. Sriramkumar
Professor
Department of Physics, Indian Institute of Technology Madras, Chennai 600036

Members

Prof. Arul Lakshminarayan (Chairperson)
Professor
Department of Physics, Indian Institute of Technology Madras, Chennai 600036

Dr. Dawood Kothawala
Associate Professor
Department of Physics, Indian Institute of Technology Madras, Chennai 600036

Prof. James Libby
Professor
Department of Physics, Indian Institute of Technology Madras, Chennai 600036

Prof. Anil Prabhakar
Professor
Department of Electrical Engineering, Indian Institute of Technology Madras, Chennai 600036